FABRÍCIO MARQUES DE OLIVEIRA

SÍNTESE, CÁLCULOS TEÓRICOS, CARACTERIZAÇÃO ESTRUTURAL E AVALIAÇÃO DAS ATIVIDADES FITOTÓXICA E INIBITÓRIA DE UREASE DE NOVOS FOSFORAMIDATOS

Tese apresentada à Universidade Federal de Viçosa, como parte das exigências do Programa de Pós-Graduação em Agroquímica, para obtenção do título de *Doctor Scientiae.*

VIÇOSA
MINAS GERAIS – BRASIL
2014

Ficha catalográfica preparada pela Biblioteca Central da Universidade Federal de Viçosa - Câmpus Viçosa

T

O48s
2014

Oliveira, Fabricio Marques de, 1983-
Síntese, cálculos teóricos, caracterização estrutural e avaliação das atividades fitotóxica e inibitória de urease de novos fosforamidatos / Fabricio Marques de Oliveira. - Viçosa, MG, 2014.
xxvi, 266f. : il. (algumas color.) ; 29 cm.

Inclui anexos.
Orientador : Luiz Cláudio de Almeida Barbosa.
Tese (doutorado) - Universidade Federal de Viçosa.
Inclui bibliografia.

1. Compostos organofosforados. 2. Compostos organofosforados - Síntese. 3. Urease. 4. Fitoxicidade. I. Universidade Federal de Viçosa. Departamento de Química. Programa de Pós-graduação em Agroquímica. II. Título.

CDD 22. ed. 547.07

FABRICIO MARQUES DE OLIVEIRA

SÍNTESE, CÁLCULOS TEÓRICOS, CARACTERIZAÇÃO ESTRUTURAL E AVALIAÇÃO DAS ATIVIDADES FITOTÓXICA E INIBITÓRIA DE UREASE DE NOVOS FOSFORAMIDATOS

Tese apresentada à Universidade Federal de Viçosa, como parte das exigências do Programa de Pós-Graduação em Agroquímica, para obtenção do título de *Doctor Scientiae.*

APROVADA: 15 de dezembro de 2014.

_____	_____
Teodorico de Castro Ramalho	Róbson Ricardo Teixeira
_____	_____
Paulo Henrique Fidêncio	Antônio Jacinto Demuner

_____
Luiz Cláudio de Almeida Barbosa
(Orientador)

Não há saber mais ou menos. Há saberes diferentes.
(Paulo Freire)

Se o conhecimento pode criar problemas, não é através da ignorância que podemos solucioná-los.
(Isaac Asimov)

O gênio consiste em um por cento de inspiração e noventa e nove por cento de transpiração.
(Thomas A. Edison)

Pesquisa é o processo de entrar em vielas para ver se elas são becos sem saída.

(Marston Bates)

AGRADECIMENTOS

A DEUS, pela vida e pela saúde!

À Universidade Federal de Viçosa e ao Departamento de Química, pela oportunidade de realização deste trabalho de pesquisa.

Ao professor Luiz Cláudio de Almeida Barbosa, pela amizade e orientação segura e competente.

Aos professores Célia Regina Álvares Maltha e Antônio Jacinto Demuner, pela amizade, pela disponibilidade, pelo estímulo e pela ajuda imprescindíveis à realização deste trabalho.

Aos técnicos José Luiz Pereira, Eduardo Rezende, Onesina Batista, Márcio Alvarenga e Cristiane Isaac Cerceau, pela colaboração na realização deste trabalho e pelos bons momentos de convívio.

Aos meus pais Neli Marques de Oliveira e Anides de Oliveira Filho, pelo apoio incondicional e pela presença constante.

Aos meus irmãos Evandro Marques de Oliveira e Rodrigo Marques de Oliveira, pelos momentos de alegria e estímulo.

À minha sobrinha Ângela Quinelato Oliveira e à sua mãe Rosangela Aparecida Quinelato Oliveira, pelo carinho.

A toda a minha família, em especial aos tios Carlos Monteiro de Almeida e Maria das Graças Silva Almeida e aos primos Vinícius Silva Monteiro e Vanessa Silva Monteiro, sempre presentes, e que me ofereceram condições para que eu progredisse na minha caminhada.

Aos amigos que passaram pela república em Viçosa ao longo desses anos, e aos amigos do Laboratório de Análise e Síntese de Agroquímicos (LASA).

Aos amigos e professores Róbson Ricardo Teixeira e Sergio Antonio Fernandes, pelo apoio e incentivo nos momentos de dificuldade.

Aos demais colegas do DEQ, pelos momentos de alegria.

Ao Rodrigo Corrêa, da USP de São Carlos, pela colaboração com os experimentos de difração de raios X.

Ao Prof. Walkimar Carneiro e Mikhail Kabeshov pelo auxílio na realização dos cálculos DFT.

Aos amigos e professores do Instituto Federal de Minas Gerais (IFMG), campus Ouro Branco.

À pequena Guidoval-MG, pelo calor humano e pelas lições de humildade.

A todos que de alguma forma, direta ou indiretamente, contribuíram para a realização deste trabalho.

ÍNDICE

LISTA DE FIGURAS

CAPÍTULO 1

CAPÍTULO 2

Página

CAPÍTULO 3

CAPÍTULO 4

CAPÍTULO 5

CAPÍTULO 6

Página

CAPÍTULO 7

ANEXO

LISTA DE ESQUEMAS

CAPÍTULO 1

CAPÍTULO 2

CAPÍTULO 4

Página

CAPÍTULO 7

Página

LISTA DE TABELAS

CAPÍTULO 2

CAPÍTULO 3

CAPÍTULO 4

CAPÍTULO 5

CAPÍTULO 7

LISTA DE ABREVIATURAS

ADMET	Absorção, distribuição, metabolismo, excreção e toxicidade em farmacocinética
ATP	Adenosina tri-fosfato
Bn	Benzil
CCD	Cromatografia em camada delgada
CG/EM	Cromatografia gasosa acoplada à espectrometria de massas
d	Dupleto
dd	Duplo dupleto
dt	Duplo tripleto
δ	Deslocamento químico
DCM	Diclorometano
DMG	Dimetilglicina
DNA	Ácido desoxirribonucleico
Et_2O	Éter dietílico
EtOAc	Acetato de etila
FDA	Food and Drug Administration
THF	Tetraidrofurano
Hz	Hertz
IV	Infravermelho
L-Ala	*L*-Alanina
L-Leu	*L*-Leucina
L-Ile	*L*-Isoleucina
J	Constante de acoplamento escalar
m	Multipleto
MHz	Megahertz

m/v	Massa/volume
NBPT	*N*-(n-butil) tiofosfórico triamida
NBPTO	*N*-(n-butil) fosfórico triamida
ppm	Partes por milhão
q	quarteto
R_f	Fator de retenção
RMN de ^{13}C	Ressonância magnética nuclear de carbono-13
RMN de ^{1}H	Ressonância magnética nuclear de hidrogênio
RNA	Ácido ribonucleico
s	Simpleto
t	Tripleto
t.a.	Temperatura ambiente
t.r.	Tempo de reação
T_f	Temperatura de fusão
v/v	Volume/volume

RESUMO

OLIVEIRA, Fabricio Marques de, D. Sc., Universidade Federal de Viçosa, Dezembro de 2014. **Síntese, cálculos teóricos, caracterização estrutural e avaliação das atividades fitotóxica e inibitória de urease de novos fosforamidatos.** Orientador: Luiz Cláudio de Almeida Barbosa. Co-orientadores: Antônio Jacinto Demuner e Célia Regina Álvares Maltha.

Os fosforamidatos são uma classe de compostos que apresentam pelo menos um grupo $–NR_1R_2$ (R_1 e R_2 = alquila, arila) em suas estruturas. Relatos na literatura evidenciam diversas atividades biológicas, seja na área médica, agrícola ou industrial para esses compostos. O presente trabalho teve por objetivo sintetizar novos fosforamidatos, visando à avaliação de suas atividades fitotóxica e inibitória de urease. A síntese baseou-se em fenóis substituídos como material de partida. O tratamento dos fenóis com cloreto de fosforila na presença de trietilamina forneceu os respectivos compostos organofosfatos diclorados. A subsequente reação destes organofosfatos com aminas na presença de trietilamina resultou na formação de 19 compostos fosforamidatos. Estes compostos foram reunidos com mais 12 substâncias dessa classe sintetizados no Laboratório de Síntese e Análise de Agroquímicos e suas atividades biológicas foram avaliadas contra *Sorghum bicolor* e *Cucumis sativus*. Os compostos *tris*(4-bromofenil)fosfato e 4-fluorofenil-*N,N´*-dimorfolin-1-ilfosfinato apresentaram valores de inibição superiores ao observado para o Glifosato sobre *S. bicolor*, enquanto que para *C. sativus* os mais ativos foram os compostos 4-clorofenil-di(piperidin-1-il)fosfinato e *bis*(3-clorofenil)-dietilfosforamidato, que apresentaram 82 e 83% de inibição, respectivamente, sobre o sistema aéreo na maior concentração (1 mmol L^{-1}). Essas substâncias também tiveram suas atividades avaliadas contra a inibição de urease. Das 25 substâncias testadas, seis apresentaram atividade comparável ou superior ao controle positivo (tiouréia), sendo que o composto *bis*(4-bromofenil)-*N*-cicloexilamidofosfato parece ser o mais promissor. As propriedades ADMET

previstas para estes fosforoamidatos estão de acordo com os requisitos gerais para potenciais fármacos, confirmando que estes compostos possuem propriedades físico-químicas que os qualificam para apresentarem satisfatórias farmacocinética e biodisponibilidade. Além disso, não foram observadas violações da regra de Lipinski para a maioria dos fosforoamidatos. A relação estrutura-atividade analisada para as 25 substâncias sugere que a presença do grupo cicloexila é uma característica estrutural importante associada com a atividade inibitória apresentada pelos compostos contra a enzima. Cálculos baseados na teoria de funcional da densidade foram realizados para obtenção dos valores de energia de HOMO e LUMO, momento de dipolo molecular e potencial eletrostático dos compostos avaliados.

Descrevemos ainda neste trabalho um estudo experimental e teórico combinando estrutura molecular e RMN dos fosforoamidatos furano-2-il-*N,N*-diisopropilamidoclorofosfato e furan-2-il-*N,N,N´,N´*-diciclohexilamidofosfato. Na escala de tempo da RMN uma rotação livre das ligações simples C-N/P-N foi observada em temperatura ambiente (298 K), enquanto que a rotação é interrompida abaixo de 195 K para o furano-2-il-*N,N*-diisopropilamidoclorofosfato. A partir das análises dos dados da RMN, a energia de ativação livre ($\Delta G^{\#}$) para a rotação das ligações C-N/P-N foi calculada como 9,9 ± 0,3 kcal mol^{-1}. Os dados experimentais foram reforçados por cálculos teóricos utilizando o método da teoria da densidade funcional B3LYP e conjunto de bases 6-31G(d) que forneceu energia de ativação ($\Delta E^{\#}$) igual a 9,2 kcal mol^{-1}. As estruturas dos compostos foram investigadas por difração de raios-X, e verificou-se que o furano-2-il-*N,N*-diisopropilamidoclorofosfato está na forma de mistura racêmica.

Por fim, foram determinados os deslocamentos químicos de RMN de ^{1}H e ^{13}C para três fosforamidatos empregando-se cálculos DFT, nos níveis B3LYP, WP04, TPSSh, M062X and wB97XD, e diferentes bases, levando-se em consideração a distribuição de Boltzamann para cada confôrmero. Os valores experimentais foram comparados com os teóricos e avaliados usando correlação linear, erro absoluto médio, desvio médio quadrático. Para o caso do RMN de ^{13}C, os resultados obtidos com GIAO/wB97XD/cc-pVTZ/SCRF apresentaram o menor RMSD (2,073), mas requerendo maior tempo de processamento. O melhor custo-benefício neste caso foi obtido empregando-se

GIAO/B3LYP/6-31G(d,p)/SCRF que forneceu o valor de desvio médio quadrático igual a 2,121 a um custo de CPU vinte e seis vezes menor. No caso do RMN de ^{1}H a combinação CSGT/TPSSh/cc-pVTZ/SCRF forneceu o valor de desvio médio quadrático igual a 0,070. Reduzindo o tempo computacional uma vez e meia (CSGT/B3LYP/6-311++G(2d,p)/SCRF) foi possível obter um bom resultado (desvio médio quadrático igual a 0,088). De modo geral, avaliando-se os parâmetros estatísticos, o método que se mostrou mais adequado a essa classe de compostos foi CSGT/wB97XD/cc-pVTZ/SCRF.

ABSTRACT

OLIVEIRA, Fabrício Marques de, D. Sc., Universidade Federal de Viçosa, December 2014. **Synthesis, theoretical calculations, structural characterization and evaluation of phytotoxic and urease inhibitory activities of new phosphoramidates.** Adviser: Luiz Cláudio de Almeida Barbosa. Co-advisers: Antônio Jacinto Demuner and Célia Regina Álvares Maltha.

Phosphoramidates is a class of compounds which has at least one -NR_1R_2 group in its structure (R_1 and R_2 = alkyl, aryl). Reports in the literature show that these compounds have several biological activities, whether in medical, agricultural or industrial area. This study aimed to synthesize new phosphoramidates in order to evaluate their phytotoxic and urease inhibitory activities. Substituted phenols were used as starting material in the synthesis route. The reaction of phenols with phosphoryl chloride, in the presence of trimethylamine, provided the respective dichlorinated organophosphates compounds. The subsequent reaction of these organophosphates with amines and trimethylamine resulted in the formation of 19 phosphoramidate compounds.

These compounds were combined with 12 other substances previously synthetized at "*Laboratório de Síntese e Análise de Agroquímicos".* Their biological activities were evaluated for *Sorghum bicolor* and *Cucumis sativus.* Compunds *tris*(4-bromophenyl)phosphate and 4-fluorophenyl-*N,N'*-dimorfolin-1-ylphosphinate showed higher inhibition values than glyphosate over *Sorghum bicolor.* For *C. sativus,* the most active compounds were 4-chlorophenyl-di(piperidin-1-yl)phosphinate and *bis*(3-chlorophenyl)-diethylphosphoramidate with 82 and 83% of inhibition, respectively. This is the result for the aerial system at the higher concentration (1 mmol L^{-1}). These substances were also tested for urease inhibition. From the 25 tested substances, six had their activity comparable to or higher than the positive control (thiourea). From all the tested compounds, *bis*(4-bromophenyl)-*N*-cyclohexylaminophosphate seems to be the

most promising molecule. The predicted ADMET properties for these phosphoramidates are in accordance with the general requirements for potential drugs. This fact confirms that these compounds have the physicochemical properties that qualify them to present satisfactory pharmacokinetics and bioavailability. Furthermore, there were no violations of Lipinski rule for most phosphoramidates. The analyzed structure-activity relationship of the 25 substances suggests that the presence of the cyclohexyl group is an important structural feature for the inhibitory activity showed by these compounds against the enzyme. Calculations based on density functional theory were carried out to obtain the energy values of HOMO and LUMO, molecular dipole moment, and electrostatic potential for the evaluated compounds.

This work also presents an experimental and theoretical study combining NMR and molecular structure of the phosphoramidates furan-2-yl-*N,N*-diisopropylamidochlorophosphate and furan-2-yl-*N,N,N′,N′*-dicyclohexylamidophosphate. On a time dependent NMR study, a free rotation was observed for the single bonds C-N/P-N at room temperature (298 K). However, this rotation is not observed at temperatures lower than 195 K for furan-2-yl-*N,N*-diisopropylamidochlorophosphate. Based on the NMR data, the free activation energy ($\Delta G^{\#}$) for the rotation of C-N/P-N bonds was calculated as 9.9 ± 0.3 kcal mol^{-1}. The experimental data was supported by theoretical calculations using the density functional theory B3LYP method and the 6-31G(d) basis set, which provided an activation energy ($\Delta E^{\#}$) of 9.2 kcal mol^{-1}. The structures of the compounds were investigated by X-ray diffraction, and it was found that furan-2-yl-*N,N*-diisopropylamidochlorophosphate is in the form of racemic mixture.

Ultimately, it was determined the ^{1}H and ^{13}C NMR chemical shifts for three phosphoramidates employing DFT calculations on B3LYP, WP04, TPSSh, M062X, wB97XD levels and different bases. The distribution for each Boltzmann conformer was taken into consideration. The experimental and theoretical values were compared and evaluated using linear correlation, mean absolute error and root-mean-square deviation (RMSD). For ^{13}C NMR, the results obtained with GIAO/wB97XD/cc-pVTZ/SCRF showed the lowest RMSD (2.073), but requiring more processing time. The best cost-benefit was obtained employing GIAO/B3LYP/6-31G(d,p)/SCRF, which provided RMSD value of

2.121 with a twenty-six times smaller CPU cost. For ^{1}H NMR, the combination CSGT/TPSSh/cc-pVTZ/SCRF provided a RMSD value of 0.070. Reducing the computational time by a factor of one and a half (CSGT/B3LYP/6-311++G(2d,p)/SCRF), it was possible to obtain a good result (RMSD of 0.088). In general, after evaluating the statistical parameters, the method that was more suitable for this class of compounds was CSGT/wB97XD/cc-pVTZ/SCRF.

1. COMPOSTOS ORGANOFOSFORADOS E SUAS DIVERSAS ATIVIDADES BIOLÓGICAS

1.1. Introdução Geral

Os compostos que apresentam em suas estruturas o elemento químico fósforo são precursores indispensáveis à vida. Descoberto em 1669 por Henning Brandt, o fósforo participa da formação molecular do DNA e RNA, e é utilizado como forma de armazenamento de energia por células na forma de ATP (Figura 1). Está presente em substâncias constituintes dos tecidos ósseo e nervoso, além de atuar como agente tamponante no meio celular e ser cofator de múltiplos sistemas enzimáticos (WESTHEIMER, 1987; BORGES *et al.*, 2004).

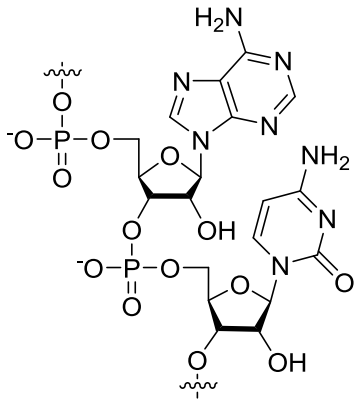

Fragmento da molécula do RNA

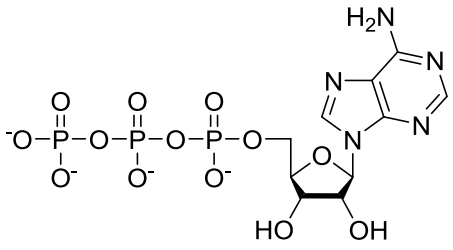

ATP

Figura 1 – Fragmento da molécula de RNA e da estrutura do trifosfato de adenosina (ATP).

A partir do conhecimento das propriedades do elemento fósforo, diversos compostos passaram a ser sintetizados pelo homem buscando atender às suas necessidades. Exemplos de compostos comerciais são apresentados na Figura 2.

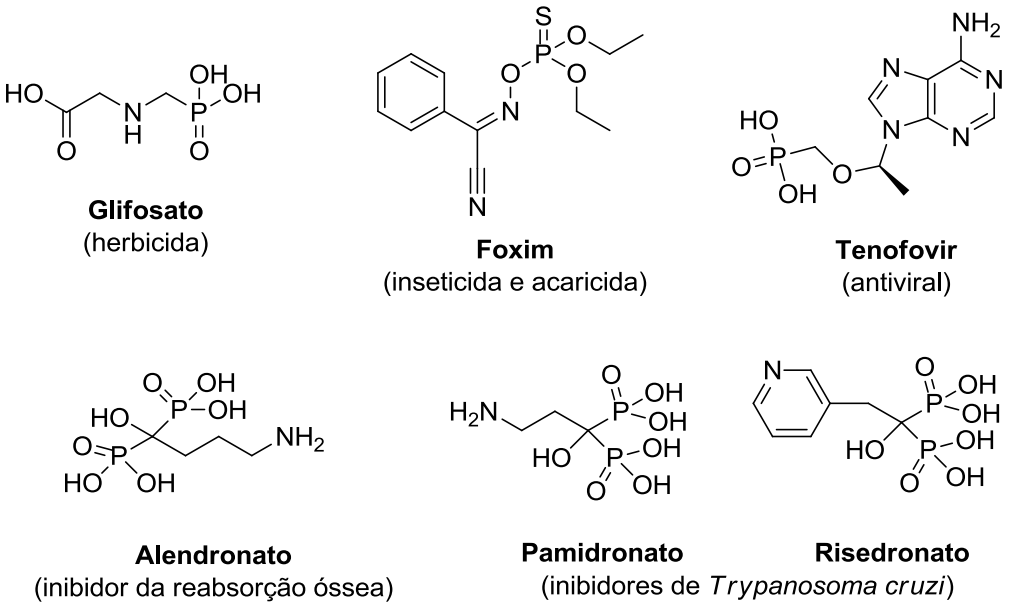

Figura 2 - Exemplos de compostos fosforados disponíveis comercialmente.

O Glifosato [*N*-fosfonometilglicina] (Figura 2) é o princípio ativo do Roundup®, herbicida comercial mais vendido no mundo. Somente o glifosato representa em torno de 40% do consumo de agroquímicos no Brasil (CARNEIRO, 2012). As principais características que colaboram para a grande aceitação do glifosato no mercado são o amplo espectro de ação, além de ser toxicologicamente e ambientalmente seguro. Somam-se a estas propriedades a boa translocação nas plantas e sua ação lenta (DUKE, 2008).

O Foxim® (Figura 2) é um inseticida organofosfato que é produzido pela Bayer Corporation, apresentando também propriedade acaricida. A substituição em sua estrutura de um grupo etoxi por um grupo metoxi levou à obtenção de um análogo com atividade de 20-30% mais ativo sobre as espécies de inseto *Pieris rapae*, *Lygocoris lucorum* e *Ostrinia furnacalis*, quando comparado ao inseticida comercial (SUN, 2011).

O composto Tenofovir (Figura 2), comercializado com o nome Viread®, atua inibindo a transcriptase reversa nucleotídeo e é empregado no coquetel anti-HIV (KARIM, 2010). Em 2009 essa mesma droga passou a ser utilizada no Brasil também na supressão do vírus da hepatite B (BENHAMOU, 2006; Ministério da Saúde, 2009).

Outro exemplo de composto organofosforado utilizado como fármaco é o Alendronato (Figura 2), princípio ativo de medicamentos como Fosamax®,

Bonalen®, Endronax®, Osteoform®, Recalfe®, Cleveron®, Osteoral®, entre outros. Esse composto pertence à classe dos bisfosfonatos e é empregado no tratamento da osteoporose, principalmente em mulheres (XU, 2004). Ainda na classe dos bisfosfonatos, Pamidronato (Aredia®), Risedronato (Actonel®) e o próprio Alendronato (Figura 2), inibem o crescimento do protozoário *Trypanosoma cruzi in vitro* e *in vivo*, sem provocar toxicidade às células hospedeiras (IC_{50} = 65 μM, 65 μM e 300 μM, respectivamente) (URBINA *et al.*, 1999; MONTALVETTI *et al.*, 2011; UBGINA e DOCAMPO, 2003). Estas estruturas serviram de modelo para que estudos na busca por bisfosfonatos mais ativos conduzidos por SZAJNMAN e colaboradores (2001) levassem ao desenvolvimento do composto 1-hidroxiheptano-1,1-bisfosfonato (**1**) (Figura 3) que apresentou valor de IC_{50} igual 18,1 μM.

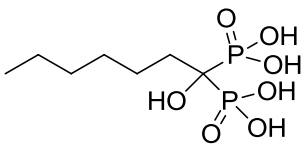

(1)

Figura 3 – Bisfosfonato com atividade sobre o protozoário *T. cruzi*.

Os compostos Fosmidomicina (**2**) e seu derivado FR900098 (**3**) (Figura 4) são membros de uma classe de produtos naturais de ácido fosfônico que são potentes e seletivos inibidores da enzima DOXP reductoisomerase, inibindo o crescimento de estirpes resistentes a múltiplos fármacos de *Plasmodium falciparum in vitro* (JOMAA *et al.*, 1999). O pró-fármaco (**4**) (Figura 4), derivado destes produtos naturais, apresentou eficácia em ratos infectados com o parasita da malária *Plasmodium vinckei* comparável à administração da droga via intraperitoneal (REICHENBERG *et al*., 2001).

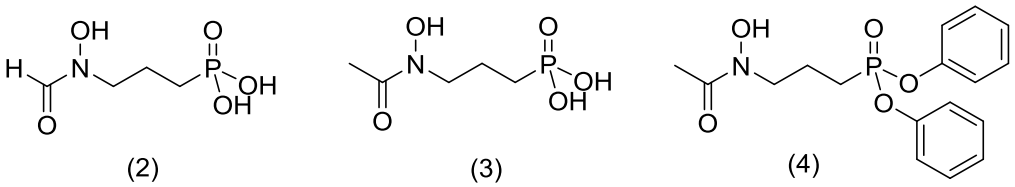

(2) (3) (4)

Figura 4 – Drogas com atividade antimalárica.

1.2. Fosforamidatos

Os compostos conhecidos como fosforamidatos caracterizam-se por apresentar pelo menos um grupo $–NR_1R_2$ (R_1 e R_2 = alquila, arila) em suas estruturas, sendo derivados do ácido fosforamídico (Figura 5) (SANTOS *et al.*, 2007).

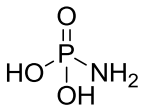

Figura 5 – Estrutura do ácido fosforamídico.

A literatura relata diversos compostos da classe dos fosforamidatos com atividade biológica, principalmente na área médica, sendo utilizados no controle de diversas patologias (DOMINGUEZ *et al.*, 2008; SUN *et al*., 2006; DUAN *et al.*, 2008; KIRAN *et al*., 2008; PRASAD *et al.*; NGUYEN e KIM, 2008; YAN *et al*., 2012; HU *et al*.; 2011; WANG *et al*.; 2010; MCGUIGAN *et al.*, 2005; MCGUIGAN *et al.*, 2009; ROMAN *et al.*, 2011; SERPI *et al.*, 2012; CHO *et al*., 2014). As estruturas de alguns compostos comercialmente disponíveis são mostradas na Figura 6.

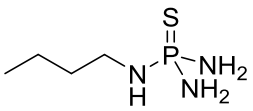

NBPT
(inibidor de urease)

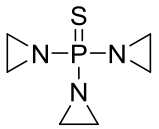

Tioetilenotiofosforamida
(antineoplásico)

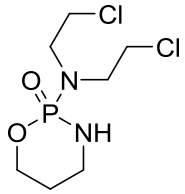

Ciclofosfamida
(antineoplásico)

Figura 6 – Fosforamidatos disponíveis comercialmente.

O NBPT [*N*-(n-butil) tiofosfórico triamida] apresenta bons resultados na inibição da atividade da enzima urease - responsável pela hidrólise da ureia, minimizando as perdas de nitrogênio por volatilização (Figura 6). Na verdade, o NBPT precisa ser oxidado ao [*N*-(n-butil) fosfórico triamida] (NBPTO), sua forma ativa. Trata-se do único princípio ativo efetivo e comercialmente disponível como inibidor de urease (Agrotain®). Pelo fato de o composto apresentar características muito similares à ureia, tais como teor de nitrogênio, solubilidade e difusividade similares, o composto atua ocupando o sítio ativo da enzima (AMTUL *et al.*, 2002; UPADHYAY, 2012). Muitas espécies de bactérias

produzem urease, incluindo a *Helicobacter pylori*, bactéria responsável pelas úlceras do estômago. Nessa linha de pesquisa, Dominguez e colaboradores (2008) descreveram a síntese de diversos fosforamidatos (Figura 7) que apresentaram elevada atividade biológica sobre a enzima (IC_{50} na ordem de nanomolar).

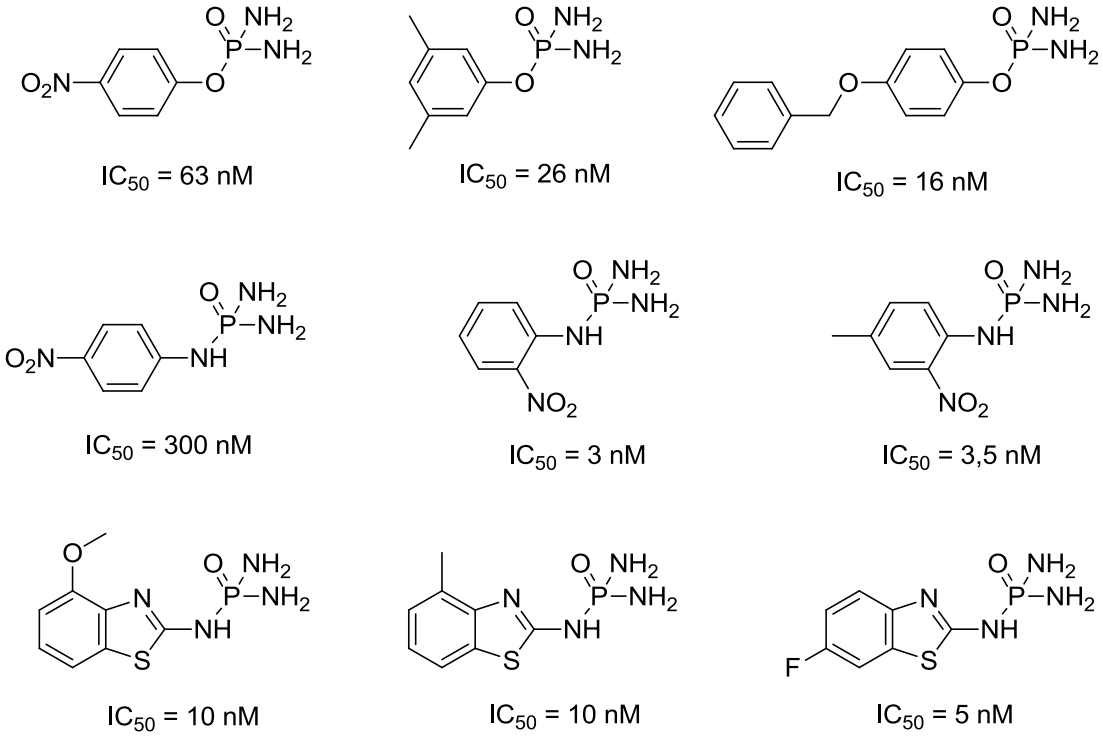

Figura 7 - Compostos fosforamidatos sintetizados por DOMINGUEZ *et al*. (2008) com atividade sobre urease.

Na linha de atividade antineoplásica destacam-se os compostos tioetilenotiofosforamida e ciclofosfamida (Figura 6). O primeiro deles, conhecido também como Tio-TEPA®, é indicado para o tratamento de câncer na bexiga e no ovário, e apresenta efeito similar ao do cloreto de mecloroetamina (**5**) (Figura 8), um dos agentes tumorais amplamente empregados (SANTOS *et al.*, 2007). A ciclofosfamida [2-[*bis*(2-cloroetil)amino]-2-oxo-1,3,2-oxazafosforinana] (Figura 6), princípio ativo do Endoxan®, é derivada da mostarda nitrogenada, e utilizada no tratamento de diversos tipos de câncer (SUN *et al.*, 2006; SANTOS *et al.*, 2007). Este composto serviu de modelo para a síntese do derivado TH-302 (**6**) (Figura 8) que se demonstrou efetivo no controle de células tumorais pancreáticas MIA PaCa-2, estável ao metabolismo microssomal e eficaz como antitumoral em combinação com o fármaco Gemcitabina® em ensaios *in vivo*

com camundongos. Por causa das suas propriedades pré-clínicas atrativas, o composto **6** encontra-se em fase 1 de testes clínicos para o tratamento de tumores sólidos (DUAN *et al.*, 2008).

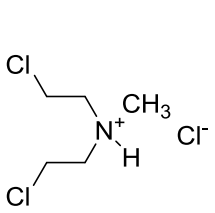

(5)

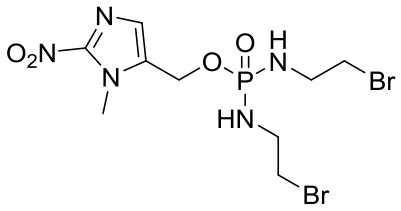

(6)

Figura 8 – Estrutura de compostos com propriedades antitumorais.

Diversos compostos fosforamidatos heterocíclicos (**7-17**) com atividade antibacteriana estão descritos na literatura (PRASAD *et al*., 2006; MADHAVA *et al*., 2012). Os compostos **7-15** são mais ativos sobre *Staphylococcus aureus*, *Bacillus subtilis*, *Escherichia coli*, *Pseudomonas aeruginosa*, *Salmonella typhimurium* e *Klebsiella pneumoniae* do que a Ciprofloxacina® (**18**), um antibiótico da classe das quinolonas (Figura 9) (PRASAD *et al*., 2006). Na mesma linha, os compostos difenilfosforamidatos **16** e **17** apresentaram-se duas vezes mais ativos sobre *Bacillus subtillis*, *Staphylococcus aureus*, *Pseudomonas aeruginosa* e *Escherichia coli*, quando comparados ao padrão comercial **18** (Figura 9) (MADHAVA *et al*., 2012).

Ar = C_6H_5
2-MeC_6H_4
4-$O_2NC_6H_4$
2-MeC_6H_4
4-ClC_6H_4
2-ClC_6H_4
2,4-$Cl_2C_6H_3$
4-BrC_6H_4
2,5-$Me_2C_6H_3$

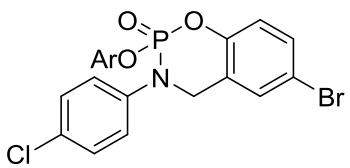

(7-15)

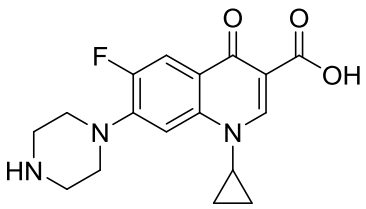

Ciprofloxacina (18)
(antibiótico)

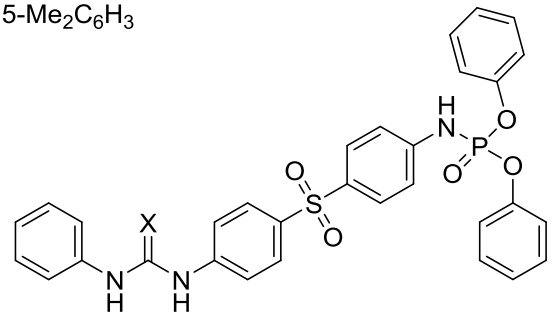

(16) X = S
(17) X = O

Figura 9 – Estrutura da Ciprofloxacina® e fosforamidatos com atividade antibacteriana.

Compostos fosforamidatos mostarda (Figura 10) apresentaram elevada atividade sobre *Trypanosoma brucei*, sendo que para **24** e **25** foram evidenciados valores de IC_{50} na ordem de namomolar (HU *et al*., 2011).

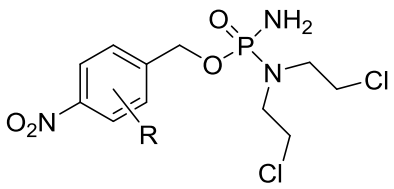

(19) R = H; IC_{50} = 3,4 μM
(20) R = 2-OCH_3; IC_{50} = 1,2 μM
(21) R = 2-CF_3; IC_{50} = 0,15 μM
(22) R = 2-F; IC_{50} = 0,27 μM
(23) R = 3-F; IC_{50} = 3,2 μM
(24) R = 2,6-diF; IC_{50} = 0,007 μM
(25) R = 2-Cl; IC_{50} = 0,008 μM

Figura 10 – Fosforamidatos mostarda com atividade sobre *T. brucei*.

Dicloridrato de hematoporfirina (**26**) é um fármaco com propriedades antitumorais comercializado com o nome Apiabasilon® usado como modelo para síntese de análogos. Ensaios *in vitro* realizados com células tumorais de fígado (BEL-7402) evidenciaram características positivas do análogo **27**. Este composto foi seletivo para as células cancerosas e apresentou valor de IC_{50} (8,41 μM) ligeiramente inferior ao de **26** (IC_{50} = 8,93 μM), usado como controle positivo (Figura 11) (WANG *et al.*, 2010).

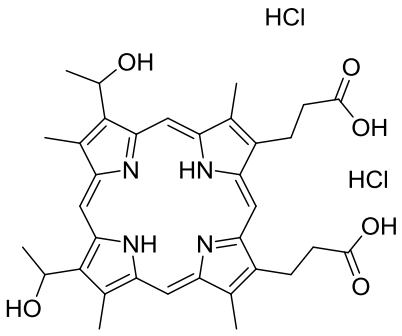

(26) IC_{50} = 8,93 μM

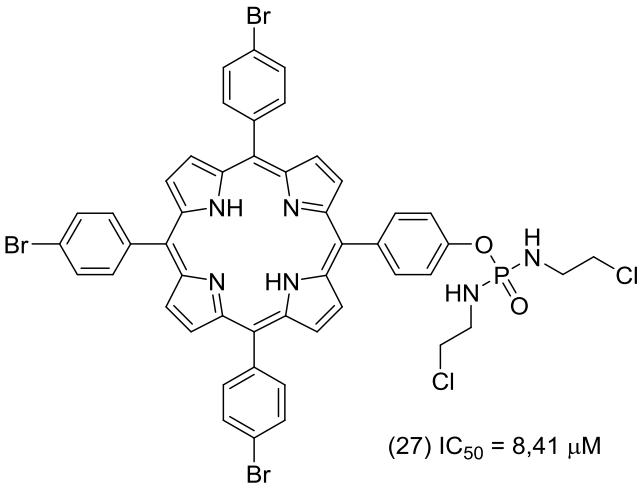

(27) IC_{50} = 8,41 μM

Figura 11 – Exemplos de compostos com atividade antitumoral.

Em estudos recentes pesquisadores têm efetuado a ligação de grupamentos fosforamidatos a nucleosídeos, uma estratégia conhecida como fosforamidato pró-nucleotídeo (do inglês “Phosphoramidate ProTide”) (MCGUIGAN *et al.*, 2005; MCGUIGAN *et al.*, 2009; DERUDAS *et al.*, 2009; DONGUI *et al.*, 2009; ROMAN *et al.*, 2011; SERPI *et al.*, 2012). Por meio dessa estratégia busca-se melhorar o potencial terapêutico de um protótipo. A

introdução desse grupamento favorece o processo de fosforilação *in vivo*, através de trifosfatos, convertendo esses nucleosídeos em suas formas ativas, denominada nucleotídeos. Esses análogos obtidos tem proporcionado significativo avanço no tratamento quimioterápico de câncer além de representarem os compostos de maior importância nos tratamentos antivirais. Nessa linha de pesquisa, a Brivudina (**28**) (Figura 12), um potente inibidor dos vírus herpes simplex tipo 1 (HSV-1) e varicela zoster (VZV), tem servido de modelo para o desenvolvimento de novos compostos. A introdução do grupamento fosforamidato levou à formação da Timectacina (**29**), desenvolvido pela New Biotics e que se encontra em fase de testes clínicos. Posteriormente, a substituição do grupamento metila na ligação éster de **29** por benzila forneceu o composto **30**, que potencializou a atividade em 175 vezes contra o câncer de cólon HT115 (Figura 12) (MCGUIGAN *et al.*, 2005).

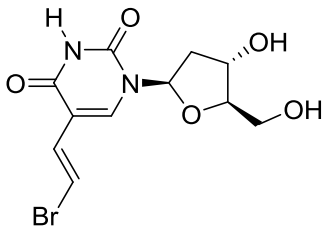

(28)

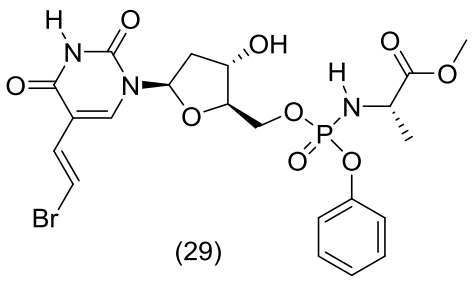

(29)

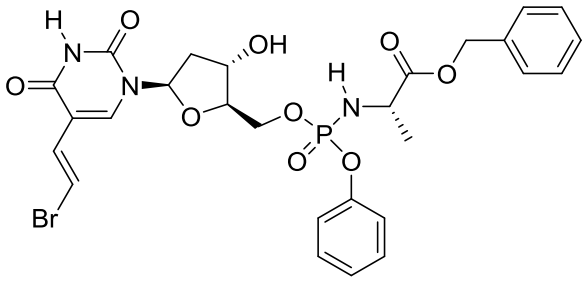

(30)

Figura 12 – Estrutura da Brivudina (**28**) e de seus derivados pró-nucleosídeos com atividade antitumoral.

Bons sistemas de liberação de fosfato foram obtidos a partir da síntese de derivados de 4´-azidocitidina (**31**). Os fosforamidatos derivados de **31** (**32-36**) foram eficientes na inibição do vírus de hepatite C, sendo obtido pro-nucleosídeo (**32**) até 3,4 vezes mais potente do que **31** (Figura 13).

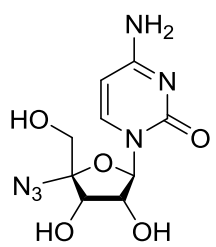

(31) EC_{50} = 1,28 μM

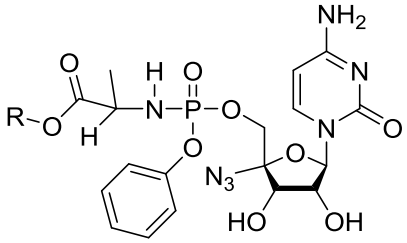

(32) R = Et; EC_{50} = 0,38 μM
(33) R = *i*Pr; EC_{50} = 0,99 μM
(34) R = nBu; EC_{50} = 0,94 μM
(35) R = 2-Bu; EC_{50} = 0,62 μM
(36) R = *t*-Bu; EC_{50} = 0,72 μM

Figura 13 – Estrutura de 4´-azidocitidina (**31**) e de pro-nucleosídeos com atividade anti-hepatite C.

O Aciclovir® (**37**) (também disponível comercialmente como Zovirax®), é um nucleosídeo análogo da purina, sintético, com atividade inibitória *in vitro* e *in vivo* contra os vírus do herpes humano, incluindo Herpes simplex (HSV), tipos 1 e 2, Varicella zoster, Epstein-Barr e Citomegalovirus (WAGSTAFF *et al.*, 1994). Esta substância é considerada inativa contra o vírus HSV deficiente de timidina quinase (EC_{50} = 50 μM). Pro-nucleosídeos obtidos a partir de **37** (**38-41**) foram até 35 vezes mais ativos (EC_{50} = 1,4 μM) sobre este vírus quando comparados ao material de partida (**37**) (Figura 14) (DERUDAS *et al.*, 2009).

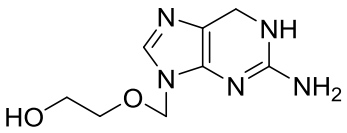

(37) EC_{50} = 50 μM

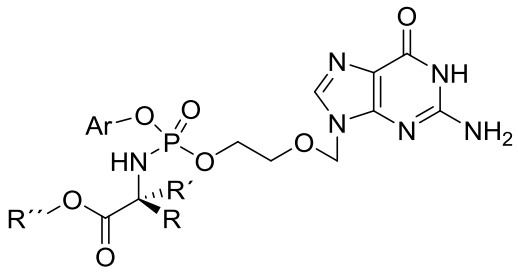

(38) Aril = *p*-F-Ph; AA = L-Ala; R´´ = Bn; EC_{50} = 1,5 μM
(39) Aril = Naftil; AA = DMG; R´´ = Bn; EC_{50} = 3,2 μM
(40) Aril = Ph; AA = L-Leu; R´´ = Bn; EC_{50} = 1,4 μM
(41) Aril = Ph; AA = L-Ile; R´´ = Bn; EC_{50} = 1,4 μM

Figura 14 – Estrutura do Aciclovir® (**37**) e dos pro-nucleosídeos (**38-41**) sintetizados por Derudas *et al*. (2009).

A atividade inseticida de compostos que contêm anéis heterocíclicos e ligações P-N é relatada na literatura (WARE, 2000; SANTOS *et al.*, 2007). Alguns exemplos de inseticidas fosforamidatos estão mostrados na Figura 15.

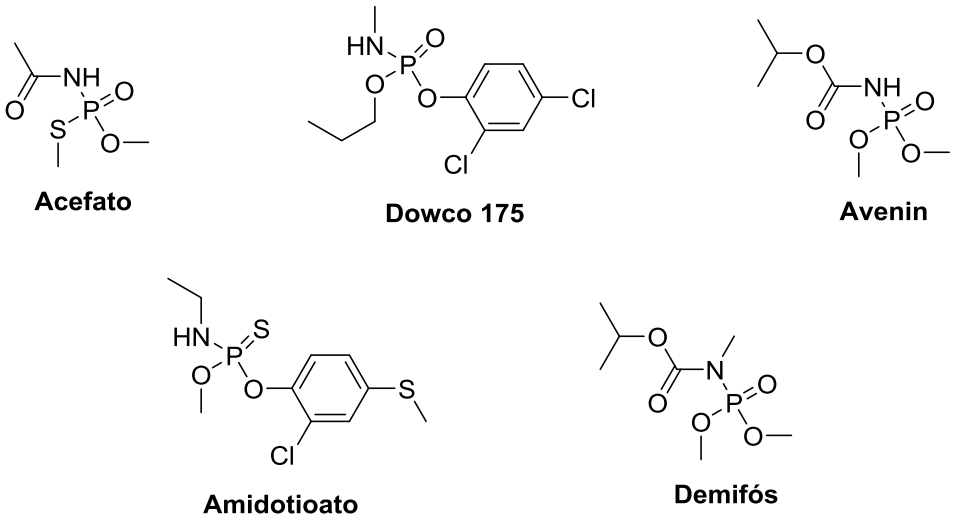

Figura 15 – Estruturas de compostos fosforamidatos com atividade inseticida.

PAULA *et al.* (2008) descreveram, recentemente, a síntese de alguns compostos da classe dos fosforamidatos. Os compostos **42**, **43** e **44** (Figura 16) apresentaram elevada atividade inseticida sobre *Ascia monuste orseis* (uma praga-chave de brássicas). Após 72h de exposição, causaram 90, 100 e 97,5% de mortalidade, respectivamente, a uma dose de 10 μg de composto/mg de inseto. Este resultado é comparado ao inseticida comercial metilcloropirifós, usado como controle positivo (100% de mortalidade).

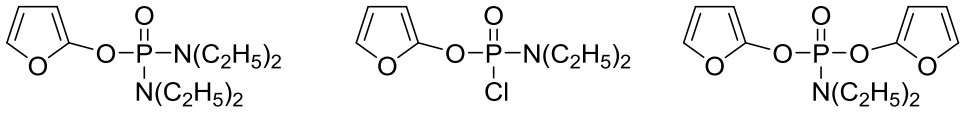

(42) (43) (44)

Figura 16 - Compostos organofosfatos com atividade inseticida descritos por PAULA *et al*. (2008).

Dando continuidade ao trabalho, OLIVEIRA *et al*. (2012) avaliaram mais detalhadamente a atividade biológica destes fosforamidatos e também sintetizaram outros compostos inéditos dessa classe. Entre os compostos avaliados, os compostos furan-2-il *N,N*-diisopropilamidoclorofosfato (**45**) e difuran-2-il piperidin-1-ilfosfonato (**46**) (Figura 17) apresentaram intervalo de mortalidade superior a 87,50% contra *A. monuste,* a uma dose de 1 μg de composto/mg de inseto, comparável com a de metilcloropirifós, utilizado como padrão de eficiência.

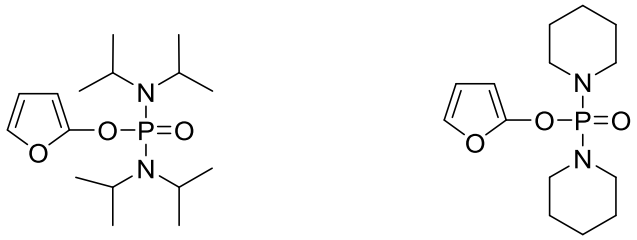

(45) (46)

Figura 17 - Compostos organofosfatos com atividade inseticida descritos por OLIVEIRA *et al*. (2012).

Em se tratando do setor agrícola, ainda, uma série de compostos fosforados heterocíclicos (**47**, **48** e **49**; Figura 18) foram sintetizados (KIRAN *et al*. 2007). Estes compostos tiveram a atividade biológica avaliada contra o fungo *Ustilago scitaminea*, responsável por perdas de até 100% em culturas de cana de açúcar. Além de secarem completamente a região tomada pelo fungo, os compostos ainda promovem o crescimento da planta, produzindo perfilhos laterais saudáveis na moita sem novas infecções. Este efeito secundário não foi observado para o padrão Bavistina (**50**) (comercialmente disponível como Carbendazim®), o que evidencia características positivas dos análogos descritos.

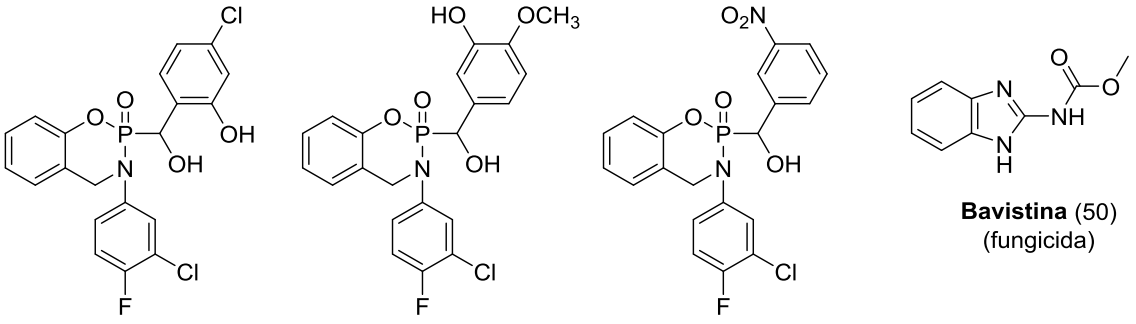

(47) (48) (49) **Bavistina** (50) (fungicida)

Figura 18 – Estrutura da Bavistina e dos compostos fosforados heterocíclicos com atividade contra o fungo *Ustilago scitaminea*.

Ainda neste contexto, vale destacar a atividade herbicida dos compostos Amiprofos-metílico (**51**) e Butamifos (**52**), disponíveis comercialmente. Estes compostos atuam inibindo a polimerização de microtúbulos em células vegetais, impedindo a formação de fusos cromáticos e induzindo a separação dos cromossomas metafásicos (MARA *et al*., 2011).

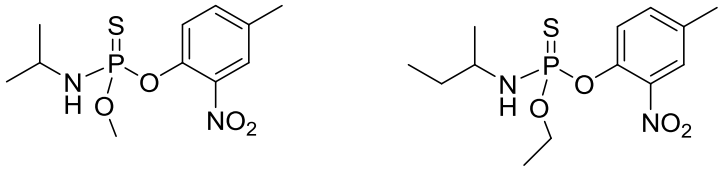

(51) (52)

Figura 19 – Estrutura dos herbicidas comerciais Amiprofos-metílico (**51**) e Butamifos (**52**).

Os compostos da classe dos fosforamidatos também vêm sendo explorados para a obtenção de retardadores de chama, substâncias que ajudam a retardar ou impedir a combustão. Por exemplo, o fosforamidato difenil piperazina-1,4-diil*bis*(metilfosfinato) (DPPMP, **53**) (Figura 20) foi sintetizado e testado como aditivo em policarbonato (PC), poli (tereftalato de butileno) (PBT), copolímeros de etileno-acetato de vinila (EVA) e acrilonitrilabutadieno-estireno (ABS) como agente retardador de chama (NGUYEN e KIM, 2008). A adição de DPPMP melhorou o efeito de retardamento de chama dos polímeros anteriormente citados de acordo com o estudo. Os polifosforamidatos PDMPD (**54**) e PDEPD (**55**) podem ser utilizados como retardadores de chama termicamente estáveis para plásticos ou materiais poliméricos, onde baixa inflamabilidade é necessária (Figura 20) (TAI *et al*., 2001).

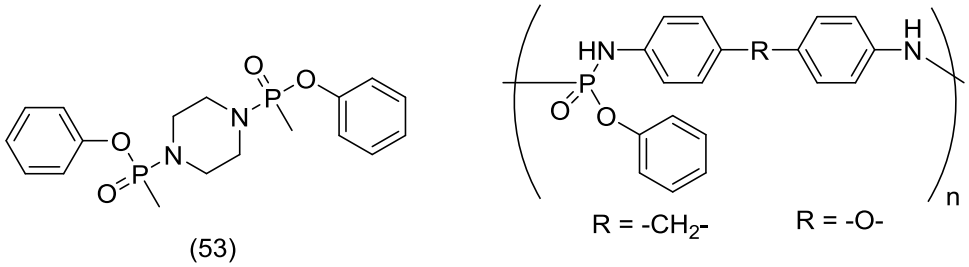

(53) (54) (55)

Figura 20 – Estruturas de substâncias da classe dos fosforamidatos com potencial efeito retardador de chama.

Os compostos **56** e **57** (Figura 21) foram aplicados como aditivos para lubrificantes em óleo e comparados com os aditivos lubrificantes comerciais dodecan-1-butil-7-amônio metiloctil fosfato (**58**) e dibutil-fosfonato (**59**) (Figura 21). Os resultados evidenciaram propriedades dos compostos contra desgaste, redutores de fricção, além de resistirem a pressões elevadas. Sugere-se que o

mecanismo de proteção é baseado na formação de uma película contendo fosfato e/ou polifosfato sobre a superfície esfregada (YAN *et al*., 2012).

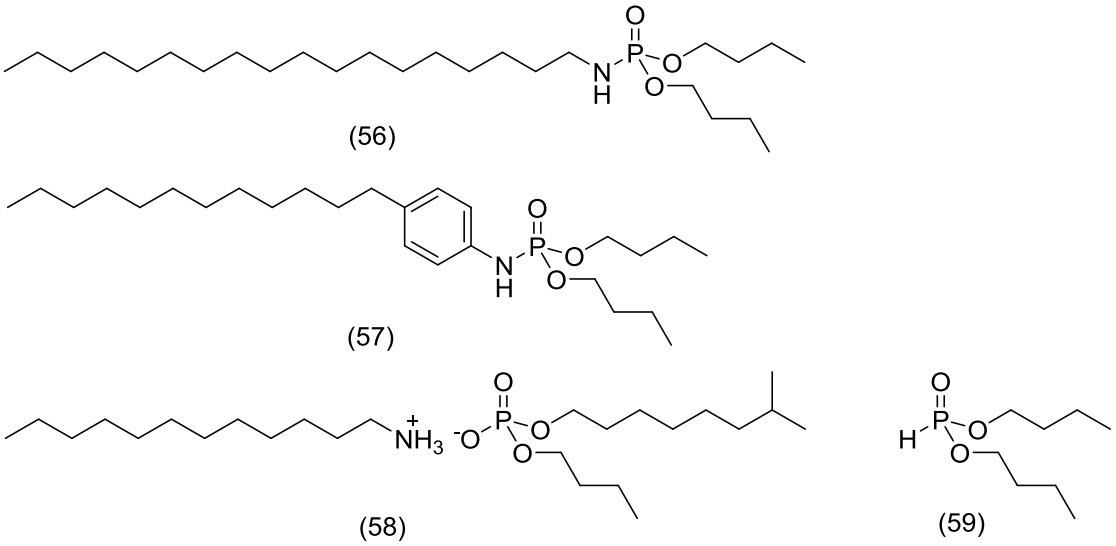

Figura 21 – Compostos fosforados aplicados como aditivos para lubrificantes em óleo.

1.3. Justificativa do Trabalho

Conforme discutido anteriormente, a literatura relata uma ampla versatilidade e aplicabilidade dos compostos organofosforados, seja aplicado à área agrícola, industrial ou medicinal. No Laboratório de Análise e Síntese de Agroquímicos (LASA), PAULA *et al*. (2008) e OLIVEIRA *et al*. (2012) sintetizaram compostos dessa classe que apresentaram elevada atividade inseticida (Figuras 16 e 17). Assim, buscou-se com esse trabalho a síntese de novos compostos que possam melhorar as condições de vida da sociedade e/ou dar uma contribuição científica no que diz respeito a essa classe de compostos.

Inicialmente pretendia-se manter anéis furânicos aos compostos, uma vez que muitos produtos naturais biologicamente ativos apresentam esse grupamento (LIU *et al*., 2006). Entretanto, o baixo rendimento das reações descritas por PAULA *et al*. (2008) e OLIVEIRA *et al*. (2012), bem como as excelentes atividades biológicas apresentadas por alguns compostos descritos na literatura apresentando o grupamento fenoxi ligado ao átomo de fósforo

motivaram a substituição do anel furânico por anéis fenólicos, conforme análise retrossintética mostrada no Esquema 1:

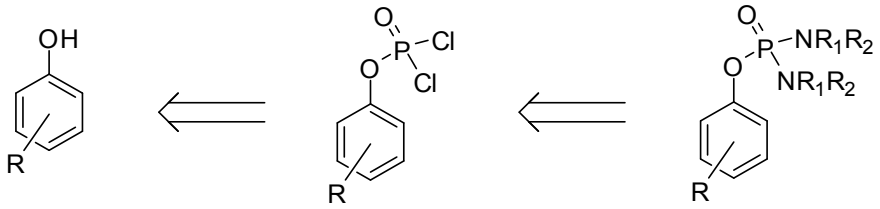

Esquema 1 – Análise retrossintética para obtenção dos fosforamidatos.

A presença de halogênios como substituintes no fenol em diversas posições é bastante interessante do ponto de vista biológico. Nos últimos 30 anos houve grande expansão do uso de halogênios em compostos utilizados como pesticida. A presença de mais de um tipo de halogênio tem sido importante para desempenho da atividade biológica (Figura 22). Além disso, diversos estudos vêm sendo realizados no intuito de entender a correlação da estrutura com a atividade biológica, propriedades físico-químicas dos compostos bem como susceptibilidade metabólica (JESCHKE, 2012).

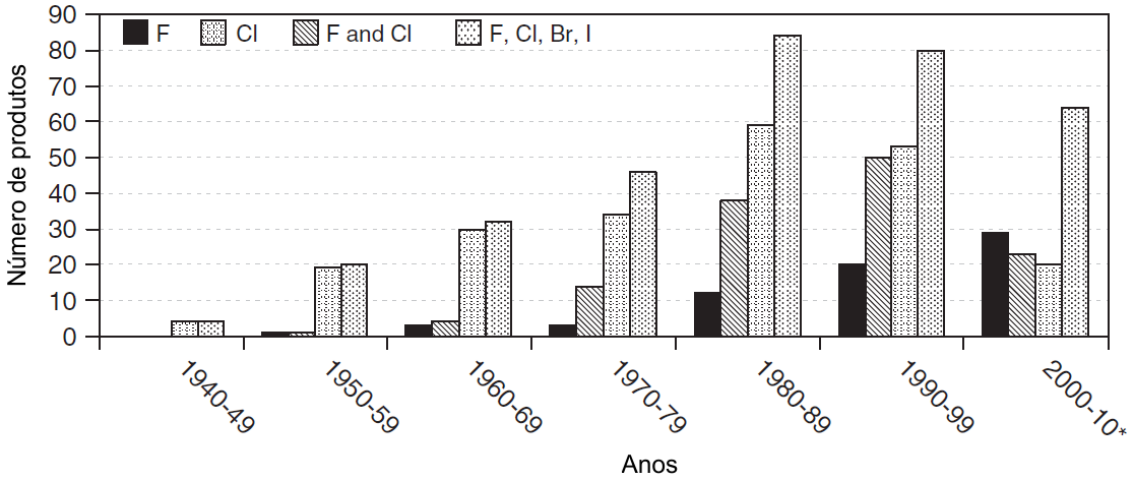

Figura 22 – Evolução mundial da síntese de compostos halogenados no período de 1940-2010 (extraído de JESCHKE, 2012).

1.4. Referências Bibliográficas

AMTUL, Z.; RAHMAN, A.; SIDDIQUI, R.A.; CHOUDHARY, M.I. Chemistry and mechanism of urease inhibition, *Current Medicinal Chemistry*, v. 9, p. 1323-1348, 2002.

ANVISA (2009). Agência Nacional de Vigilância Sanitária. Disponível em: <http://www.anvisa.gov.br>. Acesso em: 23 de março de 2013.

BENHAMOU, Y.; FLEURY, H.; TRIMOULET, P.; PELLEGRIN, I.; URBINELLI, R.; KATLAMA, C.; ROZENBAUM, W.; TEUFF, G.L.; TRYLESINSKI, A.; PIKETTY, C. Anti-hepatitis B virus efficacy of tenofovir disoproxil fumarate in HIV-infected patients. *Hepatology*, v. 43, p. 548-555, 2006.

BORGES, V.C.; FERRINI, M.T.; CAMPOS, F.G; WAITSZERG, D.L.; OLIVEIRA, G.P.C.; BOTTONI, A. Minerais. *In* Nutrição oral, enteral e parenteral na prática clínica. 3.ed. São Paulo: Editora Atheneu, 2004. 117p.

CARNEIRO, F.F.; PIGNATI, W.; RIGOTTO, R.M.; AUGUSTO, L.G.S.; RIZZOLO, A.; FARIA, N.M.X.; ALEXANDRE, V.P.; FRIEDRICH, K.; MELLO, M. S.C. Dossiê ABRASCO – Um alerta sobre os impactos dos agrotóxicos na saúde. Parte 1 - Agrotóxicos, Segurança Alimentar e Nutricional e Saúde. Rio de Janeiro: ABRASCO, 2012.

CHO, A.; ZHANG, L.; XU, J.; LEE, R., BUTLER, T.; METOBO, S.; AKTOUDIANAKIS, V.; LEW, W.; YE, H.; CLARKE, M.; DOERFFLER, E.; BYUN, D.; WANG, T.; BABUSIS, D.; CAREY, A.C.; GERMAN, P.; SAUER, D.; ZHONG, W.; ROSSI, S.; FENAUX, M.;. MCHUTCHISON, J.G., PERRY, J., FENG, J., RAY, A.S., KIM, C.U. Discovery of the First C-Nucleoside HCV Polymerase Inhibitor (GS-6620) with Demonstrated Antiviral Response in HCV Infected Patients. *Journal of Medicinal Chemistry*, v.57, p.1812-1825, 2014.

DERUDAS, M.; CARTA, D.; BRANCALE, A.; VANPOUILLE, C.; LISCO, A.; MARGOLIS, L.; BALZARINI, J.; MCGUIGAN, C. The application of phosphoramidate protide technology to acyclovir confers anti-HIV inhibition. *Journal of Medicinal Chemistry*, v. 52, p. 5520-5530, 2009.

DONGHI, M.; ATTENNI, B.; GARDELLI, C.; MARCO, A. D.; FIORE, F.; GIULIANO, C.; LAUFER, R.; LEONE, J. F.; PUCCI, V.; ROWLEY, M.; NARJES, F. Synthesis and evaluation of novel phosphoramidate prodrugs of 2'-methyl cytidine as inhibitors of hepatitis C virus NS5B polymerase. *Bioorganic & Medicinal Chemistry Letters*, v. 19, p. 1392-1395, 2009.

DUAN, J.; JIAO, H.; KAIZERMAN, J.; STANTON, T.; EVANS, J.W.; LAN, L.; LORENTE, G.; BANICA, M.; JUNG, D.; WANG, J.; MA, H.; LI, X.; YANG, Z.; HOFFMAN, R.M.; AMMONS, W.S.; HART, C.P.; MATTEUCCI, M. Potent and highly selective hypoxia-activated achiral phosphoramidate mustards as anticancer drugs. *Journal of Medicinal Chemistry*, v. 51, p. 2412-2420, 2008.

DUKE, S.O.; POWLES, S.B. Glyphosate: a once-in-a-century herbicide. *Pest Management Science*, v. 64, p. 319-325, 2008.

GUYEN, C.; KIM, J. Synthesis of a novel nitrogen-phosphorus flame retardant based on phosphoramidate and its application to PC, PBT, EVA, and ABS. *Macromolecular Research*, v. 16, p. 620-625, 2008.

HU, L.; WU, X.; HAN, J.; CHEN, L.; VASS, S.O.; BROWNE, P.; HALL, B.S.; BOT, C.; GOBALAKRISHNAPILLAI, V.; SEARLE, P.F.; KNOX, R.J.; WILKINSON, S.R. Synthesis and structure–activity relationships of nitrobenzyl phosphoramide mustards as nitroreductase-activated prodrugs. *Bioorganic & Medicinal Chemistry Letters*, v. 21, p. 3986–3991, 2011.

JESCHKE, P. The Unique Role of Halogen Substituents in the Design of Modern Crop Protection Compounds, in Modern Methods in Crop Protection Research (eds P. Jeschke, W. Krämer, U. Schirmer and M. Witschel), Wiley-VCH Verlag GmbH & Co. KGaA, p.73-128, Weinheim, Germany. doi: 10.1002/9783527655908.ch4., 2012.

JOMAA, H.; WIESNER, J.; SANDERBRAND, S.; ALTINCICEK, B.; WEIDEMEYER, C.; HINTZ, M.; TURBACHOVA, I.; EBERL, M.; ZEIDLER, J.; LICHTENTHALER, H.K.; SOLDATI, D.; BECK, E. Inhibitors of the

nonmevalonate pathway of isoprenoid biosynthesis as antimalarial drugs. *Science*, v. 285, p.1573-1576, 1999.

KARIM, Q.A.; KARIM, S.S.A; FROHLICH, J.A.; GROBLER, A.C.; BAXTER, C.; MANSOOR,L.E.; KHARSANY, A.B.M; SIBEKO, S.; MLISANA,K.P.; OMAR,Z.; GENGIAH,T.N.; MAARSCHALK,S.; ARULAPPAN, N.; MLOTSHWA, M.; MORRIS, L.; TAYLOR, D. Effectiveness and safety of tenofovir gel, an antiretroviral microbicide, for the prevention of hiv infection in women. *Science*, v. 329, p. 1168-1174, 2010.

KIRAN, Y.B.; REDDY, P.V.; REDDY, C.D. [3-(3-chloro-4-fluorophenyl)-2-oxo-3,4-dihydro-2H-2λ^5-benzo[*e*][1,3,2]oxazaphosphinin-2-yl]-(aryl/alkyl) methanols and their bioactivity on sugarcane smut. *Journal of Agricultural and Food Chemistry*, v.55, p.6933-6939, 2007.

LIU, Y.; ZHANG, S.; ABREU, P.J.M. Heterocyclic terpenes: linear furano- and pyrroloterpenoids. *Natural Product Reports*, v. 23, p. 630-651, 2006.

MADHAVA, G.; SUBBAIAH, K.V.; SREENIVASULU, R.; RAJU, C.N. Synthesis of novel urea and thiourea derivatives of diphenylphosphoramidate and their antimicrobial activity. *Der Pharmacia Lettre*, v. 4, p. 1194-1201, 2012.

MARA, C.; DEMPSEY, E.; BELL, A.; BARLOW, J.W. Synthesis and evaluation of phosphoramidate and phosphorothioamidate analogues of amiprophos methyl as potential antimalarial agents. *Bioorganic & Medicinal Chemistry Letters*, v. 21, p. 6180–6183, 2011.

MC DOWELL, L R. Minerals in Animal and Human Nutrition. Ed. L.R. McDowell. Academic Press. p. 27-77. New York, 1992.

MCGUIGAN, C.; THIERY, J.; DAVERIO, F.; JIANG, W.G.; DAVIES, G.; MASON, M. Anti-cancer ProTides: tuning the activity of BVDU phosphoramidates related to thymectacin. *Bioorganic & Medicinal Chemistry*, v. 13, p. 3219–3227, 2005.

MCGUIGAN, C.; KELLEHE, M.R.; PERRONE, P.; MULREADY, S.; LUONI, G.; DAVERIO, F.; RAJYAGURU, S.; POGAM, S.L.; NAJERA, I.; MARTIN, J.A.; KLUMPP, K.; SMITH, D.B. The application of phosphoramidate ProTide technology to the potent anti-HCV compound 4´-azidocytidine (R1479). *Bioorganic & Medicinal Chemistry Letters*, v.19, p.4250–4254, 2009.

MINISTÉRIO DA SAÚDE. Departamento de DST, Aids e Hepatites Virais. Disponível em: <http://www.aids.gov.br>. Acesso em: 23 de março de 2013.

MONTALVETTI, A.; BAILEY, B.N.; MARTIN, M.B.; SEVERIN, G.W.; OLDFIELD, E.; DOCAMPO, R. Bisphosphonates are potent inhibitors of *trypanosoma cruzi* farnesyl pyrophosphate synthase. *The Journal of Biological Chemistry*, v. 276, p. 33930–33937, 2001.

NGUYEN, C.; KIM, J. Synthesis of a novel nitrogen-phosphorus flame retardant based on phosphoramidate and its application to PC, PBT, EVA, and ABS. *Macromolecular Research*, v. 16, p. 620-625, 2008.

OLIVEIRA, F.M.; BARBOSA, L.C.A.; TEIXEIRA, R.R.; DEMUNER, A.J.; MALTHA, C.R.A.; PICANÇO, M.C.; SILVA, G.A.; PAULA, V.F. Synthesis and insecticidal activity of new phosphoramidates. *Journal of Pesticide Science*, v. 37, p. 85-88, 2012.

PAULA, V.F.; BARBOSA, L.C.A.; TEIXEIRA, R.R.; PICANÇO, M.C.; SILVA, G.A. Synthesis and insecticidal activity of new 3-benzylfuran-2-yl *N,N,N´,N´*-tetraethyldiamidophosphate derivatives. *Pest Management Science*, v. 64, p. 863–872, 2008.

PRASAD, G.S.; BABU, B.H.; REDDY, K.R.K.K.; HARANATH, P.R.; REDDY, C.S.; Synthesis and antibacterial activity of new 2-aryloxy-6-bromo-3-(4-chlorophenyl)-3,4-dihydrobenzo[e][1,3,2]oxazaphosphinine-2-oxides.*ARKIVOC*, v.xiii, p.165-170, 2006.

REICHENBERG, A.; WIESNER, J.; WEIDEMEYER, C.; DREISEIDLER, E.; SANDERBRAND, S.; ALTINCICEK, B.; BECK, E.; SCHLITZERC, M.; JOMA, H.

Diaryl ester prodrugs of FR900098 with improved *in vivo* antimalarial activity, *Bioorganic & Medicinal Chemistry Letters*, v. 11, p. 833–835, 2001.

ROMAN, C.R.; WASSERTHAL, P. BALZARINI, J.; MEIER, C. Diastereoselective synthesis of (aryloxy)phosphoramidate prodrugs. *European Journal of Organic Chemistry*, p. 4899–4909, 2011.

SANTOS, V.M.R.; DONNICI, C.L.; DACOSTA, J.B.N.; CAIXEIRO, J.M.R. Compostos organofosfatos pentavalentes: histórico, métodos sintéticos de preparação e aplicações como inseticidas e agentes antitumorais. *Química Nova*, v. 30, p. 159-170, 2007.

SERPI, M.; BIBBO, R.; RAT, S.; ROBERTS, H.; HUGHES, C.; CATERSON, B.; ALCARAZ, M. J.; GIBERT, A. T.; VERSON, C. R. A.; MCGUIGAN, C. Novel phosphoramidate prodrugs of n-acetyl-(D)-glucosamine with antidegenerative activity on bovine and human cartilage explants. *Journal of Medicinal Chemistry*, v. 55, p. 4629-4639, 2012.

SUN, D.; YANG, C.; MING, W.; SUN, L.; ZHANG, L.; ZHANG, Q.; CHAI, Y.; Preparation and activity study of new organophosphate insecticide candidates. *Journal of Pesticide Science*, v. 36, p. 44–47, 2011.

SUN, Q.; LIA, R.; GUO, W.; CUI, J.; CHENGA, T.; GE, Z. Novel class of cyclophosphamide prodrug: cyclophosphamide spiropiperaziniums (CPSP). *Bioorganic & Medicinal Chemistry Letters*, v. 16, p. 3727-3730, 2006.

SZAJNMAN, S.H.; BAILEY, B.N.; DOCAMPO, R.; RODRIGUEZ, J.B. Bisphosphonates derived from fatty acids are potent growth inhibitors of *Trypanosoma cruzi*. *Bioorganic & Medicinal Chemistry Letters*, v. 11, p. 789-192, 2001.

TAI, Q.; HU, Y.; YUEN, R.K.K.; SONG, L.; LU, H. Synthesis, structure–property relationships of polyphosphoramides with high char residues. *Journal of Materials Chemistry*, v. 21, p. 6621–6627, 2011.

UPADHYAY, L.S.B. Urease inhibitors: A review. *Indian Journal of Biotechnology*, v. 11, p. 381-388, 2012.

URBINA, J.A.; DOCAMPO, R. Specific chemotherapy of chagas disease: controversies and advances. *Trends in Parasitology*, v. 19, p. 495-501, 2003.

URBINA, J.A.; MORENO, B.; VIERKOTTER, S.; OLDFIELD, E.; PAYARES, G.; SANOJA, C.; BAILEY, B.N.; YAN, W.; SCOTT, D.A.; MORENO, S.N.J.; DOCAMPO, R. *Trypanosoma cruzi* contains major pyrophosphate stores, and its growth *in vitro* and *in vivo* is blocked by pyrophosphate analogs. *The Journal of Biological Chemistry*, v. 274, p. 33609-33615, 1999.

WAGSTAFF, A.J.; FAULDS, D.; GOA, K.L. Aciclovir. A Reappraisal of its Antiviral Activity, Pharmacokinetic properties and therapeutic efficacy. *Drugs*, v. 47, p. 153-205, 1994.

WANG, Z.; GUO, C.; XIE, W.; LIU, C.; XIAO, C.; TAN, Z.; Novel phosphoramidates with porphine and nitrogenous drug: one-pot synthesis and orientation to cancer cells. *European Journal of Medicinal Chemistry*, v. 45, p. 890–895, 2010.

WARE, G.W. The pesticide book. Fresno: Thomson Publications, 2000, 418p.

WESTHEIMER, F. H. Why Nature Chose Phosphates. *Science*, v. 235, p. 1173-1178, 1987.

WILSON, R.H. Novel therapeutic developments other than EGFR and VEGF inhibition in colorectal cancer. *The Oncologist*, v. 11, p. 1018-1024, 2006.

XU, G.; XIE, Y.; WU, X. A facile and direct synthesis of alendronate from pyrrolidone. *Organic Preparations and Procedures International: The New Journal for Organic Synthesis*, v. 36, p. 185-187, 2004.

YAN, J.; BU, J.; BAI, X.; LI, J.; REN, T.; ZHAO, Y. The tribological study of novel phosphorous–nitrogen type phosphoramidate additives in rapeseed oil. *Journal of Engineering Tribology*, v. 226, p. 377-388, 2012.

CAPÍTULO 2

2. SÍNTESE E CARACTERIZAÇÃO DE FOSFORAMIDATOS

2.1. Introdução

Os primeiros estudos na química orgânica do fósforo foram realizados em 1820 por Jean Lassaigne quando esterificou o ácido fosfórico empregando álcool etílico. Em meados do século XX, Michaelis deu grande contribuição no desenvolvimento na química dos compostos organofosforados, explorando a nucleofilicidade do elemento. Dentre os diversos trabalhos conduzidos por Michaelis, vale destacar a contribuição para a química de compostos contendo a ligação P-N, entre os quais se encontram os fosforamidatos (MCMURRAY *et al.*, 2001; SANTOS *et al.*, 2007).

Características como polarizabilidade do elemento, baixa a média eletronegatividade e variável número de coordenação favorecem a diversidade de compostos sintetizados. As diferentes atividades biológicas dos organofosforados estão relacionadas, evidentemente, com características estruturais, tais como o tipo de heteroátomo ou grupo funcional ligado ao átomo de fósforo e seu estado de oxidação. Os fosforamidatos, conforme discutido no primeiro capítulo, são largamente usados para fins industriais e exibem uma grande diversidade de atividades biológicas, dentre as quais destacamos a antiviral, antitumoral, antibacteriana, antimalárico, antiprotozoários e inibidores das enzimas urease, acetil e butirilcolinesterase (SANTOS *et al.*, 2007).

A ligação P-N, característica dessa classe de compostos, é geralmente obtida através de reações de cloretos de fósforo (PCl_3) ou compostos trivalentes de fósforo com diferentes aminas (SANTOS *et al.*, 2007) (Esquema 1).

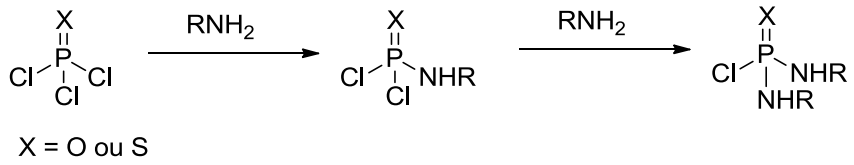

Esquema 1 – Representação geral da reação de cloretos de fósforo com aminas.

Em 1945, compostos fosforamidatos passaram a ser obtidos a partir de fosfonatos clorados, obtidos como intermediários de reação em meio anidro (ATHERTON *et al*., 1945) (Esquema 2)

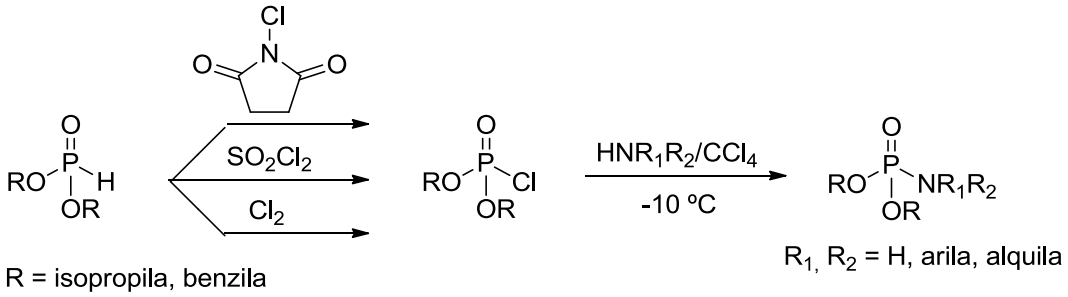

Esquema 2 – Obtenção de fosforamidatos a partir de fosfonato de dialquila.

Rendimentos igualmente satisfatórios foram obtidos empregando-se fosfonatos de dialquila em reação com aminas e tetracloreto de carbono em meio básico (SANTOS *et al*., 2007; ATHERTON *et al*., 1945). Essa metodologia sintética ficou conhecida como reação de Atherton-Todd e se mostrou efetiva na obtenção de fosforamidatos (Esquema 3), com geração da espécie P(O)-Cl *in situ*. Este procedimento é vantajoso na medida em que ocorre em uma única etapa, há grande diversidade de compostos P-H disponíveis comercialmente e não há necessidade de uma etapa posterior de oxidação (WAGNER *et al*., 2012).

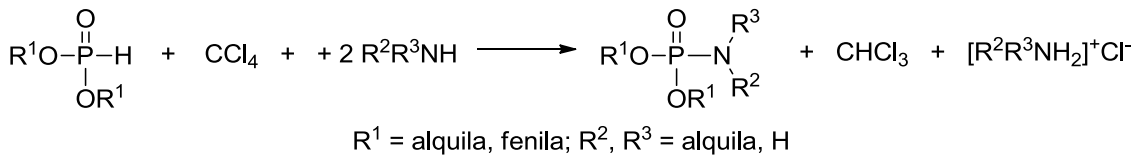

Esquema 3 – Reação geral descrita por Atherton e Todd para obtenção de fosforamidatos.

Por meio desta metodologia sintética, o fosfonato de dialquila encontra-se em equilíbrio com a sua forma fosfito (Esquema 4). O hidrogênio ácido desta espécie é removido por meio de reação ácido-base em meio aquoso e ocorre um ataque nucleofílico do fósforo do intermediário gerado ao tetracloreto de carbono. Na sequencia, há o ataque nucleofílico da amina ao átomo de fósforo resultando no correspondente fosforamidato. O mecanismo, proposto na década de 40, está representado no esquema 4 (ATHERTON *et al*., 1945).

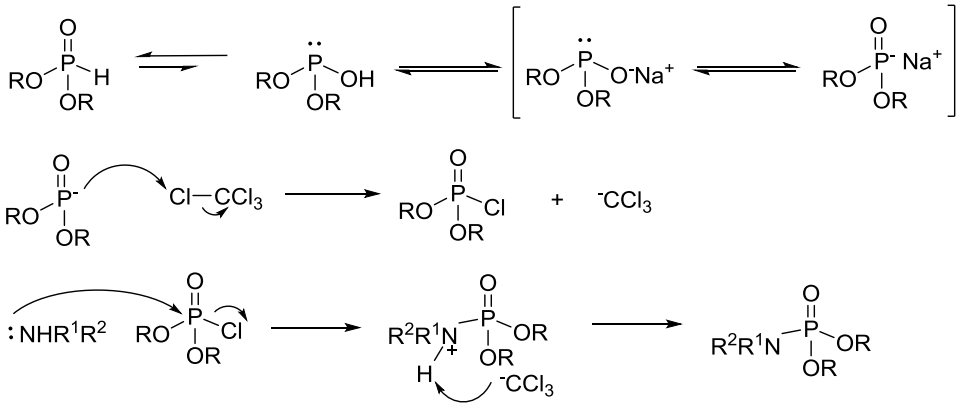

Esquema 4 - Mecanismo proposto por Atherton e Todd para obtenção de fosforamidato a partir de fosfonato.

Contudo, GEORGIEV *et al*. (1993) realizaram cálculos *ab initio* e propuseram um mecanismo diferente para a etapa inicial do mecanismo das reações de Atherton e Todd com aminas. Pela proposta, há formação do sal de fosfônio a partir da reação da amina com o fosfonato, a qual atua como base. Na sequencia, há desprotonação do fosfonato e é gerado o ânion fosfito e o monoéster fosfonato. Ocorre um ataque nucleofílico do fósforo negativo da espécie fosfito ao cloro do tetracloreto de carbono, formando assim o intermediário fosforoclorado. Por fim, o ânion triclorometanídeo reage com o monoéster fosfonato gerado na etapa anterior formando mais uma vez o sal de fosfônio, conforme esquema 5.

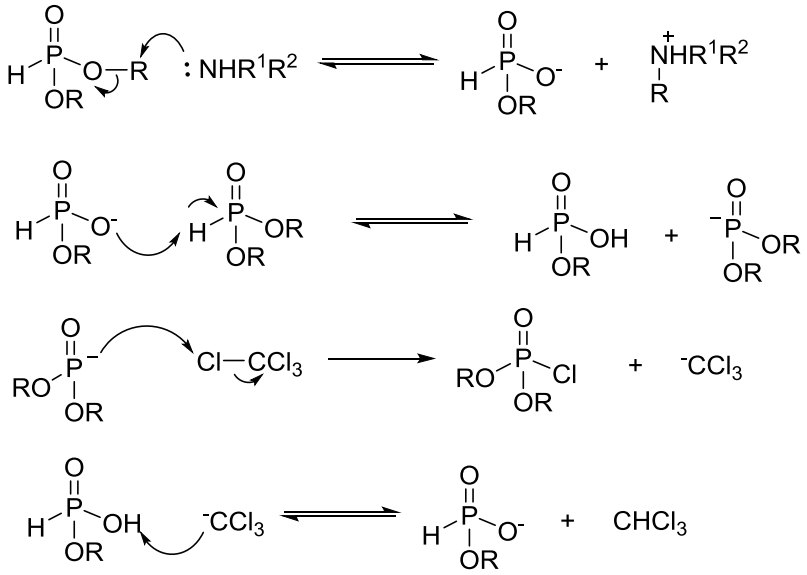

Esquema 5 - Mecanismo proposto por Georgiev *et al*. (1993) para reação de Atherton e Todd.

Outra forma de se obter compostos fosforamidatos é a partir de cloreto de fosforila ($POCl_3$), que foi primeiramente reportado em 1946 por Charles Wurtz. Uma grande variedade estrutural de compostos fosforados é possível de ser obtida, uma vez que $POCl_3$ reage com álcoois, fenóis e aminas (MCMURRAY *et al*., 2001). Diversos compostos com promissora atividade biológica vem sendo sintetizados a partir do $POCl_3$, conforme se observa na Figura 1 (MCGUIGAN, *et al*., 2009; DERUDAS *et al*., 2009; RUDA *et al*., 2010; WANG *et al*., 2010). Diante dos bons resultados descritos na literatura, a metodologia empregando-se $POCl_3$ foi usada neste trabalho.

Nesse capítulo descreve-se, portanto, a síntese e a caracterização estrutural de uma série de fosforamidatos. Essas substâncias foram preparadas com vistas à avaliação de suas atividades fitotóxica e inibitória de urease.

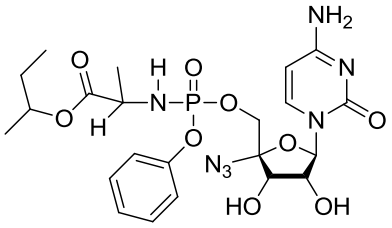

Inibidor do HCV
(MCGUIGAN *et al*., 2009)

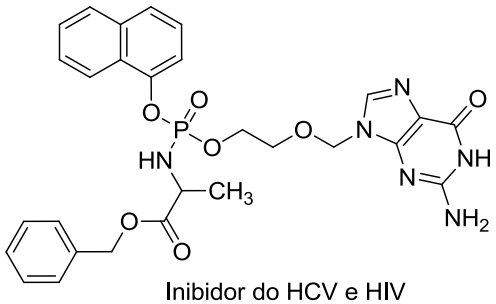

Inibidor do HCV e HIV
(DERUDAS *et al*., 2010)

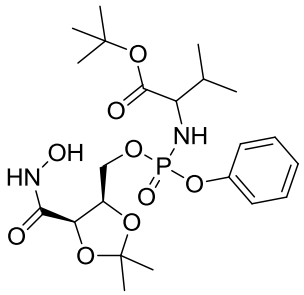

Inibidor de *Trypanosoma brucei*
(RUDA *et al*., 2010)

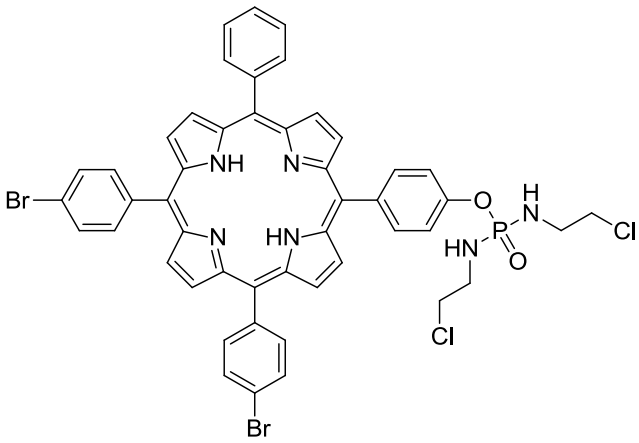

Antitumoral
(WANG *et al*., 2010)

Figura 1 – Exemplos de compostos fosforamidatos obtidos a partir do $POCl_3$.

2.2. Material e Métodos

2.2.1. Generalidades Metodológicas

Os solventes utilizados nas reações foram de grau P.A., devidamente secos. De modo geral, foram secos por refluxo sobre um agente secante, destilados e armazenados sobre peneira molecular, sendo mantidos sob atmosfera de nitrogênio, de acordo com os procedimentos descritos por PERRIN e ARMAREGO (1994).

As análises por CCD foram realizadas empregando-se placas cromatográficas de sílica-gel impregnadas sobre alumínio (espessura de 250 μm). Os solventes utilizados como eluente foram previamente destilados.

As placas CCD foram reveladas com solução alcoólica de ácido fosfomolíbdico (12 g de $2H_3PO_4.20MoO_3.H_2O$/250 mL de etanol) e, ou, solução

aquosa de $KMnO_4$ (3 g de $KMnO_4$, 20 g de K_2CO_3, 5 mL de NaOH 5%/300 mL de água) (CASEY *et al*., 1990), após terem sido observadas sob lâmpada ultravioleta (λ = 254 e 365 nm).

As separações cromatográficas em coluna foram feitas utilizando-se sílica-gel (70-230 mesh ou 230-400 mesh) como fase estacionária.

As temperaturas de fusão foram determinadas em aparelho MQAPF-301 e não foram corrigidas.

Os espectros no infravermelho foram obtidos por meio de um detector de reflectância difusa acentuada (PIKE GLADATR), em espectrofotômetro FT-IR-VARIAN 660 (Departamento de Química-UFV)

Os espectros de ressonância magnética nuclear de hidrogênio (RMN de ^1H, 300 MHz) e de carbono (RMN de ^{13}C, 75 MHz) foram obtidos em espectrômetros VARIAN MERCURY 300 (Departamento de Química – UFV). Utilizou-se como solvente clorofórmio deuterado ($CDCl_3$) ou dimetilsulfóxido deuterado (DMSO). Como padrão de referência interna utilizou-se o cloreto de tetrametilsilano (δ_H 0). As constantes de acoplamento escalar (*J*) foram expressas em Hertz (Hz).

Os espectros de massas, por impacto eletrônico, foram registrados em equipamento CG-EM SHIMADZU GCMS-QP5050A.

Nas purificações por recristalização utilizaram-se os métodos convencional, descrito por SHRINER *et al*. (1980), e por pares de solventes, descrito por GONÇALVES *et al*. (1988). Por este método, solubiliza-se o composto em um solvente no qual ele seja solúvel a frio, adicionando-se a seguir, a quente, um outro no qual ele seja muito pouco solúvel. A mistura é então resfriada até a recristalização e, por filtração ou decantação, separam-se os cristais da água-mãe.

2.2.2. Procedimentos sintéticos

2.2.2.1. Furan-2(*5H*)-ona (**60**)

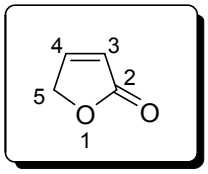

A um balão bitubulado de 500 mL, adaptado a um condensador e a um funil de adição, adicionaram-se 33,0 g (343 mmol) de 2-furaldeído (furfural), previamente purificado conforme descrito por PERRIN e ARMAREGO (1994), juntamente com 140 mL de DCM. A adição de 14,7 g de sulfato de sódio foi seguida, imediatamente, da adição de 10,30 g (0,091 mol) de *N,N*-dietiletanolamina. Em seguida, 31,60 g de ácido fórmico foram adicionados à mistura, cuidadosamente, por dois minutos. Após esse tempo, 6,90 mL de peróxido de hidrogênio 30% v/v foram adicionados à mistura, que foi então vigorosamente agitada, e 55 mL de peróxido de hidrogênio 30% v/v foram adicionados gota a gota por cinco horas. Ao final da adição, a mistura foi mantida sob agitação e refluxo por 18 horas. A fase orgânica foi separada e a fase aquosa, extraída com DCM (3 x 15 mL). Os extratos orgânicos foram combinados, e a fase orgânica resultante foi lavada com solução saturada de tiossulfato de sódio (2 x 10 mL). Em seguida, a fase orgânica foi seca com $MgSO_4$ e filtrada. A fase orgânica resultante desse procedimento foi testada para verificar a possível presença de peróxido de hidrogênio. Dois tubos de ensaio foram empregados na realização do teste. Em cada tubo adicionaram-se 5,0 mL de solução de sulfato ferroso amoniacal (1% m/v), 0,50 mL de solução de H_2SO_4 (0,5 mol L^{-1}) e 0,5 mL de uma solução aquosa 0,1 mol L^{-1} de tiocianato de potássio. A um dos tubos adicionaram-se 5 mL de fase orgânica. Este tubo foi agitado vigorosamente. A ausência de peróxido foi evidenciada pelo não aparecimento de uma coloração marrom-avermelhada. Após a realização do teste, a fase orgânica foi concentrada sob pressão reduzida e o líquido amarelado resultante foi fracionado em coluna de sílica-gel eluída com hexano-EtOAc 1:1 v/v. Esse procedimento resultou na obtenção de 14,04 g (0,167 mol) da lactona **60** com 49% de rendimento.

Os dados espectroscópicos obtidos da lactona **60** foram consistentes com os descritos na literatura (TEIXEIRA, 2008).

2.2.2.2. furan-2-il *N,N,N',N'*-tetraetildiamido fosfato (**42**)

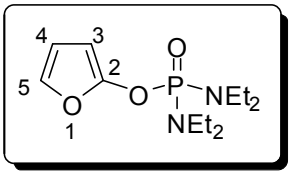

Primeira abordagem sintética - A um balão de fundo redondo bitubulado (25 mL), conectado a um tubo de cloreto de cálcio, adicionaram-se a lactona furan-2(*5H*)-ona (2,0 g; 23,8 mmol) e 5,0 mL de DCM anidro. Em seguida, cloreto de fosforila ($POCl_3$) (2,2 mL; 24 mmol) foi adicionado à mistura de uma só vez. Trietilamina (4,8 mL; 36 mmol) dissolvida em 4,0 mL de DCM anidro foi adicionada à mistura reagente, gota a gota, ao longo de um período de uma hora. Após essa adição, a mistura resultante foi agitada por 18 horas. Decorrido esse período, adicionou-se mais 0,80 mL (6,0 mmol) de trietilamina. Agitou-se a mistura por mais 24 horas. O solvente foi, então, removido em um evaporador rotatório. Ao resíduo resultante adicionaram-se, cuidadosamente, 12 mL de éter dietílico anidro seguido de 6,0 mL de pentano. O frasco foi selado e a mistura foi agitada por dois minutos à temperatura ambiente. O precipitado formado foi removido por filtração a vácuo. O filtrado foi imediatamente lavado com 6,0 mL de éter dietílico e 12 mL de pentano. O frasco contendo o filtrado foi hermeticamente fechado e a mistura foi mantida em um refrigerador por 12 horas. Após esse tempo, a solução sobrenadante foi transferida para um balão tritubulado de 100 mL. O solvente foi cuidadosamente removido sob pressão reduzida. O material resultante não foi purificado. Adicionaram-se 10 mL de éter dietílico anidro a esse material. Ao balão tritubulado adaptou-se um tubo de cloreto de cálcio e um funil de adição. O balão contendo a mistura reagente foi resfriado em uma mistura de gelo e sal. Carregou-se o funil de adição com dietilamina (18 mL; 180 mmol), que foi adicionada lentamente à mistura reagente por um período de uma hora. Terminada a adição, permitiu-se que a temperatura da mistura se igualasse à temperatura ambiente e fosse elevada a 35 ^{o}C. A agitação da mistura, a esta temperatura, foi continuada por 24 horas. O precipitado formado na reação foi

removido por filtração a vácuo, sendo lavado várias vezes com éter dietílico anidro. O filtrado foi concentrado sob pressão reduzida, resultando em um material de coloração marrom. O material foi fracionado em coluna de sílica-gel eluída com hexano-EtOAc 3:1; 2:1; 1:1 v/v, resultando no isolamento da substância **44** com rendimento de 6,2% (0,37 g; 1,3 mmol) e do composto **42** com rendimento de 46% (3,01 g; 11,0 mmol).

Substância 44: *bis* (furan-2-il) *N,N*-dietilamidofosfato

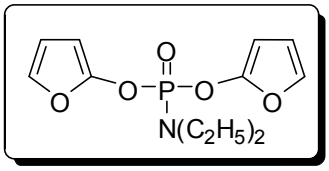

Os dados espectroscópicos obtidos para os compostos **42** e **44** foram consistentes com os descritos na literatura (TEIXEIRA, 2008).

Segunda abordagem sintética - A um tubo selado adicionou-se furan-2(*5H*)-ona (100 mg; 1,2 mmol) dissolvida em 3,0 mL de éter dietílico anidro. Em seguida, cloreto de fosforila ($POCl_3$) (0,17 mL; 1,8 mmol) foi adicionado à mistura de uma só vez. Trietilamina (0,3 mL; 2,4 mmol) dissolvida em 0,5 mL de éter dietílico anidro foi adicionada à mistura reagente, gota a gota, ao longo de um período de 5 minutos. Após essa adição, a mistura resultante foi agitada por 48 horas. Decorrido esse período, o tudo selado foi resfriado em uma mistura de gelo e sal. Adicionou-se dietilamina (0,37 mL; 3,6 mmol) lentamente à mistura reagente por um período de 2 minutos. Terminada a adição, permitiu-se que a temperatura da mistura se igualasse à temperatura ambiente. A agitação da mistura, a esta temperatura, foi continuada por 24 horas. O precipitado formado na reação foi removido por filtração a vácuo, sendo lavado várias vezes com éter dietílico anidro. O filtrado foi concentrado sob pressão reduzida, resultando em um material de coloração marrom. O material foi fracionado em coluna de sílica-gel eluída com hexano-EtOAc 3:1; 2:1; 1:1 v/v, resultando no isolamento da substância **43** com 20% de rendimento (58 mg; 0,24 mmol), da substância **42** com rendimento de 15% (49 mg; 0,18 mmol) e da substância **61** com rendimento de 17% (18 mg; 0,31 mmol).

Os dados espectroscópicos obtidos para os compostos **42** e **43** foram consistentes com os descritos na literatura (TEIXEIRA, 2008). O subproduto **61** foi caracterizado apenas por espectrometria de massas.

Substância 61: dicloreto dietilfosforamídico

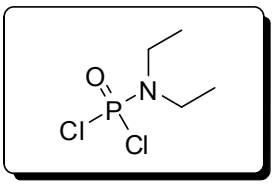

EM, *m/z* (%): 191 ($C_4H_{10}Cl_2NOP$ $[M+2]^{+\bullet}$, 6); 189 ($C_4H_{10}Cl_2NOP$ $[M]^{+\bullet}$, 10); 178 (7); 176 (51); 174 (77); 156 (6); 154 (17); 150 (10); 148 (64); 146 (100); 126 (5); 124 (5); 119 (7); 117 (9); 154 (17); 112 (5); 110 (17); 71 (18); 47 (34); 44 (20); 42 (53); 41 (12); 40 (5).

2.2.2.3. 4-bromofenil fosforodicloridato (**62**)

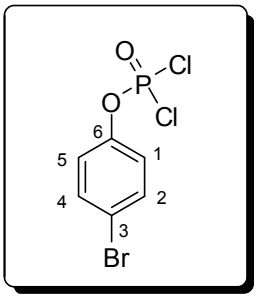

O procedimento descrito a seguir foi baseado no trabalho publicado por UCKUN *et al*. (2005).

A um balão de fundo redondo (50 mL) adicionou-se cloreto de fosforila (1,0 mL; 10,8 mmol) em éter dietílico anidro (10 mL) sob atmosfera de nitrogênio. O balão foi resfriado a 0 ºC em banho de gelo. Uma solução de 4-bromofenol (1,700 g; 9,8 mmol) e trietilamina (1,5 mL; 10,8 mmol) em éter dietílico anidro (25 mL) foi adicionada ao balão gota a gota durante o período de 1 hora. Após esse período o banho de gelo foi removido e deixou-se que a temperatura da mistura retornasse à temperatura ambiente gradualmente. A mistura reacional foi mantida sob agitação por 18 horas. Na sequencia o precipitado formado foi removido por filtração à vácuo em funil de vidro sinterizado e o precipitado lavado com éter dietílico anidro. A mistura reacional foi concentrada em evaporador rotatório levando à formação de um óleo

amarelo claro, contendo o 4-bromofenil fosforodicloridato (**62**) (2,760 g; 9,5 mmol). Este óleo não foi submetido a nenhum processo de purificação posterior (97% de rendimento).

Característica: óleo amarelo claro, sem ser submetido a qualquer processo de purificação.

Rendimento: 97% (2,760 g; 9,5 mmol) a partir de 9,8 mmol do correspondente 4-bromofenol, utilizado como material de partida.

CCD: R_f = 0,36 (hexano-EtOAc 1:1 v/v).

IV ($\overline{\nu}_{máx}$/cm^{-1}): 3095; 1479; 1300; 1182; 1159; 1067; 1008; 931; 824; 760; 610; 549; 516.

RMN de ^{1}H (300 MHz, $CDCl_3$) δ (multiplicidade, *J*/Hz, número de hidrogênios, atribuição): 7,08-7,23 (d; 2H; H-1/H-5); 7,42-7,59 (d, 2H; H-2/H-4).

RMN de ^{13}C (75 MHz, $CDCl_3$) δ (multiplicidade, *J*/Hz, atribuição): 122,55 (C-3); 133,6 (d, $^3J_{C,P}$ = 2,0; C-1/C-5); 148,77 (s, C-2/C-4); 148,77 (s, C-6).

EM, *m/z* (%): 292 ($C_6H_4BrCl_2O_2P$ $[M+4]^{+\bullet}$, 44); 290 ($C_6H_4BrCl_2O_2P$ $[M+2]^{+\bullet}$, 100); 288 ($C_6H_4BrCl_2O_2P$ $[M]^{+\bullet}$, 61); 254 (49); 252 (36); 173 (35); 75 (36); 64 (33); 63 (63).

Os compostos 2-bromofenil fosforodicloridato (**63**), 4-nitrofenil fosforodicloridato (**64**) e 4-fluorofenil fosforodicloridato (**65**) foram preparados utilizando-se o procedimento experimental descrito para a síntese do composto (**62**). As estruturas das substâncias (**63**), (**64**) e (**65**) foram confirmadas pelos dados experimentais descritos a seguir.

2.2.2.4. 2-bromofenil fosforodicloridato (**63**)

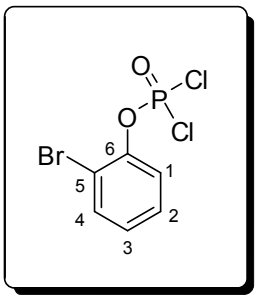

Característica: óleo amarelo claro, sem ser submetido a qualquer processo de purificação.

Rendimento: 99% (2,810 g; 9,7 mmol) a partir de 9,8 mmol do correspondente 2-bromofenol, utilizado como material de partida.

CCD: R_f = 0,41 (hexano-EtOAc 1:1 v/v).

IV ($\bar{\nu}_{máx}$/cm^{-1}): 3069; 2360; 1976; 1578; 1470; 1442; 1297; 1260; 1200; 1160; 1122; 1044; 1011; 934; 760; 750; 703; 652; 563; 539.

RMN de ^{1}H (300 MHz, $CDCl_3$) δ (multiplicidade, *J*/Hz, número de hidrogênios, atribuição): 6,95-7,28 (m, 2H; H-1/H-3); 7,32-7,50 (m, 1H; H-2); 7,52-7,70 (m, 1H; H-4).

RMN de ^{13}C (75 MHz, $CDCl_3$) δ (multiplicidade, *J*/Hz, atribuição): 115,28 (s; C-5); 121,91 (s, C-1); 127,18 (s, C-3); 128,95 (s, C-2); 134,03 (s; C-4); 147,70 (d, $^2J_{C,P}$ = 8,2; C-6).

EM, *m/z* (%): 292 ($C_6H_4BrCl_2O_2P$ $[M+4]^{+\bullet}$, 5); 290 ($C_6H_4BrCl_2O_2P$ $[M+2]^{+\bullet}$, 10); 288 ($C_6H_4BrCl_2O_2P$ $[M]^{+\bullet}$, 6); 211 (64); 209 (100); 145 (13); 143 (13); 119 (8); 117 (10); 63 (32); 50 (11); 38 (20); 32 (9).

2.2.2.5. 4-nitrofenil fosforodicloridato (**64**)

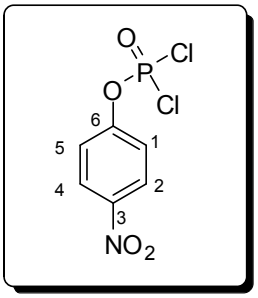

Característica: óleo amarelo escuro, sem ser submetido a qualquer processo de purificação.

Rendimento: 95% (2,970 g; 11,6 mmol) a partir de 12,2 mmol do correspondente 4-nitrofenol, utilizado como material de partida.

CCD: R_f = 0,55 (hexano-EtOAc 2:1 v/v).

IV ($\bar{\nu}_{máx}$/cm^{-1}): 3122; 3079; 2991; 1523; 1346; 1190; 1159; 1107; 935; 747; 550

RMN de ^{1}H (300 MHz, $CDCl_3$) δ (multiplicidade, *J*/Hz, número de hidrogênios, atribuição): 7,30-7,51 (m; 2H; H-1/H-5); 8,18-8,39 (m, 2H; H-2/H-4).

RMN de ^{13}C (75 MHz, $CDCl_3$) δ (multiplicidade, *J*/Hz, atribuição): 121,50 (s, C-1/C-5); 126,36 (s, C-2/C-4); 145,28 (s, C-3); 155,36 (s, C-6).

EM, *m/z* (%): 259 ($C_6H_4Cl_2NO_4P$ $[M+4]^{+\bullet}$, 3); 257 ($C_6H_4Cl_2NO_4P$ $[M+2]^{+\bullet}$, 16); 255 ($C_{16}H_{24}BrN_2O_2P$ $[M]^{+\bullet}$, 29); 225 (39); 127 (19); 117 (22); 99 (17); 92 (13); 75 (71); 63 (61); 47 (29); 38 (38); 32 (100).

2.2.2.6. 4-fluoro fosforodicloridato (**65**)

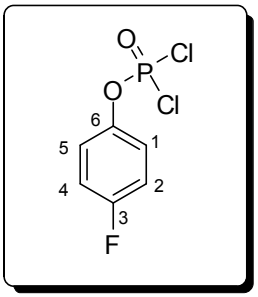

Característica: óleo amarelo claro, sem ser submetido a qualquer processo de purificação.

Rendimento: 91% (2,050 g; 9,0 mmol) a partir de 9,8 mmol do correspondente 4-fluorofenol, utilizado como material de partida.

CCD: R_f = 0,39 (hexano-EtOAc 1:1 v/v).

IV ($\bar{\nu}_{máx}$/cm^{-1}): 3119; 3079; 1501; 1302; 1240; 1190; 1175; 1090; 946; 838; 691; 563.

RMN de ^{1}H (300 MHz, $CDCl_3$) δ (multiplicidade, *J*/Hz, número de hidrogênios, atribuição): 6,97-7,22 (m; 2H; H-1/H-5); 7,24-7,32 (m, 2H; H-2/H-4).

RMN de ^{13}C (75 MHz, $CDCl_3$) δ (multiplicidade, *J*/Hz, atribuição): 116,87 (m, C-2/C-4); 122,10 (m, C-1/C-5); 145,46 (m, C-6); 160,90 (d, $^{2}J_{C,F}$ = 245,5; C-6).

EM, *m/z* (%): 232 ($C_6H_4Cl_2FO_4P$ $[M+4]^{+\bullet}$, 6); 230 ($C_6H_4Cl_2FO_4P$ $[M+2]^{+\bullet}$, 41); 228 ($C_6H_4Cl_2FO_4P$ $[M]^{+\bullet}$, 62); 194 (22); 192 (67); 111 (92); 94 (10); 83 (100); 81 (10); 75 (14); 63 (15); 63 (15); 57 (57); 47 (22).

2.2.2.7. 4-bromofenil *N,N´*-dicicloexilaminafosfinato (**66**)

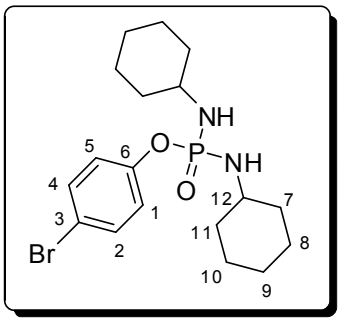

O procedimento descrito a seguir foi baseado no trabalho publicado por UCKUN *et al*. (2005).

A um balão de fundo redondo (50 mL) adicionou-se *p*-bromofenil fosforodicloridato (**62**) (0,500 mg; 1,7 mmol) em DCM anidro (10 mL) sob atmosfera de nitrogênio. O balão foi resfriado a 0 ºC em banho de gelo. Ao balão adicionou-se trietilamina anidra (0,50 mL; 3,6 mmol). Uma solução de cicloexilamina (0,340 g; 3,5 mmol) em DCM anidro (20 mL) foi adicionada ao balão gota a gota durante o período de 1 hora. Após esse período o banho de gelo foi removido e deixou-se que a temperatura da mistura retornasse à temperatura ambiente gradualmente. A mistura reacional foi mantida sob agitação por 18 horas. Na sequencia o precipitado formado foi removido por filtração à vácuo em funil de vidro sinterizado e o precipitado foi lavado com DCM anidro. A mistura reacional foi concentrada em evaporador rotatório levando à formação de um óleo amarelo claro. O material foi purificado em coluna de sílica-gel em gradiente de concentração (Hex:AcEt 3:1). O produto (**66**) isolado como um sólido branco com rendimento de 29% (0,201 g; 0,5 mmol) e (**67**) como um sólido amarelado com rendimento de 8% (0,064 g; 0,1 mmol).

Substância 66

Característica: sólido branco amorfo, purificado por cromatografia em coluna de sílica-gel, empregando-se como eluente hexano-EtOAc 3:1 v/v.

Rendimento: 29% (0,201 g; 0,5 mmol) a partir de 1,7 mmol do correspondente *p*-bromofenil fosforodicloridato, utilizado como material de partida.

CCD: R_f = 0,46 (hexano-EtOAc 2:1 v/v).

T_f = 89,4-91,4 ºC.

IV ($\bar{\nu}_{máx}$/cm^{-1}): 3223; 2927; 2852; 1483; 1449; 1213; 1095; 1009; 908; 828; 738; 639; 537.

RMN de ^{1}H (300 MHz, $CDCl_3$) δ (multiplicidade, *J*/Hz, número de hidrogênios, atribuição): 1,05-1,92 (m, 20H, -C<u>H</u>$_2$); 2,59 (t, $J_{N\underline{H},P} \approx J_{N\underline{H},12} \approx$ 10,0; 2H, -N<u>H</u>); 2,98-3,14 (m, 2H; H-12); 7,08-7,13 (m, 2H; H-1/H-5); 7,36-7,41 (m, 2H; H-2/H-4).

RMN de ^{13}C (75 MHz, $CDCl_3$) δ (multiplicidade, *J*/Hz, atribuição): 25,32 (C-8/C-10)*; 25,58 (C-9)*; 36,18 (tripleto aparente, $^3J_{C,P}$ = 5,1; C-7/C-11); 50,86 (s, C-12); 116,99 (s, C-3); 122,25 (d, $^3J_{C,P}$ = 4,9; C-1/C-5); 132,65 (s, C-2/C-4); 150,83 (d, $^2J_{C,P}$ = 6,5; C-6). * Estas atribuições podem estar invertidas.

EM, *m/z* (%): 416 ($C_{18}H_{28}BrN_2O_2P$ $[M+2]^{+\bullet}$, 5); 414 ($C_{18}H_{28}BrN_2O_2P$ $[M]^{+\bullet}$, 5); 373 (12); 371 (12); 161 (12); 98 (100); 81 (15); 79 (17); 56 (29); 55 (35); 43 (10); 41 (30).

Substância 67: *bis* (4-bromofenil) *N*-cicloexilamidofosfato

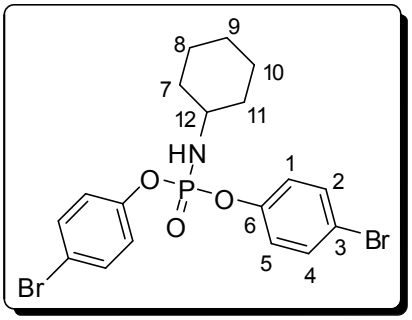

Característica: sólido amarelado, purificado por cromatografia em coluna de sílica-gel, empregando-se como eluente hexano-EtOAc em gradiente de concentração (6:1, 5:1, 4:1, 3:1 v/v).

Rendimento: 8% (0,064 g; 0,1 mmol) a partir de 1,7 mmol do correspondente *p*-bromofenil fosforodicloridato, utilizado como material de partida.

CCD: R_f = 0,43 (hexano-EtOAc 2:1 v/v).

T_f = 143,5-144,9 ºC.

IV ($\bar{\nu}_{máx}$/cm^{-1}): 3177; 2929; 2855; 1583; 1481; 1197; 915; 830; 737; 521.

RMN de ^{1}H (300 MHz, $CDCl_3$) δ (multiplicidade, *J*/Hz, número de hidrogênios, atribuição): 1,04-1,94 (m, 10H, -C<u>H</u>$_2$); 2,99 (t, $J_{N\underline{H},P} \approx J_{N\underline{H},12} \approx$ 12,3; 2H, -N<u>H</u>);

3,06-3,27 (m, 2H; H-12); 7,09-7,16 (m, 4H; H-1/H-5); 7,40-7,47 (m, 4H; H-2/H-4).

RMN de ^{13}C (75 MHz, $CDCl_3$) δ (multiplicidade, *J*/Hz, atribuição): 24,87 (C-8/C-10)*; 25,17 (C-9)*; 35,44 (d, $^3J_{C,P}$ = 5,1; C-7/C-11); 51,31 (C-12); 117,85 (C-3); 121,89 (d, $^3J_{C,P}$ = 5,1; C-1/C-5); 132,65 (C-2/C-4); 149,83 (d, $^2J_{C,P}$ = 6,9; C-6). * Estas atribuições podem estar invertidas.

EM, *m/z* (%): 491 ($C_{18}H_{20}Br_2NO_3P$ $[M+4]^{+\bullet}$, 16); 489 ($C_{18}H_{20}Br_2NO_3P$ $[M+2]^{+\bullet}$, 41); 487 ($C_{18}H_{20}Br_2NO_3P$ $[M]^{+\bullet}$, 19); 446 (100); 408 (37); 316 (9); 236 (16); 172 (33); 98 (71); 55 (54); 41 (43).

Os compostos 4-bromofenil-*N,N´*-dipipiridin-1-ilfosfinato (**68**), 4-bromofenil-*N,N,N´,N´*-tetraetildiamidofosfato (**69**), 4-bromofenil-*N,N´*-difenilfosfato (**70**), *tris*(4-bromofenil)fosfato (**71**), 4-bromofenildimorfolinofosfinato (**72**), 4-bromofenil-4,4´-dimetil-(*N,N´*-difenil) fosfato (**73**), 4-bromofenil-*N,N*-diisopropilamidoclorofosfato (**74**), 2-bromofenil-*N,N´*-dicicloexilamidofosfinato (**75**), 2-bromofenil-*N,N´*-dipepiridin-1-ilfosfinato (**76**), 2-bromofenil-*N,N,N´,N´*-tetraetildiamidofosfato (**77**), 4-nitrofenil-*N,N´*-dicicloexilamidofosfinato (**78**), *bis*(4-nitrofenil)-*N*-cicloexilamidofosfato (**79**), *bis*(4-nitrofenil)morfolinofosfonato (**80**), 4-fluorofenil-*N,N,N´,N´*-tetraetildiamidofosfato (**81**), 4-fluorofenil-*N,N´*-dimorfolin-1-ilfosfinato (**82**), 4-fluorofenildi(piperidin-1-il)fosfinato (**83**), 4-fluorofenil-*N,N´*-dicicloexilamidofosfinato (**84**) foram preparados utilizando-se o procedimento experimental descrito para a síntese do composto (**66**). Especificamente no caso do composto **70**, o DCM utilizado como solvente foi substituído por acetonitrila sob refluxo. As estruturas das substâncias (**68-84**) foram confirmadas pelos dados experimentais descritos a seguir.

2.2.2.8. 4-bromofenil *N,N´*-dipepiridin-1-ilfosfinato (**68**)

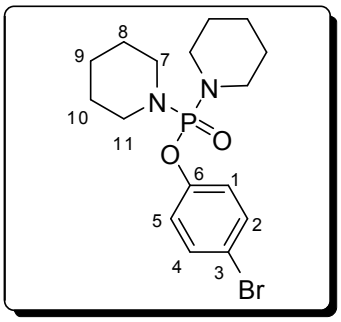

Característica: óleo amarelado claro, purificado por cromatografia em coluna de sílica-gel, empregando-se como eluente hexano-EtOAc 2:1 v/v.

Rendimento: 32% (0,212 g; 0,5 mmol) a partir de 1,7 mmol do correspondente *p*-bromofenil fosforodicloridato, utilizado como material de partida.

CCD: R_f = 0,30 (hexano-EtOAc 2:1 v/v).

IV ($\overline{\nu}_{máx}$/cm^{-1}): 2932; 2849; 1719; 1528; 1482; 1339; 1219; 1199; 1157; 1113; 1065; 1027; 1009; 956; 904; 830; 758; 729; 631; 608; 560; 473.

RMN de ^{1}H (300 MHz, $CDCl_3$) δ (multiplicidade, *J*/Hz, número de hidrogênios, atribuição): 1,39-1,61 (m, 12H, H-8/H-9/H-10); 3,03-3,15 (m, 8H, H-7/H-11); 7,06-7,15 (m, 2H; H-1/H-5); 7,35-7,45 (m, 2H; H-2/H-4).

RMN de ^{13}C (75 MHz, $CDCl_3$) δ (multiplicidade, *J*/Hz, atribuição): 24,69 (C-9); 26,29 (d, $^3J_{C\text{-}P}$ = 2,4; C-8/C-10); 45,77 (d, $^2J_{C\text{-}P}$ = 2,4; C-7/C-11); 116,93 (C-3); 122,26 (d, $^3J_{C\text{-}P}$ = 2,4; C-1/C-5); 132,64 (C-2/C-4); 150,92 (d, $^2J_{C\text{-}P}$ = 6,2; C-6).

EM, *m/z* (%): 388 ($C_{16}H_{24}BrN_2O_2P$ $[M+2]^{+\bullet}$, 3); 386 ($C_{16}H_{24}BrN_2O_2P$ $[M]^{+\bullet}$, 3); 238 (4); 240 (3); 216 (2); 215 (18); 132 (5); 130 (5); 86 (3); 85 (11); 84 (100); 55 (9); 42 (9).

2.2.2.9. 4-bromofenil *N,N,N´,N´*-tetraetildiamido fosfato (**69**)

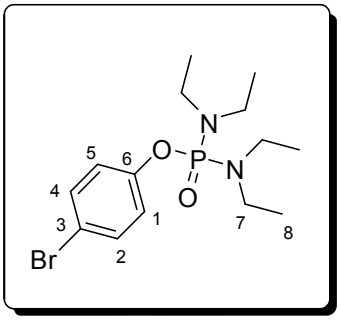

Característica: óleo amarelado claro, purificado por cromatografia em coluna de sílica-gel, empregando-se como eluente hexano-EtOAc 2:1 v/v.

Rendimento: 13% (0,081 g; 0,2 mmol) a partir de 1,7 mmol do correspondente *p*-bromofenil fosforodicloridato, utilizado como material de partida.

CCD: R_f = 0,33 (hexano-EtOAc 2:1 v/v).

IV ($\bar{\nu}_{máx}$/cm^{-1}): 2971; 2922; 2877; 1482; 1206; 1163; 893; 830; 718.

RMN de ^{1}H (300 MHz, $CDCl_3$) δ (multiplicidade, *J*/Hz, número de hidrogênios, atribuição): 0,99-1,13 (m, 12H, H-8); 3,04-3,20 (m, 8H, H-7); 7,06-7,15 (m, 2H; H-1/H-5); 7,36-7,46 (m, 2H; H-2/H-4).

RMN de ^{13}C (75 MHz, $CDCl_3$) δ (multiplicidade, *J*/Hz, atribuição): 14,33 e 13,90 (d, $^3J_{C\text{-}P} \approx 2,2$; C-8); 40,08 e 39,86 (d, $^2J_{C\text{-}P} \approx 4,7$; C-7); 118,16 e 116,73 (C-3); 122,28 e 122,20 (d, $^3J_{C\text{-}P} \approx 2,4$; C-1/C-5); 132,81 e 132,56 (C-2/C-4); 149,76 e 150,96 (d, $^2J_{C\text{-}P} \approx 5,8$; C-6).

EM, *m/z* (%): 364($C_{14}H_{24}BrN_2O_2P$ $[M+2]^{+\bullet}$,3); 362 ($C_{14}H_{24}BrN_2O_2P$ $[M]^{+\bullet}$,3); 349 (17); 347 (17); 191 (38); 72 (100); 58 (19); 56(17); 44 (33); 42 (28); 32 (81).

2.2.2.10. 4-bromofenil *N,N´*-difenil fosfato (**70**)

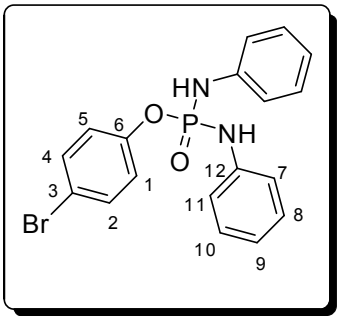

Característica: sólido cristalino, purificado por cromatografia em coluna de sílica-gel, empregando-se como eluente hexano-EtOAc 2:1 v/v.

Rendimento: 16% (0,056 g; 0,14 mmol) a partir de 0,9 mmol do correspondente *p*-bromofenil fosforodicloridato, utilizado como material de partida.

CCD: R_f = 0,26 (hexano-EtOAc 2:1 v/v).

T_f = 189,8-191,4 ºC.

IV ($\bar{\nu}_{máx}$/cm^{-1}): 3362; 3139; 2906; 1476; 1203; 912; 745; 506.

RMN de ^{1}H (300 MHz, $CDCl_3$) δ (multiplicidade, *J*/Hz, número de hidrogênios, atribuição): 5,93 (d, 2H, $J_{N\underline{H}\text{-}P}$ = 8,9; -N<u>H</u>); 6,96-7,11 (m, 8H, H-1/H-5/H-7/H-9/H-11); 7,18-7,38 (m, 6H; H-2/H-4/H-8/H-10).

RMN de ^{13}C (75 MHz, $CDCl_3$) δ (multiplicidade, *J*/Hz, atribuição): 118,59 (C-3)*; 118,69 (C-7/C-11)*; 122,61 (C-9)**; 122,69 (C-1/C-5)**; 122,90 (C-8/C-10)**; 129,67 (C-2/C-4); 132,95 (C-12); 138,85 (C-6). * Essas atribuições podem estar invertidas. ** Essas atribuições podem estar invertidas.

EM, *m/z* (%): 404 ($C_{18}H_{16}BrN_2O_2P$ $[M+2]^{+\bullet}$, 5); 402 ($C_{16}H_{24}BrN_2O_2P$ $[M]^{+\bullet}$, 5); 311 (35); 247 (22); 172 (74); 155 (27); 139 (40); 92 (100); 75 (27); 65 (69); 39 (33).

2.2.2.11. *tris* (4-bromofenil) fosfato (**71**)

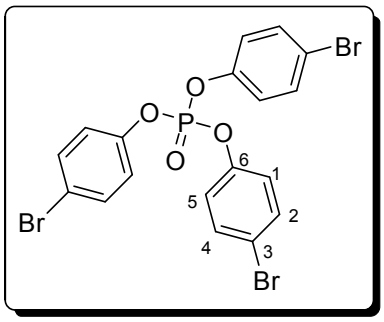

Característica: sólido cristalino, purificado por cromatografia em coluna de sílica-gel, empregando-se como eluente hexano-EtOAc 5:1 v/v.

Rendimento: 26% (0,084 g; 0,15 mmol) a partir de 1,7 mmol do correspondente *p*-bromofenil fosforodicloridato, utilizado como material de partida. Nessa reação empregava-se 2,3-diidroxibenzaldeído como nucleófilo, mas o produto esperado não foi formado.

CCD: R_f = 0,37 (hexano-EtOAc 5:1 v/v).

T_f = 105,0-106,3 ºC.

IV ($\bar{\nu}_{máx}$/cm^{-1}): 2959; 2920; 2850; 2364; 1578; 1476; 1399; 1297; 1230; 1182; 1160; 1067; 1012; 976; 953; 936; 922; 823; 773; 632; 538; 492; 452.

RMN de ^{1}H (300 MHz, $CDCl_3$) (multiplicidade, *J*/Hz, número de hidrogênios, atribuição): 7,06-7,13 (m, 6H, H-1/H-5); 7,43-7,51 (m, 6H; H-2/H-4).

RMN de ^{13}C (75 MHz, $CDCl_3$) (multiplicidade, *J*/Hz, atribuição): 149,40 (d, $^{2}J_{C,P}$ = 7,6; C-6), 133,26 (C-2/C-4), 122,03 (d, $^{3}J_{C,P}$ = 5,1; C-1/C-5), 119,25 (C-3).

EM, *m/z* (%): 564 ($C_{18}H_{12}Br_3O_4P$ $[M+4]^{+\bullet}$, 92); 562 ($C_{18}H_{12}Br_3O_4P$ $[M+2]^{+\bullet}$, 100); 560 ($C_{18}H_{12}Br_3O_4P$ $[M]^{+\bullet}$, 34); 328 (30); 174 (71); 173 (59); 172 (72); 171 (44); 168 (66); 155 (33); 145 (52); 143 (54); 75 (65); 64 (37); 50 (44).

2.2.2.12. 4-bromofenil dimorfolinofosfinato (**72**)

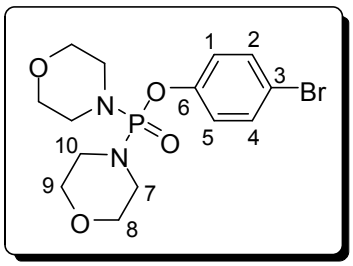

Característica: cristal branco, purificado por cromatografia em coluna de sílica-gel, empregando-se como eluente hexano-EtOAc em gradiente de concentração (9:1, 6:1, 5:1, 4:1, 3:1 v/v).

Rendimento: 46% (0,307 g; 0,8 mmol) a partir de 1,7 mmol do correspondente *p*-bromofenil fosforodicloridato, utilizado como material de partida.

CCD: R_f = 0,60 (hexano-EtOAc 3:1 v/v).

T_f = 112,7-113,9 ºC.

IV ($\bar{\nu}_{máx}$/cm^{-1}): 2956; 2846; 1482; 1232; 1111; 967; 904; 840; 734; 473

RMN de ^{1}H (300 MHz, $CDCl_3$) δ (multiplicidade, *J*/Hz, número de hidrogênios, atribuição): 3,15-3,22 (m, 8H, H-7/H-10); 3,59-3,61 (m, 8H, H-8/H-9); 7,09-7,15 (m, 2H; H-1/H-5); 7,41-7,47 (m, 2H; H-2/H-4).

RMN de ^{13}C (75 MHz, $CDCl_3$) δ (multiplicidade, *J*/Hz, atribuição): 44,74 (s, C-7/C-10); 66,96 (d, $^3J_{C,P}$ = 5,8; C-8/C-9); 117,37 (s, C-3); 121,83 (d, $^3J_{C,P}$ = 5,0; C-1/C-5); 132,68 (s, C-2/C-4); 150,09 (d, $^2J_{C,P}$ = 5,9; C-6).

EM, *m/z* (%): 392 ($C_{14}H_{20}BrN_2O_4P$ $[M+2]^{+\bullet}$, 11); 390 ($C_{14}H_{20}BrN_2O_4P$ $[M]^{+\bullet}$, 10); 377 (5); 361 (15); 347 (12); 335 (24); 134 (10); 86 (100); 56 (46); 42 (21).

2.2.2.13. 4-bromofenil 4,4´-dimetil-(*N,N´*-difenil) fosfato (**73**)

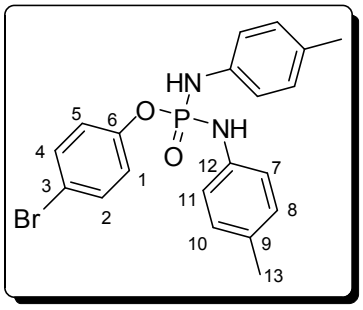

Característica: sólido branco amorfo, purificado por cromatografia em coluna de sílica-gel, empregando-se como eluente hexano-EtOAc 3:1 v/v.

Rendimento: 13% (0,099 g; 0,2 mmol) a partir de 1,7 mmol do correspondente *p*-bromofenil fosforodicloridato, utilizado como material de partida.

CCD: R_f = 0,51 (hexano-EtOAc 2:1 v/v).

T_f = 104,7-106,1 ºC.

IV ($\bar{\nu}_{máx}$/cm^{-1}): 3377; 3139; 1616; 1482; 1202; 991; 817; 493.

RMN de ^{1}H (300 MHz, $CDCl_3$) δ (multiplicidade, *J*/Hz, número de hidrogênios, atribuição): 1,67 (s, 6H, -C<u>H</u>$_3$); 6,48-6,65 (m, 10H, H-1/H-5/H-7/H-8/H-10/H-11); 6,88-6,92 (m, 2H, H-2/H-4); 7,32 (d, 2H, $J_{N\underline{H}\text{-}P}$ = 9,9; -N<u>H</u>).

RMN de ^{13}C (75 MHz, $CDCl_3$) δ (multiplicidade, *J*/Hz, atribuição): 19,44 (C-13); 116,18 (C-3); 116,88 (d, $^2J_{C,P}$ = 7,4; C-7/C-11); 121,71 (d, $^2J_{C,P}$ = 4,6; C-1/C-5); 128,35 (C-9); 129,19 (C-8/C-10); 131,20 (C-2/C-4); 136,68 (C-12); 148,75 (d, $^2J_{C,P}$ = 6,4; C-6).

EM, *m/z* (%): 432 ($C_{20}H_{20}BrN_2O_2P$ [M+2]$^{+\bullet}$, 44); 430 ($C_{20}H_{20}BrN_2O_2P$ [M]$^{+\bullet}$, 41); 261 (21); 241 (14); 107 (100); 79 (32).

2.2.2.14. 4-bromofenil *N,N*-diisopropilamidoclorofosfato (**74**)

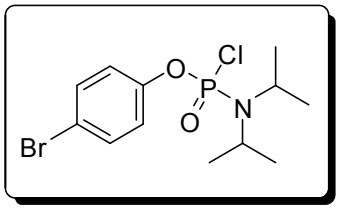

EM, *m/z* (%): 357 ($C_{12}H_{18}BrClNO_2P$ [M+4]$^{+\bullet}$, 2); 355 ($C_{12}H_{18}BrClNO_2P$ [M+2]$^{+\bullet}$, 7); 353 ($C_{12}H_{18}BrClNO_2P$ [M]$^{+\bullet}$, 5); 340 (44); 338 (31); 300 (26); 298 (100); 296 (76); 124 (8); 44 (43); 43 (38); 42 (38); 41 (77); 36 (25).

O composto **74** não foi isolado, ficando adsorvido à sílica ou alumina após fracionamento.

2.2.2.15. 2-bromofenil *N,N´*-dicicloexilamidofosfinato (**75**)

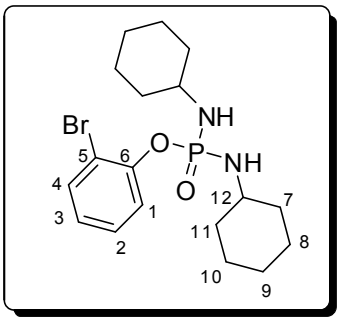

Característica: sólido branco em agulha, purificado por cromatografia em coluna de sílica-gel, empregando-se como eluente hexano-EtOAc 2:1 v/v.

Rendimento: 36% (0,250 g; 0,6 mmol) a partir de 1,7 mmol do correspondente *o*-bromofenil fosforodicloridato, utilizado como material de partida.

CCD: R_f = 0,22 (hexano-EtOAc 2:1 v/v).

T_f = 111,6-113,2 ºC.

IV ($\bar{\nu}_{máx}$/cm^{-1}): 3208; 2928; 2850; 1474; 1219; 1087; 908; 756; 506.

RMN de ^{1}H (300 MHz, $CDCl_3$) δ (multiplicidade, *J*/Hz, número de hidrogênios, atribuição): 1,20-2,03 (m, 20H, -C<u>H</u>$_2$); 2,69 (t, 2H, -N<u>H</u>); 3,05-3,25 (m, 2H; H-12); 6,94-7.00 (m, 1H; H-3); 7,21-7,27 (m, 1H; H-2); 7,50-7,58 (m, 2H; H-1/H-4).

RMN de ^{13}C (75 MHz, $CDCl_3$) δ (multiplicidade, *J*/Hz, atribuição): 25,04 (C-8/C-10); 25,33 (C-9); 35,88 (d, $^3J_{C\text{-}P}$ = 4,8; C-7/C-11); 50,55 (C-12); 114,47 (C-5); 121,86 (d, $^3J_{C\text{-}P}$ = 2,9; C-1); 125,18 (C-3); 128,59 (C-2); 133,11 (C-4); 148,61 (d, $^2J_{C\text{-}P}$ = 6,0; C-6)

EM, *m/z* (%): 416 ($C_{18}H_{28}BrN_2O_2P$ $[M+2]^{+\bullet}$, 4); 414 ($C_{18}H_{28}BrN_2O_2P$ $[M]^{+\bullet}$, 4); 373 (21); 371 (21); 335 (57); 291 (9); 289 (10); 253 (14); 236 (10); 161 (11); 98 (100); 79 (21); 55 (46); 41 (50); 32 (39).

2.2.2.16. 2-bromofenil *N,N´*-dipepiridin-1-ilfosfinato (**76**)

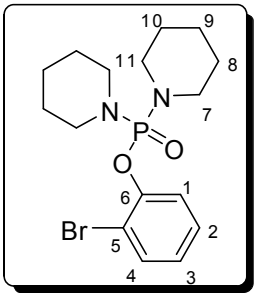

Característica: sólido amarelo claro amorfo, purificado por cromatografia em coluna de sílica-gel, empregando-se como eluente hexano-EtOAc 1:1 v/v.

Rendimento: 34% (0,230 g; 0,6 mmol) a partir de 1,7 mmol do correspondente *o*-bromofenil fosforodicloridato, utilizado como material de partida.

CCD: R_f = 0,32 (hexano-EtOAc 1:1 v/v).

T_f = 60,7-62,4 ºC.

IV ($\bar{\nu}_{máx}$/cm^{-1}): 2931; 2848; 1474; 1228; 1206; 1161; 904

RMN de ^{1}H (300 MHz, $CDCl_3$) δ (multiplicidade, *J*/Hz, número de hidrogênios, atribuição): 1,45-1,56 (m, 12H, H-8/H-9/H-10); 3,13-3,24 (m, 8H, H-7/H-11); 6,95 (td, *J* = 8,1 e *J* = 1,5; 1H; H-3); 7,25 (td, *J* = 8,1 e *J* = 1,5; 1H; H-2); 7,53 (dt, *J* = 8,1 e *J* = 1,5; 1H; H-1); 7,60 (dt, *J* = 8,1 e *J* = 1,5; 1H; H-4).

RMN de ^{13}C (75 MHz, $CDCl_3$) δ (multiplicidade, *J*/Hz, atribuição): 24,72 (C-9); 26,28 (d, $^3J_{C\text{-}P}$ = 5,1; C-8/C-10); 45,84 (d, $^2J_{C\text{-}P}$ = 2,4; C-7/C-11); 114,21 (d, $^2J_{C\text{-}P}$ = 8,4; C-5); 121,11 (d, $^3J_{C\text{-}P}$ = 2,8; C-1); 125,00 (C-3); 128,68 (C-2); 133,47 (C-4); 149,11 (d, $^2J_{C\text{-}P}$ = 4,9; C-6).

EM, *m/z* (%): 388 ($C_{16}H_{24}BrN_2O_2P$ $[M+2]^{+\bullet}$, 2); 386 ($C_{16}H_{24}BrN_2O_2P$ $[M]^{+\bullet}$, 2); 307 (11); 215 (15); 84 (100); 55 (14); 42 (13).

2.2.2.17. 2-bromofenil *N,N,N´,N´*-tetraetildiamido fosfato (**77**)

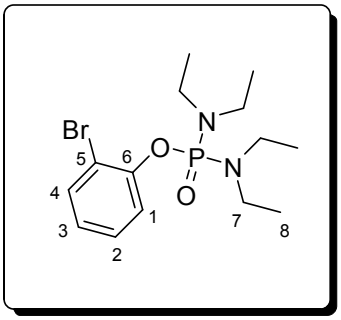

EM, *m/z* (%): 364($C_{14}H_{24}BrN_2O_2P$ $[M+2]^{+\bullet}$,3); 362 ($C_{14}H_{24}BrN_2O_2P$ $[M]^{+\bullet}$,3); 349 (22); 347 (22); 290 (23); 283 (23); 191 (50); 72 (100); 58 (17); 56 (21); 44 (32); 42 (30).

O composto **77** não foi isolado, ficando adsorvido à sílica após coluna de sílica-gel (eluente hexano-EtOAc 2:1 v/v).

2.2.2.18. 4-nitrofenil *N,N´*-dicicloexilamidofosfinato (**78**)

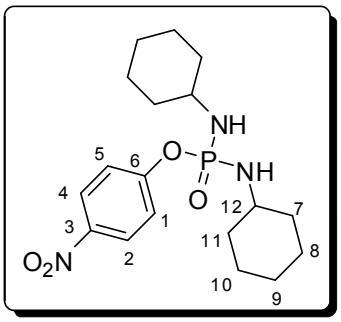

Característica: sólido branco amorfo, purificado por cromatografia em coluna de sílica-gel, empregando-se como eluente hexano-EtOAc 3:1 v/v.

Rendimento: 32% (0,245 g; 0,6 mmol) a partir de 1,7 mmol do correspondente *p*-nitrofenil fosforodicloridato, utilizado como material de partida.

CCD: R_f = 0,18 (hexano-EtOAc 1:1 v/v).

T_f = 144,7-145,6 ºC.

IV ($\overline{\nu}_{máx}$/cm^{-1}): 3377; 3184; 2924; 2851; 1340; 1224; 1109; 889; 742; 522

RMN de ^{1}H (300 MHz, $CDCl_3$) δ (multiplicidade, *J*/Hz, número de hidrogênios, atribuição): 1,01-2,00 (m, 20H, -C<u>H</u>$_2$); 2,11-2,70 (sinal alargado, 2H, -N<u>H</u>); 2,98-3,18 (m, 2H; H-12); 7,33-7,43 (m, 2H; H-1/H-5); 8,14-8,24 (m, 2H; H-2/H-4).

RMN de ^{13}C (75 MHz, $CDCl_3$) δ (multiplicidade, *J*/Hz, atribuição): 25,28 (C-8/C-10)*; 25,51 (C-9)*; 36,12 (d, $^3J_{C,P}$ = 4,5; C-7/C-11); 51,03 (s, C-12); 120,4 (d, $^3J_{C,P}$ = 5,4; C-1/C-5); 125,75 (s, C-2/C-4); 144,00 (s, C-3); 156,95 (d, $^2J_{C,P}$ = 5,8; C-6). * Estas atribuições podem estar invertidas.

EM, *m/z* (%): 381 ($C_{18}H_{28}N_3O_4P$ $[M]^{+\bullet}$, 3); 338 (13); 256 (8); 98 (39); 81 (11); 79 (11); 65 (10); 56 (27); 55 (25); 41 (28); 39 (44); 32 (100).

O 4-nitrofenil *N,N´*-dicicloexilaminafosfinato (**78**) foi o segundo composto eluído no processo de separação cromatográfica, isolado com rendimento de 32% (0,245 g; 0,6 mmol) como um sólido branco amorfo. A primeira fração da separação cromatográfica foi constituída pelo composto *bis* (4-nitrofenil) *N*-cicloexilaminafosfato (**79**) isolado, com rendimento de 12% (0,088 g; 0,2 mmol).

2.2.2.19. *bis* (4-nitrofenil) *N*-cicloexilaminafosfato (**79**)

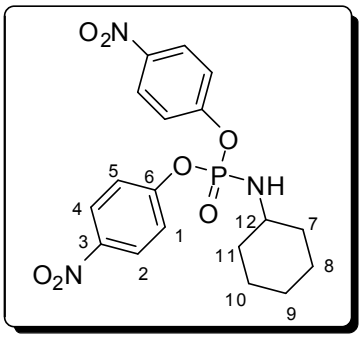

Característica: sólido branco em agulha, purificado por cromatografia em coluna de sílica-gel, empregando-se como eluente hexano-EtOAc 3:1 v/v.

Rendimento: 12% (0,088 g; 0,2 mmol) a partir de 1,7 mmol do correspondente *p*-nitrofenil fosforodicloridato, utilizado como material de partida.

CCD: R_f = 0,31 (hexano-EtOAc 1:1 v/v).

T_f = 175,4-176,7 ºC.

IV ($\bar{\nu}_{máx}$/cm^{-1}): 3160; 3114; 2926; 2851; 1512; 1341; 1207; 1105; 920; 854; 748; 532.

RMN de ^{1}H (300 MHz, $CDCl_3$) δ (multiplicidade, *J*/Hz, número de hidrogênios, atribuição): 1,16-1,90 (m, 10H, -C<u>H</u>$_2$); 3,15-3,37 (m, 2H, -N<u>H</u>/H-12); 7,39-7,44 (m, 4H; H-1/H-5); 8,22-8,28 (m, 4H; H-2/H-4).

RMN de ^{13}C (75 MHz, $CDCl_3$) δ (multiplicidade, *J*/Hz, atribuição): 24,79 (C-8/C-10)*; 25,02 (C-9)*; 35,37 (d, $^3J_{C,P}$ = 5,1; C-7/C-11); 51,64 (s, C-12); 120,58 (d, $^3J_{C,P}$ = 5,6; C-1/C-5); 125,74 (s, C-2/C-4); 144,73 (s, C-3); 155,55 (d, $^2J_{C,P}$ = 6,4; C-6). * Estas atribuições podem estar invertidas.

EM, *m/z* (%): 421 ($C_{18}H_{20}N_3O_7P$ $[M]^{+\bullet}$, 6); 378 (59); 340 (18); 139 (14); 109 (11); 98 (14); 81 (16); 65 (23); 55 (32); 41 (46); 39 (44); 32 (100).

2.2.2.20. *bis*(4-nitrofenil) morfolinofosfonato (**80**)

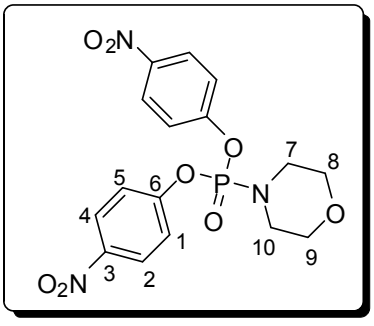

Característica: cristal branco, purificado por cromatografia em coluna de sílica-gel, empregando-se como eluente hexano-EtOAc em gradiente de concentração (3:1, 2:1, 1:1 v/v).

Rendimento: 11% (0,087 g; 0,2 mmol) a partir de 1,7 mmol do correspondente *p*-nitrofenil fosforodicloridato, utilizado como material de partida.

CCD: R_f = 0,38 (hexano-EtOAc 1:1 v/v).

T_f = 161,5-162,9 ºC.

IV ($\bar{\nu}_{máx}$/cm^{-1}): 2858; 1588; 1513; 1342; 1199; 908; 846; 745; 471.

RMN de ^{1}H (300 MHz, $CDCl_3$) δ (multiplicidade, *J*/Hz, número de hidrogênios, atribuição): 3,30-3,38 (m, 4H, H-7/H-10); 3,60-3,67 (m, 4H, H-8/H-9); 7,38-7,45 (m, 4H; H-1/H-5); 8,24-8,31 (m, 4H; H-2/H-4).

RMN de ^{13}C (75 MHz, $CDCl_3$) δ (multiplicidade, *J*/Hz, atribuição): 44,67 (s, C-7/C-10); 66,59 (dupleto, $^3J_{C,P}$ = 5,7; C-8/C-9); 120,55 (dupleto, $^3J_{C,P}$ = 5,4; C-1/C-5); 125,87 (s, C-2/C-4); 144,95 (s, C-3); 155,04 (d, $^2J_{C,P}$ = 6,5; C-6).

EM, *m/z* (%): 409 ($C_{16}H_{16}N_3O_8P$ $[M]^{+\bullet}$, 2); 366 (100); 352 (55); 271 (11); 213 (8); 150 (50); 75 (29); 56 (38); 44 (29).

2.2.2.21. 4-fluorofenil *N,N,N´,N´*-tetraetildiamido fosfato (**81**)

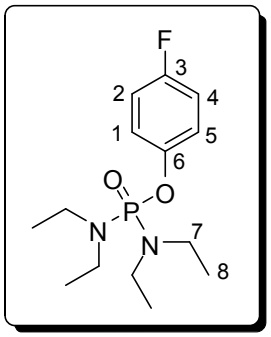

Característica: cristal branco, purificado por cromatografia em coluna de sílica-gel, empregando-se como eluente hexano-EtOAc 3:1 v/v.

Rendimento: 25% (0,134 g; 0,4 mmol) a partir de 1,7 mmol do correspondente *p*-fluorofenil fosforodicloridato, utilizado como material de partida.

CCD: R_f = 0,53 (hexano-EtOAc 3:1 v/v).

IV ($\bar{\nu}_{máx}$/cm^{-1}): 2973; 1501; 1380; 1168; 1025; 900; 817; 500.

RMN de ^{1}H (300 MHz, $CDCl_3$) δ (multiplicidade, *J*/Hz, número de hidrogênios, atribuição): 1,07 (t, *J* = 7,2; 12H, -C$\underline{H}_3$); 3,11 (dq, *J* = 7,2 e *J* = 18,3; 8H, -C$\underline{H}_2$); 6,91-7,03 (m, 2H; H-2/H-4); 7,13-7,20 (m, 2H; H-1/H-5).

RMN de ^{13}C (75 MHz, $CDCl_3$) δ (multiplicidade, *J*/Hz, atribuição): 14,05 (d, $^3J_{C,P}$ = 2,1; C-8); 39,63 (d, $^2J_{C,P}$ = 4,7; C-7); 115,97 (d, $^2J_{C,F}$ = 23,0; C-2/C-4); 121,43 (q, *J* = 4,8 e *J* = 8,1; C-1/C-5); 147,39 (s, C-6); 158,96 (d, $^2J_{C,F}$ = 239,9; C-3).

EM, *m/z* (%): 303 ($C_{14}H_{24}FN_2O_2P$ $[M+1]^{+\bullet}$, 3); 302 ($C_{14}H_{24}FN_2O_2P$ $[M]^{+\bullet}$, 18); 287 (73); 230 (55); 216 (44); 191 (68); 166 (14); 120 (14); 111 (21); 72 (100); 58 (29); 44 (42).

2.2.2.22. 4-fluorofenil *N,N´*-dimorfolin-1-ilfosfinato (**82**)

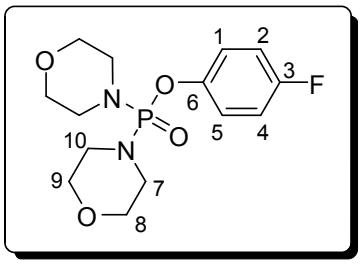

Característica: cristal branco, purificado por cromatografia em coluna de sílica-gel, empregando-se como eluente hexano-EtOAc 3:1 v/v.

Rendimento: 55% (0,317 g; 1,0 mmol) a partir de 1,7 mmol do correspondente *p*-fluorofenil fosforodicloridato, utilizado como material de partida.

CCD: R_f = 0,57 (hexano-EtOAc 3:1 v/v).

T_f = 128,7-130,1 ºC.

IV ($\bar{\nu}_{máx}$/cm^{-1}): 2974; 2851; 1502; 1230; 1109; 965; 907; 843; 741; 489

RMN de ^{1}H (300 MHz, $CDCl_3$) δ (multiplicidade, *J*/Hz, número de hidrogênios, atribuição): 3,14-3,23 (m, 8H, H-7/H-10); 3,58-3,65 (m, 8H, H-8/H-9); 6,97-7,05 (m, 2H; H-2/H-4); 7,13-7,21 (m, 2H; H-1/H-5).

RMN de ^{13}C (75 MHz, $CDCl_3$) δ (multiplicidade, *J*/Hz, atribuição): 44,72 (s, C-7/C-10); 66,94 (d, $^2J_{C,P}$ = 5,8; C-8/C-9); 116,22 (d, $^2J_{C,F}$ = 23,3; C-2/C-4); 121,35 (q, *J* = 4,9 e *J* = 8,4; C-1/C-5); 146,82 (q, *J* = 2,8 e *J* = 5,8; C-6); 159,31 (d, $^2J_{C,F}$ = 241,8; C-3).

EM, *m/z* (%): 331 ($C_{14}H_{20}FN_2O_4P$ $[M+1]^{+\bullet}$, 4); 330 ($C_{14}H_{20}FN_2O_4P$ $[M]^{+\bullet}$, 24); 315 (13); 299 (33); 287 (26); 273 (57); 134 (16); 123 (22); 86 (100); 56 (52); 42 (25).

2.2.2.23. 4-fluorofenil di(piperidin-1-il)fosfinato (**83**)

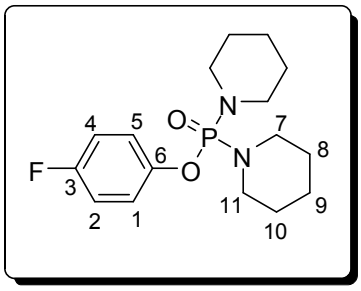

Característica: óleo amarelo claro, purificado por cromatografia em coluna de sílica-gel, empregando-se como eluente hexano-EtOAc 3:1 v/v.

Rendimento: 30% (0,168 g; 0,5 mmol) a partir de 1,7 mmol do correspondente *p*-fluorofenil fosforodicloridato, utilizado como material de partida.

CCD: R_f = 0,51 (hexano-EtOAc 3:1 v/v).

IV ($\overline{\nu}_{máx}$/cm^{-1}): 2933; 2849; 1501; 1339; 1193; 1071; 903; 817; 733; 477.

RMN de ^{1}H (300 MHz, $CDCl_3$) δ (multiplicidade, *J*/Hz, número de hidrogênios, atribuição): 1,42-1,59 (m, 12H, H-8/H-9/H-10); 3,06-3,13 (m, 8H, H-7/H-11); 6,93-7,01 (m, 2H; H-2/H-4); 7,13-7,19 (m, 2H; H-1/H-5).

RMN de ^{13}C (75 MHz, $CDCl_3$) δ (multiplicidade, *J*/Hz, atribuição): 24,44 (s, C-9); 26,04 (d, $^3J_{C,P}$ = 5,3; C-7/C-11); 45,49 (d, $^3J_{C,P}$ = 2,3; C-8/C-10); 115,87 (d, $^2J_{C,F}$ = 23,1; C-2/C-4); 121,41 (q, *J* = 4,8 e *J* = 8,3; C-1/C-5); 147,40 (s, C-6); 158,99 (d, $^2J_{C,F}$ = 240,8; C-3).

EM, *m/z* (%): 327 ($C_{16}H_{24}FN_2O_2P$ $[M+1]^{+\bullet}$, 3); 326 ($C_{16}H_{24}FN_2O_2P$ $[M]^{+\bullet}$, 16); 242 (8); 215 (32); 178 (12); 130 (12); 84 (100); 55 (22); 42 (12).

2.2.2.24. 4-fluorofenil *N, N´*-dicicloexilamidofosfinato (**84**)

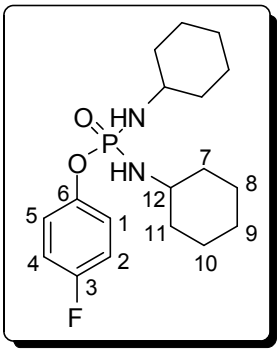

Característica: sólido branco amorfo, purificado por cromatografia em coluna de sílica-gel, empregando-se como eluente hexano-EtOAc 3:1 v/v.

Rendimento: 28% (0,172 g; 0,5 mmol) a partir de 1,7 mmol do correspondente *p*-fluorofenil fosforodicloridato, utilizado como material de partida.

CCD: R_f = 0,39 (hexano-EtOAc 2:1 v/v).

T_f = 117,9-119,3 ºC.

IV ($\overline{\nu}_{máx}$/cm^{-1}): 3232; 2926; 2853; 1503; 1435; 1198; 1087; 892; 812; 484.

RMN de ^{1}H (300 MHz, $CDCl_3$) δ (multiplicidade, *J*/Hz, número de hidrogênios, atribuição): 1,03-1,97 (m, 20H, -C<u>H</u>$_2$); 2,53 (t, *J* = 2,4; 2H, -N<u>H</u>); 2,99-3,16 (m, 2H; H-12); 6,92-7,02 (m, 2H; H-2/H-4); 7,13-7,21 (m, 2H; H-1/H-5).

RMN de ^{13}C (75 MHz, $CDCl_3$) δ (multiplicidade, *J*/Hz, atribuição): 25,05 (C-8/C-10)*; 25,34 (C-9)*; 35,94 (tripleto aparente, $^3J_{C,P}$ = 5,0; C-7/C-11); 50,58 (s, C-12); 115,93 (d, $^2J_{C,F}$ = 23,2; C-2/C-4); 121,48 (q, *J* = 4,8 e *J* = 8,2; C-1/C-5); 147,31 (q, *J* = 2,1 e *J* = 6,2; C-6); 159,11 (d, $^2J_{C,F}$ = 240,8; C-3). * Estas atribuições podem estar invertidas.

EM, *m/z* (%): 355 ($C_{18}H_{28}FN_2O_2P$ $[M+1]^{+\bullet}$, 7); 354 ($C_{18}H_{28}FN_2O_2P$ $[M]^{+\bullet}$, 33); 311 (57); 273 (15); 243 (20); 229 (33); 191 (24); 161 (22); 98 (100); 79 (29); 55 (62); 41 (35).

2.3. Resultados e Discussão

O presente estudo objetivou, inicialmente, dar continuidade aos trabalhos de PAULA *et al.* (2008) e OLIVEIRA *et al*. (2012), uma vez que os fosforamidatos **42-46** apresentaram elevada atividade inseticida. Além disso, há outros relatos de atividade biológica descritos na literatura para essa classe de organofosfatos (SANTOS *et al.*, 2007).

A presença de um grupo das furanonas (**60**) na estrutura das substâncias é uma característica importante, uma vez que são conhecidos heterociclos com diversas atividades biológicas descritas na literatura: antiinflamatória, antimicrobiana, antifúngica, anticâncer, antiviral HIV, fitotóxica, inseticida, fago inibidor, entre outros (SOUZA *et al.*, 2005).

Os fosforamidatos **42-46** foram sintetizados conforme análise retrossintética mostrada no Esquema 6.

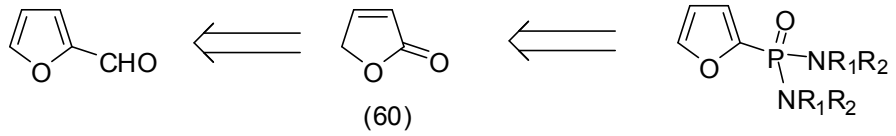

(60)

Esquema 6 - Metodologia sintética empregada na síntese dos fosforamidatos.

A reação de oxidação de Bayer Villiger do furfuraldeído com ácido perfórmico, gerado *in situ* pela reação do peróxido de hidrogênio com ácido fórmico, fornece a lactona **60** com rendimento de 49% (Esquema 7), similar àquele documentado na literatura (NÄSMAN, 1990).

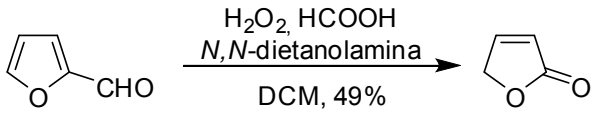

(60)

Esquema 7 - Síntese da furan-2(*5H*)ona **(60)** a partir do furfuraldeído.

Os dados espectroscópicos obtidos para a lactona **60** são consistentes com os descritos na literatura (TEIXEIRA, 2008).

Na sequencia, a lactona **60** é submetida à reação segundo adaptação da rota sintética descrita por Näsman (1990), conforme Esquema 8. O intermediário **85** não isolado após o tratamento de **60** com cloreto de fosforila ($POCl_3$), é imediatamente submetido à reação de substituição nucleofílica com as aminas etilamina, cicloexilamina, diisopropilamina e piperidina.

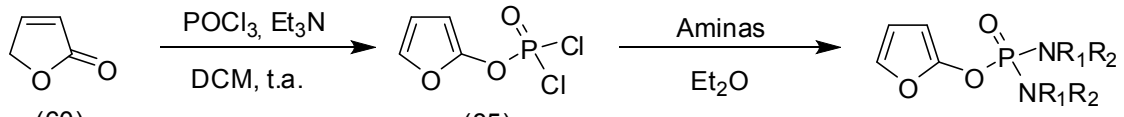

(60) (85)

Esquema 8 - Reação para a síntese dos fosforamidatos a partir da lactona **60**.

Empregando a lactona **60** como material de partida, os fosforamidatos foram obtidos com rendimentos variando de 6,4 a 46,0% (OLIVEIRA *et al.*, 2012). O melhor rendimento (46%) foi obtido empregando-se etilamina como nucleófilo.

2.3.1. Tentativa de otimização da síntese do furan-2-il *N,N,N',N'*-tetraetildiamidofosfato (42)

Diante dos baixos rendimentos alcançados por OLIVEIRA *et al*. (2012), buscou-se otimizar o procedimento de síntese do furan-2-il *N,N,N',N'*-tetraetildiamidofosfato (**42**) para então dar continuidade ao projeto de desenvolvimento de novas substâncias.

A tentativa de otimização de síntese da substância **42** consistiu na variação de condições reacionais bem como na simplificação de etapas (Tabela 1). O procedimento geral pode ser consultado na segunda alternativa descrita em 2.1.2.2.

Tabela 1 – Resultados experimentais da síntese do composto **42**

Experimento	Condições	Tempo final da reação (h)	Solvente	Rendimento (%)[a]			
				42	**43**	**61**	**86**
1	(i)lactona **60** (1,0 equiv.), $POCl_3$ (1,5 equiv.), Et_3N (2,0 equiv); 24h (ii) Et_2NH (3,0 equiv.)	48	DCM	-	8	6	11
2	(i)lactona **60** (1,0 equiv.), $POCl_3$ (1,5 equiv.), Et_3N (2,0 equiv); 24h (ii) Et_2NH (3,0 equiv.)	48	Et_2O	-	16	8	-
3[b]	(i)lactona **60** (1,0 equiv.), $POCl_3$ (1,5 equiv.), Et_3N (2,0 equiv); 24h (ii) Et_2NH (3,0 equiv.)	72	Et_2O	15	20	17	-
4	(i)lactona **60** (1,0 equiv.), $POCl_3$ (1,5 equiv.), Et_3N (2,0 equiv); 24h (ii) Et_2NH (3,0 equiv.)	48	THF	-	10	7	-
5	(i)lactona **60** (1,0 equiv.), $POCl_3$ (1,5 equiv.), Et_3N (2,0 equiv); 5 min (ii) Et_2NH (3,0 equiv.)	24	Et_2O	5	34	28	7
6	(i)lactona **60** (1,0 equiv.), $POCl_3$ (1,5 equiv.), Et_3N (2,0 equiv); 5 min (ii) Et_2NH (3,0 equiv.)	24	DCM	12	14	12	-

Tabela 1 – Resultados experimentais da síntese do composto **42** (continuação)

Experimento	Condições	Tempo final da reação (h)	Solvente	Rendimento (%)[a]			
				42	**43**	**61**	**86**
7	(i)lactona **60** (1,0 equiv.), $POCl_3$ (1,5 equiv.), Et_3N (2,0 equiv); 5 min (ii) Et_2NH (3,0 equiv.)	24	THF	-	9	7	12
8	(i)lactona **60** (1,0 equiv.), $POCl_3$ (2,5 equiv.), Et_3N (2,0 equiv); 5 min (ii) Et_2NH (3,0 equiv.)	24	Et_2O	-	3	2	12
9	(i)lactona **60** (1,0 equiv.), $POCl_3$ (2,5 equiv.), Et_3N (2,0 equiv); 5 min (ii) Et_2NH (3,0 equiv.)	24	DCM	-	16	8	-
10	(i)lactona **60** (1,0 equiv.), $POCl_3$ (2,5 equiv.), Et_3N (3,0 equiv); 5 min (ii) Et_2NH (3,0 equiv.)	24	Et_2O	-	16	8	-
11	(i)lactona **60** (1,0 equiv.), $POCl_3$ (2,5 equiv.), Et_3N (3,0 equiv); 5 min (ii) Et_2NH (3,0 equiv.)	24	THF	-	14	7	-
12	(i)lactona **60** (1,0 equiv.), $POCl_3$ (1,5 equiv.), Et_3N (6,0 equiv); 5 min (ii) Et_2NH (3,0 equiv.)	24	Et_2O	-	19	16	23
13	(i)lactona **60** (1,0 equiv.), $POCl_3$ (2,5 equiv.), Et_3N (2,0 equiv); 24h (ii) Et_2NH (3,0 equiv.)	48	THF	-	18	9	-
14	(i)lactona **60** (1,0 equiv.), $POCl_3$ (2,5 equiv.), Et_3N (2,0 equiv); 24h (ii) Et_2NH (3,0 equiv.)	48	DCM	-	14	7	-
15	(i)lactona **60** (1,0 equiv.), $POCl_3$ (1,5 equiv.), Et_3N (3,0 equiv); 24h (ii) Et_2NH (3,0 equiv.)	72	Et_2O	9	14	12	-
16	(i)lactona **60** (1,0 equiv.), $POCl_3$ (2,5 equiv.), Et_3N (2,0 equiv); 24h (ii) Et_2NH (4,0 equiv.)	48	Et_2O	12	13	11	-

Tabela 1 – Resultados experimentais da síntese do composto **42** (continuação)

Experimento	Condições	Tempo final da reação (h)	Solvente	Rendimento (%)[a]			
				42	**43**	**61**	**86**
17	(i)lactona **60** (1,0 equiv.), $POCl_3$ (2,5 equiv.), Et_3N (3,0 equiv); 24h (ii) Et_2NH (3,0 equiv.)	72	Et_2O	11	17	14	-
18	(i)lactona **60** (1,0 equiv.), $POCl_3$ (1,5 equiv.), Et_3N (2,0 equiv); DMAP (1 mol%); 24h (ii) Et_2NH (3,0 equiv.)	72	Et_2O	11	14	12	-
19	(i)lactona **60** (1,0 equiv.), $POCl_3$ (1,5 equiv.), Et_3N (2,0 equiv); DMAP (5 mol%); 24h (ii) Et_2NH (3,0 equiv.)	72	Et_2O	13	15	17	-

[a] Rendimentos expressos para os compostos **42** e **43** foram calculados considerando-se a lactona **60** como limitante, enquanto para os compostos **61** e **86** o limitante foi o $POCl_3$.
[b] Para condição **3** todos os detalhes experimentais são descritos em 2.1.2.2.
[c] Todas as reações foram conduzidas sob nitrogênio.

Nos experimentos **1, 2** e **4** (Tabela 1), realizou-se a variação do solvente empregado durante a reação, sendo testados diclorometano, éter dietílico e tetraidrofurano, devidamente anidros. O tempo reacional para a etapa **i)** foi de 24 horas. Em nenhum dos casos o solvente favoreceu a formação do produto de interesse (**42**). Entretanto, observa-se que no caso do experimento **2**, no qual emprega-se éter dietílico, o subproduto monoclorado (**43**) foi obtido em maior rendimento (16%) quando comparado aos outros dois experimentos (8 e 10%). Mantendo-se o éter dietílico como solvente e aumentando-se o tempo de reação (experimento **3**) observou-se a formação da substância **42** em 15% de rendimento, e do subproduto **43** em 20%. Reduzindo-se o tempo da etapa **i)** para 5 min, a formação de **42** foi evidenciada nos experimentos **5** (5%) e **6** (12%) nos quais se utiliza éter dietílico e diclorometano, respectivamente. No caso do experimento **7**, que empregou THF como solvente, tal produto não foi formado.

Uma vez que a etapa de formação do intermediário **85** corresponde a um equilíbrio (Esquema 9), pelo incremento de $POCl_3$ e/ou trietilamina, esperava-se deslocar o equilíbrio para a formação de **85**. Por esse

procedimento, tentou-se aumentar o rendimento dessa etapa de formação do composto **85**, uma vez que Näsman (1990) isolou esse intermediário com rendimento de 60-65%.

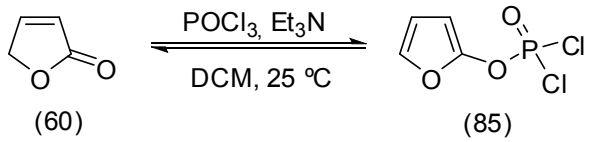

(60) (85)

Esquema 9 - Etapa de formação do intermediário **85**.

O aumento da quantidade de $POCl_3$, conforme descrito nos experimentos **8-11** não favoreceu a formação do composto **42**. Aumentando-se o tempo reacional da etapa **i)** para 24 horas (experimentos **14** e **16**), o composto **42** foi formado em 12% de rendimento quando se usou éter dietílico como solvente (experimento **16**). Realizou-se um acréscimo de 1 equivalente de $POCl_3$ no experimento **17** comparado ao **15**; entretanto, não foi significativo o aumento no rendimento do composto **42** (de 9 para 11%) e do subproduto **43** (de 14 para 17%). No experimento **12** triplicou-se o número de equivalentes de trietilamina comparado ao experimento **5**. Consequentemente, o produto de interesse não foi formado e o subproduto **43** obtido em 19%.

Segundo TIMPERLEY e WATERS (2005), a síntese dos compostos dialquil *N*-fluoroalquilfosforamidatos **87** e **88** só foi possível quando o material de partida foi submetido às condições reacionais na presença do catalisador 4-dimetilaminopiridina (DMAP) e, mesmo assim, com rendimentos moderados (Esquema 10).

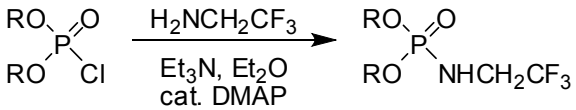

R = *n*-Pr (87) 49%
i-Pr (88) 25%

Esquema 10 - Síntese dos dialquil *N*-fluoroalquilfosforamidatos **87** e **88** descrita por TIMPERLEY e WATERS (2005).

Dessa forma, a lactona **60** foi submetida às condições descritas na condição **3**, que em maior rendimento forneceu o composto **42** de interesse (15%). Porém, utilizou-se o catalisador DMAP em quantidades de **1** e **5** mol% (condições **18** e **19**, respectivamente). Surpreendentemente, o produto **42** foi

obtido em menor rendimento nas duas situações, não sendo alcançado o objetivo.

Os compostos **61** e **86** foram caracterizados apenas por espectrometria de massas devido às estruturas simples. A presença do pico do íon molecular em *m/z* 189 para o composto **61** (Figura 2) é consistente com a fórmula molecular deste composto ($C_4H_{10}Cl_2NOP$).

Com relação ao composto **86** observou-se em seu espectro de massas a presença de um pequeno pico de valor *m/z* 226, que corresponde ao pico do íon molecular. Além disso, o pico de valor de *m/z* igual a 72 apresentou intensidade igual a 100%. A grande intensidade para este pico é devido à presença de dois grupos etila ligados a nitrogênio na estrutura do composto (Figura 3).

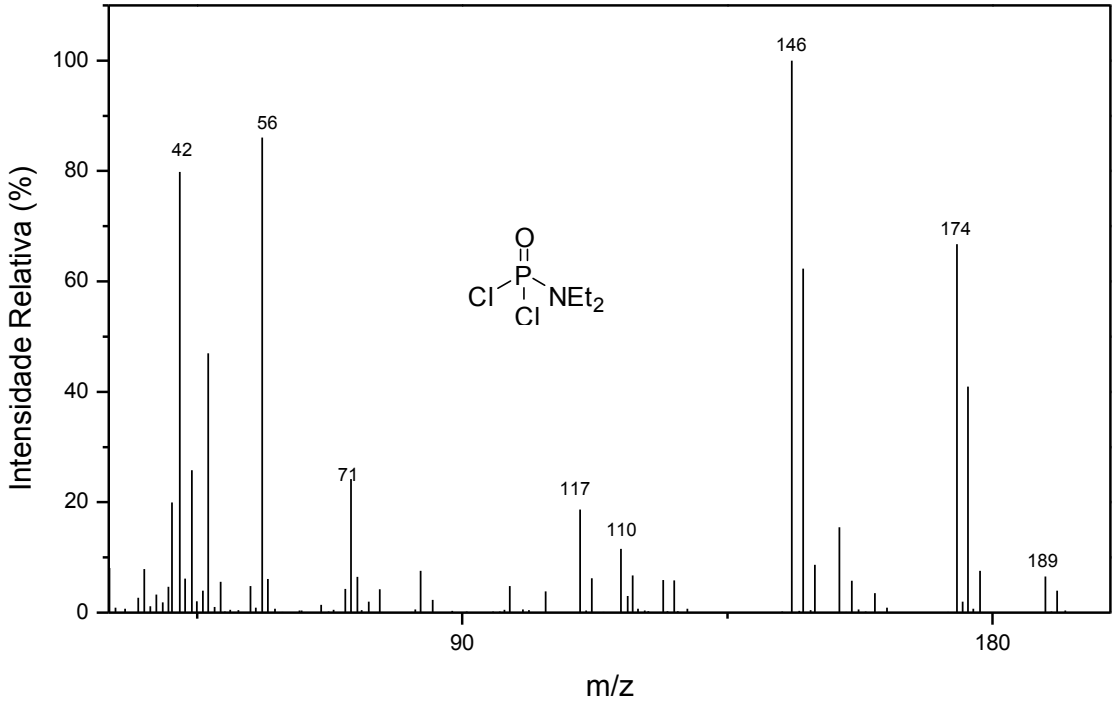

Figura 2 – Espectro de massas do subproduto **61**.

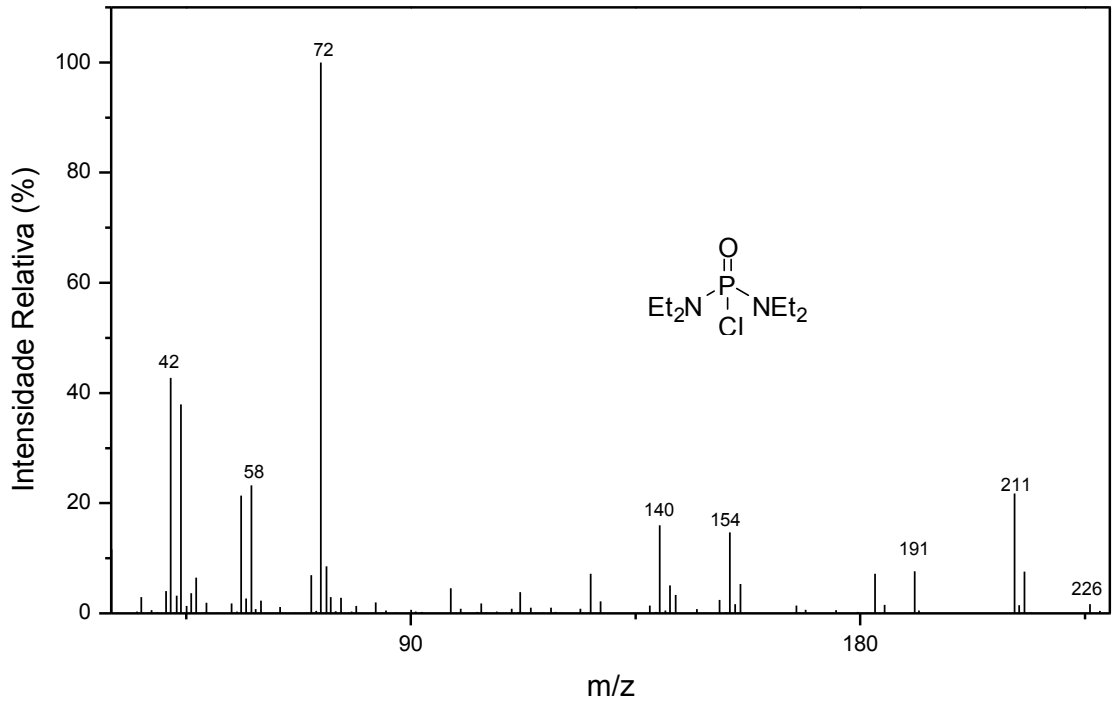

Figura 3 – Espectro de massas do subproduto **86**.

2.3.2. Síntese de compostos fenólicos organofosfatos diclorados

Diante das tentativas infrutíferas de otimização da síntese dos fosforamidatos contendo o anel lactônico, buscou-se na literatura grupos interessantes do ponto de vista químico e biológico para desenvolvimento de novos fosforamidatos.

Compostos apresentando fenóxidos diretamente ligados ao átomo de fósforo são comuns na literatura e apresentam diversidade de atividades biológicas: anticâncer (MCGUIGAN *et al*., 2005; VOORDE *et al*., 2011; BORRELO *et al*., 2009; CONGIATU *et al*., 2006; KIRAN *et al*., 2008; MCGUIGAN *et al*., 2011a); anti-HIV (UCKUN *et al*., 2005; DERUDAS *et al*., 2009); antimalárico (MARA *et al*., 2011); anti hepatite C (GARDELLI *et al*., 2009; MCGUIGAN *et al*., 2011b); inibidores de *Trypanosoma cruzi* (RUDA *et al*., 2010), herpes simplex e vírus influenza dos tipos A e B (DERUDAS *et al*., 2010), bem como inibidores de urease (DOMINGUEZ *et al*., 2008). Neste último caso, particularmente, vale a pena chamar a atenção para o fenilfosforodiamidato (PPD), que apresenta estrutura semelhante aos compostos que são objetivo desse trabalho. Juntamente com os compostos *N*-n-butiltiofosforiltriamida (NBPT), *N*-n-butilfosforiltriamida (NBPTO) e *N*-

diaminofosforil-4-fluorobenzamida (Flurofamida), são usados como modelo no desenvolvimento de novas substâncias com potencial atividade inibidora de urease (Esquema 11).

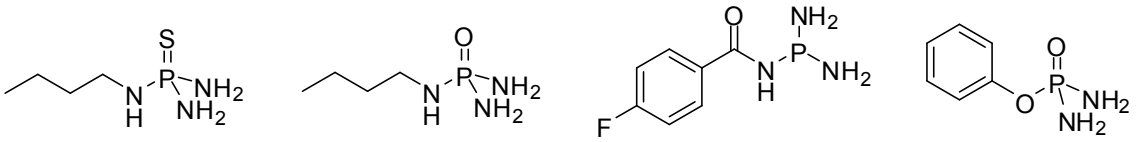

NBPT **NBPTO** **Flurofamida** **PPD**

Esquema 11 – Alguns inibidores de urease usados como modelo para design de novos compostos.

Uma vantagem da substituição da lactona **60** por fenóis substituídos é a maior nucleofilicidade dos fenóxidos comparado ao oxigênio carbonílico da lactona, o que pode favorecer a obtenção de substâncias em maior rendimento. DERUDAS *et al*. (2010) relatam, inclusive, a obtenção de produtos resultantes do tratamento do α-naftol com $POCl_3$ em 95% de rendimento.

Com base em todo esse conhecimento precedente da literatura, idealizou-se que os fosforamidatos poderiam ser obtidos a partir do tratamento inicial de fenóis substituídos com $POCl_3$ e posterior reação com aminas. A primeira etapa do desenvolvimento do presente estudo consistiu, portanto, na síntese de compostos organofosfatos fenólicos diclorados.

DERUDAS *et al*. (2010) prepararam o diclorado correspondente à reação do α-naftol (1 equivalente) gotejando-se a esse reagente uma mistura de $POCl_3$ (1 equivalente) e TEA anidra (1 equivalente) a -78 ºC por um período de 30 minutos. Na sequencia, a mistura foi mantida sob agitação ao longo da noite à temperatura ambiente, levando à formação do produto de interesse em 95% de rendimento. O tratamento do 4-bromofenol, um dos materiais de partida neste trabalho, segundo as condições descritas por DERUDAS *et al*. (2010) (Esquema 12) não levou ao produto desejado.

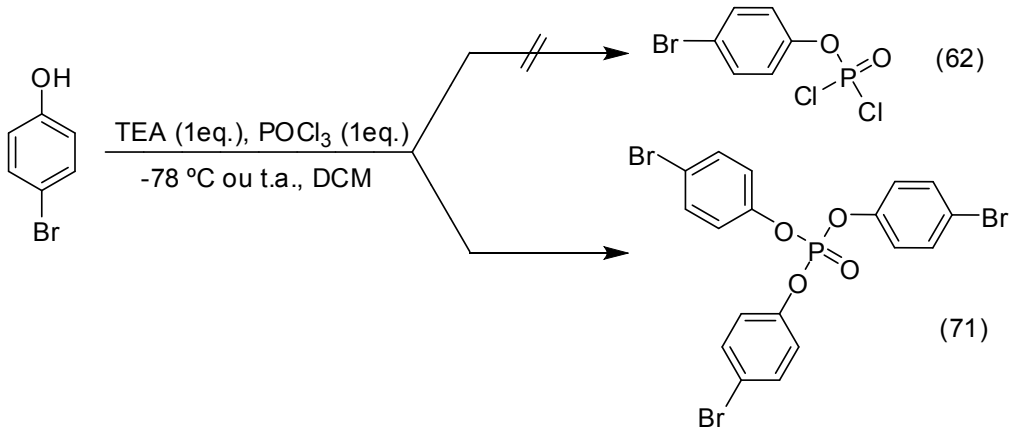

Esquema 12 – Tentativa de síntese do 4-bromofenil fosforodicloridato **(62)** segundo condições descritas por DERUDAS *et al*. (2010).

A adição gota-a-gota da mistura de TEA e $POCl_3$ por 30 minutos ao fenol, seja à temperatura ambiente ou à -78 ºC, favoreceu a formação do composto **71** em detrimento do composto de interesse (**62**). A formação de triarilfosfato já havia sido evidenciada por DHAWAN e REDMORE (1986) ao tratarem 2 equivalentes de fenóis substituídos com 1 equivalente de $POCl_3$ na presença de ácido de Lewis ($AlCl_3$), levando a uma mistura dos produtos monoarilfosfato e triarilfosfato. No entanto, a formação do diarilfosfato não foi evidenciada.

Buscou-se na literatura alternativas que pudessem auxiliar na resolução do problema encontrado. Notou-se que as sínteses baseavam-se na mesma metodologia, porém, alterando-se o número de equivalentes adicionados ou a ordem como as substâncias são adicionadas, conforme sumarizado na Tabela 2:

Tabela 2: Condições reacionais para síntese de fosforados diclorados **62-65**

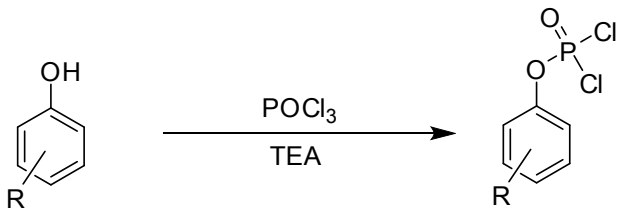

Condição	Condições	Solvente	Referências, (Rendimento) (%)
1	i) $POCl_3$ (1 equiv.); ii) fenol (1 equiv.); iii) TEA (1 equiv.), –78ºC; iv) -78 ºC → t.a.; t.r.=12-16h.	Et_2O	MCGUIGAN *et al*. (2005), (78) Patente US 7951787 (77) YUAN *et al*. (2009), (n.i.)* RUDA *et al*. (2010), (n.i.)* DERUDAS *et al*. (2009), (n.i.)*
2	i) $POCl_3$ (30 equiv.); ii) fenol (1 equiv.); iii) TEA (1 equiv.) a 20 ºC; t.r.=1h	DCM	WANG *et al*. (2010), (51)
3	i) $POCl_3$ (1,1 equiv.); ii) fenol (1 equiv.) + TEA (1 equiv.), 0ºC; 2-3h; iv) 0 ºC → t.a.; t.r.=12-16h; v) refluxo, 2h	Et_2O	UCKUN *et al*. (2005), (n.i.)*
4	i) $POCl_3$ (6 equiv.) + $AlCl_3$ (3,4 mol%); ii) fenol (1 equiv.); refluxo, 6h	DCM	ORLOFF *et al*. (1958), (77)
5	i) $POCl_3$ (1 equiv.) + $AlCl_{3(cat)}$; ii) fenol (2 equiv.); refluxo, 6h	DCM	DHAWAN *et al*. (1986), (n.i.)*

* n.i. = composto não isolado

Diferentemente do que foi observado no experimento representado no Esquema 4, reações realizadas segundo as condições **1-2** da Tabela 2 favoreceram a formação do produto de interesse. Entretanto, foi evidenciada via CG/EM a formação do subproduto **71**. Tentativas de separação dos compostos por coluna de sílica gel, sílica gel neutralizada com 1% de trietilamina ou alumina, foram infrutíferas. Independentemente do solvente utilizado nas condições **1** e **2**, éter dietílico ou diclorometano, os resultados obtidos foram similares. Entretanto, observou-se que o sal formado é insolúvel em éter dietílico, enquanto o composto de interesse **62** é solúvel, o que favoreceria a etapa posterior de filtração.

Diante da dificuldade de se isolar o composto **62**, optou-se pela realização da reação conforme descrito na condição **3**. A implementação da metodologia sintética para obtenção do composto **62** a partir de 4-bromofenol

mostrou-se bem sucedida segundo as condições descritas por UCKUN *et al*. (2005).

Uma mistura contendo o fenol (1 equivalente) e TEA anidra (1,1 equivalente) dissolvidos em éter dietílico anidro foi preparada e adicionada gota-a-gota a um balão contendo $POCl_3$ (1,1 equivalente) dissolvido em éter dietílico anidro, em ambiente de nitrogênio. A adição foi realizada por um período de 1h, sendo a mistura mantida resfriada a 0 ºC. Posteriormente, permitiu-se que a temperatura da mistura retornasse à temperatura ambiente gradualmente. À medida que se adicionava uma gota da mistura já era possível observar a formação do sal que permanecia em suspensão. Acreditava-se, portanto, que a reação poderia ser interrompida após alguns minutos. No entanto, após 6 horas de reação evidenciou-se ainda a presença de fenol via cromatografia em camada delgada. Por isso, o meio reacional foi mantido sob agitação por um período de 18 horas, o que levou ao total consumo do fenol, não sendo necessário refluxar a reação conforme descrito na condição **3**. A proposta mecanística para a formação dos compostos **62-65** está representada no Esquema 13.

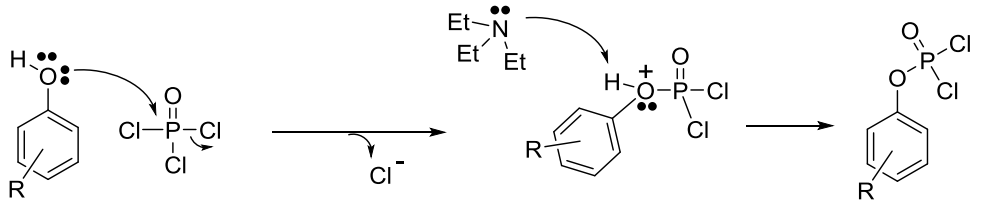

R = *p*-Br (62)
o-Br (63)
p-NO_2 (64)
p-F (65)

Esquema 13 - Proposta mecanística para a formação dos compostos **62-65**.

Na sequencia o precipitado formado foi removido por filtração à vácuo em funil de vidro sinterizado e o precipitado lavado com éter dietílico anidro. A mistura reacional foi exaustivamente concentrada a baixa pressão em evaporador rotatório levando à formação de um óleo amarelo claro.

Procedimento similar efetuado com as substâncias 2-bromofenol, 4-nitrofenol e 4-fluorofenol resultou na obtenção dos respectivos diclorados em excelentes rendimentos (Esquema 14). Esses resultados demonstram que a metolodogia corresponde a uma alternativa viável para obtenção dos organofosfatos diclorados.

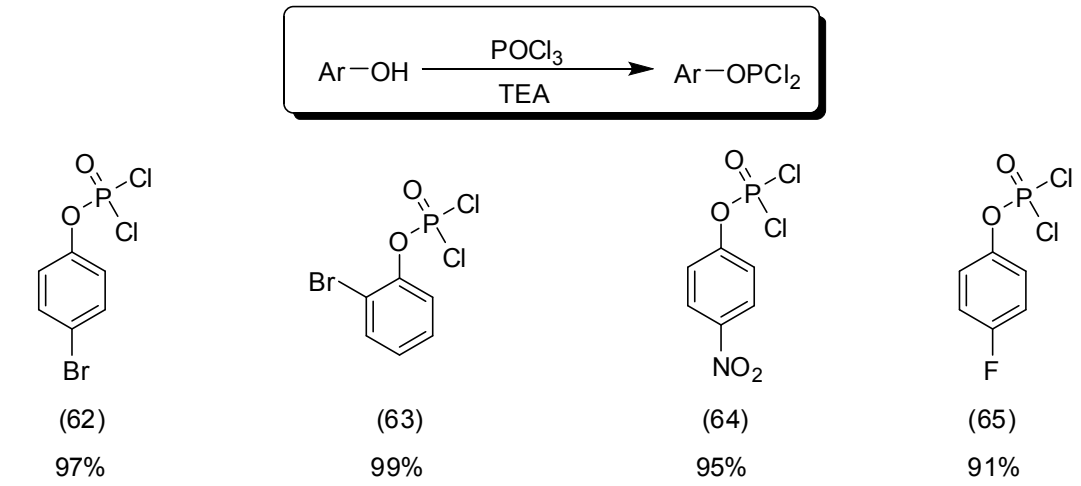

Esquema 14 – Produtos diclorados obtidos a partir do tratamento de fenóis com $POCl_3$ e TEA.

É importante salientar que esses compostos não foram purificados devido à elevada reatividade e instabilidade apresentada. No entanto, a pureza observada via CG/EM foi satisfatória (acima de 91%). RUDA *et al*. (2010) sintetizaram compostos diclorados derivados de fenóis substituídos em posição *para* ($–NO_2$, $-OCH_3$ e $–CH_3$), e nas posições *meta* e *orto* ($–CH_3$). Todos os compostos foram submetidos a reações na sequencia sem purificação prévia devido à instabilidade dos mesmos. Buscando verificar um possível produto de degradação, uma alíquota do composto **62** foi deixada exposta ao ar em uma bancada do laboratório durante 24 horas. Transcorrido esse tempo, o óleo amarelado adquiriu um aspecto sólido. O material foi avaliado via CG/EM antes e após exposição ao ar e constatou-se que o diclorado se decompunha ao fenol correspondente. A reatividade e instabilidade de organofosfatos diclorados é destacada também por ROMAN *et al*. (2011). O diclorado formado, sem purificação prévia, foi reagido com fenóis substituídos para fornecer os respectivos produtos monoclorados, também instáveis, com rendimento variando de 59 a 93% (Esquema 15).

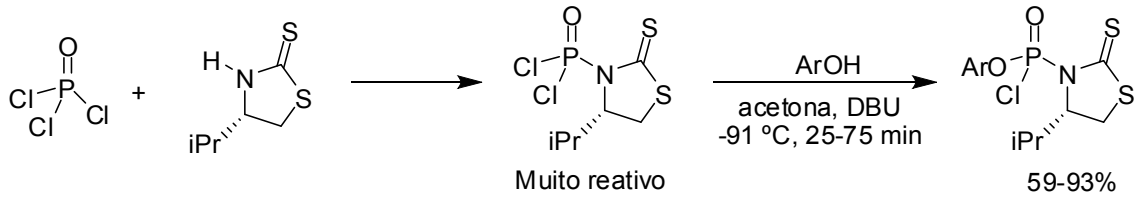

Esquema 15 – Estrutura geral de compostos fosforados reativos e instáveis descritos por ROMAN *et al*. (2011).

Além de substituintes halogênios no fenol, uma opção bastante interessante é a presença do grupo $–NO_2$ em posição *para*. Um bom grupo abandonador ligado ao átomo de fósforo contribui para a atividade inseticida, e o substituinte $–NO_2$ em posição *para* torna o fenóxido ainda melhor abandonador. Este efeito está relacionado com o mecanismo de ação do paration etílico, inseticida disponível comercialmente. Em sua forma ativada, paraoxon etílico, a inativação da acetilcolinesterase ocorre via ataque nucleofílico de um grupo hidroxila do aminoácido serina, presente na enzima, ao átomo de fósforo do inibidor, carregado parcial positivamente. Consequentemente, tem-se a formação de um complexo enzima-inibidor bastante estável, e a enzima torna-se inibida (Esquema 16) (FUKUTO, 1990).

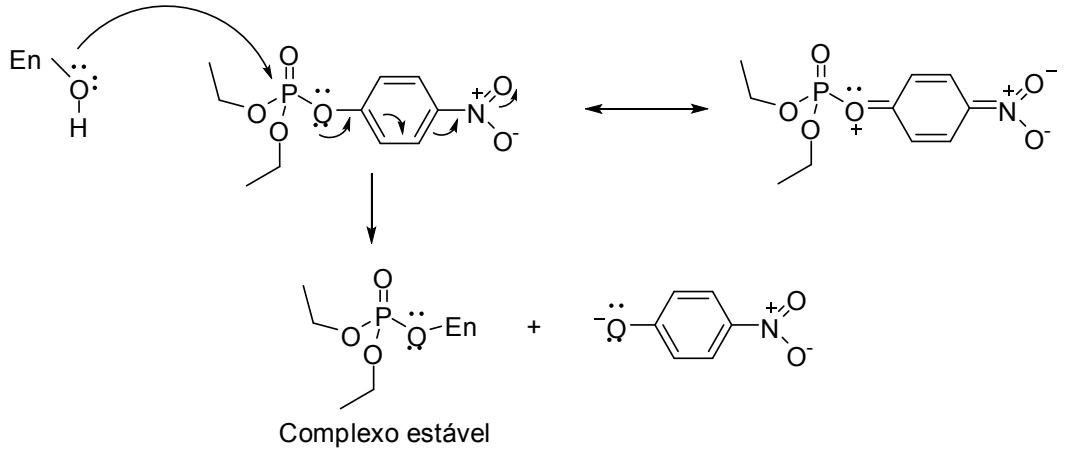

Esquema 16 – Efeito de um substituinte retirador de elétrons na reatividade do paraoxon etílico (forma ativada do paration etílico).

Em primeiro momento foram então sintetizados quatro diclorados (**62-65**) e caracterizados via espectroscopia no IV e de RMN, bem como espectrometria de massas. As informações espectroscópicas e espectrométricas obtidas são apresentadas nas Seções 2.1.2.3 a 2.1.2.6.

A ausência da banda na faixa de 3400-3600 cm^{-1} no espectro no IV do composto **62** (Figura 4), correspondente ao estiramento do grupo hidroxila de fenol, confirmou o consumo do material de partida da reação. As duas bandas observadas em 1182 e 1159 cm^{-1} podem ser atribuídas ao estiramento de ligação P = O, uma vez que a banda relacionada a este grupamento pode aparecer como um dupleto. Quanto aos demais diclorados (**63-65**), as bandas de absorção referentes ao estiramento de ligação P = O foram observadas, respectivamente, em 1200 e 1160 cm^{-1}, 1190 e 1159 cm^{-1} e 1175 e 1091 cm^{-1}.

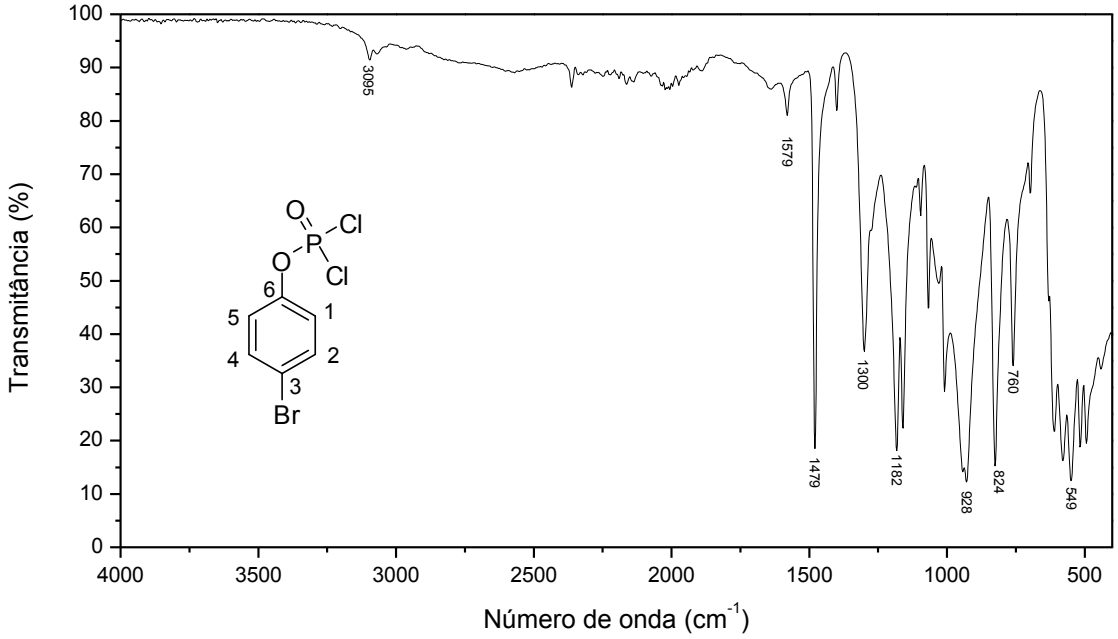

Figura 4 – Espectro no IV do diclorado **62**.

O espectro de RMN de ^{1}H do composto **62** é apresentado na Figura 5. O sinal correspondente aos hidrogênios aromáticos H-1 e H-5, mais blindados por estarem em posição *orto* em relação ao oxigênio, foi observado em δ_H 7,08-7,23. Para o diclorado **64**, o sinal para os hidrogênio H-1 e H-5 foi observado ao redor de δ_H 7,30-7,51, enquanto para **65** foi observado em δ_H 6,97-7,22. Os hidrogênio aromáticos H-2 e H-4, mais desblindados, apresentaram sinal em δ_H 7,42-7,59, δ_H 8,18-8,39 e δ_H 7,24-7,32 para os compostos **62**, **64** e **65**, respectivamente. Esses sinais são aqueles esperados para um anel aromático 1,4-dissubstituído (SILVERSTEIN *et al*., 2006). O sinal em δ_H 6,95-7,28 no espectro de RMN de ^{1}H do composto **63**, integrado para 2 hidrogênios, são referentes a H-1 e H-3, devido ao maior efeito de blindagem pelo oxigênio nas posições *orto* e *para.* O sinal em δ_H 7,32-7,50 é referente a H-2, e δ_H 7,52-7,70 a H-3.

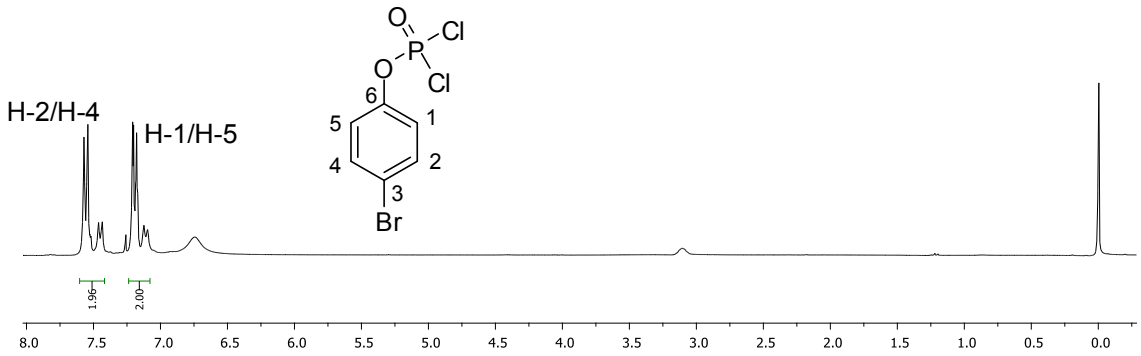

Figura 5 – Espectro de RMN de ^{1}H (300 MHz, $CDCl_3$) do diclorado **62**.

No espectro de RMN de ^{13}C do diclorado **62** (Figura 6), o sinal correspondente a C-6 foi observado em δ_C 148,77. Quanto aos demais diclorados, os sinais para este carbono foram observados em δ_C 147,70 (d, $^{2}J_{C,P}$ = 8,2, C-6) (**63**), 155,36 (**64**) e 145,46 (**65**). O desdobramento do sinal de C-6 é decorrente do acoplamento do átomo de carbono com fósforo. Os espectros de RMN de ^{1}H e ^{13}C dos compostos **63**, **64** e **65** foram obtidos em qualidade razoável, uma vez que as substâncias não foram previamente purificadas devido à capacidade de degradarem na sílica.

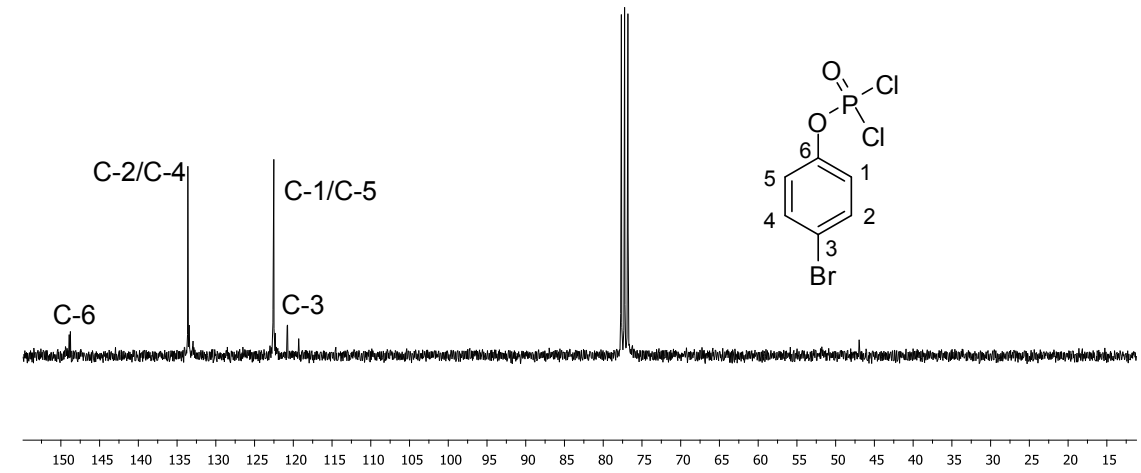

Figura 6 – Espectro de RMN de ^{13}C (75 MHz, $CDCl_3$) do diclorado **62**.

No espectro de massas do diclorado **62** (Figura 7), a presença do pico em *m/z* 288 é consistente com a fórmula molecular deste composto ($C_6H_4BrCl_2O_2P$). O pico do íon molecular também foi observado nos espectros dos diclorados **63** (*m/z* 288), **64** (*m/z* 255) e **65** (m/z 228).

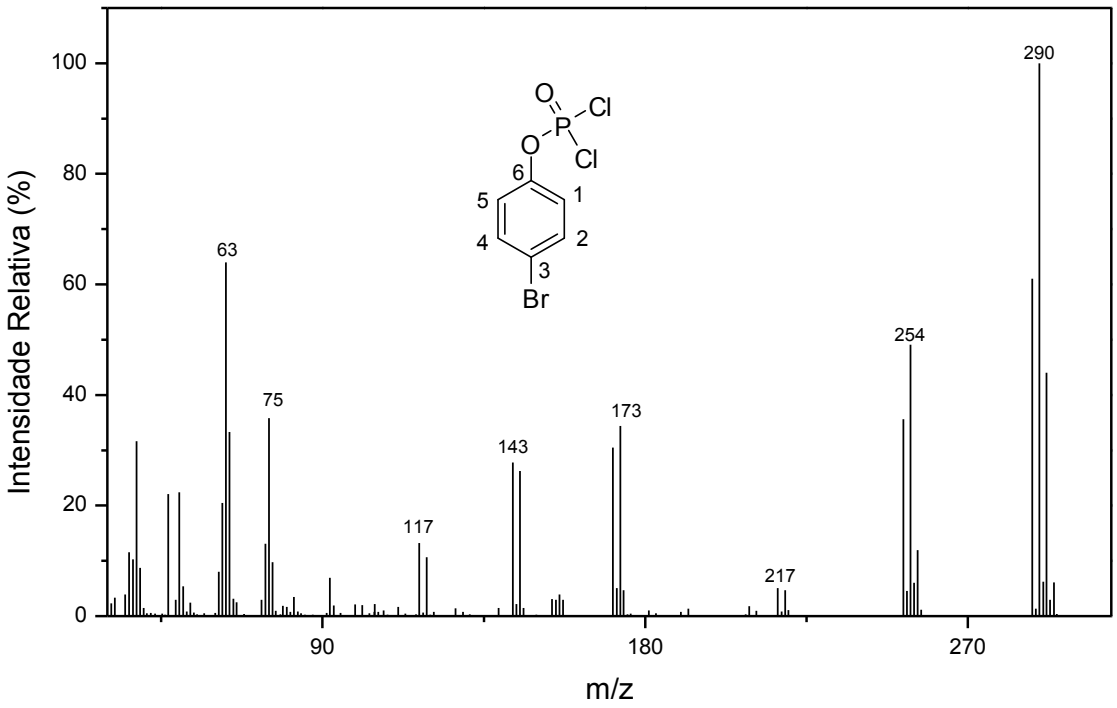

Figura 7 - Espectro de massas do composto **62**.

Os picos observados nos espectros de massas dos diclorados **62** e **63** em *m/z* 290 ($[M+2]^{+\bullet}$, 100 e 10%, respectivamente) confirmaram a presença do elemento bromo nas estruturas. Além do elemento bromo, a presença de dois átomos do elemento cloro nos compostos **62** e **63** justificou os picos observados em *m/z* 292 ($[M+4]^{+\bullet}$, 44 e 5%, respectivamente). Os picos observados em *m/z* 259 e *m/z* 232 para os diclorados **64** e **65**, respectivamente, referentes a $[M+4]^{+\bullet}$, confirmaram a presença de dois átomos de cloro nas estruturas.

2.3.3. Síntese dos fosforamidatos

Tendo assegurada a síntese dos fosforados diclorados **62-65** na primeira etapa em excelentes rendimentos (91-99%), voltou-se a atenção para a obtenção dos fosforamidatos.

Normalmente a reação é realizada empregando-se o organofosfato diclorado na presença de uma base, e posterior adição das aminas. Trietilamina (ROMAN *et al*., 2011; MARA *et al*., 2011; GARDELLI *et al*., 2009; RUDA *et al*., 2010; VOORDE *et al*., 2011; TAI *et al*., 2011, UCKUN *et al*., 2005) e *N*-metilimidazol (VOORDE *et al*., 2001; MCGUIGAN *et al*., 2005;

BORRELO *et al*., 2009; CHO *et al*., 2011; CONGIATU *et al*., 2006; RUDA *et al*., 2010) são as bases mais comumente empregadas nesse tipo de reação (Esquema 17).

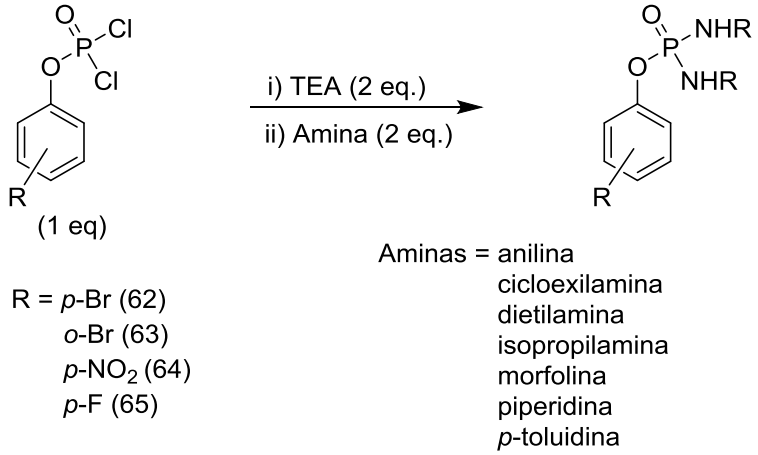

Esquema 17 – Esquema geral para síntese de fosforamidatos, a partir dos compostos diclorados **62-65**.

A segunda etapa empregada na síntese dos fosforamidatos foi realizada conforme metodologia descrita por UCKUN *et al*. (2005). Os organofosfatos diclorados **62-65**, sem prévia purificação, foram submetidos à reação de substituição nucleofílica com aminas, na presença de trietilamina a 0 ºC (UCKUN *et al*., 2005; ROMAN *et al*., 2011). À medida que ocorre a adição da amina, ligeiro aquecimento da mistura é observado. A literatura relata, ainda, o processo de adição de trietilamina à temperatura de -78 ºC (CONGIATU *et al*., 2006; DERUDAS, *et al*., 2009; VOORDE, *et al*., 2011). Após o fracionamento em coluna de sílica-gel foram isolados os compostos **66-73, 75-76 e 78-84**.

A estrutura dos compostos obtidos e os correspondentes rendimentos são apresentados na Tabela 3. As condições de reação não foram otimizadas. No entanto, de modo geral, as reações se completaram 18 horas após a adição de trietilamina, à temperatura ambiente.

Tabela 3 - Resultados experimentais da reação de síntese dos compostos fosforados **66-84**

Código (Rendimento %)	Estrutura	Código (Rendimento %)	Estrutura
66 (29)	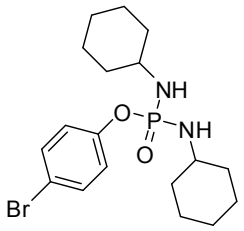	**67** (8)	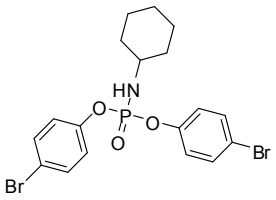
68 (32)	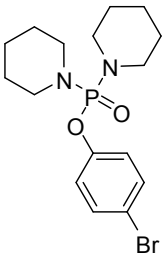	**69** (13)	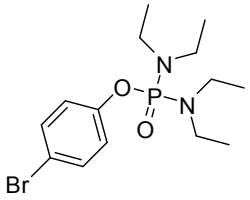
70 (16)	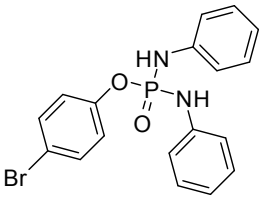	**71** (26)	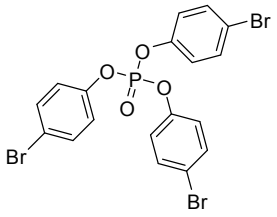
72 (46)	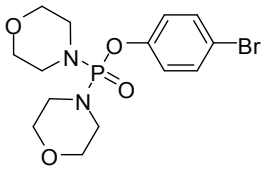	**73** (13)	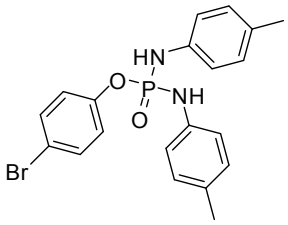
74 (0)	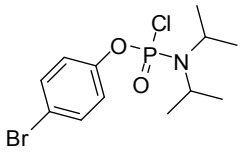	**75** (36)	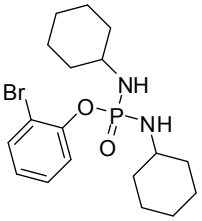
76 (34)	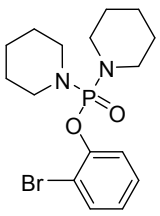	**77** (0)	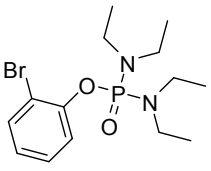

Tabela 3 - Resultados experimentais da reação de síntese dos compostos fosforados **66-84** (continuação)

Código (Rendimento %)	Estrutura	Código (Rendimento %)	Estrutura
78 (32)	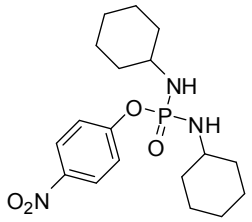	**79** (12)	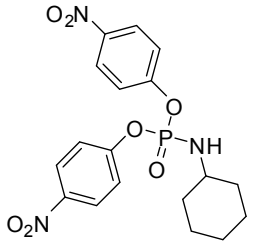
80 (11)	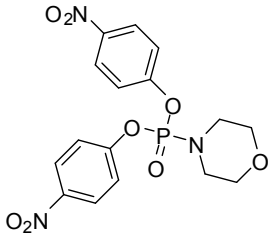	**81** (25)	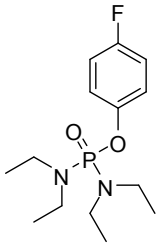
82 (55)	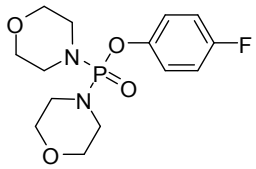	**83** (30)	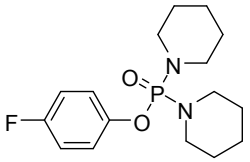
84 (28)	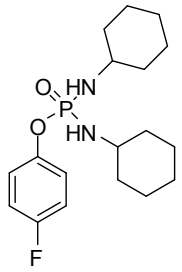		

Os dados espectroscópicos correspondentes aos compostos **66-84** estão descritos nas seções 2.1.2.7 a 2.1.2.24. Os espectros no infravermelho, de RMN de ^{1}H e de ^{13}C, bem como o espectro de massas dos compostos **66-73, 75-76 e 78-84** encontram-se em anexo.

Um dos primeiros compostos sintetizados foi o de número **66**. Uma descrição do processo de caracterização deste composto será apresentada a seguir.

Obtida como um sólido branco amorfo (T_f = 89,4-91,4 ^{o}C), a substância foi caracterizada empregando-se técnicas de espectroscopia no IV e de RMN de ^{1}H e ^{13}C e espectrometria de massas.

A banda de estiramento de –NH no IV do composto **66** (Figura 8) apresentou-se alargada em 3223 cm^{-1} devido à formação de ligações de hidrogênio intermoleculares. Segundo Pretsch (1989), o estiramento de ligação P-N-C pode aparecer como duas bandas em 1110-930 e 770-680 cm^{-1}, de modo que é razoável atribuir as bandas em 1095 e 738 cm^{-1} a esse estiramento.

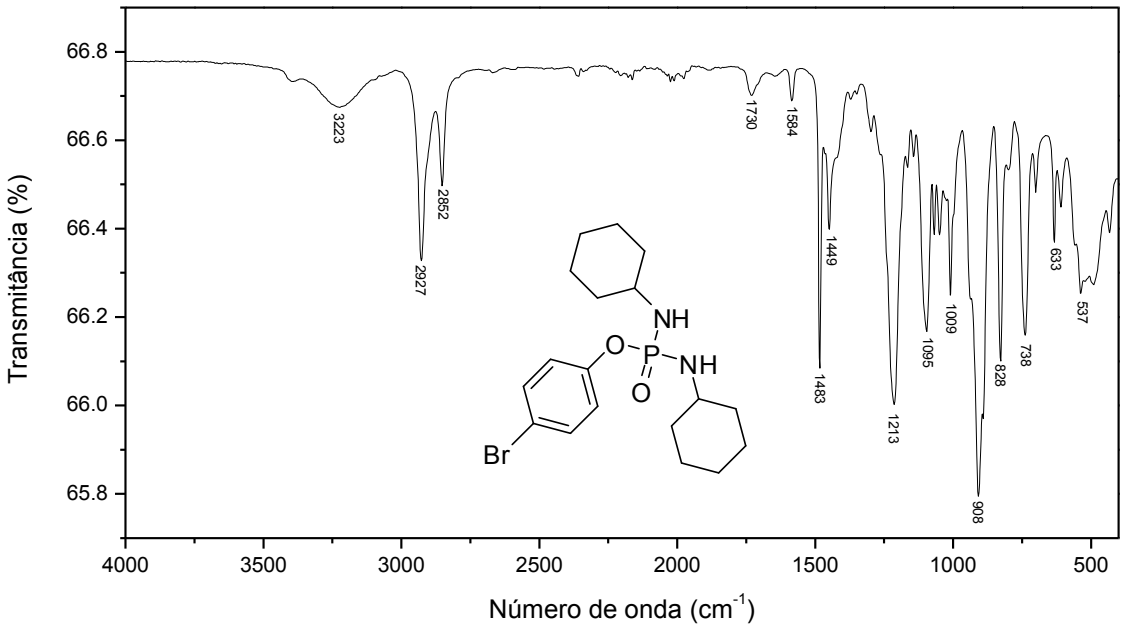

Figura 8 - Espectro no IV do composto **66**.

No espectro de RMN de ^{1}H (Figura 9) o multipleto em δ_H 1,05-1,92, integrado para 20 hidrogênios, é referente aos átomos de hidrogênio metilênicos dos anéis do grupo cicloexila. O sinal em δ_H 2,59, um tripleto integrado para dois átomos de hidrogênio (t, $J_{N\underline{H},P} \approx J_{N\underline{H},12} \approx 10,0$; 2H, -N<u>H</u>), refere-se aos átomos de hidrogênio do grupo amino (-N<u>H</u>), e o sinal em δ_H 2,98-3,14, multipleto integrado para dois átomos de hidrogênio, corresponde aos átomos de hidrogênio –C<u>H</u> dos anéis cicloexila. Observaram-se ainda sinais em δ_H 7,08-7,13 e δ_H 7,36-7,41, referentes aos hidrogênios (H-1/H-5) e (H-2/H-4), respectivamente, do aromático.

Similarmente ao que ocorreu com os diclorados **62-65**, alguns sinais no espectro de RMN de ^{13}C (Figura 10) encontraram-se desdobrados devido aos acoplamentos C-P. Os carbonos C-8/C-9/C-10 apresentaram-se como simpletos em δ_C 25,32 e 25,58, o que está de acordo com os valores de

deslocamento químico descritos na literatura para um grupo cicloexila ligado ao átomo de nitrogênio (PRETSCH, 1989). Em razão da proximidade dos deslocamentos químicos, as atribuições referentes a esses carbonos podem estar invertidas. O sinal em δ_C 36,18 (tripleto aparente, $^3J_{C\text{-}P}$ = 5,1 Hz) é referente aos átomos de carbono metilênicos C-7/C-11. Estes sinais apresentaram-se como um aparente tripleto, provavelmente devido à sobreposição dos sinais referentes a dois dupletos. Pelo fato de a substância possuir dois anéis de seis membros, embora exista aparente simetria entre eles, pode haver algum arranjo diferenciando-os ligeiramente, o que justificaria a formação desses dupletos. Observaram-se ainda sinais em δ_C 50,86, referente ao átomo de carbono C-12; em δ_C 116,99, referente ao C-3; em δ_C 122,25, referente ao átomo C-1/C-5 (d; $^3J_{C\text{-}P}$ = 4,9 Hz); em δ_C 132,65 referente ao átomo C-2/C-4 e em δ_C 150,83 (d, $^2J_{C\text{-}P}$ = 6,5 Hz) referente ao carbono C-6. Os valores das constantes de acoplamento encontram-se de acordo com a literatura (TORRES *et al*., 2008; SOUZA *et al*., 2006; SOUZA *et al*., 2004). Curiosamente, para os compostos **78** e **79** foi observado acoplamento do fósforo com o carbono apenas em longas sequencias PNCC (^3J), mas não foi observado com sequencia PNC (^2J). Esta situação também é relatada por SOUZA *et al*. (2006).

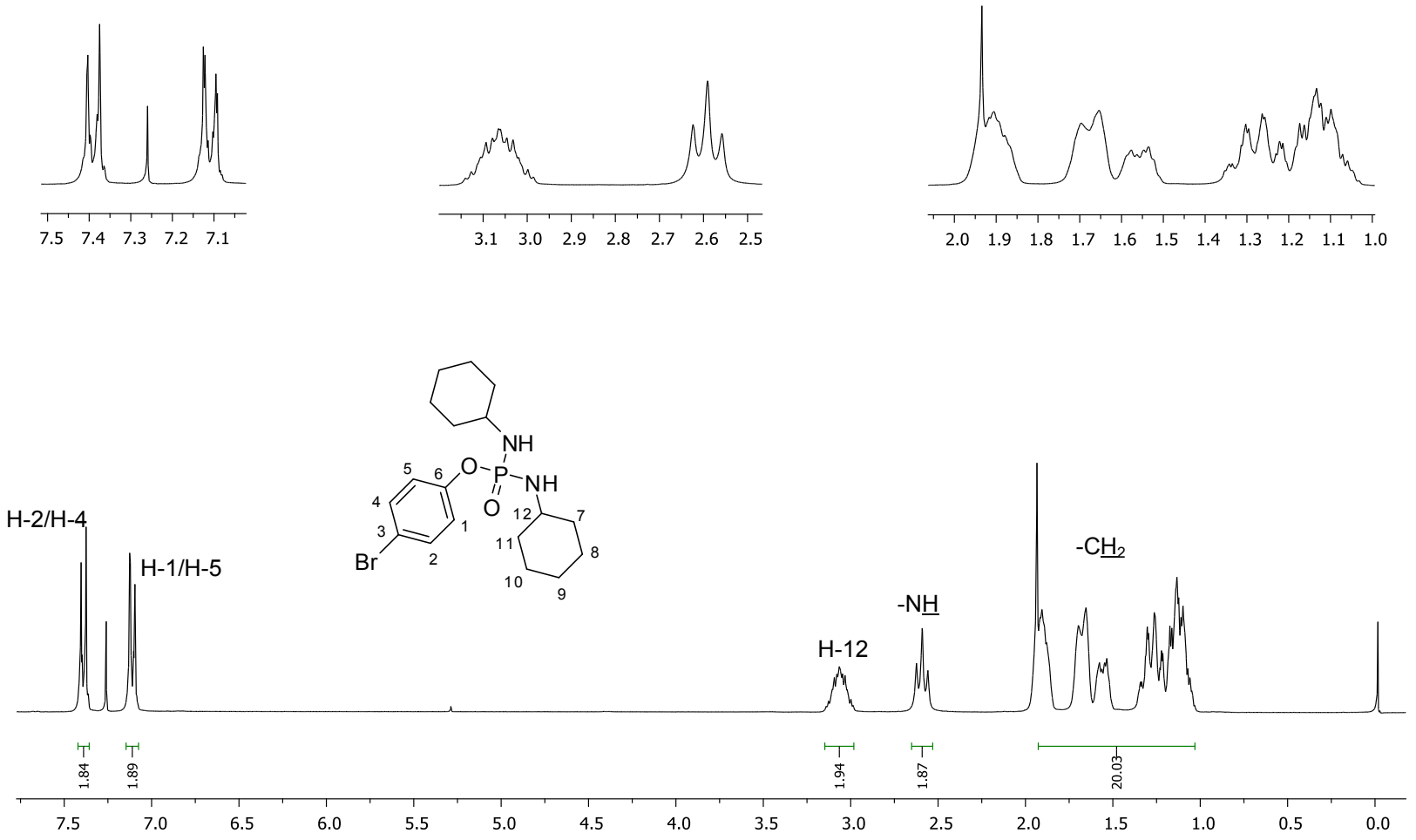

Figura 9 - Espectro de RMN de ^{1}H (300 MHz, $CDCl_3$) do composto **66**.

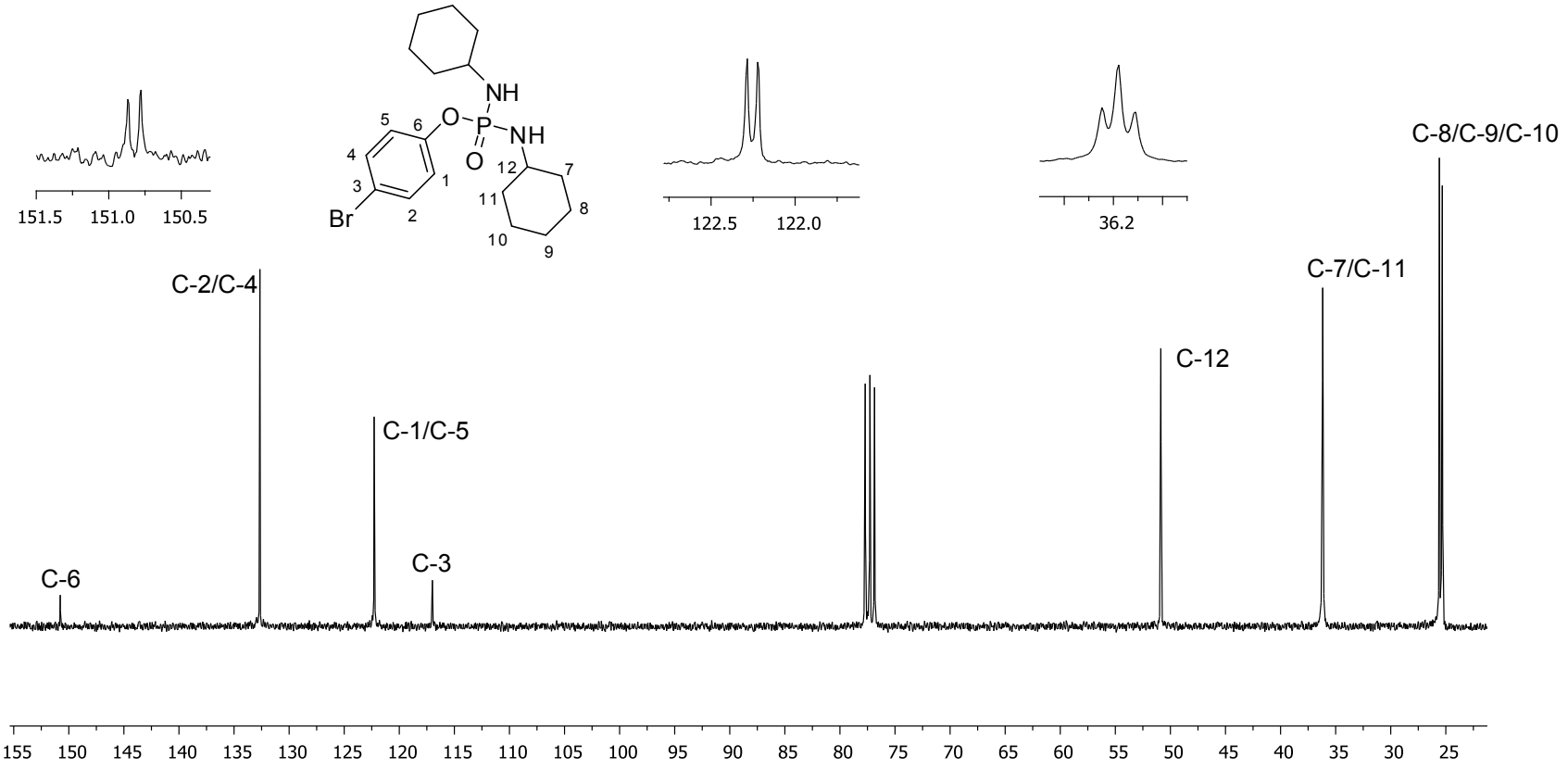

Figura 10 - Espectro de RMN de ^{13}C (75 MHz, $CDCl_3$) do composto **66**.

Ainda com relação ao composto **66**, isolado em 29% de rendimento, observou-se em seu espectro de massas a presença de um pequeno pico de valor *m/z* 414, que corresponde ao pico do íon molecular. Além disso, o pico de valor de *m/z* igual a 98 apresentou intensidade igual a 100%. A grande intensidade para este pico é devido à presença de dois grupos cicloexila na estrutura do composto, uma vez que o valor de *m/z* igual a 98 poderia ser atribuído a um anel cicloexila mais um grupo -NH (ver estrutura do fragmento correspondente a *m/z* 98 para o composto **66** na Figura 11). Ainda com respeito ao espectro de massas do fosforado **66**, o fragmento com valor de *m/z* 98 é comum aos compostos **67**, **75**, **78**, **79** e **84**.

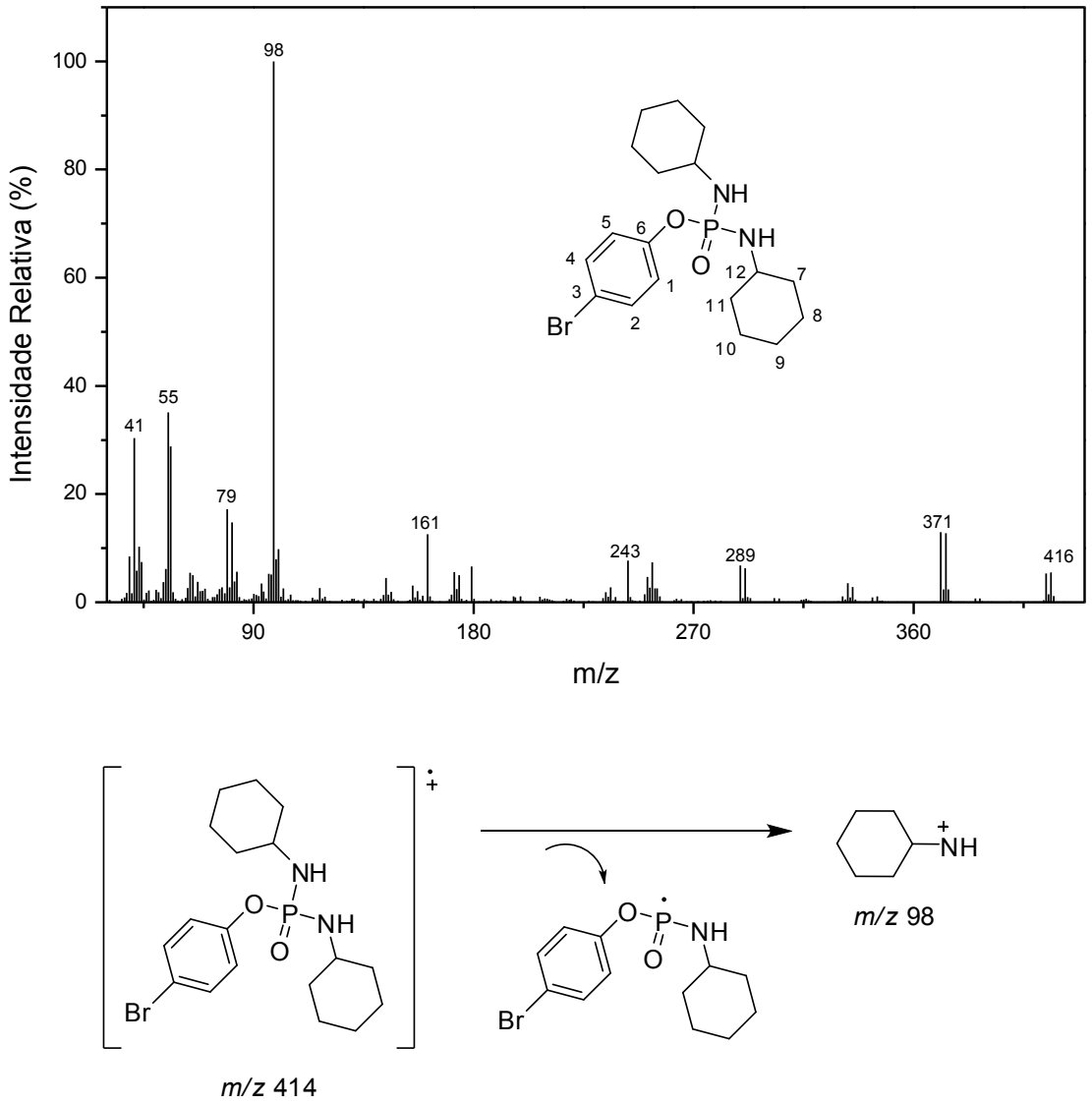

Figura 11 - Espectro de massas e principal processo de fragmentação do composto **66**.

Todas as substâncias mostradas na Tabela 3 foram também completamente caracterizadas com base nas informações da espectroscopia no IV, de RMN de ^{1}H e ^{13}C, bem como espectrometria de massas.

Embora os rendimentos obtidos das reações dos diclorados **62-65** com aminas primárias e secundárias tenham sido baixos (0-55%), o trabalho publicado por TAI *et al*. (2011) nos motivou a empregar anilina como nucleófilo, embora seja menos nucleofílica do que as aminas até então testadas. Naquele trabalho, o tratamento do fenol com $POCl_3$, e posteriormente com derivados da anilina resultou na formação de polímeros em rendimentos variando de 78 a 92% (Esquema 18).

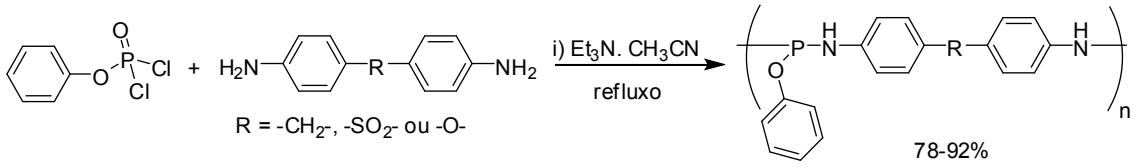

Esquema 18 – Polímeros sintetizados por TAI *et al*. (2011).

O tratamento do diclorado **63** (átomo de bromo em posição *orto* no anel aromático) com anilina anidra, sob as condições descritas em 2.1.2.6 não nos forneceu o produto de interesse. Partimos então para a substituição do material de partida **63** pelo **62**, que apresenta o átomo de bromo em posição *para* no anel aromático, na tentativa de reduzir possível impedimento espacial (condições descritas na Tabela 4). Entretanto, o produto esperado (**70**) não foi obtido (condição **1**).

Tabela 4 - Condições reacionais para síntese do produto **70**

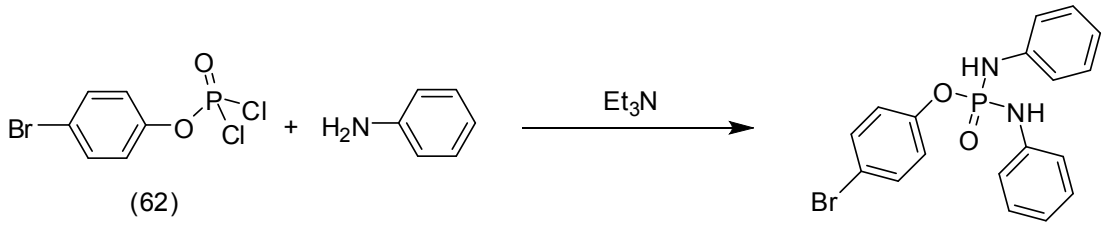

(62) (70)

Condição	Condições	Solvente	Rendimento (%)
1	i) anilina (2 equiv.); ii) TEA (4 equiv.); iii) substância **62** (1 equiv.), 0ºC, 20 min; iv) ºC → t.a.; t.r.=20h.	DCM[a]	0
2	i) anilina (2 equiv.); ii) TEA (4 equiv.); iii) DMAP 5 mol%; iv) substância **62** (1 equiv.), 0ºC, 20 min; v) ºC → t.a.; t.r.=20h.	DCM[a]	0
3	i) anilina (2 equiv.); ii) TEA (4 equiv.); iii) substância **62** (1 equiv.),0ºC, 20 min; iv) refluxo; t.r.=20h.	Tolueno[a]	10
4	i) anilina (2 equiv.); ii) TEA (4 equiv.); iii) substância **62** (1 equiv.),0ºC, 20 min; iv) refluxo; t.r.=20h.	Tolueno[b]	9
5	i) anilina (2 equiv.); ii) TEA (4 equiv.); iii) substância **62** (1 equiv.), 0ºC, 20 min; iv) refluxo; t.r.=20h.	CH_3CN[a]	16
6	i) anilina (2 equiv.); ii) TEA (4 equiv.); iii) substância **62** (1 equiv.), 0ºC, 20 min; iv) refluxo; t.r.=20h.	CH_3CN[b]	14

[a] Empregou-se 0,5 mL de solvente para 100 mg do material de partida **62**.

[b] Empregou-se 5 mL de solvente para 100 mg do material de partida **62**.

O emprego de 5 mol% de DMAP, conforme descrito por TYMPERLEY e WATERS (2005) não favoreceu a formação da substância desejada (condição **2**). Entretanto, a substituição do DCM por tolueno anidro, e posterior aquecimento até o refluxo, mesmo na ausência de DMAP, favoreceu a formação do produto **70** em 10% de rendimento (condição **3**). Uma vez que nas condições **1-3** empregou-se menor quantidade de solvente (solução mais concentrada do que na condição descrita em 2.1.2.6), optou-se por realizar o procedimento reacional em condição mais diluída a fim de verificar se haveria interferência. Entretanto, conforme verificado na condição **4** não houve

influência significativa. Partimos então para a reação segundo as condições descritas por TAI *et al*. (2011), na qual se emprega CH_3CN como solvente. Observou-se que o sal formado ao longo da reação solubiliza-se quando submetido ao refluxo, o que pode favorecer o processo. Após refluxo por 20h o produto foi obtido em 16% de rendimento (Esquema 19). Novamente, a diluição do meio reacional (condição **6**) não influenciou significativamente no rendimento.

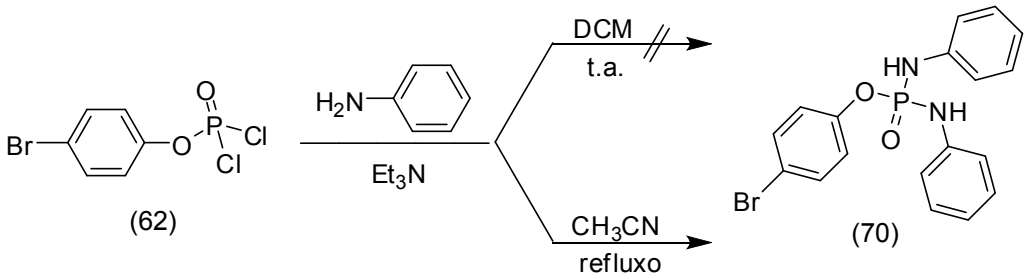

Esquema 19 – Síntese do fosforamidato **70** segundo condições descritas por TAI *et al*. (2011).

Os compostos **74** e **77**, particularmente, tiveram sua formação evidenciada apenas por espectrometria de massas (Figuras 12 e 13, respectivamente). Os sinais em *m/z* em 357 ($[M+4]^{+\bullet}$, 2), *m/z* 355 ($[M+2]^{+\bullet}$, 7) e *m/z* 353 ($[M]^{+\bullet}$, 5) estão de acordo com a presença de um átomo de cloro e um átomo de bromo na estrutura do composto **74** (Figura 12).

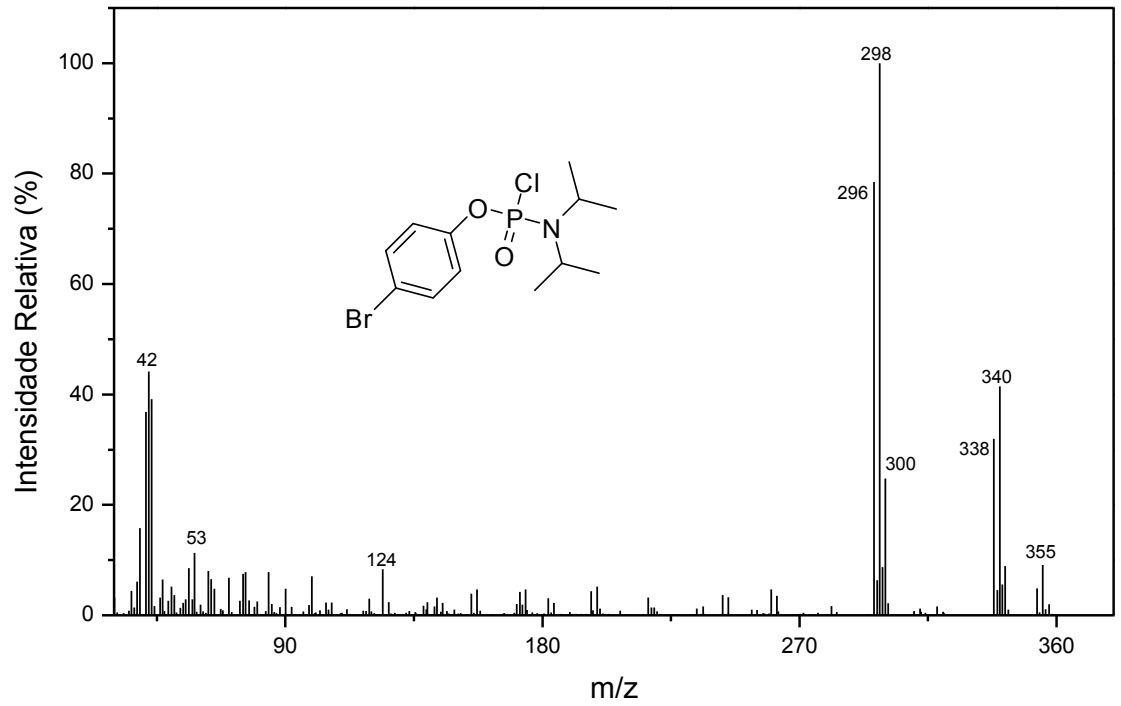

Figura 12 – Espectro de massas do composto **74**.

Durante a etapa de purificação por coluna de sílica gel, nenhum material de interesse foi recuperado. No caso da substância **74**, por apresentar um átomo de cloro ligado ao fósforo, a instabilidade do composto em sílica era esperada. Dessa forma, foi realizado o fracionamento em coluna de alumina, o que não contornou o problema enfrentado.

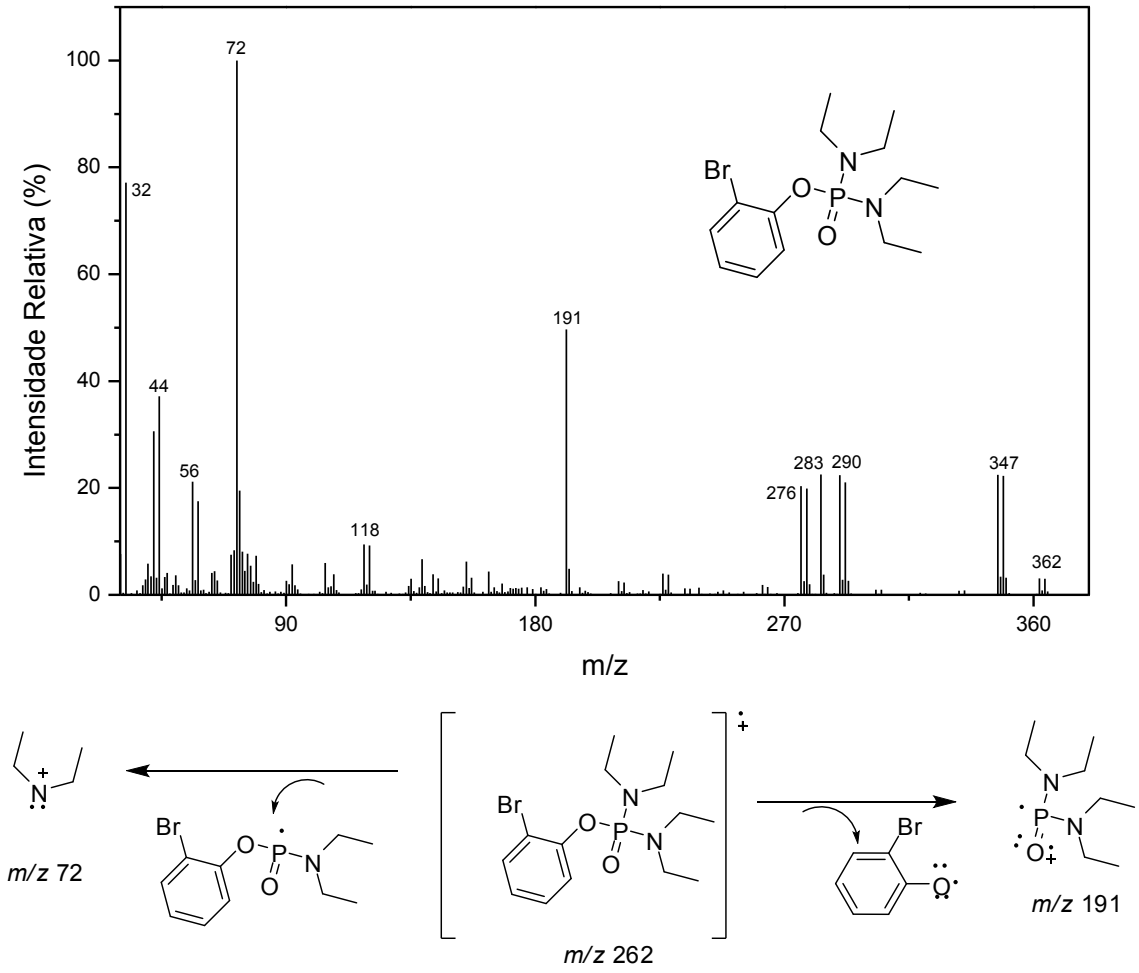

Figura 13 – Espectro de massas e processos de fragmentação mais importantes do composto **77**.

Situação semelhante à descrita foi observada por TIMPERLEY e WATERS (2005) ao tratar vários dicloretos fosforados com dois equivalentes de 2,2,2-trifluoroetilamina e trietilamina, levando à obtenção de misturas de produtos de difícil purificação e, em alguns casos, instáveis.

Por fim, foram realizadas tentativas de síntese de compostos heterocíclicos conforme estruturas **89** e **90**, a partir da reação do diclorado **62** com álcool 2-aminobenzílico e 2,3-diidroxibenzaldeído, respectivamente (Figura 14). Relatos na literatura evidenciam a possibilidade desse tipo de reação

(ALONSO *et al*. (2011) e GHOLIVAND *et al*. (2007). No entanto, não conseguimos obter os produtos desejados. Não foi realizada etapa de otimização.

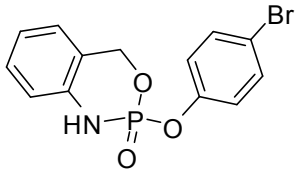

(89)

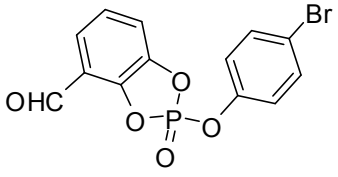

(90)

Figura 14 – Estrutura dos compostos heterocíclicos **89** e **90** que não foram formados.

2.4. Conclusões

Descreveram-se neste capítulo as etapas envolvidas na preparação de 19 fosforados inéditos. A tentativa de otimização para síntese dos fosforamidatos contendo grupo das furanonas não foi bem sucedida. No entanto, o tratamento de fenóis substituídos com cloreto de fosforila ($POCl_3$) levou à obtenção de intermediários organofosfatos diclorados (**62-65)** em excelentes rendimentos (91-99%). Os compostos **62-65**, sem prévia purificação, foram submetidos à reação de substituição nucleofílica com diferentes aminas, segundo condições descritas por UCKUN *et al*. (2005), resultando nos produtos (**66-73, 75-76 e 78-84**) desejados em rendimentos variando de 8 a 55%. Dois compostos foram formados (**74** e **77**), porém, não foram recuperados após coluna de sílica-gel.

Os dezessete fosforados sintetizados e isolados foram caracterizados via espectroscopia no IV e de RMN, bem como espectrometria de massas.

2.5. Referências Bibliográficas

ALONSO, C.; SANTOS, J.; VICARIO, J.; PALACIOS, F. Phosphorus substituted hydroxylamine and hydroxamic acid derivatives: synthesis and reactivity. *Arkivoc*, v. (iii), p. 221-253, 2011.

ATHERTON, F.R.; TODD, A.R.; OPENSHAW, H.T. Studies on phosphorylation. Part II. The reaction of dialkyl phosphites with polyhalogen compounds in presence of bases. A new method for the phosphorylation of amines, *Journal of the Chemical Society*, p. 660-663, 1945.

BORRELO, L.; CHIACCHIO, U.; CORSARO, A.; PISTARA, V.; IANNAZZO, D. Phosphoroamidate derivatives of N,O-nucleosides as inhibitors of reverse transcriptase. *Arkivoc*, v. (viii), p. 112-124, 2009.

CASEY, M.; LEONARD, J.; LYGO, B. *Advanced practical organic chemistry*. New York: Chapman and Hall, 1990, 264p.

CHO, J.H.; AMBLARD, F.; COATS, S.J.; SCHINAZI, R.F. Efficient synthesis of nucleoside aryloxy phosphoramidate prodrugs utilizing benzyloxycarbonyl protection. *Tetrahedron*, v. 67, p. 5487-5493, 2011.

CONGIATU, C.; BRANCALE, A.; MASON, M.D.; JIANG, W.G.; MCGUIGAN, C. Novel Potential Anticancer Naphthyl Phosphoramidates of BVdU: Separation of Diastereoisomers and Assignment of the Absolute Configuration of the Phosphorus Center. *Journal of Medicinal Chemistry*, v. 49, p. 452-455, 2006.

DERUDAS, M.; BRANCALE, A.; NAESENS, L.; NEYTS, J.; BALZARINI, J.; MCGUIGAN, C. Application of the phosphoramidate ProTide approach to the antiviral drug ribavirin. *Bioorganic & Medicinal Chemistry*, v. 18, p. 2748–2755, 2010.

DERUDAS, M.; CARTA, D.; BRANCALE, A.; VANPOUILLE, C.; LISCO, A.; MARGOLIS, L.; BALZARINI, J.; MCGUIGAN, C. The application of phosphoramidate protide technology to acyclovir confers anti-HIV inhibition. *Journal of Medicinal Chemistry*, v. 52, p. 5520-5530, 2009.

DHAWAN, B.; REDMORE, D. Metalation-Induced Double Migration of Phosphorus from O→C. Convenient Preparation of *Bis*(2-hydroxyary1)phosphinic Acids. *Journal of Organic Chemistry*, v. 51, p. 179-183, 1986.

DOMINGUEZ, M.J.; SANMARTIN, C.; FONT, M.; PALOP, J.A.; FRANCISCO, S.S.; URRUTIA, O.; HOUDUSSE, F.; GARCIA-MINA, J.E. Design, Synthesis, and Biological Evaluation of Phosphoramide Derivatives as Urease Inhibitors. *Journal of Agricultural and Food Chemistry*, v. 56, p. 3721-3731, 2008.

FUKUTO, T.R. Mechanism of action of organophosphorus and carbamate insecticide. *Environmental Health Perspectives*, v. 87, p. 245-254, 1990.

GARDELLI, C.; ATTENNI, B.; DONGHI, M.; MEPPEN, M.; PACINI, B.; HARPER, S.; MARCO, A.; FIORE, F.; GIULIANO, C.; PUCCI, V.; LAUFER, R.; GENNARI, N.; MARCUCCI, I.; LEONE, J.F.; OLSEN, D.B.; MACCOSS, M.; ROWLEY, M.; NARJES, F. Phosphoramidate Prodrugs of 20-C-Methylcytidine for Therapy of Hepatitis C Virus Infection. *Journal of Medicinal Chemistry*, v. 52, p. 5394–5407, 2009.

GEORGIEV, E. M.; KANETI, J., TROEV, K.; ROUNDHILL, D. M.; "An *ab initio* study of the mechanism of the Atherton-Todd reaction between dimethyl phosphonate and chloro- and fluoro-substituted methanes". *Journal of the American Chemical Society*, v.115, p.10964-10973, 1993.

GHOLIVAND, K.; SHARIATINIA, Z.; MAHZOUNI, H.R.; AMIRI, S. Phosphorus heterocycles: synthesis, spectroscopic study and X-ray crystallography of some new diazaphosphorinanes. *Structural Chemistry*, v. 18, p. 653–660, 2007.

GONÇALVES, D.; WAL, E.; ALMEIDA, R.R. *Química Orgânica Experimental***.** São Paulo: Mcgraw-Hill, 1988, 269p.

KIRAN, Y.B.; REDDY, C.D.; GUNASEKAR, D.; REDDY, C.S.; LEON, A.; BARBOSA, L.C.A. Synthesis and anticancer activity of new class of bisphosphonates/phosphanamidates. *European Journal of Medicinal Chemistry*, v. 43, p. 885-892, 2008.

MARA, C.; DEMPSEY, E.; BELL, A.; BARLOW, J.W. Synthesis and evaluation of phosphoramidate and phosphorothioamidate analogues of amiprophos methyl as potential antimalarial agents. *Bioorganic & Medicinal Chemistry Letters*, v. 21, p. 6180–6183, 2011.

MCGUIGAN, C.; KELLEHE, M.R.; PERRONE, P.; MULREADY, S.; LUONI, G.; DAVERIO, F.; RAJYAGURU, S.; POGAM, S.L.; NAJERA, I.; MARTIN, J.A.; KLUMPP, K.; SMITH, D.B. The application of phosphoramidate ProTide technology to the potent anti-HCV compound 4´-azidocytidine (R1479). *Bioorganic & Medicinal Chemistry Letters*, v.19, p.4250–4254, 2009.

MCGUIGAN, C.; MADELA, K.; ALJARAH, M.; GILLES, A.; BATTINA, S.K.; RAMAMURTY, C.V.S.; RAO, C.S.; VERNACHIO, J.; HUTCHINS, J.; HALL, A.; KOLYKHLOV, A.; HENSON, G.; CHAMBERLAIN, S. Dual pro-drugs of 20-C-methyl guanosine monophosphate as potent and selective inhibitors of hepatitis C virus. *Bioorganic & Medicinal Chemistry Letters*, v. 21, p. 6007–6012, 2011b.

MCGUIGAN, C. *Phosphoramidate compounds and methods of use*. Patente US 7951787, 2011.

MCGUIGAN, C.; MURZIANI, P.; SLUSARCZYK, M.; GONCZY, B.; VOORDE, J.V.; LIEKENS, S.; BALZARINI, J. Phosphoramidate ProTides of the Anticancer Agent FUDR Successfully Deliver the Preformed Bioactive Monophosphate in Cells and Confer Advantage over the Parent Nucleoside. *Journal of Medicinal Chemistry*, v. 54, p. 7247-7258, 2011a.

MCGUIGAN, C.; THIERY, J.; DAVERIO, F.; JIANG, W.G.; DAVIES, G.; MASON, M. Anti-cancer ProTides: tuning the activity of BVDU phosphoramidates related to thymectacin. *Bioorganic & Medicinal Chemistry*, v. 13, p. 3219–3227, 2005.

MCMURRAY, J. S.; IV, D. R. C.; WANG, W.; CAMPBELL, M. L., The synthesis of phosphopeptides, *Biopolymers*, v. 60, p.3-31, 2001.

NÄSMAN, J.H. 3-methyl-2(*5H*)-furanone. *Organic Syntheses*, v. 68, p. 162, 1990.

OLIVEIRA, F.M.; BARBOSA, L.C.A.; TEIXEIRA, R.R.; DEMUNER, A.J.; MALTHA, C.R.A.; PICANÇO, M.C.; SILVA, G.A.; PAULA, V.F. Synthesis and insecticidal activity of new phosphoramidates. *Journal of Pesticide Science*, v. 37, p. 85-88, 2012.

ORLOFF, H.; WORREL, C. J.; MARLEY, F. X. The Synthesis of Alkyl Aryl Phosphates from Aryl Phosphorochloridates. I. The Sodium Alkoxide Route. *Journal of the American Chemical Society*, v. 80, p. 727-734, 1958.

PAULA, V.F.; BARBOSA, L.C.A.; TEIXEIRA, R.R.; PICANÇO, M.C.; SILVA, G.A. Synthesis and insecticidal activity of new 3-benzylfuran-2-yl *N,N,N´,N´*-tetraethyldiamidophosphate derivatives. *Pest Management Science*, v. 64, p. 863–872, 2008.

PERRIM, D.D. & ARMAREGO, W. L. F. *Purification of laboratory chemicals*. 3ed. Oxford: Pergation Press, 1994, 340p.

PRETSCH, E.; SIMON, W.; SEIBL, J.; CLERC, T. *Tables of Spectral data for structure determination of organic compounds*. 2nd ed.; Berlin: Springer-Verlag, 1989.

ROMAN, C.R.; WASSERTHAL, P. BALZARINI, J.; MEIER, C. Diastereoselective synthesis of (aryloxy)phosphoramidate prodrugs. *European Journal of Organic Chemistry*, v. 2011, p. 4899–4909, 2011.

RUDA, G.F.; WONG, P.E.; ALIBU, V.P.; NORVAL, S.; READ, K.D.; BARRET, M.P.; GILBERT, I.H. Aryl Phosphoramidates of 5-Phospho Erythronohydroxamic Acid, A New Class of Potent. *Journal of Medicinal Chemistry*, v. 53, p. 6071–6078, 2010.

SANTOS, V.M.R.; DONNICI, C.L.; DACOSTA, J.B.N.; CAIXEIRO, J.M.R. Compostos organofosfatos pentavalentes: histórico, métodos sintéticos de preparação e aplicações como inseticidas e agentes antitumorais. *Química Nova*, v. 30, p. 159-170, 2007.

SHRINER, R.L.; FUSON, R.C.; CURTIN, D.Y.; MORRILL, T.C. *The systematic identification of organic compounds*. 6ed. New York: John Wiley & Sons, 1980, 604p.

SILVERSTEIN, R.M.; WEBSTER, F.X.; KIEMLE, D.J. *Identificação Espectrométrica de Compostos Orgânicos*, 7. ed.; Rio de Janeiro: LTC, 2006, 490 p.

SOUZA, M.V.N. The Furan-2(5*H*)-ones: Recent Synthetic Methodologies and its Application in Total Synthesis of Natural Products. *Mini-Reviews in Organic Chemistry*, v. 2, p. 139-145, 2005.

SOUZA, M.C.; MACEDO, W.P.; SILVA, M.C.M.; COSTA, G. One-pot synthesis of N-alkyl substituted phosphory guanidines. *Phosphorus, Sulfur, and Silicon*, v. 179, p. 1047–1054, 2004.

SOUZA, M.C.; MACEDO, W.P.; TORRES, T.S.; PEDROSA, L.F.; ALT, H.G. Selective Monophosphorylation of Aliphatic Diamines. *Phosphorus, Sulfur, and Silicon*, v. 181, p. 1885–1893, 2006.

TAI, Q.; HU, Y.; YUEN, R.K.K.; SONG, L.; LU, H. Synthesis, structure–property relationships of polyphosphoramides with high char residues. *Journal of Materials Chemistry*, v. 21, p. 6621–6627, 2011.

TEIXEIRA, R. R. *Síntese e avaliação das atividades fitotóxica e citotóxica de compostos análogos aos nostoclídeos*. Belo Horizonte-MG: UFMG, Tese (Doutorado) – Universidade Federal de Minas Gerais, 2008.

TIMPERLEY, C.M; WATERS, M. Fluorinated phosphorus compounds Part 11. The reactions of some fluorinated amines with dialkyl and *bis*(fluoroalkyl) phosphorochloridates. *Journal of Fluorine Chemistry*, v. 126, p. 1144-1149, 2005.

TORRES, T.S.; MACEDO, W.P.; PEDROSA, L.F.; SOUZA, M.C.B.V.; FERREIRA, V.F.; CUNHA, A.C.; FOGEL, T.; SANTOS, F.C.; MARQUES, I.P.; PAIXÃO, I.C.P.; SOUZA, M.C. Synthesis and Anti-HSV-1 *In Vitro* Activity of New Phosphoramidates with 4-oxoquinoline and Phtalimidic Nuclei, *Letters in Organic Chemistry*, v. 5, p. 644-650, 2008.

UCKUN, F.M.; VENKATACHALAM, T.K.; ERBECK, D.; CHEN, C.L.; PETKEVICH, A.S.; VASSILEV, A. Zidampidine, an aryl phosphate derivative of AZT: *in vivo* pharmacokinetics, metabolism, toxicity, and anti-viral efficacy against hemorrhagic fever caused by Lassa virus. *Bioorganic & Medicinal Chemistry*, v. 13, p. 3279–3288, 2005.

VOORDE, J.V.; LIEKENS, S.; MCGUIGAN, C.; MURZIANI, P.G.S.; SLUSARCZYK, M.; BALZARINI, J. The cytostatic activity of NUC-3073, a phosphoramidate prodrug of 5-fluoro-20-deoxyuridine, is independent of activation by thymidine kinase and insensitive to degradation by phosphorolytic enzymes. *Biochemical Pharmacology*, v. 82, p. 441–452, 2011.

WAGNER, S.; RAKOTOMALALA, M.; BYKOV, Y.; WALTER. O.; DORING, M. Synthesis of New Organophosphorus Compounds Using the Atherton–Todd Reaction as a Versatile Tool. *Heteroatom Chemistry*, v. 23, p. 216-222, 2012.

WANG, Z.; GUO, C.; XIE, W.; LIU, C.; XIAO, C.; TAN, Z.; Novel phosphoramidates with porphine and nitrogenous drug: one-pot synthesis and orientation to cancer cells. *European Journal of Medicinal Chemistry*, v. 45, p. 890–895, 2010.

YUAN, J.; CHENA, X.; QUA, L.; QUA, Z.; ZHOUA, Y.; ZHAO, Y. Synthesis of a Novel Type of Phosphoramidate Derivatives of 2-Arylquinolone. *Journal of the Chinese Chemical Society*, v. 56, p. 51-58, 2009.

CAPÍTULO 3

3. AVALIAÇÃO DA ATIVIDADE FITOTÓXICA DE FOSFORAMIDATOS

3.1. Introdução

Segundo o Fundo de População das Nações Unidas, UNFPA, nos últimos 50 anos, o número de habitantes do mundo mais que duplicou, passando de 2 bilhões e 500 mil em 1950 para 7 bilhões de pessoas em outubro de 2011. Este número mostra a população em processo de envelhecimento, sendo que a proporção global de pessoas com mais de 60 anos, que era de 8% em 1950, cresceu para 11% em 2009 e está projetada para alcançar 22% em 2050. Ainda que, na maioria dos países, as taxas de natalidade estejam descrescendo, a população mundial segue aumentando e, estima-se que será alcançada a marca de 8 bilhões e 900 mil pessoas até 2050 (UNFPA, 2013).

Diante deste aumento populacional, alguns desafios precisam ser vencidos, tais como inclusão social, redução da pobreza e aumento da produtividade agropastoril associada com a sustentabilidade ambiental e responsabilidade social, sem, entretanto, aumentar a área cultivada (UNFPA, 2013). Por essa razão, o uso de técnicas de manejo de culturas, melhoramento animal e vegetal, conservação dos solos, sistemas de irrigação, combate a pragas e aplicação de fertilizantes se traduzem em maior produtividade com reflexo direto na produção de alimento (NICHOLSON, 2007).

Diante da necessidade de proteger as produções agrícolas contra ataque de pragas, milhões de dólares são gastos anualmente com defensivos agrícolas. Assim, o produtor agrícola precisa recorrer a diferentes métodos de

controle, como o químico, genético, biológico ou mecânico (BARBOSA, 2004). No Brasil, em 2012, as vendas de defensivos agrícolas totalizaram US$ 9,71 bilhões, 14,4% a mais do que as de 2011. Em reais, a comercialização somou cerca de R$ 19,5 bilhões, de acordo com dados do Sindicato Nacional da Indústria de Produtos para Defesa Agrícola (SINDAG). Os segmentos líderes foram os inseticidas, com 37,3% das vendas, os herbicidas, com 32,3%, e os fungicidas, com 25,2%. Embora esteja em segundo lugar em valor de vendas, os herbicidas responderam por 57,1% da quantidade total vendida em produto comercial (Figura 1) (SINDAG, 2013).

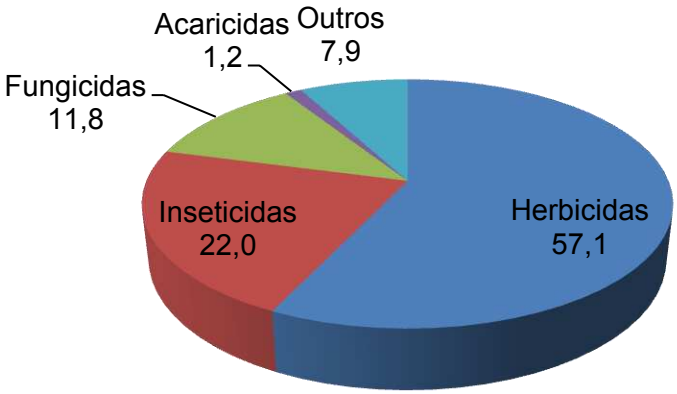

Figura 1 – Participação das classes na quantidade vendida de defensivos agrícolas, em produto comercial, Brasil, 2012.

O Brasil reúne as maiores áreas agricultáveis disponíveis, bem como 20% do volume de água doce do mundo, podendo-se tornar o maior produtor de grãos, carnes e biocombustíveis do mundo. Esse potencial poderá ser viabilizado se houver maior controle sobre as pragas, se o mercado brasileiro reduzir a dependência externa de fertilizantes nitrogenados e houver maior incentivo a projetos de produção de fertilizantes (MAPA, 2013).

Embora seja grande o número de compostos disponíveis comercialmente com atividade fitotóxica, é crescente a necessidade de desenvolvimento de novas substâncias com esta atividade biológica. Esta demanda justifica-se na medida em que se buscam compostos que sejam mais seletivos e menos tóxicos ao homem e animais domésticos, que possam ser utilizados em menores doses, que apresentem novos mecanismos de ação, além de serem pouco persistentes no meio ambiente. Soma-se a estes fatores,

a necessidade de novos produtos que possam combater biótipos de plantas daninhas resistentes aos herbicidas comercialmente disponíveis. A resistência aos herbicidas é um resultado normal e previsível do processo de seleção natural. Os primeiros registros foram feitos na década de 1960, e hoje se estima que existem 416 biótipos resistentes e 222 espécies (129 dicotiledôneas e 93 monocotiledôneas) de plantas daninhas que apresentem resistência a um ou mais sítios de ação (resistência múltipla) (MACIAS *et al*., 2000; BECKIE, 2006; SILVA *et al*., 2007; HEAP, 2013; HEAP, 2014).

Dentro deste cenário, vale a pena chamar a atenção para a atividade fitotóxica apresentada pelos compostos amiprofos-metílico e butamifos, disponíveis comercialmente, que são fosforotioamidatos (Figura 2). Estes compostos fazem parte de um pequeno grupo que atua inibindo a polimerização de microtúbulos em células vegetais, impedindo a formação de fusos cromáticos e induzindo a separação dos cromossomas metafásicos (MARA *et al*., 2011). É importante chamar a atenção para a presença do grupo fenol diretamente ligado ao átomo de fósforo e da ligação P-N, similarmente às estruturas sintetizadas neste trabalho.

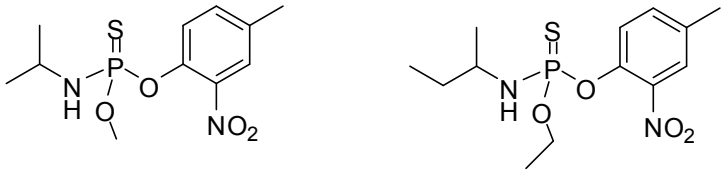

Amiprofos-metílico Butamifos

Figura 2 – Estrutura dos herbicidas comerciais Amiprofos-metílico e Butamifos.

Além destes compostos supracitados, relatam-se, ainda, os compostos fosforados Benzulida (fosforoditioato que atua inibindo a síntese de lipídeos), Glifosato e Sulfosato (glicinas com atividade sobre a enzima 5-enolpiruvoil-chiquimato-3-fosfato sintetase – EPSPS -, que sintetiza os aminoácidos aromáticos fenilalanina, tirosina e triptofano), além de Amônio-glufosinato e Bialafos (ácidos fosfínicos que inibem a glatamina sintetase) (Figura 3). Dentre estes compostos destaca-se o glifosato, princípio ativo do Roundup®, herbicida mais vendido no mundo. No Brasil, segundo dados de 2009, suas vendas responderam por cerca de um terço do volume total de praguicidas comercializados, sendo usado em mais de uma centena de culturas (QUEIROZ, 2011).

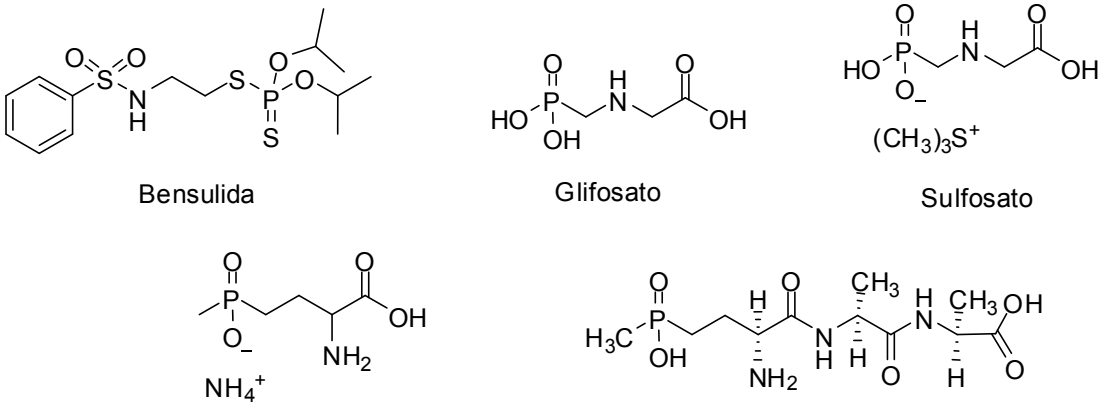

Figura 3 – Estrutura de compostos fosforados com atividade fitotóxica disponíveis comercialmente.

Descreve-se, neste capítulo, os resultados referentes à avaliação da atividade fitotóxica dos fosforamidatos sintetizados no Laboratório de Análise e Síntese de Agroquímicos. Além dos compostos sintetizados neste trabalho, avaliou-se a atividade biológica dos compostos descritos por PEREIRA (2013), cujas estruturas estão representadas na Tabela 1:

Tabela 1 – Fosforamidatos descritos por PEREIRA (2013)

Código	Estrutura	Código	Estrutura
91	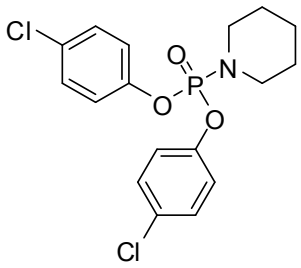	**92**	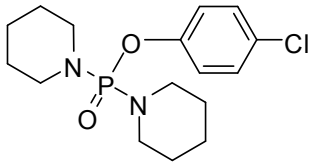
93	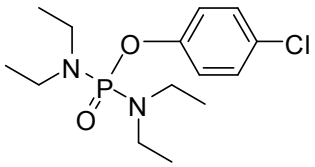	**94**	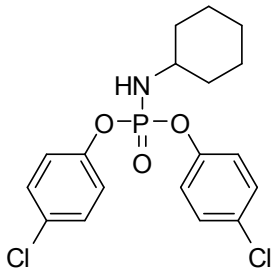
95	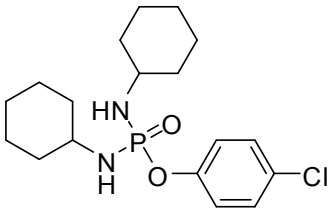	**96**	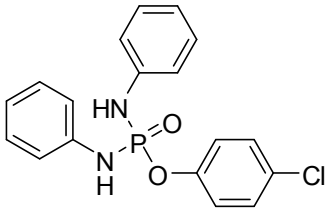
97	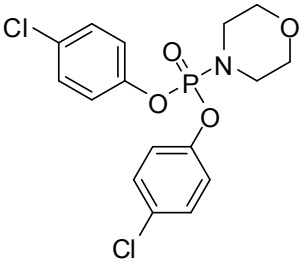	**98**	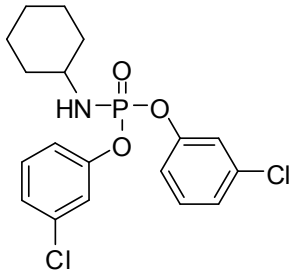
99	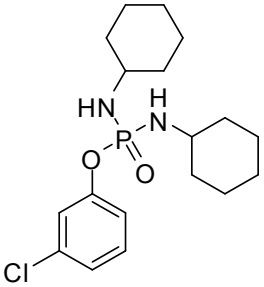	**99**	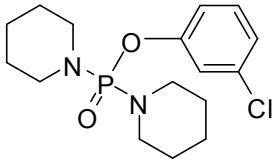
101	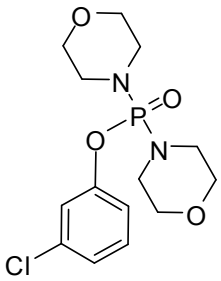	**100**	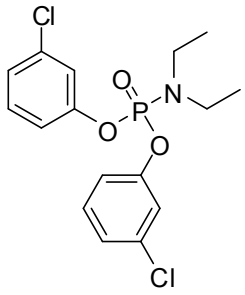

3.2. Materiais e Métodos

3.2.1. Avaliação da atividade fitotóxica sobre o desenvolvimento radicular e da parte aérea de pepino (*Cucumis sativus*) e de sorgo (*Sorghum bicolor*)

Foram preparadas soluções-estoque dos fosforamidatos **66-73, 75-76, 78-84** e **91-100** nas concentrações de 0,125; 0,250; 0,500 e 1,00 mmol L^{-1}. Em balão volumétrico, uma quantidade adequada dessas substâncias foi dissolvida em dimetil sulfóxido (DMSO; 1,0% v/v) e o volume completado com água deionizada. Para cada uma das concentrações foram preparadas três placas de Petri recobertas com papel de germinação. Em seguida, 20 sementes da espécie de interesse (*C. sativus* ou *S. bicolor*) foram espalhadas sobre cada placa de Petri, para então serem umidecidas uniformemente com 5 mL da solução-estoque. As placas foram seladas com plástico filme, envolvidas com papel alumínio e incubadas em câmara de germinação a 25 °C por 7 dias (para pepino) ou 10 dias (para sorgo). Decorrido este período, o crescimento foi avaliado por medição das radículas (caule e raiz) com régua graduada em milímetros e os resultados expressos em percentagem de crescimento comparado ao controle. Considerou-se a média das medidas para cada unidade experimental (placa de Petri).

Como controle positivo empregou-se o herbicida comercial glifosato (Glifosato Plus Pikapau 480 g/L), exemplo de organofosforado, e o Pivot (Imazetapir 100 g/L) preparados nas mesmas condições/concentrações descritas anteriormente, e uma solução de DMSO em água (1% v/v) foi usada como branco. As percentagens de inibição (ou estimulação) foram calculadas em comparação com esse controle.

3.3. Resultados e Discussão

Uma vez realizada a síntese dos compostos fosforamidatos, procedeu-se à avaliação da atividade fitotóxica destas substâncias sobre espécies que apresentam respostas eficazes em curto espaço de tempo. Dessa forma, foram escolhidas as espécies *Sorghum bicolor* (sorgo), representante das

monocotiledôneas, e *Cucumis sativus* (pepino), como representante das dicotiledôneas. Estas espécies são comumente utilizadas em “screening” para selecionar espécies potencialmente fitotóxicas (EINHELLING *et al.*, 1983).

Os efeitos dos compostos **66-73, 75-76, 78-84** e **91-100** sobre a germinação e o crescimento do sistema radicular de *S. bicolor* e de *C. sativus*, em testes realizados em placas de Petri nas concentrações de 0,125; 0,250; 0,500 e 1,00 mmol L^{-1} estão apresentados nas Tabelas 2 e 3. Os valores negativos representam inibição da atividade, enquanto os valores positivos indicam que houve estímulo.

Ao longo dos experimentos utilizou-se uma solução de DMSO em água (1% v/v) como branco, de forma a garantir que a solução usada para solubilizar os compostos não estava inibindo o desenvolvimento das espécies avaliadas. Além disso, os percentuais de inibição foram calculados comparativamente a esse branco.

O comportamento apresentado pelos herbicidas comerciais Glifosato (pós-emergente) e Pivot (pré-emergente) foram utilizados como parâmetro para garantir que os experimentos estavam sendo realizados segundo condições adequadas. À medida que se reduziu a concentração do princípio ativo, reduziu-se também a porcentagem de inibição sobre as espécies avaliadas, o que é o comportamento esperado, como se pode observar para o herbicida Glifosato (Figura 4). Embora o herbicida mais adequado para ser utilizado como controle positivo neste tipo de ensaio seja o Pivot, devido ao fato de ser utilizado como pré-emergente, a discussão nesse trabalho será realizada em comparação com o herbicida Glifosato. Essa decisão justifica-se na medida em que: i) a inibição apresentada pelos dois herbicidas comerciais não diferiu significativamente em nenhuma das duas espécies; ii) o glifosato, por ser um composto organofosforado, apresenta estrutura mais semelhante aos compostos em estudo.

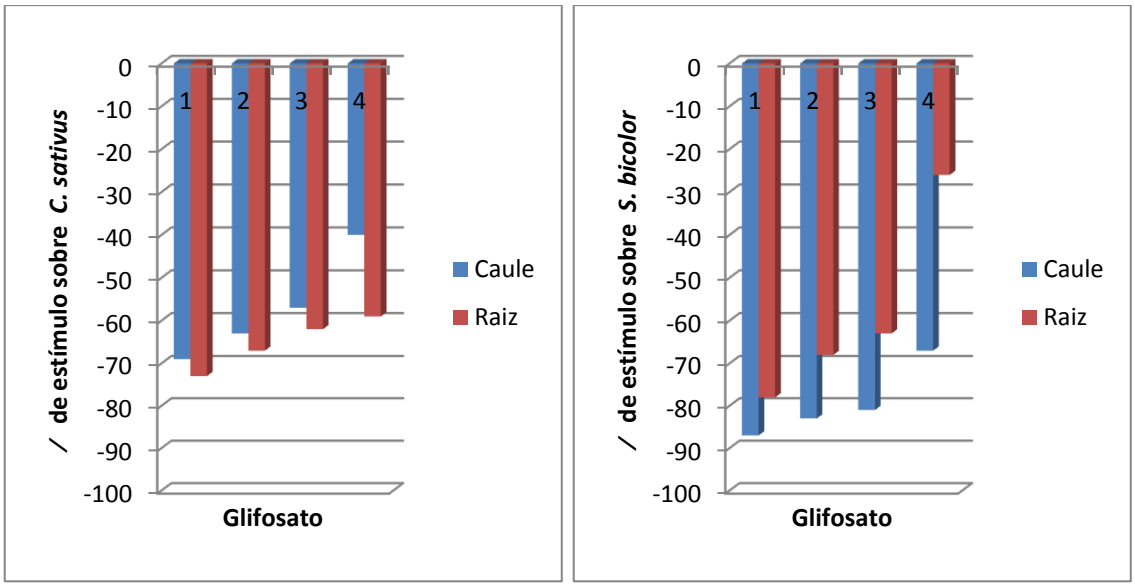

Figura 4 - Efeito do herbicida comercial glifosato sobre o crescimento radicular e da parte aérea de pepino (*C. sativus*) e de sorgo (*S. bicolor*). Os números 1, 2, 3 e 4 referem-se, respectivamente, às concentrações 1,00; 0,500; 0,250 e 0,125 mmol L^{-1}.

A maioria dos compostos avaliados foi considerada pouco ativa sobre as espécies testadas, sendo que os compostos **70** e **80** estimularam o crescimento da parte aérea em até 40% (composto **70** a 1 mmol L^{-1}). É importante mencionar que não houve inibição significativa sobre a germinação das sementes, havendo pelo menos 80% de germinação em todos os casos avaliados.

Observou-se para os compostos organofosforados **71** e **82** uma maior atividade inibitória sobre o sistema radicular de *S. bicolor* em comparação com a parte aérea (Figura 5). Os valores de inibição obtidos são superiores ao observado para o controle positivo Glifosato. Outras substâncias que merecem destaque são os compostos **92** e **93**, que inibiram o crescimento do caule dessa espécie em 65 e 69%, respectivamente, e o crescimento de raiz em 53 e 62%, respectivamente.

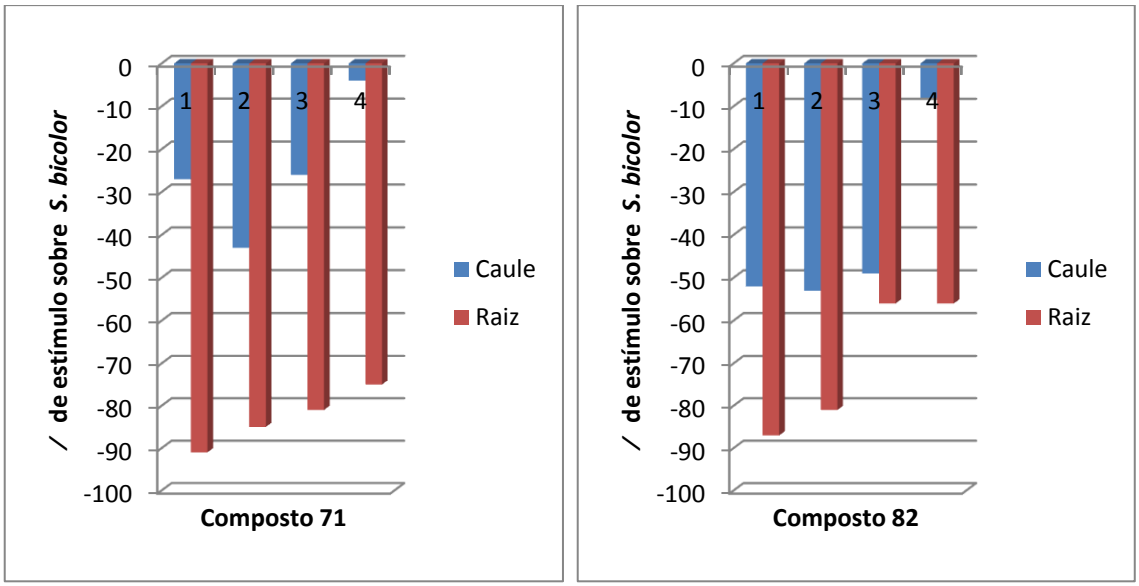

Figura 5 - Efeito dos fosforados **71** e **82** sobre o crescimento radicular e da parte aérea de sorgo (*S. bicolor*). Os números 1, 2, 3 e 4 referem-se, respectivamente, às concentrações 1,00; 0,500; 0,250 e 0,125 mmol L^{-1}.

Em se tratando da espécie *C. sativus*, os melhores resultados foram observados para os compostos **92** e **100**. Estes compostos apresentaram 82 e 83% de inibição, respectivamente, sobre o sistema aéreo na maior concentração (1 mmol L^{-1}). Estes compostos apresentaram, ainda, elevada atividade sobre a raiz dessa espécie, com 72 e 75% de inibição, respectivamente, nessa mesma concentração.

Outras substâncias que merecem destaque são os compostos **68**, **76** e **81**, que apresentaram atividade inibitória sobre o caule de pepino no valor de 77, 77 e 80%, respectivamente, na maior concentração.

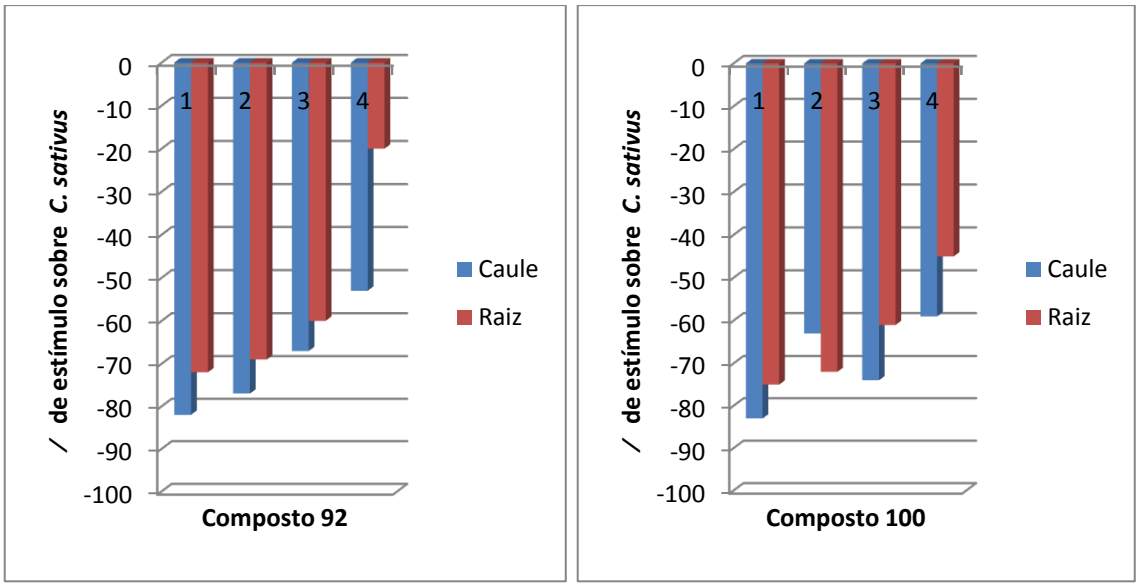

Figura 6 - Efeito dos fosforados **92** e **100** sobre o crescimento radicular e da parte aérea de pepino (*C. sativus*). Os números 1, 2, 3 e 4 referem-se, respectivamente, às concentrações 1,00; 0,500; 0,250 e 0,125 mmol L^{-1}.

A partir dos valores de inibição observados não foi possível estabelecer uma correlação entre a fitotoxicidade e a estrutura dos compostos fosforamidatos. Uma vez que para a maioria dos compostos não há uma obediência à condição de que, menor quantidade de princípio ativo, menor será a atividade biológica, não foi possível determinar o valor de EC_{50}. Esse parâmetro seria fundamental para auxiliar na correlação da atividade biológica com parâmetros como energia de HOMO e LUMO, momento de dipolo e volume molecular.

Dessa forma, esses resultados nos mostram que há substâncias potencialmente ativas dentro dessa classe avaliada. No entanto, ensaios mais elaborados precisam ser realizados de forma que se possa estabelecer correlações da atividade biológica com as propriedades físico-químicas dos compostos.

Tabela 2. Efeito dos compostos **66-73**, **75-76**, **78-84** e **91-100** e do herbicida glifosato sobre a espécie *S. bicolor* (sorgo)

	Caule				Raiz			
Compostos	1,0 mol L^{-1}	0,50 mol L^{-1}	0,25 mol L^{-1}	0,12 mol L^{-1}	1,0 mol L^{-1}	0,50 mol L^{-1}	0,25 mol L^{-1}	0,12 mol L^{-1}
66	-37	-6	2	-19	-25	-10	1	-5
67	46	-10	24	49	-39	-63	-36	-3
68	-49	-44	-16	-48	-56	-37	-27	-36
69	-52	-70	-49	-58	-50	-71	-53	-19
70	-10	54	-47	-55	-18	31	-53	-46
71	-27	-43	-26	-4	-91	-85	-81	-75
72	-67	-68	-49	-17	-50	-52	-61	-43
73	-51	-27	-63	-37	-47	-27	-34	-32
75	-32	-36	-25	4	18	-12	1	25
76	-38	-54	-41	-21	-37	-39	-41	-17
78	-3	-40	-39	-51	-15	-38	-28	-55
79	-40	-63	-55	-39	-51	-63	-71	-43
80	-41	-41	-9	-47	-28	-34	-3	-47
81	-42	-65	-50	-8	-61	-57	-54	-20
82	-52	-53	-49	-8	-87	-81	-56	-56
83	-43	-57	-2	-55	-40	-60	-13	-57
84	-44	-54	-54	-53	-44	-44	-52	-55

Tabela 2. Efeito dos compostos **66-73**, **75-76**, **78-84** e **91-100** e do herbicida glifosato sobre a espécie *S. bicolor* (sorgo (continuação)

	Caule				Raiz			
Compostos	1,0 mol L^{-1}	0,50 mol L^{-1}	0,25 mol L^{-1}	0,12 mol L^{-1}	1,0 mol L^{-1}	0,50 mol L^{-1}	0,25 mol L^{-1}	0,12 mol L^{-1}
91	4	-17	-41	-48	8	-21	-30	-35
92	-65	-37	-55	-40	-53	-34	-48	-50
93	-69	-43	-53	-30	-62	-43	-48	-41
94	-32	-48	-38	-10	-13	-39	-34	-8
95	-22	7	-22	-18	-25	-8	-9	2
96	18	-45	-44	-24	-2	-27	-33	-22
97	-11	-26	-39	-36	-23	-31	-36	-18
98	-49	-30	-49	-23	-38	-35	-39	-29
99	-36	-43	-27	-18	-49	-45	-23	-17
100	-36	-48	-70	-29	-24	-43	-58	-34
101	-46	-43	-52	-31	-47	-23	-42	-28
102	-38	-46	-68	-6	-44	-53	-73	-31
Glifosato	-87	-83	-81	-67	-78	-68	-63	-26
Pivot	-89	-84	-81	-72	-81	-73	-69	-59

Tabela 3. Efeito dos compostos **66-73**, **75-76**, **78-84** e **91-100** e do herbicida glifosato sobre a espécie *C. sativus* (pepino)

	Caule				Raiz			
Compostos	1,0 mol L^{-1}	0,50 mol L^{-1}	0,25 mol L^{-1}	0,12 mol L^{-1}	1,0 mol L^{-1}	0,50 mol L^{-1}	0,25 mol L^{-1}	0,12 mol L^{-1}
66	-51	-72	-52	-57	-55	-64	-49	-38
67	14	-1	-27	-11	16	-16	-26	-13
68	-77	-64	-57	-51	-72	-67	-53	-17
69	-62	-52	-52	-13	-40	-31	-23	-15
70	40	39	27	35	37	35	-11	8
71	18	14	19	0	7	0	-2	20
72	-34	-26	26	-32	3	-26	33	-20
73	11	36	29	-8	10	4	9	5
75	-31	-32	-50	-45	-12	-34	-48	-29
76	-77	-79	-49	-61	-71	-64	-38	-47
78	-10	-52	-7	-31	-2	-55	-25	-25
79	33	7	40	-8	3	-6	19	-17
80	35	41	25	7	16	7	-4	-19
81	-80	-64	-47	-50	-77	-63	-34	-4
82	35	-15	2	14	24	-16	-21	10
83	-61	-76	-38	-23	-84	-77	-62	-55
84	-45	-31	-39	-57	-54	-18	-32	-62

Tabela 3. Efeito dos compostos **66-73**, **75-76**, **78-84** e **91-100** e do herbicida glifosato sobre a espécie *C. sativus* (pepino) (continuação)

	Caule				Raiz			
Compostos	1,0 mol L^{-1}	0,50 mol L^{-1}	0,25 mol L^{-1}	0,12 mol L^{-1}	1,0 mol L^{-1}	0,50 mol L^{-1}	0,25 mol L^{-1}	0,12 mol L^{-1}
91	-30	-19	-1	-42	8	6	27	-33
92	-82	-77	-67	-53	-72	-69	-60	-20
93	-79	-65	-57	-48	-63	-59	-11	-23
94	-3	16	23	33	25	29	3	33
95	-51	-29	-54	-35	-37	-17	-50	-32
96	-9	5	4	-30	-13	18	16	-7
97	-21	-40	-40	9	-1	-13	-33	14
98	20	6	5	31	19	12	-15	48
99	-31	-31	-35	-25	-32	-29	-20	-23
100	-83	-63	-74	-59	-75	-72	-61	-45
101	-56	-13	2	-9	-22	5	22	-23
102	-37	-32	-8	29	-16	-16	-10	24
Glifosato	-69	-63	-57	-40	-73	-67	-62	-59
Pivot	-73	-68	-63	-52	-75	-69	-66	-61

3.4. Considerações Finais

A avaliação da atividade fitotóxica contra as espécies sorgo e pepino evidenciou a potencial atividade de 8 compostos fosforamidatos (**68**, **71**, **76**, **81**, **82**, **92**, **93** e **100**). Os resultados mostraram uma variação de atividade em decorrência das concentrações utilizadas e do tipo de cultura. Para *S. bicolor* os compostos mais ativos foram **71**, **82**, **92** e **93**, que chegaram a inibir em até 91% (**71** a 1 mmol L^{-1}) o crescimento de raiz dessa espécie. Dentre as substâncias testadas, as que mostraram maior inibição da parte aérea para *C. sativus* foram os compostos **92** e **100**, que inibiram em até 83% na maior concentração.

3.5. Referências Bibliográficas

BARBOSA, L.C.A. *Os pesticidas, o homem e o meio ambiente*. Viçosa: Editora UFV, 2004, 215p.

BECKIE, H. J. Herbicide-resistant weeds: management tactics and practices. *Weed Technology*, v. 20, p. 793-814, 2006.

EINHELLING, F. A.; SCHON, M. K.; RASMUSSEN, J. A. Synergistic effects of four cinnamic acid compounds on grain sorghum. *Journal of Plant Growth Regulation*, v.1, p.251-258, 1983.

HEAP, I. Global perspective of herbicide-resistant weeds. *Pest Management Science*, v. 70, p. 1306-1315*,* 2014.

HEAP, I. *International survey of herbicide resistant weeds*. Disponível em <http://www.weedscience.org>. Acesso em: 15 de dezembro de 2013.

MACIAS, F.A.; CASTELLANO, D.; MOLINILLO, J.M.G. Search for a standard phytotoxic bioassay for allelochemicals. Selection of standard target species. *Journal of Agricultural and Food Chemistry*, v. 48, p. 2512-2521, 2000.

MAPA, *Ministério da Agricultura, Pecuária e Abastecimento*. Disponível em: <http://www.agricultura.gov.br>. Acesso em: 15 de dezembro de 2013.

MARA, C.; DEMPSEY, E.; BELL, A.; BARLOW, J.W. Synthesis and evaluation of phosphoramidate and phosphorothioamidate analogues of amiprophos methyl as potential antimalarial agents. *Bioorganic & Medicinal Chemistry Letters*, v. 21, p. 6180-6183, 2011.

NICHOLSON, G.M. Fighting the global pest problem: Preface to the special Toxicon issue on insecticidal toxins and their potential for insect pest control. *Toxicon*, v. 49, p. 413-422, 2007.

PEREIRA, S. R. Síntese de Fosforamidatos e Avaliação da atividade herbicida e Inibidora de Urease. *Relatório de Iniciação Científica*, 2013. *Dados ainda não publicados.*

QUEIROZ, G.M.P.; SILVA, M.R.; BIANCO, R.J.F.; PINHEIRO, A.; KAUFMANN, V. Transporte de glifosato pelo escoamento superficial e por lixiviação em um solo agrícola. *Química Nova*, v. 34, p. 190-195, 2011.

SILVA, A.A.; VARGAS, L.; FERREIRA, E.A. *Herbicidas: Resistência de plantas*. In: SILVA, A.A., SILVA, J.F. (Eds.). *Tópicos em manejo de plantas daninhas*. Editora UFV: Viçosa, 2007. p. 279-324.

SINDAG. *Sindicato Nacional da Indústria de Produtos para Defesa Agrícola*. Disponível em: <http://www.sindag.org.br/>. Acesso em: 15 de dezembro de 2013.

UNFPA: *United Nations Population Fund*. Disponível em: <http://www.unfpa.org.br/>. Acesso em: 15 de dezembro de 2013.

CAPÍTULO 4

4. SYNTHESIS, MOLECULAR PROPERTIES AND DFT STUDIES OF NEW PHOSPHORAMIDATES AS POTENTIAL UREASE INHIBITORS

4.1. Abstract

In this work new phosphoramidates were prepared and screened for their putative urease inhibitory activity. The importance of this class of compounds is related to the wide range of biological activities which they exhibit. Consequently, higher activity shown by phosphoramidates **3a**, **4b**, **5a**, **5b**, **5c** and **9a** suggests they could serve as lead substances for the development of novel synthetic compounds with enhanced inhibitory ureolitic activity. Their predicted ADMET properties are also in accordance with the general requirements for drug-like compounds. Structure-activity relationship (SAR) analyses suggest that the presence of cyclohexylamine group is an important structural feature associated with enhanced activities. DFT calculations were performed to obtain the energy values of HOMO and LUMO, and dipole moment.

4.2. Introduction

Urease is a nickel-containing metalloenzyme that catalyzes hydrolysis of urea to ammonia and carbon dioxide and occur in a wide variety of organisms (ROBERTS *et al*., 2012; KRAJEWSKA, 2009; FOLLMER, 2010). High concentrations of ammonia arising from these reactions is responsible for the

endurance of bacteria *Helicobacter pylori* to acidic pH of the stomach during colonization (FOLLMER, 2010; AMTUL *et al.,* 2002). The enzymatic activity of urease plays an effective role in pathogenesis of urinary and gastrointestinal tracts, causing diseases such as gastritis, peptic ulcers and gastric cancer (FOLLMER, 2010). Urease inhibitors play an important role in the treatment of infections caused by urease producing bacteria (KRAJEWSKA, 2009). Among such bacteria are *H. pylori*, a well-recognized pathogen that infects two-thirds of world population causing 2% to 4% mortality among infected humans (ROBERTS *et al*., 2012; DUCKWORTH *et al*., 2009). Currently, the treatment of infections caused by *H. pylori* has been accomplished through a combination of drugs due to the high level of antibiotic resistance exhibited by this bacteria (ROBERTS *et al.,* 2012). This highlights the need for the development of new antimicrobials to treat *H. pylori* infections, and one important line of research is to target the urease produced by this bacteria (FOLLMER, 2010; AMTUL *et al*., 2002; LI *et al*., 2009).

Amongst the several classes of compounds known to inhibit ureases, the phosphoramidates represent the most active (VASSILIOU *et al*., 2008). This class of compounds have attracted much attention due to their wide range of biological activities such as insecticides (PAULA *et al*., 2008; OLIVEIRA *et al*., 2012a), anti-HCV (MCGUIGAN *et al*., 2009), anti-HIV (DERUDAS *et al.*, 2009; MEHELLOU *et al*., 2009), antiviral (HARRIS *et al*., 2001; DERUDAS *et al*., 2010), inhibitor of reverse transcriptase (BORRELLO *et al*., 2009), antimalarial (MARA *et al*., 2011) and inhibitor of hepatitis C virus (DONGHI *et al*., 2009).

Thus, in the present work, new phosphoramidates were prepared and screened for inhibitory activity against urease from *Jack bean* using thiourea and hydroxyurea as reference urease inhibitors. Urease activity was determined by measuring the ammonia production using the indophenol method (WEATHERBURN, 1967). In addition, the map of the electrostatic potential (MEP) and the value of the frontier orbitals HOMO and LUMO and the dipole moment for optimized geometries from DFT calculations were investigated, as these features may be related to the interaction of the molecules with their target sites. *In silico* physico-chemical properties of the evaluated compounds were determined and the results are also discussed.

The target compounds were synthesized by employing a short synthetic sequence (Scheme 1) according to a procedure adapted from the literature (UCKUN *et al*., 2005). In the initial step a mixture of substituted phenols, phosphoryl chloride and triethylamine in dry diethyl ether was stirred for 18 hours at room temperature resulting in the intermediates **1a-1f**, that were used without purification as shown in Scheme 1.

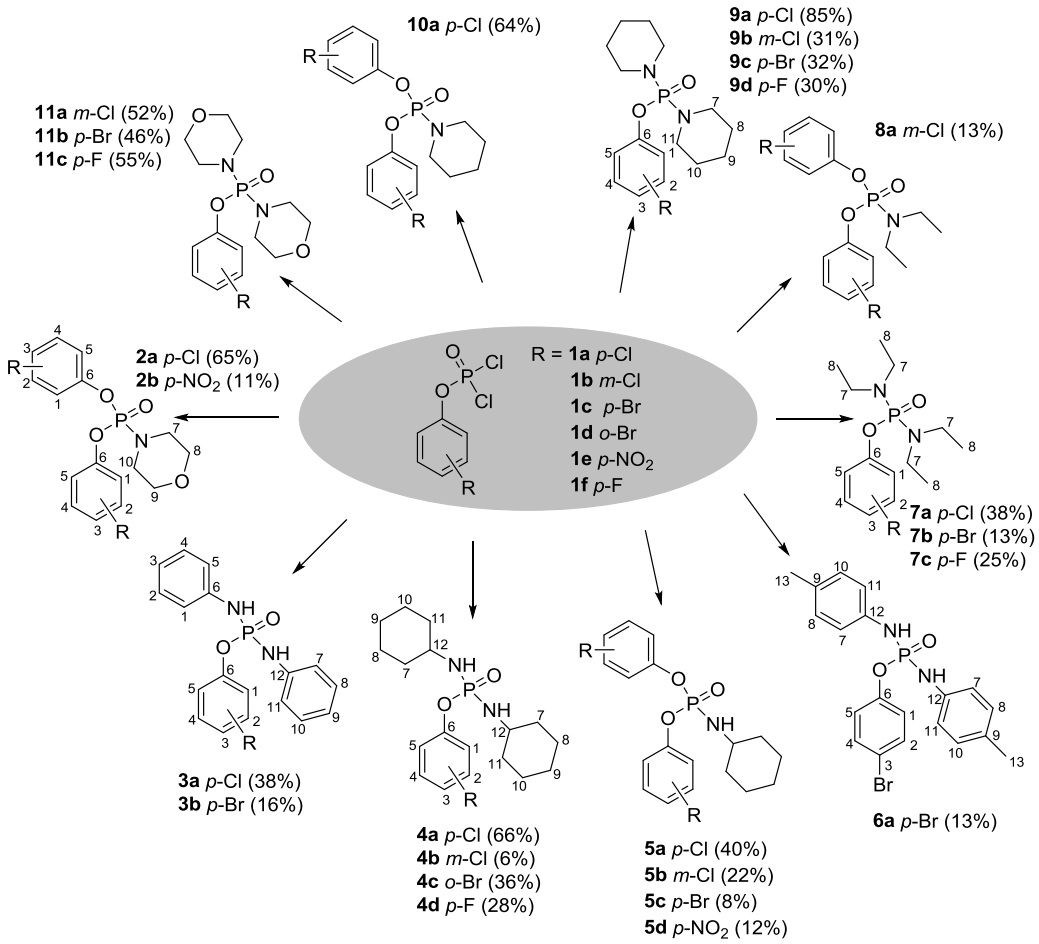

Scheme 1 - Structural formulas of the phosphoramidates synthesized. In general, the conversion of **1a-f** to compounds **2-11** was achieved by reaction with different amines.

The intermediates **1a-1f** were treated with different amines (two equivalents) and triethylamine (two equivalents) in anhydrous dichloromethane and the mixture maintained under magnetic stirring for 18 h. In sequence the precipitate formed was removed by vacuum filtration on a sintered glass funnel and the precipitate washed with anhydrous dichloromethane to afford the

required products **2-11** (Scheme 1). Several attempts to optimize this reaction were carried out, varying the amount of solvent, temperature, reaction time, etc. However in some cases only a small amount of the required product was formed and in general the yields of the required compounds varied from 6% to 91% after purification on a silica gel column. The formation of bisarylphosphonates compounds (**5a-d, 8a, 10a**) may have been favored since the intermediates **1a-1f** were used in the next step without further purification. Moreover, these intermediates can be degraded to the respective phenols. Spectroscopic data (IR, ^{1}H NMR, ^{13}C NMR) of all the synthesized compounds were in full agreement with the proposed structures (see Experimental)

The effect of each compound was assessed by comparing the inhibitory characteristic of the phosphoramidates with that of thiourea and hydroxyurea, the standard compounds which belong to the urease inhibitor group of molecules. The inhibition of ureolitic activity of tested compounds varied from 4% to 83%. Compounds **4c**, **4d**, **5d**, **9c**, **9d**, **11b** and **11c**, however, were found to be positive allosteric effectors on urease as they stimulated urea hydrolysis assisted by this enzyme (Table 1).

The phosphoramidates **11a** and **2b** stimulated urease activity only in experiments carried out with urea concentrations as high as 20 mM. The phosphoramidates **3a**, **4b**, **5a**, **5b**, **5c** and **9a** were found to be the most promising urease inhibitors (Table 1). Thus, these compounds were further investigated and their IC_{50} (concentration necessary to inhibit urease by 50%) were determined.

Table 1. *In vitro* urease inhibitory activities of phosphoramidates **2-11**

	Urea (mM)	
Compound	**10.0**	**20.0**
2a	36.53 ± 0.81	29.07 ± 3.83
2b	5.20 ± 1.73	-4.05 ± 5.95
3a	29.00 ± 7.30	50.74 ± 3.44
3b	50.25 ± 1.61	29.45 ± 1.93
4a	33.77 ± 2.68	30.95 ± 1.56
4b	36.00 ± 4.80	83.60 ± 0.36
4c	-31.97 ± 4.68	-11.43 ± 14.43
4d	-13.47 ± 2.13	-5.28 ± 2.60
5a	69.42 ± 4.00	79.45 ± 3.03
5b	46.00 ± 11.00	50.54 ± 7.38
5c	72.05 ± 6.15	74.04 ± 6.96
5d	-39.39 ± 0.56	-11.34 ± 0.45
6a	39.49 ± 10.77	52.37 ± 4.14
7a	23.32 ± 0.30	10.22 ± 2.74
7b	16.44 ± 5.13	23.75 ± 1.84
7c	5.15 ± 5.37	17.00 ± 6.41
8a	15.61 ± 5.34	3.97 ± 10.94
9a	62.05 ± 2.27	47.00 ± 0.33
9b	17.00 ± 4.56	13.29 ± 19.61
9c	-25.37 ± 0.57	-8.95 ± 3.56
9d	-9.29 ± 0.46	-5.25 ± 0.01
10a	30.24 ± 1.15	33.65 ± 0.44
11a	15.69 ± 0.23	-3.89 ± 1.48
11b	-47.70 ± 5.56	-20.55 ± 1.52
11c	-45.76 ± 0.78	-16.64 ± 2.16
Hydroxyurea (HU)	80.02 ± 6.03	71.18 ± 6.07
Thiourea (TU)	22.62 ± 13.78	20.33 ± 11.32

Values are the mean ± S.D. from three experiments (n = 3). Hydroxyurea and thiourea were used as reference of urease inhibitors.

Table 2 shows that compound **5c** was approximately as potent as hydroxyurea and four times more potent than the reference urease inhibitor thiourea, under the test experimental conditions. The second best urease inhibitor was the compound **5b** followed by **5a**, **9a**, **4b** and **3a**. From the results presented in Table 2, it can be observed that with exception of **3a** all the other compounds were more potent than thiourea.

Table 2. Concentration of promising phosphoramidates necessary to inhibit urease by 50% (IC_{50}).

Compound	IC_{50} (mM)
3a	2.77
4b	2.28
5a	1.16
5b	0.98
5c	0.69
9a	1.44
Hydroxyurea (HU)	0.61
Thiourea (TU)	2.72

Reactions were carried out in the presence of urea 10 mM.

Since the phosphoramidates inhibited the urease activity at different extents a cluster analysis employing data obtained at 10 μM and 20 μM was obtained in order to facilitate the grouping of these compounds and a comparison with standard urease inhibitors hydroxyurea and thiourea (Figure 1).

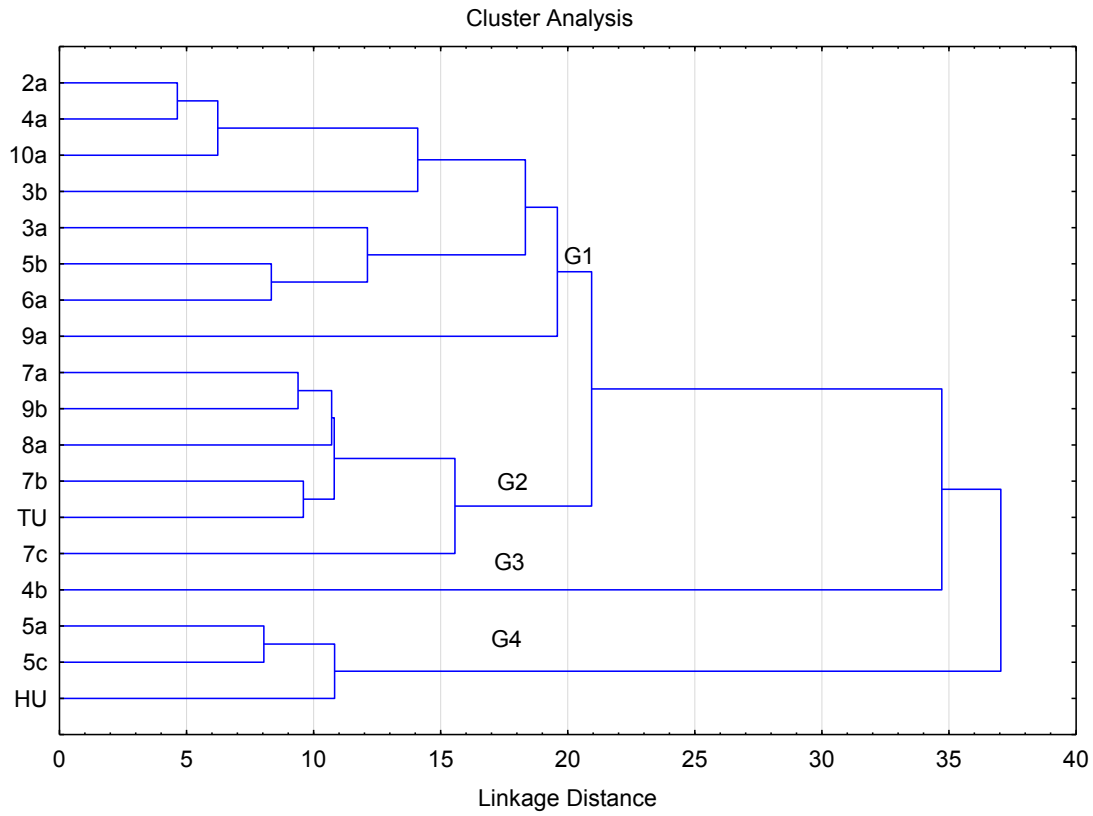

Figure 1 - Cluster analysis for phosphoramidates. (TU = thiourea and HU = hydroxyurea)

As can be observed in Figure 1, four main groups of compounds were formed: G1 and G2 include compounds that are poor urease inhibitors, including the reference thiourea (TU); G3 and G4 include compounds that are better active urease inhibitors compared with the standard hydroxyurea (HU). The inhibitory ureolitic activity of compounds **5a** and **5c** was comparable to that of the hydroxyurea, **5c** being the most active one. Among the three most active phophoramidates (shown in G3 and G4), all of them bear the cyclohexylamine group, which highlights the importance of this unit for biological activity. The phenoxy group seems to not contribute for the inhibitory ureolitic activity of the synthesized phosphoramidates as such group is present in all compounds, including those that function as positive allosteric effectors. Compounds prepared from *p*-bromophenol (**1c**, **3b**, **5c**, **6a**, **7b**, **9c** and **11b**), *p*-chlorophenol (**1a**, **2a**, **3a**, **4a**, **5a**, **7a**, **9a** and **10a**) or *m*-chlorophenol (**1b**, **4b**, **5b**, **8a**, **9b** and **11a**) were among the most active, while compounds derived from *p*-nitrophenol (**1e**, **2b** and **5b**), *o*-bromophenol (**1d** and **4c**) or *p*-fluorophenol (**1f**, **4d**, **7c**, **9d** and **11c**) were less active. However, it is important to highlight that the presence of phenol groups per se is not the main feature associated with biological activity since some compounds containing *p*-chlorophenol (**2a**, **3a**, **4a**, **10a**) and *p*-bromophenol (**3b** and **6a**) were poorly active.

A computational study was carried out to predict their physicochemical properties, since it is related to the absorption, distribution, metabolism, excretion and toxicity (ADMET) properties (MANGAL *et al*., 2013). Screening was conducted to evaluate the characteristics of the candidate drugs based on Lipinski's Rule of Five (LIPINSKI *et al*., 1997) and other related criteria added by Veber and co-workers (VEBER *et al*., 2002). The molecular attributes analyzed included the calculated octan-1-ol/water partition coefficient (cLogP ≤ 5); number of hydrogen-bond donors (HBD ≤ 5); number of hydrogen bond acceptors (HBA ≤ 10); molecular weight (MW ≤ 500); number of rotatable bonds (nRotb < 10); and topological polar surface area (TPSA < 140 $Å^2$). Values in parentheses represent the ideal values according to Lipinski (LIPINSKI *et al*., 1997) and Veber (VEBER *et al*., 2002). Physicochemical parameters (Tables 3 and 4) were calculated using Osiris Property Explorer (Tetko, 2005) and Molinspiration (http://www.molinspiration.com/cgi-bin/properties), good free

computational tools which help to predict pharmacokinetic properties of candidate drugs used by several research groups (ALAFEEFY *et al*., 2012; OLIVEIRA *et al*., 2012b; TEIXEIRA *et al*., 2013).

Normally, the drugs interacting with enzymes inside the body have LogP values between 2 and 5 (TAMBUNAN *et al*., 2011). In this respect, most of the 25 compounds present LogP values within this range, the exceptions being compounds **5a**, **5b**, **5c** and **6a** (Tables 2 and 3). Interestingly to note is that despite the high LogP values, compounds **5a**, **5b**, **5c** are among the most actives.

Analysis of theoretical toxicity risks revealed that all compounds examined might not be tumorigenic or irritating (Table 3). However, five compounds might have mutagenic effect (**3b**, **5c**, **6a**, **9c** and **11b**) and two could possibly have some effect on mammalian reproduction (**4d** and **2b**) (Table 3). With regard to solubility in water of organic molecules (log S), only compounds **5c** (logS = -6.57) and **6a** (logS = -7.19) present solubility values outside the limits (-6.5 – 0.5).(Maalej *et al*., 2011) The negative values of the drug-likeness calculations, between -28.83 and -11.68 (Table 3) indicate that compounds of the series **2-11** do not contain fragments that are frequently present in commercial drugs (LIPINSKI *et al*., 2001; PROUDFOOT, 2002).

Table 3. Predicted drug-likeness properties and toxicity risks of compounds calculated by Osiris package

Comp.	*cLogP*	Log*S*	MW	*Toxicity risks*[a]				Drug-likeness	Drug-Score
				M	T	I	R		
2a	3.61	-4.45	388	-	-	-	-	-15.79	0.33
2b	0.3	-1.87	357	-	-	-	±	-23.46	0.36
3a	4.37	-6.40	358	-	-	-	-	-11.68	0.23
3b	4.46	-6.5	403	±	-	-	-	-15.17	0.17
4a	4.62	-5.99	370	-	-	-	-	-16.24	0.23
4b	4.62	-5.99	370	-	-	-	-	-17.52	0.23
4c	4.70	-6.09	415	-	-	-	-	-21.01	0.21
4e	4.07	-5.57	354	-	-	-	-	-18.55	0.27
5a	5.4	-6.37	400	-	-	-	-	-21.03	0.19
5b	5.4	-6.37	400	-	-	-	-	-22.31	0.19
5c	5.57	-6.57	489	±	-	-	-	-24.22	0.12
5d	4.07	-5.57	354	-	-	-	-	-18.55	0.27
6a	5.09	-7.19	431	±	-	-	-	-16.61	0.14
7a	3.77	-3.21	318	-	-	-	-	-15.72	0.39
7b	3.21	-2.79	363	-	-	-	-	-18.05	0.42
7c	3.21	-2.79	302	-	-	-	-	-18.05	0.42
8a	4.97	-4.98	374	-	-	-	-	-21.84	0.26
9a	3.46	-3.92	342	-	-	-	-	-11.95	0.37
9b	3.46	-3.92	342	-	-	-	-	-13.09	0.37
9c	3.54	-4.02	387	±	-	-	-	-15.0	0.28
9d	2.9	-3.50	326	-	-	-	-	-14.14	0.41
10a	4.82	-5.84	386	-	-	-	-	-16.74	0.25
11a	1.04	-2.15	346	-	-	-	-	-12.13	0.45
11b	1.12	-2.24	391	±	-	-	-	-14.04	0.34
11c	0.49	-1.72	330	-	-	-	-	-13.19	0.46
HU	-1.45	-1.00	76.0	-	-	-	-	-0.19	0.09
TH	-0.95	-0.88	76.0	-	-	-	-	-2.21	0.54

HU, Hydroxyurea; TH, Thiourea; clogP, calculated lipophilicity; logS, logarithm of aqueous solubility measured in M; MW, molecular weight; M, mutagenic effect; T, tumorigenic effect; I, irritating effect; R, reproductive effect, [a]Ranked according to: (-), no bad effect; (±), medium bad effect; (+), bad effect

Compound **2b** is the one with the highest HBA number (equal to 9), close to the limit of 10 predicted by Lipinsky's rule. On the other hand some compounds (**4a**, **3a**, **4b**, **4c**, **4d**, **3b** and **6a**) show values of HBD = 2, while hydroxyurea presents HBD = 4. From the data presented so far for compounds of the series **2-11**, the parameters described in Lipinski's rules, are within the limit set by such rules. Among the compounds studied, eleven of them have one rule violation, which is within the limits established (two) (Lipinski *et al.*, 2001). Only compounds **4d** (TPSA = 96.18) and **2b** (TPSA = 97.07) (Table 4) are

expected to exhibit moderate bioavailability, based on the acceptable range (61 ≤ TPSA ≤ 140), while for others it is expected a good bioavailability. TPSA was used to calculate the percentage of absorption (%ABS) as reported (ERTL *et al*., 2000). From all these parameters, it can be observed that all the title compounds exhibited a great %ABS ranging from 75.51% to 97.69%. In general the compounds in this series possess a high number of rotatable bonds (4–8) and therefore, exhibit large conformational flexibility, while the standard´s compounds presented nRotB = 0 (Table 4).

Table 4. Drug-likeness calculations of compounds by using Molinspiration Cheminformatics software

Comp.	TPSA[b]	HBD	HBA	Lipinski's violations	Volume	nRotB	%ABS[c]
2a	48.01	0	5	0	306.974	5	92.44
2b	97.07	0	9	0	300.977	5	75.51
3a	50.36	2	4	0	302.533	6	91.63
3b	50.36	2	4	1	306.882	6	91.63
4a	50.35	2	4	1	339.705	6	91.63
4b	50.36	2	4	1	339.705	6	91.63
4c	50.36	2	4	1	344.055	6	91.63
4e	50.36	2	4	0	331.101	6	91.63
5a	47.57	1	4	1	331.237	6	92.59
5b	47.57	1	4	1	331.237	6	92.59
5c	47.57	1	4	1	339.936	6	92.59
5d	50.36	2	4	0	331.101	6	91.63
6a	50.36	2	4	1	340.004	6	91.63
7a	32.78	0	4	0	293.93	8	97.69
7b	32.78	0	4	0	298.279	8	97.69
7c	32.781	0	4	0	285.325	8	97.69
8a	38.78	0	4	1	308.349	7	95.62
9a	32.78	0	4	0	306.813	4	97.69
9b	32.78	0	4	0	306.813	4	97.69
9c	32.78	0	4	0	311.162	4	97.69
9d	32.78	0	4	0	298.208	4	97.69
10a	38.77	0	4	1	314.791	5	95.62
11a	51.25	0	6	0	291.179	4	91.32
11b	51.25	0	6	0	295.528	4	91.32
11c	51.249	0	6	0	282.574	4	91.32
HU[d]	75.349	4	4	0	63.327	0	83.00
TU[d]	52.046	2	4	0	63.074	0	91.04

[a] HBD, number of hydrogen bond donor; HBA, number of hydrogen bond acceptor.

[b] TPSA: Total polar surface area

[c] %ABS = 109 - 0.345 x TPSA(Ertl *et al.*, 2000)

[d] HU, Hydroxyurea; TU, Thiourea

One factor closely related to the affinity of a receptor is the molecular volume. This parameter does not seem to have a direct relationship with the biological activity, since the compound used as a positive control (hydroxyurea) showed small molecular volume (63 A^3) compared to compound **5c** (339.936 A^3). In an attempt to find some correlation between electronic properties and biological activity (CORREA-BASURTO *et al*., 2007; ARANTES *et al*., 2011) the HOMOs and LUMOs of the compounds were examined. The calculated energies gaps are also listed in Table 5. The computational calculations were performed using Spartan (HEHRE and OHLINGER, 2010) and Gaussian (FRISCH *et al*., 2009).

Table 5. Descriptors Quantum-Chemical for compounds of series **2-11** and references

Comp.	HOMO	LUMO	GAP[a]	Moment dipole
2a	-6.61	-0.92	-5.69	4.14
2b	-6.35	-2.99	-3.36	8.35
3a	-6.19	-0.88	-5.32	5.78
3b	-6.01	-0.49	-5.52	5.77
4a	-6.50	-0.82	-5.68	6.55
4b	-6.56	-0.83	-5.72	8.62
4c	-6.36	-0.38	-5.98	3.44
4d	-6.58	-0.81	-5.77	6.63
5a	-6.67	-0.92	-5.75	6.44
5b	-6.86	-0.92	-5.94	5.55
5c	-6.49	-0.77	-5.72	6.43
5d	-7,05	-2,57	-4,48	5,96
6a	-5.98	-0.89	-5.10	6.27
7a	-6.32	-0.82	-5.51	7.25
7b	-6.09	-0.36	-5.72	6.72
7c	-6.04	-0.31	-5.74	6.28
8a	-6.77	-0.91	-5.86	3.39
9a	-6.31	-0.82	-5.49	7.03
9b	-6.29	-0.82	-5.47	4.89
9c	-6.21	-0.40	-5.82	6.99
9d	-6.39	-0.80	-5.59	6.51
10a	-6.66	-0.91	-5.74	6.28
11a	-6.28	-0.84	-5.44	2.45
11b	-6.26	-0.52	-5.73	4.51
11c	-6.23	-0.47	-5.76	4.07
Hydroxyurea	-7.60	-0.19	-7.41	5.00
Thiourea	-6.06	-0.33	-5.73	7.70

[a] GAP = HOMO-LUMO

The IC_{50} values were converted to their related negative logarithmic state, which is $\log(1/IC_{50})$ and further used as dependent variable in developing the QSAR models. The descriptors used in the regression analysis are cLogP, HOMO energy, LUMO energy, GAP energy, moment dipole and molecular volume (Tables 2, 3 and 4).

Preliminary analysis was carried out in terms of a correlation analysis between $-LogIC_{50}$ and various molecular descriptors and the results are presented in Table 6. This was done to remove the chances of intercorrelation among the molecular descriptors that may lead to false predicting models.

Table 6. Correlation matrix for $-LogIC_{50}$ with molecular descriptors.

	$-LogIC_{50}$	HOMO	LUMO	GAP	Moment dipole	Volume	cLogP
$-LogIC_{50}$	1.000						
HOMO	0,645	1.000					
LUMO	0.363	0.365	1.000				
GAP	0.649	0.927	0.686	1.000			
Moment dipole	0.589	0.578	0.105	0.503	1.000		
Volume	0.248	0.290	0.970	0.614	0.143	1.000	
cLogP	0.178	0.285	0.963	0.609	0.078	0.984	1.000

The values of the selected descriptors used in the regression analysis are presented in Tables 3, 4 and 5. The models were built using the multiple linear regression (MLR) method as employed in the BuildQsar software (DE OLIVEIRA and GAUDIO, 2001). The data depicted in Table 6, indicated poor correlation between urease activity with these descriptors (see graphs in the supplemental material). Thus, models using multiple linear regression (MLR) method were obtained since it was not possible to validate using the Leave One Out (LOO) method (DE OLIVEIRA and GAUDIO, 2001).

It appears that there is a correlation between the structure of compounds **HU**, **5b**, **5a**, **9a**, **TU** and **4b** with the inhibitory activity of urease. Compounds **3a** and **5c** would be outliers in this linear regression ($-LogIC_{50}$ = -0.1333MD + 0.7885; R^2 = 0.9823). However, no plausible explanation to justify the removal of these compounds (**3a** and **5c**) can be proposed. Furthermore, the structures of the compounds used as positive control (**HU** and **TU**) differ significantly from the compounds synthesized in this work.

The highest and lowest energy difference between the HOMO and LUMO (gap energies) were observed for compounds **4c** (-5.98 eV) and **2b** (-4.37 eV), respectively. However, it was not observed for these compounds under discussion a clear correlation of biological activity with the measures of nucleophilicity and electrophilicity (HOMO and LUMO energies, respectively). Figure 2 shows the distributions and energy levels of the frontier molecular orbital computed at the B3LYP/6–311++G(2d,p) level for the most active compound (**5c**).

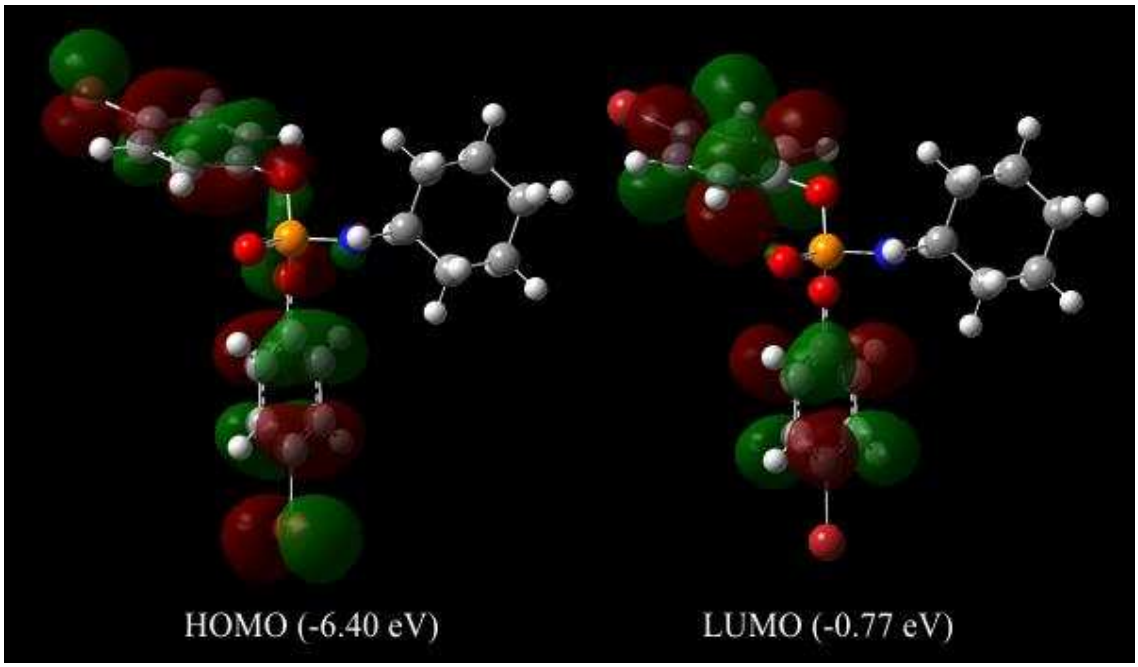

Figure 2 - Molecular orbital surfaces and energy levels given in parentheses for the HOMO and LUMO of the most active compound computed at B3LYP/6–311++G(2d,p) level in water.

4.3. Experimental

4.3.1. Chemistry

All the chemicals were purchased from Sigma Aldrich (Milwaukee, WI, USA) and used without purification. The ^{1}H- and ^{13}C-NMR spectra were recorded on a Varian Mercury 300 instrument (300 MHz and 75 MHz respectively). Tetramethylsilane was used as internal standard (δ = 0) and deuterated DMSO as solvent. IR spectra were obtained using a Perkin Elmer

Paragon 1000 FTIR spectrophotometer, using potassium bromide (1% v/v) disks, scanning from 600 to 4000 cm^{-1}. HRMS data were recorded under ESI conditions on a micrOTOF-QII Bruker spectrometer. The melting points were determined using a MQAPF-301 melting point apparatus (Microquimica, Brazil) and were not corrected. Analytical thin layer chromatography analysis was conducted on aluminum backed pre-coated silica gel plates. Flash column chromatography was performed using silica gel 60 (63–230 μm).

4.3.1.1. General method of preparation of phosphorodichloridate derivatives (**1a-1f**).

Phosphorus oxychloride (1.0 mL, 10.8 mmol) in dry diethyl ether (10.0 mL) was placed under a nitrogen atmosphere in a 50 mL round bottom flask. The contents were cooled to 0 ºC using an ice bath. A solution of substituted phenols (9.8 mmol) and triethylamine (1.5 mL, 10.8 mmol) in anhydrous diethyl ether (25 mL) was added dropwise while maintaining the temperature at 0 ºC throughout the addition (ca: 1 h). After this period, the ice bath was removed and the mixture was allowed to gradually warm up to room temperature and was stirred vigorously for 18 hours. The precipitated triethylammonium salt was filtered through a sintered glass funnel under vacuum and the precipitate was washed with additional anhydrous diethyl ether. The organic layers were combined and the solvent was evaporated under vacuum using a rotary evaporator to yield crude phosphorodichloridate (**1a-1f**) as viscous oil that were used without further purification. The spectroscopic and spectrometric data of all compounds are consistent with predicted in the literature.

4.3.1.2. General method of preparation of phosphoramidates.

Phosphorodichloridate derivatives (**1a-1f**) (500 mg, 1.7 mmol) were placed into a round bottom flask under nitrogen atmosphere. Using a dry syringe, anhydrous dichloromethane (10 mL) was added and the mixture was cooled to 0 ºC. A solution of different amines (6.9 mmol) in anhydrous dichloromethane (20 mL) was added dropwise with vigorous stirring over a period of 1 h. After completion of the addition, the reaction mixture was allowed to gradually warm to room temperature and stirred for 18–22 h until the reaction

was complete as evidenced from TLC analyses. The crude products were concentrated in vacuum, anhydrous diethyl ether (15 mL) was added and the precipitated triethylammonium hydrochloride salt was filtered. The precipitate was further washed with additional diethyl ether (2 x 15 mL). The combined ether extracts were combined and concentrated in a rotary evaporator under reduced pressure to afford the required compounds. The synthesis of compounds **2a**, **3a**, **4a**, **5a** and **10a** is described in the literature (Krishnan *et al.*, 1985; Ruveda *et al.*, 1975; Roubinek *et al.*, 1980; Cramer and Hennrich, 1961; Kašpárek and Mollin, 1980).

4.3.1.3. Spectral data

*bis(4-chlorophenyl) morpholinophosphonate (**2a**)*. It was obtained as a light yellow amorphous solid in 65% yield (purified by silica gel column chromatography, using hexane/acetone 4:1 v/v as the eluting solvent): TLC R_f = 0.45 (hexane/acetone 4:1 v/v); mp: 73.1-74.6 ºC. IR (ATR, cm^{-1}) $\bar{\nu}_{max}$ 2965, 2857, 2363, 1588, 1484, 1259, 1193, 1089, 911, 830, 771, 683, 538, 482. ^1H NMR (300 MHz, $CDCl_3$) δ 3.23-3.31 (4H, m, H-7, H-10), 3.55-3.62 (4H, m, H-8, H-9), 7.13-7.21 (4H, m, H-1, H-5), 7.25-7.34 (4H, m, H-2, H-4). ^{13}C NMR (75 MHz, $CDCl_3$) δ 44.93 (CH_2, C-7, C-10), 66.71 (CH_2, d, J = 5.3 Hz, C-8, C-9), 121.63 (CH, d, J = 4.9 Hz, C-1, C-5), 130.07 (CH, C-2, C-4), 130.80 (C, C-3), 149.29 (C, d, J = 6.8 Hz, C-6). GC-MS *m/z*: 387 $[M]^{+\bullet}$. HREIMS m/z (M + H^+): calcd for $C_{16}H_{16}Cl_2NO_4P$, 388.0267; found, 388.0158.

*bis(4-nitrophenyl) morpholinophosphonate (**2b**)*. It was obtained as a white crystal in 11% yield (purified by silica gel column chromatography, using hexane/ethyl acetate 1:1 v/v as the eluting solvent): TLC R_f = 0.32 (hexane/ethyl acetate 1:1 v/v); mp: 161.5-162.9 ºC. IR (ATR, cm^{-1}) $\bar{\nu}_{max}$ 2858, 1588, 1513, 1342, 1199, 908, 846, 745, 471; ^1H NMR (300 MHz, $CDCl_3$) δ 3.30-3.38 (4H, m, H-7, H-10), 3.60-3.67 (4H, m, H-8, H-9), 7.38-7.45 (4H, m, H-1, H-5), 8.24-8.31 (4H, m, H-2, H-4). ^{13}C NMR (75 MHz, $CDCl_3$) δ 44.67 (CH_2, C-7, C-10), 66.59 (CH_2, d, J = 5.7 Hz, C-8, C-9), 120.55 (CH, d, J = 5.4 Hz, C-1, C-5), 125.87 (CH, C-2, C-4), 144.95 (C, C-3), 155.04 (C, d, J = 6.5 Hz, C-6). GC-

MS *m/z*: 409 $[M]^{+\bullet}$. HREIMS m/z (M + H^+): calcd for $C_{16}H_{16}N_3O_8P$, 410.0748; found, 410.0759.

*4-chlorophenyl N,N´-diphenyl phosphate (**3a**)*. It was obtained as a colorless crystal in 38% yield (purified by silica gel column chromatography, using hexane/ethyl acetate 1:1 v/v as the eluting solvent): TLC R_f = 0.63 (hexane/ethyl acetate 1:1 v/v); mp: 169.4 – 170.0 ºC. IR (ATR, cm^{-1}) $\bar{\nu}_{max}$ 3374, 3142, 2980, 2906, 2367, 1600, 1476, 1394, 1298, 1204, 911, 845, 746, 686, 508. ^{1}H NMR (300 MHz, DMSO) δ 6.85 (2H, t, *J* = 6.9 Hz, -NH), 7.08-7.28 (10H, m, H-7, H-8, H-9, H-10, H-11), 7.42-7.46 (2H, m, H-1, H-5), 8.50 (2H, m, H-2, H-4). ^{13}C NMR (75 MHz, DMSO) δ 118.08 (CH, d, *J* = 7.8 Hz, C-7, C-11), 121.57 (CH, C-9), 122.97 (CH, d, *J* = 4.7 Hz, C-1, C-5), 129.44 (C, C-3), 129.65 (CH, C-8, C-10), 130.31 (CH, C-2, C-4), 141.32 (C, d, *J* = 1.7 Hz, C-12), 149.85 (C, d, *J* = 6.3 Hz, C-6). GC-MS *m/z*: 358 $[M]^{+\bullet}$. HREIMS m/z (M + H^+): calcd for $C_{18}H_{16}ClN_2O_2P$, 359.0711; found, 359.0607.

*4-bromophenyl N,N´-diphenyl phosphate (**3b**)*. It was obtained as a colorless crystal in 16% yield (purified by silica gel column chromatography, using hexane/ethyl acetate 2:1 v/v as the eluting solvent): TLC R_f = 0.26 (hexane/ethyl acetate 2:1 v/v); mp: 189.8-191.4 ºC; IR (ATR, cm^{-1}) $\bar{\nu}_{max}$ 3362, 3139, 2906, 1476, 1203, 912, 745, 506. ^{1}H NMR (300 MHz, $CDCl_3$) δ 5.93 (2H, d, *J* = 8.9 Hz, -NH), 6.96-7.11 (8H, m, H-1, H-5, H-7, H-9, H-11), 7.18-7.38 (6H, m, H-2, H-4, H-8, H-10). ^{13}C NMR (75 MHz, $CDCl_3$) δ 118.59 (C, C-3), 118.69 (CH, C-7, C-11), 122.61 (CH, C-9), 122.69 (CH, C-1, C-5), 122.90 (CH, C-8, C-10), 129.67 (CH, C-2, C-4), 132.95 (C, C-12), 138.85 (C, C-6). GC-MS *m/z*: 402 $[M]^{+\bullet}$. HREIMS m/z (M + H^+): calcd for $C_{18}H_{16}BrN_2O_2P$, 403.0206; found, 403.0071.

*4-chlorophenyl N,N´-dicyclohexylamidophosphinate (**4a**)*. It was obtained as an amorphous solid in 66% yield (purified by silica gel column chromatography, using hexane/ethyl acetate 3:1 v/v as the eluting solvent): TLC R_f = 0.12 (hexane/ethyl acetate 3:1 v/v); mp: 106.6-107.6 ºC; IR (ATR, cm^{-1}) $\bar{\nu}_{max}$ 3230, 2925, 2851, 1488, 1434, 1310, 1204, 1087, 1002, 888, 834, 754, 648, 648, 529,

486. ^{1}H NMR (300 MHz, $CDCl_3$) δ 0.97-2.00 (20H, m, -C<u>H</u>$_2$), 2.46 (2H, broad s, -N<u>H</u>), 3.0-3.15 (2H, m, H-12), 7.07-7.19 (2H, m, H-1, H-5), 7.20-7.35 (2H, m, H-2, H-4). ^{13}C NMR (75 MHz, $CDCl_3$) δ 25.31 (CH_2, C-8, C-10), 25.59 (CH_2, C-9), 36.18 (CH_2, t, J = 5.0 Hz, C-7, C-11), 50.86 (CH, C-12), 121.79 (CH, d, J = 5.1 Hz, C-1, C-5), 129.40 (C, C-3), 129.67 (CH, C-2, C-4), 150.28 (C, d, J = 6.5 Hz, C-6). GC-MS *m/z*: 370 $[M]^{+\bullet}$. HREIMS m/z (M + H^+): calcd for $C_{18}H_{28}ClN_2O_2P$, 371.1650; found, 371.1571.

*3-chlorophenyl N,N´-dicyclohexylamidophosphinate (**4b**)*. It was obtained as a white amorphous solid in 6% yield (purified by silica gel column chromatography, using hexane/ethyl acetate 1:1 v/v as the eluting solvent): TLC R_f = 0.43 (hexane/ethyl acetate 1:1 v/v); mp: 92.0-93.0 ºC. IR (ATR, cm^{-1}) $\bar{\nu}_{max}$ 3377, 3176, 2927, 2851, 1589, 1424, 1207, 1092, 1017, 930, 774, 666, 526. ^{1}H NMR (300 MHz, $CDCl_3$) δ 1.02-1.99 (20H, m, -C<u>H</u>$_2$), 2.50 (2H, broad s, -N<u>H</u>), 3.0-3.17 (2H, m, H-12), 7.04-7.31 (4H, m, H-1, H-2, H-3, H-5). ^{13}C NMR (75 MHz, $CDCl_3$) δ 25.31 (CH_2, C-8, C-10), 25.59 (CH_2, C-9), 36.15 (CH_2, t, J = 4.5 Hz, C-7, C-11), 50.90 (CH, C-12), 118.80 (CH, d, J = 4.9 Hz, C-5), 121.02 (CH, d, J = 5.4 Hz, C-1), 124.51 (CH, C-3), 130.43 (CH, C-2), 134.85 (C, C-4), 152.28 (C, d, J = 6.3 Hz, C-6). GC-MS *m/z*: 370 $[M]^{+\bullet}$. HREIMS m/z (M + H^+): calcd for $C_{18}H_{28}ClN_2O_2P$, 371.1650; found, 371.1574.

*2-bromophenyl N,N´-dicyclohexylamidophosphinate (**4c**)*. It was obtained as a white solid in 36% yield (purified by silica gel column chromatography, using hexane/ethyl acetate 2:1 v/v as the eluting solvent): TLC R_f = 0.22 (hexane/ethyl acetate 2:1 v/v); mp: 111.6-113.2 ºC; IR (ATR, cm^{-1}) $\bar{\nu}_{max}$ 3208, 2928, 2850, 1474, 1219, 1087, 908, 756, 506. ^{1}H NMR (300 MHz, $CDCl_3$) δ 1.20-2.03 (20H, m, -C<u>H</u>$_2$), 2.69 (2H, t, J = 9.9 Hz, -N<u>H</u>), 3.05-3.25 (2H, m, H-12), 6.94-7.00 (1H, m, H-3), 7.21-7.27 (1H, m, H-2), 7.50-7.58 (2H, m, H-1, H-4). ^{13}C NMR (75 MHz, $CDCl_3$) δ 25.04 (CH_2, C-8, C-10), 25.34 (CH_2, C-9), 35.88 (CH_2, d, J = 4.8 Hz, C-7, C-11), 50.55 (CH, C-12), 114.47 (C, C-5), 121.86 (CH, d, J = 2.9 Hz, C-1), 125.18 (CH, C-3), 128.59 (CH, C-2), 133.11 (CH, C-4), 148.61 (C, d, J = 6.0 Hz, C-6). GC-MS *m/z*: 416 $[M]^{+\bullet}$. HREIMS m/z (M + H^+): calcd for $C_{18}H_{28}BrN_2O_2P$, 415.1145; found, 415.0993.

*4-fluorophenyl N,N´-dicyclohexylamidophosphinate (**4d**)*. It was obtained as a white amorphous solid in 28% yield (purified by silica gel column chromatography, using hexane/ethyl acetate 2:1 v/v as the eluting solvent): TLC R_f = 0.39 (hexane/ethyl acetate 2:1 v/v); mp 117.9-119.3 ºC; IR (ATR, cm^{-1}) $\bar{\nu}_{max}$ 3232, 2926, 2853, 1503, 1435, 1198, 1087, 892, 812, 484. ^{1}H NMR (300 MHz, $CDCl_3$) δ 1.03-1.97 (20H, m, -C$\underline{H}_2$), 2.53 (2H, t, *J* = 2.4 Hz, -N$\underline{H}$), 2.99-3.16 (2H, m, H-12), 6.92-7.02 (2H, m, H-2, H-4), 7.13-7.21 (2H, m, H-1, H-5). ^{13}C NMR (75 MHz, $CDCl_3$) δ 25.05 (CH_2, C-8, C-10), 25.34 (CH_2, C-9), 35.94 (CH_2, C-7, C-11), 50.58 (CH, C-12), 115.93 (CH, d, *J* = 23.2 Hz, C-2, C-4), 121.48 (CH, q, *J* = 4.8 Hz and *J* = 8.2 Hz, C-1, C-5), 147.31 (C, q, *J* = 2.1 Hz and *J* = 6.2 Hz, C-6), 159.11 (C, d, *J* = 240.8 Hz, C-3). GC-MS *m/z*: 354 $[M]^{+\bullet}$. HREIMS m/z (M + H^+): calcd for $C_{18}H_{28}FN_2O_2P$, 355.1945; found, 355.1963.

*bis(4-chlorophenyl) cyclohexylphosphoramidate (**5a**)*. It was obtained as a colorless solid in 40% yield (purified by silica gel column chromatography, using hexane/ethyl acetate 3:1 v/v as the eluting solvent): TLC R_f = 0.60 (hexane/ethyl acetate 3:1 v/v); mp: 123.7-124.2 ºC. IR (ATR, cm^{-1}) $\bar{\nu}_{max}$ 3192, 2933, 2854, 1589, 1483, 1201, 1092, 1014, 918, 834, 770, 661, 519. ^{1}H NMR (300 MHz, $CDCl_3$) δ 1.06-1.93 (11H, m, -C$\underline{H}_2$, H-12), 3.17-3.22 (1H, m, -N$\underline{H}$), 7.15-7.22 (4H, m, H-1, H-5), 7.28-7.32 (4H, m, H-2, H-4). ^{13}C NMR (75 MHz, $CDCl_3$) δ 25.14 (CH_2, C-8, C-10), 25.43 (CH_2, C-9), 35.67 (CH_2, d, *J* = 5.0 Hz, C-7, C-11), 51.56 (CH, C-12), 121.73 (CH, d, *J* = 5.1 Hz, C-1, C-5), 129.91 (CH, C-2, C-4), 130.48 (C, C-3), 149.56 (C, d, *J* = 6.9 Hz, C-6). GC-MS *m/z*: 399 $[M]^{+\bullet}$. HREIMS m/z (M + H^+): calcd for $C_{18}H_{20}Cl_2NO_3P$, 400.0631; found, 400.0520.

*bis(3-chlorophenyl) cyclohexylphosphoramidate (**5b**)*. It was obtained as a white amorphous solid in 22% yield (purified by silica gel column chromatography, using hexane/ethyl acetate 4:1 v/v as the eluting solvent): TLC R_f = 0.28 (hexane/ethyl acetate 4:1 v/v); mp: 89.3-89.7 ºC. IR (ATR, cm^{-1}) $\bar{\nu}_{max}$ 3184, 2933, 2850, 1584, 1468, 1249, 1199, 1112, 940, 776, 674, 613. ^{1}H NMR (300 MHz, $CDCl_3$) δ 1.09-1.93 (11H, m, -C$\underline{H}_2$, H-12), 3.07-3.29 (1H, m, -N$\underline{H}$), 7.10-

7.34 (8H, m, H-1, H-2, H-3, H-5). ^{13}C NMR (75 MHz, $CDCl_3$) *δ* 25.13 (CH_2, C-8, C-10), 25.43 (CH_2, C-9), 35.65 (CH_2, d, *J* = 5.0 Hz, C-7, C-11), 51.62 (CH, C-12), 118.7 (CH, d, *J* = 4.9 Hz, C-5), 121.02 (CH, d, *J* = 5.5 Hz, C-1), 125.53 (CH, C-3), 130.65 (CH, C-2), 135.13 (C, C-4), 151.45 (C, d, *J* = 7.0 Hz, C-6). GC-MS *m/z*: 399 $[M]^{+\bullet}$. HREIMS m/z (M + H^+): calcd for $C_{18}H_{20}Cl_2NO_3P$, 400.0631; found, 400.0530.

*bis(4-bromophenyl) cyclohexylphosphoramidate (**5c**)*. It was obtained as a light yellow amorphous solid in 8% yield (purified by silica gel column chromatography, using hexane/ethyl acetate 2:1 v/v as the eluting solvent): TLC R_f = 0.46 (hexane/ethyl acetate 2:1 v/v); mp: 143.5-144.9 ºC; IR (ATR, cm^{-1}) $\bar{\nu}_{max}$ 3177, 2929, 2855, 1583, 1481, 1197, 915, 830, 737, 521. ^{1}H NMR (300 MHz, $CDCl_3$) *δ* 1.04-1.94 (10H, m, -C<u>H</u>$_2$), 2.99 (1H, t, *J* = 12.3 Hz, -N<u>H</u>), 3.06-3.27 (1H, m, H-12), 7.09-7.16 (4H, m, H-1, H-5), 7.40-7.47 (4H, m, H-2, H-4). ^{13}C NMR (75 MHz, $CDCl_3$) *δ* 24.87 (CH_2, C-8, C-10), 25.17 (CH_2, C-9), 35.44 (CH_2, d, *J* = 5.1 Hz, C-7, C-11), 51.31 (CH, C-12), 117.85 (C, C-3), 121.89 (CH, d, *J* = 5.1 Hz, C-1, C-5), 132.65 (CH, C-2, C-4), 149.83 (C, d, *J* = 6.9 Hz, C-6). GC-MS *m/z*: 487 $[M]^{+\bullet}$. HREIMS m/z (M + H^+): calcd for $C_{18}H_{20}Br_2NO_3P$, 487.9620; found, 487.9512.

*bis(4-nitrophenyl) cyclohexylphosphoramidate (**5d**)*. It was obtained as a white solid in 12% yield (purified by silica gel column chromatography, using hexane/ethyl acetate 3:1 v/v as the eluting solvent): TLC R_f = 0.31 (hexane/ethyl acetate 3:1 v/v); mp: 175.4-176.7 ºC. IR (ATR, cm^{-1}) $\bar{\nu}_{max}$ 3157, 2926, 2851, 1589, 1512, 1341, 1207, 1105, 920, 854, 748, 618, 532. ^{1}H NMR (300 MHz, $CDCl_3$) *δ* 1.16-1.90 (10H, m, -C<u>H</u>$_2$), 3.15-3.37 (2H, m, -N<u>H</u>, H-12), 7.39-7.44 (4H, m, H-1, H-5), 8.22-8.28 (4H, m, H-2, H-4). ^{13}C NMR (75 MHz, $CDCl_3$) *δ* 24.79 (CH_2, C-8, C-10), 25.02 (CH_2, C-9), 35.37 (CH_2, d, *J* = 5.1 Hz, C-7, C-11), 51.64 (CH, C-12), 120.58 (CH, d, *J* = 5.6 Hz, C-1, C-5), 125.74 (CH, C-2, C-4), 144.73 (C, C-3), 155.55 (C, d, *J* = 6.4 Hz, C-6). GC-MS *m/z*: 421 $[M]^{+\bullet}$. HREIMS m/z (M + H^+): calcd for $C_{18}H_{20}N_3O_7P$, 422.1112; found, 422.1027.

*4-bromophenyl 4,4´-dimethyl-(N,N´-diphenyl) phosphate (**6a**)*. It was obtained as a white amorphous solid in 13% yield (purified by silica gel column chromatography, using hexane/ethyl acetate 2:1 v/v as the eluting solvent): TLC R_f = 0.51 (hexane/ethyl acetate 2:1 v/v); mp: 104.7-106.1 ºC; IR (ATR, cm^{-1}) $\bar{\nu}_{max}$ 3377, 3139, 1616, 1482, 1202, 991, 817, 493. ^{1}H NMR (300 MHz, $CDCl_3$) δ 1.67 (6H, s, -C$\underline{H}_3$), 6.48-6.65 (10H, m, H-1, H-5, H-7, H-8, H-10, H-11), 6.88-6.92 (2H, m, H-2, H-4), 7.32 (2H, d, *J* = 9.9 Hz, -N$\underline{H}$). ^{13}C NMR (75 MHz, $CDCl_3$) δ 19.44 (CH_3, C-13), 116.18 (C, C-3), 116.88 (CH, d, *J* = 7.4 Hz, C-7, C-11), 121.71 (CH, d, *J* = 4.6 Hz, C-1, C-5), 128.35 (C, C-9), 129.19 (CH, C-8, C-10), 131.20 (CH, C-2, C-4), 136.68 (C, C-12), 148.75 (C, d, *J* = 6.4 Hz, C-6). GC-MS *m/z*: 430 $[M]^{+\bullet}$. HREIMS m/z (M + H^+): calcd for $C_{20}H_{20}BrN_2O_2P$, 431.0519; found, 431.0532..

*4-chlorophenyl N,N,N´,N´-tetraethyldiamidophosphinate (**7a**)*. It was obtained as a light yellow oil in 38% yield (purified by silica gel column chromatography, using hexane/ethyl acetate 3:1 v/v as the eluting solvent): TLC R_f = 0.33 (hexane/ethyl acetate 3:1 v/v); IR (ATR, cm^{-1}) $\bar{\nu}_{max}$ 2972, 2933, 2874, 1592, 1486, 1380, 1163, 1091, 1025, 897, 763, 541. ^{1}H NMR (300 MHz, $CDCl_3$) δ 1.07 (12H, t, *J* = 7.2 Hz, -C$\underline{H}_3$), 3.10 (8H, dq, *J* = 7.2 Hz and *J* = 3.0 Hz, -C$\underline{H}_2$), 7.12-7.19 (2H, m, H-1, H-5), 7.21-7.28 (2H, m, H-2, H-4). ^{13}C NMR (75 MHz, $CDCl_3$) δ 14.32 (CH_3, d, *J* = 2.2 Hz, C-8), 39.95 (CH_2, d, *J* = 11.4 Hz, C-7), 121.76 (CH, d, *J* = 5.3 Hz, C-1, C-5); 129.14 (C, C-3), 129.70 (CH, C-2, C-4), 150.40 (C, d, *J* = 6.0 Hz, C-6). GC-MS *m/z*: 318 $[M]^{+\bullet}$. HREIMS m/z (M + H^+): calcd for $C_{14}H_{24}ClN_2O_2P$, 319.1337; found, 319.1235.

*4-bromophenyl N,N,N´,N´-tetraethyldiamidophosphinate (**7b**)*. It was obtained as a light yellow oil in 13% yield (purified by silica gel column chromatography, using hexane/ethyl acetate 2:1 v/v as the eluting solvent): TLC R_f = 0.33 (hexane/ethyl acetate 2:1 v/v); IR (ATR, cm^{-1}) $\bar{\nu}_{max}$ 2971, 2922, 2877, 1482, 1206, 1163, 893, 830, 718. ^{1}H NMR (300 MHz, $CDCl_3$) δ 0.99-1.13 (12H, m, -C$\underline{H}_3$), 3.04-3.20 (8H, m, -C$\underline{H}_2$), 7.06-7.15 (2H, m, H-1, H-5), 7.36-7.46 (2H, m, H-2, H-4). ^{13}C NMR (75 MHz, $CDCl_3$) δ 14.33 and 13.90 (CH_3, d, *J* = 2.2 Hz, C-8), 40.08 and 39.86 (CH_2, d, *J* = 4.7 Hz, C-7), 118.16 and 116.73 (C, C-3),

122.28 and 122.20 (CH, d, *J* = 2.4 Hz, C-1, C-5), 132.81 and 132.56 (CH, C-2, C-4), 149.76 and 150.96 (C, d, *J* = 5.8 Hz, C-6). GC-MS *m/z*: 362 $[M]^{+\bullet}$. HREIMS m/z (M + H^+): calcd for $C_{14}H_{24}BrN_2O_2P$, 363.0832; found, 363.0743.

*4-fluorophenyl N,N,N´,N´-tetraethyldiamidophosphinate (**7c**)*. It was obtained as a white crystal in 25% yield (purified by silica gel column chromatography, using hexane/ethyl acetate 3:1 v/v as the eluting solvent): TLC R_f = 0.53 (hexane/ethyl acetate 3:1 v/v); IR (ATR, cm^{-1}) $\bar{\nu}_{max}$ 2973, 1501, 1380, 1168, 1025, 900, 817, 500. ^{1}H NMR (300 MHz, $CDCl_3$) δ 1.07 (12H, t, *J* = 7.2 Hz, -C<u>H</u>$_3$), 3.11 (8H, dq, *J* = 7.2 Hz and *J* = 18.3 Hz, -C<u>H</u>$_2$), 6.91-7.03 (2H, m, H-2, H-4), 7.13-7.20 (2H, m, H-1, H-5). ^{13}C NMR (75 MHz, $CDCl_3$) δ 14.05 (CH_3, d, *J* = 2.1 Hz, C-8), 39.63 (CH_2, d, *J* = 4.7 Hz, C-7), 115.97 (CH, d, *J* = 23.0 Hz, C-2, C-4), 121.43 (CH, q, *J* = 4.8 Hz and *J* = 8.1 Hz, C-1, C-5), 147.43 (C, C-6), 158.96 (C, d, *J* = 239.9 Hz, C-3). GC-MS *m/z*: 302 $[M]^{+\bullet}$. HREIMS m/z (M + H^+): calcd for $C_{14}H_{24}FN_2O_2P$, 303.1632; found, 303.1653.

*bis(3-chlorophenyl) N,N-diethyldiamidophosphinate (**8a**)*. It was obtained as a light yellow oil in 13% yield (purified by silica gel column chromatography, using hexane/ethyl acetate 3:1 v/v as the eluting solvent): TLC R_f = 0.36 (hexane/ethyl acetate 3:1 v/v); IR (ATR, cm^{-1}) $\bar{\nu}_{max}$ 2975, 1584, 1469, 1262, 1198, 1037, 925, 775, 676, 602, 541. ^{1}H NMR (300 MHz, $CDCl_3$): δ 1.07 (6H, t, *J* = 7.1 Hz, -C<u>H</u>$_3$), 3.23 (4H, dq, *J* = 12.4 Hz and *J* = 7.1 Hz, -C<u>H</u>$_2$), 7.31-7.64 (8H, m, H-1, H-2, H-3, H-5). ^{13}C NMR (75 MHz, $CDCl_3$): δ 8.68 (CH_3, C-8), 46.78 (CH_2, C-7), 121.39-121.97 (CH, m, C-5), 129.71-129.84 (CH, m, C-1), 130.19-130.36 (CH, m, C-3), 132.52-133.10 (CH, m, C-2), 147.85-148.04 (C, m, C-4), 148.38-148.66 (C, m, C-6). GC-MS *m/z*: 373 $[M]^{+\bullet}$. HREIMS m/z (M + H^+): calcd for $C_{16}H_{18}Cl_2NO_3P$, 374.0474; found, 374.0383.

*4-chlorophenyl N,N´-dipiperidin-1-ilphosphinate (**9a**)*. It was obtained as a light yellow oil in 85% yield (purified by silica gel column chromatography, using hexane/ethyl acetate 3:1 v/v as the eluting solvent): TLC R_f = 0.23 (hexane/ethyl acetate 3:1 v/v); IR (ATR, cm^{-1}) $\bar{\nu}_{max}$ 2932, 2849, 1720, 1592, 1486, 1339, 1204, 1160, 1071, 956, 898, 832, 729, 565, 479. ^{1}H NMR (300

MHz, $CDCl_3$): δ 1.39-1.65 (12H, m, H-8, H-9, H-10), 3.05-3.15 (8H, m, H-7, H-11), 7.11-7.19 (2H, m, H-1, H-5), 7.22-7.34 (2H, m, H-2, H-4). ^{13}C NMR (75 MHz, $CDCl_3$): δ 24.71 (CH_2, C-9), 26.30 (CH_2, d, J = 5.6 Hz, C-8, C-10), 45.77 (CH_2, d, J = 2.7 Hz, C-7, C-11), 121.78 (CH, d, J = 5.3 Hz, C-1, C-5), 129.27 (C, C-3), 129.65 (CH, C-2, C-4), 150.46 (C, C-6). GC-MS *m/z*: 342 $[M]^{+\bullet}$. HREIMS m/z (M + H^+): calcd for $C_{16}H_{22}ClN_2O_2P$, 343.1337; found, 343.1211.

*3-chlorophenyl N,N´-dipiperidin-1-ilphosphinate (**9b**)*. It was obtained as a light yellow oil in 91% yield (purified by silica gel column chromatography, using hexane/ethyl acetate 1:1 v/v as the eluting solvent): TLC R_f = 0.35 (hexane/ethyl acetate 1:1 v/v); IR (ATR, cm^{-1}) $\bar{\nu}_{max}$ 2934, 2849, 1588, 1472, 1339, 1070, 923, 730, 680, 475. ^1H NMR (300 MHz, $CDCl_3$): δ 1.39-1.61 (12H, m, H-8, H-9, H-10), 3.04-3.21 (8H, m, H-7, H-11), 7.05-7.32 (4H, m, H-1, H-2, H-3, H-5). ^{13}C NMR (75 MHz, $CDCl_3$): δ 24.71 (CH_2, C-9), 26.29 (CH_2, d, J = 5.3 Hz, C-8, C-10), 45.78 (CH_2, d, J = 2.3 Hz, C-7, C-11), 118.73 (CH, d, J = 5.0 Hz, C-5), 120.97 (CH, d, J = 5.5 Hz, C-1), 124.38 (CH, C-3), 130.41 (CH, C-2), 134.82 (C, C-4), 152.45 (C, d, J = 6.1 Hz, C-6). GC-MS *m/z*: 342 $[M]^{+\bullet}$. HREIMS m/z (M + H^+): calcd for $C_{16}H_{24}ClN_2O_2P$, 343.1337; found, 343.1226.

*4-bromophenyl N,N´-dipiperidin-1-ilphosphinate (**9c**)*. It was obtained as a light yellow oil in 32% yield (purified by silica gel column chromatography, using hexane/ethyl acetate 2:1 v/v as the eluting solvent): TLC R_f = 0.30 (hexane/ethyl acetate 2:1 v/v); IR (ATR, cm^{-1}) $\bar{\nu}_{max}$ 2932, 2849, 1719, 1528, 1482, 1339, 1219, 1199, 1157, 1113, 1065, 1027, 1009, 956, 904, 830, 758, 729, 631, 608, 560, 473. ^1H NMR (300 MHz, $CDCl_3$): δ 1.39-1.61 (12H, m, H-8, H-9, H-10), 3.03-3.15 (8H, m, H-7, H-11), 7.06-7.15 (2H, m, H-1, H-5), 7.35-7.45 (2H, m, H-2, H-4). ^{13}C NMR (75 MHz, $CDCl_3$): δ 24.69 (CH_2, C-9), 26.29 (CH_2, d, J = 2.4 Hz, C-8, C-10), 45.77 (CH_2, d, J = 2.4 Hz, C-7, C-11), 116.93 (C, C-3), 122.26 (CH, d, J = 2.4 Hz, C-1, C-5), 132.64 (CH, C-2, C-4), 150.92 (C, d, J = 6.2 Hz, C-6). GC-MS *m/z*: 386 $[M]^{+\bullet}$. HREIMS m/z (M + H^+): calcd for $C_{16}H_{24}BrN_2O_2P$, 387.0832; found, 387.0677.

*4-fluorophenyl N,N´-dipiperidin-1-ilphosphinate (**9d**)*. It was obtained as a light yellow oil in 30% yield (purified by silica gel column chromatography, using hexane/ethyl acetate 3:1 v/v as the eluting solvent): TLC R_f = 0.51 (hexane/ethyl acetate 3:1 v/v); IR (ATR, cm^{-1}) $\bar{\nu}_{max}$ 2933, 2849, 1501, 1339, 1193, 1071, 903, 817, 733, 477. ^{1}H NMR (300 MHz, $CDCl_3$): δ 1.42-1.59 (12H, m, H-8, H-9, H-10), 3.06-3.13 (8H, m, H-7, H-11), 6.93-7.01 (2H, m, H-2, H-4), 7.13-7.19 (2H, m, H-1, H-5). ^{13}C NMR (75 MHz, $CDCl_3$): δ 24.44 (CH_2, C-9), 26.04 (CH_2, d, J = 5.3 Hz, C-7, C-11), 45.49 (CH_2, d, J = 2.3 Hz, C-8, C-10); 115.87 (CH, d, J = 23.1 Hz, C-2, C-4), 121.41 (CH, q, J = 4.8 Hz and J = 8.3 Hz, C-1, C-5), 147.40 (C, C-6), 158.99 (C, d, J = 240.8 Hz, C-3). GC-MS *m/z*: 326 $[M]^{+\bullet}$. HREIMS m/z (M + H^+): calcd for $C_{16}H_{24}FN_2O_2P$, 327.1632; found, 327.1663.

*bis(4-chlorophenyl)piperidin-1-ilphosphonate (**10a**)*. It was obtained as a light yellow oil in 64% yield (purified by silica gel column chromatography, using hexane/ethyl acetate 3:1 v/v as the eluting solvent): TLC R_f = 0.74 (hexane/ethyl acetate 3:1 v/v); IR (ATR, cm^{-1}) $\bar{\nu}_{max}$ 3096, 2937, 2854, 1589, 1484, 1269, 1194, 1089, 908, 829, 769, 638, 479. ^{1}H NMR (300 MHz, $CDCl_3$): δ 1.39-1.60 (6H, m, H-8, H-9, H-10), 3.15-3.29 (4H, m, H-7, H-11), 7.13-7.25 (4H, m, H-1, H-5), 7.26-7.35 (4H, m, H-2, H-4). ^{13}C NMR (75 MHz, $CDCl_3$): δ 24.33 (CH_2, C-9), 25.93 (CH_2, d, J = 4.5 Hz, C-8, C-10), 45.84 (CH_2, d, J = 2.2 Hz, C-7, C-11), 121.69 (CH, d, J = 5.4 Hz, C-1, C-5), 129.92 (C, C-3), 130.41 (CH, C-2, C-4), 149.59 (C, d, J = 6.4 Hz, C-6). GC-MS *m/z*: 385 $[M]^{+\bullet}$. HREIMS m/z (M + H^+): calcd for $C_{17}H_{18}Cl_2NO_3P$, 386.0474; found, 386.0368.

*3-chlorophenyl N,N´-dimorfolin-1-ilphosphinate (**11a**)*. It was obtained as a colorless oil in 52% yield (purified by silica gel column chromatography, using hexane/acetone 1:1 v/v as the eluting solvent): TLC R_f = 0.40 (hexane/acetone 1:1 v/v); mp: IR (ATR, cm^{-1}) $\bar{\nu}_{max}$ 2967, 2916, 2854, 1700, 1589, 1212, 1112, 930, 735, 503. ^{1}H NMR (300 MHz, $CDCl_3$): δ 3.12-3.29 (8H, m, H-7, H-10), 3.54-3.73 (8H, m, H-8, H-9), 7.09-7.33 (4H, m, H-1, H-2, H-3, H-5). ^{13}C NMR (75 MHz, $CDCl_3$): δ 44.99 (CH_2, C7, C-10), 67.20 (CH_2, d, J = 5.8 Hz, C-8, C-9), 118.57 (CH, d, J = 4.8 Hz, C-5), 120.87 (CH, d, J = 5.5 Hz, C-1), 125.10 (CH,

C-3), 130.71 (CH, C-2), 135.18 (C, C-4), 151.80 (C, d, *J* = 6.0 Hz, C-6). GC-MS *m/z*: 346 $[M]^{+\bullet}$. HREIMS m/z (M + H^+): calcd for $C_{14}H_{20}ClN_2O_4P$, 347.0922; found, 347.0841.

*4-bromophenyl N,N´-dimorfolin-1-ilphosphinate (**11b**)*. It was obtained as a white crystal in 46% yield (purified by silica gel column chromatography, using hexane/ethyl acetate 3:1 v/v as the eluting solvent): TLC R_f = 0.60 (hexane/ethyl acetate 3:1 v/v); mp. 112.7-113.9 ºC. IR (ATR, cm^{-1}) $\bar{\nu}_{max}$ 2956, 2846, 1482, 1232, 1111, 967, 904, 840, 734, 473. ^{1}H NMR (300 MHz, $CDCl_3$): *δ* 3.15-3.22 (8H, m, H-7, H-10), 3.59-3.61 (8H, m, H-8, H-9), 7.09-7.15 (2H, m, H-1, H-5), 7.41-7.47 (2H, m, H-2, H-4). ^{13}C NMR (75 MHz, $CDCl_3$): *δ* 44.74 (CH_2, C-7, C-10), 66.96 (CH_2, d, *J* = 5.8 Hz, C-8, C-9) 117.37 (C, C-3), 121.83 (CH, d, *J* = 5.0 Hz, C-1, C-5), 132.68 (CH, C-2, C-4), 150.09 (C, d, *J* = 5.9 Hz, C-6). GC-MS *m/z*: 390 $[M]^{+\bullet}$. HREIMS m/z (M + H^+): calcd for $C_{14}H_{20}BrN_2O_4P$, 391.0417; found, 391.0281.

*4-fluorophenyl N,N´-dimorfolin-1-ilphosphinate (**11c**)*. It was obtained as a white crystal in 55% yield (purified by silica gel column chromatography, using hexane/ethyl acetate 3:1 v/v as the eluting solvent): TLC R_f = 0.57 (hexane/ethyl acetate 3:1 v/v); mp. 128.7-130.1 ºC. IR (ATR, cm^{-1}) $\bar{\nu}_{max}$ 2974, 2851, 1502, 1230, 1109, 965, 907, 843, 741, 489. ^{1}H NMR (300 MHz, $CDCl_3$): *δ* 3.14-3.23 (8H, m, H-7, H-10), 3.58-3.65 (8H, m, H-8, H-9), 6.97-7.05 (2H, m, H-2, H-4), 7.13-7.21 (2H, m, H-1, H-5). ^{13}C NMR (75 MHz, $CDCl_3$): *δ* 44.72 (CH_2, C-7, C-10), 66.94 (CH_2, d, *J* = 5.8 Hz, C-8, C-9), 116.22 (CH, d, *J* = 23.3 Hz, C-2, C-4), 121.35 (CH, q, *J* = 4.9 Hz and *J* = 8.4 Hz, C-1, C-5), 146.82 (C, q, *J* = 2.8 Hz and *J* = 5.8 Hz, C-6), 159.31 (C, d, *J* = 241.8, C-3). GC-MS *m/z*: 330 $[M]^{+\bullet}$. HREIMS m/z (M + H^+): calcd for $C_{14}H_{20}FN_2O_4P$, 331.1217; found, 331.1160.

4.3.1.4. Urease inhibition assay

The screening for identifying potential urease inhibitors was done by incubating each synthesized compound at final concentration of 1.6 mM in reactions containing buffer solution (Na_2HPO_4/NaH_2PO_4 50 mM, pH 7.4), urea

(10 or 20 mM) and 1.25 x 10^{-2} U of urease (Sigma U-1500-100 kU). Each mixture was incubated for 15 min at 25 °C and the reactions were interrupted following the methodology described by Weatherburn (Weatherburn, 1967). The ammonium concentration was determined by phenol hypochloride assay (636 nm) and the inhibition percentage [INH(%)] was calculated by the following equation: INH(%) = 100 – ((A_{INH}/A_B) × 100). In this equation A_{INH} and A_B are ammonium concentration in the tubes with and without inhibitor, respectively. The inhibitory potential of the phosphoramidates was compared to those of the standard inhibitors hydroxyurea and thiourea. The phosphoramidates that were able to inhibit urease activity by over 40% were further used from 50 to 3200 μM to determine the concentration necessary to inhibit the enzyme by 50% (IC_{50}). All experiments were performed in triplicate. The cluster analysis was performed by employing unweighted pair-group average as amalgamation (joining) rule and city-block (Manhattan) distances as distance metric.

4.3.1.5. Quantum Chemical and Physicochemical Parameters

The physicochemical parameters were determined using the online software provided by Molinspiration Cheminformatics (Bratislava, Slovak Republic). Molecular attributes analyzed were n-octanol/water partition coefficient (cLogP), the amount of hydrogen bond donors (HBD), the amount of hydrogen bond acceptor (HBA), the molecular weight of the compounds (MW), number of rotatable bonds (nRotb) and total polar surface area (TPSA). The values of the total polar surface areas (TPSA) were determined using the above software employing the method described by Ertl and co-authors (Ertl *et al.*, 2000) and it was used to calculate the percentage of absorption (%ABS) according to the equation: %ABS = 109 - 0.345 x TPSA, as reported (ERTL *et al*., 2000).

Quantum mechanical calculations for compounds of the series **2-11** were performed using the Spartan 10 (HEHRE and OHLINGER, 2010) and the Gaussian 09 (FRISCH *et al*., 2009) programs. Computational geometry optimizations were carried out with the Spartan 10 software package employing semi-empirical PM6 method. The most stable conformers were fully optimized with at the B3LYP/6-31G(d,p) level of theory, where B3LYP is Becke three

parameter exchange functional, combined with the Lee-Yang-Parr correlation functional, at gas phase (BECKE, 1993). The DFT/B3LYP method is recommended for the estimation of molecular properties related to reactivity of molecules, such as the energy of the highest occupied molecular orbital (E_{HOMO}) and the energy of the lowest unoccupied molecular orbital (E_{LUMO}) (ZHANG and MUSGRAVE, 2007). Predictions of the HOMO–LUMO energies and dipole moment were performed in DFT energy calculations (B3LYP/6-311++G(2d,p)) considering the SMD solvation model and water as solvent (MARENICH *et al*., 2009). Electrostatic potentials and HOMO/LUMO maps were calculated for the geometries fully optimized that resulted from DFT calculations using Gaussian 09 at the B3LYP/6-311++G(2d,p).

4.4. Conclusions

In summary, 25 new phosphoramidates were prepared and evaluated for their inhibitory activity against urease. Of these compounds, **5c** appeared the most promising, with good activity as urease inhibitors. The ADMET properties predicted for these phosphoramidates are in accordance with the general requirements for potential drugs, confirming that these compounds possess physicochemical properties that qualify them to have good pharmacokinetics and drug bioavailability. In addition, no violations of Lipinski's rule were observed for the majority of the phosphoramidates. The structure−activity relationships suggested that the presence of cyclohexylamine group seems to increase the biological activity of the compounds. The promising biological results obtained, along with the good drug-likeness predictors that were calculated, make these compounds valid leads for further studies in therapies that require compounds with inhibitory activity ureolitic and for synthesizing new phosphoramidates which might be serve as a valuable prototype with improved potency.

4.5. Acknowledgments

We are grateful to the following Brazilian agencies: Conselho Nacional de Desenvolvimento Científico e Tecnológico (CNPq) for research fellowships (AJD, CRAM, LCAB), Fundação de Amparo à Pesquisa de Minas Gerais (FAPEMIG), Coordenação de Aperfeiçoamento de Pessoal de Nível Superior (CAPES) and FINEP for financial support.

4.6. References

ALAFEEFY, A.M.; ALQASOUMI, S.I.; ASHOUR, A.E.; MASAND, V.; AL-JABER, N.A.; BEN HADDA, T.; MOHAMED, M.A. Quinazoline-tyrphostin as a new class of antitumor agents, molecular properties prediction, synthesis and biological testing. *European Journal of Medical Chemistry,* v. 53, p. 133-140, 2012.

AMTUL, Z.; RAHMAN, A.U.; SIDDIQUI, R.A.; CHOUDHARY, M.I. Chemistry and mechanism of urease inhibition. *Current Medicinal Chemistry,* v. 9, p. 1323-1348, 2002.

ARANTES, F.F.P.; BARBOSA, L.C.A.; MALTHA, C.R.A.; DEMUNER, A.J.; FIDÊNCIO, P.H.; CARNEIRO, J.W.M. A quantum chemical and chemometric study of sesquiterpene lactones with cytotoxicity against tumor cells. *Journal of Chemometrics,* v. 25, p. 401-407, 2011.

BECKER, A.D. Density-functional thermochemistry. III. The role of exact exchange. *The Journal of Chemical Physics,* v. 98, p. 5648-5652, 1993.

BORRELLO, L.; CHIACCHIO, U.; CORSARO, A.; PISTARÀ, V.; IANNAZZO, D. Phosphoroamidate derivatives of N,O-nucleosides as inhibitors of reverse transcriptase. *Archive for Organic Chemistry,* v. 2009, p. 112-124, 2009.

CORREA-BASURTO, J.; FLORES-SANDOVAL, C.; MARIN-CRUZ, J.; ROJO-DOMINGUEZ, A.; ESPINOZA-FONSECA, L.M.; TRUJILLO-FERRARA, J.G.

Docking and quantum mechanic studies on cholinesterases and their inhibitors. *European Journal of Medical Chemistry,* v. 42, p. 10-19, 2007.

CRAMER, F.; HENNRICH, N. Imidoester, V. Die Umlagerung von Trichloracetimidaten zu N-substituierten Säureamiden. *Chemische Berichte,* v. 94, p. 976-989, 1961.

DE OLIVEIRA, D.B.; GAUDIO, A.C. BuildQSAR: A New Computer Program for QSAR Analysis. *Quantitative Structure-Activity Relationships,* v. 19, p. 599-601, 2001.

DERUDAS, M.; BRANCALE, A.; NAESENS, L.; NEYTS, J.; BALZARINI, J.; MCGUIGAN, C. Application of the phosphoramidate ProTide approach to the antiviral drug ribavirin. *Bioorganic and Medicinal Chemistry,* v. 18, p. 2748-2755, 2010.

DERUDAS, M.; CARTA, D.; BRANCALE, A.; VANPOUILLE, C.; LISCO, A.; MARGOLIS, L.; BALZARINI, J.; MCGUIGAN, C. The application of phosphoramidate protide technology to acyclovir confers anti-HIV inhibition. *Journal of Medicinal Chemistry,* v. 52, p. 5520-5530, 2009.

DONGHI, M.; ATTENNI, B.; GARDELLI, C.; MARCO, A.D.; FIORE, F.; GIULIANO, C.; LAUFER, R.; LEONE, J.F.; PUCCI, V.; ROWLEY, M.; NARJES, F. Synthesis and evaluation of novel phosphoramidate prodrugs of 2'-methyl cytidine as inhibitors of hepatitis C virus NS5B polymerase. *Bioorganic & Medicinal Chemistry Letters,* v. 19, p. 1392-1395, 2009.

DUCKWORTH, M.J.; OKOLI, A.S.; MENDZ, G.L. Novel Helicobacter pylori therapeutic targets: the unusual suspects. *Expert Review of Anti-Infective Therapy,* v. 7, p. 835-867, 2009.

ERTL, P.; ROHDE, B.; SELZER, P. Fast Calculation of Molecular Polar Surface Area as a Sum of Fragment-Based Contributions and Its Application to the Prediction of Drug Transport Properties. *Journal of Medicinal Chemistry,* v. 43, p. 3714-3717, 2000.

FOLLMER, C. Ureases as a target for the treatment of gastric and urinary infections. *Journal of Clinical Pathology,* v. 63, p. 424-430, 2010.

FRISCH, M.J.; TRUCKS, G.W.; SCHLEGEL, H.B.; SCUSERIA, G.E.; ROBB, M.A.; CHEESEMAN, J.R.; SCALMANI, G.; BARONE, V.; MENNUCCI, B.; PETERSSON, G.A.; NAKATSUJI, H.; CARICATO, M.; LI, X.; HRATCHIAN, H.P.; IZMAYLOV, A.F.; BLOINO, J.; ZHENG, G.; SONNENBERG, J.L.; HADA, M.; EHARA, M.; TOYOTA, K.; FUKUDA, R.; HASEGAWA, J.; ISHIDA, M.; NAKAJIMA, T.; HONDA, Y.; KITAO, O.; NAKAI, H.; VREVEN, T.; MONTGOMERY, J.A.; JR.; PERALTA, J.E.; OGLIARO, F.; BEARPARK, M.; HEYD, J.J.; BROTHERS, E.; KUDIN, K.N.; STAROVEROV, V.N.; KOBAYASHI, R.; NORMAND, J.; RAGHAVACHARI, K.; RENDELL, A.; BURANT, J.C.; IYENGAR, S.S.; TOMASI, J.; COSSI, M.; REGA, N.; MILLAM, J.M.; KLENE, M.; KNOX, J.E.; CROSS, J.B.; BAKKEN, V.; ADAMO, C.; JARAMILLO, J.; GOMPERTS, R.; STRATMANN, R.E.; YAZYEV, O.; AUSTIN, A.J.; CAMMI, R.; POMELLI, C.; OCHTERSKI, J.W.; MARTIN, R.L.; MOROKUMA, K.; ZAKRZEWSKI, V.G.; VOTH, G.A.; SALVADOR, P.; DANNENBERG, J.J.; DAPPRICH, S.; DANIELS, A.D.; FARKAS, Ö.; FORESMAN, J.B.; ORTIZ, J.V.; CIOSLOWSKI, J.; FOX, D.J. (2009). Gaussian '09, Revision A.1 (Version ´09): Wallingford CT.

HARRIS, S.A.; MCGUIGAN, C.; ANDREI, G.; SNOECK, R.; DE CLERCQ, E.; BALZARINI, J. Synthesis and antiviral evaluation of phosphoramidate derivatives of (*E*)-5-(2-bromovinyl)-2'-deoxyuridine. *Antiviral Chemistry and Chemotherapy,* v. 12, p. 293-300, 2001.

HEHRE, W.; OHLINGER, S. (2010). Spartan'10 Tutorial and user's guide (Version ´10): Wavefunction Inc.

KAŠPÁREK, F.; MOLLIN, J. Solvolysis of diphenyl amidophosphates in aqueous alcoholic media. *Collection of Czechoslovak Chemical Communications,* v. 52, p. 1115-1130, 1980.

KRAJEWSKA, B. Ureases I. Functional, catalytic and kinetic properties: A review. *Journal of Molecular Catalysis B: Enzymatic,* v. 59, p. 9-21, 2009.

KRISHNAN, P.; SUNDARAM, S.; VENKATASUBRAMANIAN, N. Alkaline hydrolysis of arylesters of diphenylphosphorodiamidates—evidence consistent with an elimination—addition mechanism. *Proceedings of the Indian Academy of Sciences - Chemical Sciences,* v. 94, p. 467-473, 1985.

LI, H.Q.; XIAO, Z.P.; YIN, L.; YAN, T.; LV, P.C.; ZHU, H.L. Amines and oximes derived from deoxybenzoins as Helicobacter pylori urease inhibitors. *European Journal of Medical Chemistry,* v. 44, p. 2246-2251, 2009.

LIPINSKI, C.A.; LOMBARDO, F.; DOMINY, B.W.; FEENEY, P.J. Experimental and computational approaches to estimate solubility and permeability in drug discovery and development settings. *Advanced Drug Delivery Reviews,* v. 23, p. 3-25, 1997.

LIPINSKI, C.A.; LOMBARDO, F.; DOMINY, B.W.; FEENEY, P.J. Experimental and computational approaches to estimate solubility and permeability in drug discovery and development settings. *Adv Drug Deliv Rev,* v. 46, p. 3-26, 2001.

MAALEJ, E.; CHABCHOUB, F.; SAMADI, A.; DE LOS RÍOS, C.; PERONA, A.; MORREALE, A.; MARCO-CONTELLES, J. Synthesis, biological assessment and molecular modeling of 14-aryl-10,11,12,14-tetrahydro-9*H*-benzo[5,6]chromeno[2,3-b]quinolin-13-amines. *Bioorganic & Medicinal Chemistry Letters,* v. 21, p. 2384-2388, 2011.

MANGAL, M.; SAGAR, P.; SINGH, H.; RAGHAVA, G.P.; AGARWAL, S.M. NPACT: Naturally Occurring Plant-based Anti-cancer Compound-Activity-Target database. *Nucleic Acids Research,* v. 41, p. D1124-1129, 2013.

MARA, C.; DEMPSEY, E.; BELL, A.; BARLOW, J.W. Synthesis and evaluation of phosphoramidate and phosphorothioamidate analogues of amiprophos methyl as potential antimalarial agents. *Bioorganic & Medicinal Chemistry Letters,* v. 21, p. 6180-6183, 2011.

MARENICH, A.V.; CRAMER, C.J.; TRUHLAR, D.G. Universal solvation model based on solute electron density and on a continuum model of the solvent

defined by the bulk dielectric constant and atomic surface tensions. *Journal of Physical Chemistry B,* v. 113, p. 6378-6396, 2009.

MCGUIGAN, C.; KELLEHER, M.R.; PERRONE, P.; MULREADY, S.; LUONI, G.; DAVERIO, F.; RAJYAGURU, S.; POGAM, S.L.; NAJERA, I.; MARTIN, J.A.; KLUMPP, K.; SMITH, D.B. The application of phosphoramidate ProTide technology to the potent anti-HCV compound 4′-azidocytidine (R1479). *Bioorganic & Medicinal Chemistry Letters,* v. 19, p. 4250-4254, 2009.

MEHELLOU, Y.; BALZARINI, J.; MCGUIGAN, C. An investigation into the anti-HIV activity of 2',3'-didehydro-2',3'-dideoxyuridine (d4U) and 2',3'-dideoxyuridine (ddU) phosphoramidate 'ProTide' derivatives. *Organic and Biomolecular Chemistry,* v. 7, p. 2548-2553, 2009.

OLIVEIRA, F.M.; BARBOSA, L.C.A.; TEIXEIRA, R.R.; DEMUNER, A.J.; MALTHA, C.R.A.; PICANÇO, M.C.; SILVA, G.A.; PAULA, V.F. Synthesis and insecticidal activity of new phosphoramidates. *Journal of Pesticide Science,* v. 37, p. 85-88, 2012.

OLIVEIRA, F.M.; BARBOSA, L.C.A.; VALENTE, V.M.M.; DEMUNER, A.J.; MALTHA, C.R.A.; OLIVEROS-BASTIDAS, A.J. Structure–activity relationship of pyridin-2(1*H*)-ones derivatives as urease inhibitors. *Journal of Pharmacy Research,* v. 5, p. 5326-5333, 2012.

PAULA, V.F.; BARBOSA, L.C.A.; TEIXEIRA, R.R.; PICANCO, M.C.; SILVA, G.A. Synthesis and insecticidal activity of new 3-benzylfuran-2-yl *N,N,N',N'*-tetraethyldiamidophosphate derivatives. *Pest Management Science,* v. 64, p. 863-872, 2008.

PROUDFOOT, J.R. Drugs, leads, and drug-likeness: an analysis of some recently launched drugs. *Bioorganic & Medicinal Chemistry Letters,* v. 12, p. 1647-1650, 2002.

ROBERTS, B.P.; MILLER, B.R., 3RD; ROITBERG, A.E.; MERZ, K.M., JR. Wide-open flaps are key to urease activity. *Journal of the American Chemical Society,* v. 134, p. 9934-9937, 2012.

ROUBINEK, F.; BEDRNÍK, P.; CECH, M.; DANĚK, J.; BUDĚŠÍNSKÝ, Z. Diphenylesters of amidophosphoric acids, their synthesis, determination of phosphorus and biological activity. *Ceskoslovenska Farmacie,* v. 29, p. 90-94, 1980.

RUVEDA, M.A.; ZERBA, E.N.; PODESTA, R.; DE LICASTRO, S.A. Organophosphorus chemistry—V : Thermal transformation of the cyclohexylammonium salt of O-aryl *N*-cyclohexyl phosphoramidic acids into sym-pyrophosphates. *Tetrahedron,* v. 31, p. 885-890, 1975.

TAMBUNAN, U.S.; BRAMANTYA, N.; PARIKESIT, A.A. In silico modification of suberoylanilide hydroxamic acid (SAHA) as potential inhibitor for class II histone deacetylase (HDAC). *BMC Bioinformatics,* v. 12 Suppl 13, p. S23, 2011.

TEIXEIRA, R.R.; BRESSAN, G.C.; PEREIRA, W.L.; FERREIRA, J.G.; OLIVEIRA, F.M.; THOMAZ, D.C. Synthesis and Antiproliferative Activity of C-3 Functionalized Isobenzofuran-1(3*H*)-ones. *Molecules,* v. 18, p. 1881-1896, 2013.

TETKO, I.V. Computing chemistry on the web. *Drug Discovery Today,* v. 10, p. 1497-1500, 2005.

UCKUN, F.M.; VENKATACHALAM, T.K.; ERBECK, D.; CHEN, C.L.; PETKEVICH, A.S.; VASSILEV, A. Zidampidine, an aryl phosphate derivative of AZT: in vivo pharmacokinetics, metabolism, toxicity, and anti-viral efficacy against hemorrhagic fever caused by Lassa virus. *Bioorganic and Medicinal Chemistry,* v. 13, p. 3279-3288, 2005.

VASSILIOU, S.; GRABOWIECKA, A.; KOSIKOWSKA, P.; YIOTAKIS, A.; KAFARSKI, P.; BERLICKI, L. Design, synthesis, and evaluation of novel

organophosphorus inhibitors of bacterial ureases. *Journal of Medicinal Chemistry,* v. 51, p. 5736-5744, 2008.

VEBER, D.F.; JOHNSON, S.R.; CHENG, H.Y.; SMITH, B.R.; WARD, K.W.; KOPPLE, K.D. Molecular properties that influence the oral bioavailability of drug candidates. *Journal of Medicinal Chemistry,* v. 45, p. 2615-2623, 2002.

WEATHERBURN, M.W. Phenol-hypochlorite reaction for determination of ammonia. *Analytical Chemistry,* v. 39, p. 971–974, 1967.

ZHANG, G.; MUSGRAVE, C.B. Comparison of DFT Methods for Molecular Orbital Eigenvalue Calculations. *The Journal of Physical Chemistry A,* v. 111, p. 1554-1561, 2007.

CAPÍTULO 5

5. A COMPARISON OF DENSITY FUNCTIONAL METHODS FOR THE ESTIMATION OF PROTON AND CARBON CHEMICAL SHIFTS OF PHOSPHORAMIDATES

5.1. Abstract

^{1}H and ^{13}C NMR chemical shifts were measured for three phosphoramidates and computed using the B3LYP, WP04, TPSSh, M062X and wB97xD density functional methods. The experimental and computed chemical shift values for proton and carbon were compared, and computational methods were comprehensively evaluated (using linear correlation (R^2), mean absolute error (MAE), root mean squared deviation (RMSD) and DP4 analysis criteria). Applying a linear correction to the computed data improves the absolute accuracy and reduces random errors. For ^{13}C NMR shift data, results from the GIAO/wB97xD/cc-pVTZ/SCRF combination show the lowest value of RMSD (2.073), but incurred a high CPU cost. The best compromise cost-accuracy was obtained for the GIAO/B3LYP/6-31G(d,p)/SCRF combination that provides RMSD 2.121 at a CPU cost twenty-six times smaller than GIAO/wB97xD/cc-pVTZ/SCRF. For ^{1}H NMR shift data, CSGT/TPSSh/cc-pVTZ/SCRF shows RMSD of 0.070. The method that best applies to this class of compound is CSGT/wB97xD/cc-pVTZ/SCRF. DP4 analysis was used to correlate the chemical shifts (^{1}H and ^{13}C NMR) of the compounds and indicated that the method that best applies to this class of compounds is CSGT/wB97xD/cc-pVTZ/SCRF, with DP4 analysis of 51.9%. In general, the best results were obtained when using implicit solvation model during calculations. The best

method was applied on an external test set of 6 additional molecules and provided satisfactory results.

5.2. Introduction

The organophosphorus (OP) compounds form a class of compounds having at least one phosphorus atom connected to a carbon atom in their structure and find wide application in several fields. Amongst these, one of the most common classes include phosphoramidates, which incorporate one amide functional group derived from the phosphoric acid. It has been found that these compounds have particular importance due to their expressive biological activities. These compounds are used in medicine, due to their potential applications as anticancer (CONGIATU *et al.,* 2006; DUAN *et al.,* 2008; KIRAN *et al.,* 2008; LEWANDOWSKA *et al.,* 2013; WANG *et al.,* 2010; WITTINE *et al.,* 2009), anti-HIV (MEHELLOU *et al.,* 2009; ZAKIROVA *et al.,* 2012), inhibitors of hepatitis C virus (MCGUIGAN *et al.,* 2009; PERRONE *et al.,* 2007; SOFIA *et al.,* 2012) and antimalarial agents (MARA *et al.,* 2011). Within agriculture they are reported to act as urease inhibitors (DOMÍNGUEZ *et al.,* 2008), herbicides (KATAGI, 1993) and insecticides (OLIVEIRA *et al.,* 2012; PAULA *et al.,* 2008). In industry they find application both as antifire (KIRAN *et al.,* 2007) and antirust additives in lubricating oils (YAN *et al.,* 2012). We recently published a review highlighting the main phosphoramidates with potential biological activity and applications within the medical area (OLIVEIRA *et al.,* 2014).

Continuing our work on the search for new compounds with insecticidal (OLIVEIRA *et al.,* 2012; PAULA *et al.,* 2008) and phytotoxic activities (ALVARENGA *et al.,* 2009; BARBOSA *et al.,* 2012; BARBOSA *et al.,* 2009; BARBOSA *et al.,* 2010; DEMUNER *et al.,* 2009), a series of phosphoramidates compounds were synthesized. In the last series of compounds, the inhibitory activity of urease was evaluated (OLIVEIRA *et al.,* 2014).

It is widely believed that the biological activity of the phosphoramidates is correlated with their molecular properties (CORRÊA *et al.,* 2012; TEIXEIRA *et al.,* 2009). Most studies focus on their crystal structures, DFT quantum chemical calculations and NMR (GHOLIVAND *et al.,* 2008; GHOLIVAND *et al.,* 2010;

OLIVEIRA *et al.,* 2013). Whilst the application of NMR techniques to determine the relative spatial orientation of substituents has become a routine task examples of structural and stereochemical misassignments still appear in the literature (NICOLAOU *et al.,* 2005). The accurate calculation of NMR chemical shifts with quantum chemical methods has provided an additional tool to supplement or in some cases even replace NMR assignments. Consequently, in a recent work, we have characterized phosphoramidates using quantum chemical calculations (Density Functional Theory - DFT) couple to both dynamic NMR studies and single crystal X-ray diffraction data (OLIVEIRA *et al.,* 2013). It is an important tendency nowadays that the computational chemistry methods become useful tools to help the interpretation and analysis of the experimental data.

From a theoretical standpoint, advanced computational protocols have been developed for calculating NMR chemical shifts, mainly ^{1}H and ^{13}C, as well as coupling constants of isolated molecules, in which the environmental effects are neglected (COSTA *et al.,* 2010). These effects are predominantly related to the inherently large size of such systems, making conventional *ab initio* theories either very computationally demanding or even prohibitive. The theoretical task lies in calculating the molecular second-order magnetic response properties, in which the calculation of the nuclear magnetic shielding tensor plays a relevant role (COSTA *et al.,* 2010). It is generally accepted that the calculation of these proprieties requires gauge-invariant procedures. Therefore, some theoretical methods have been proposed, in which the most commonly used approaches are: the GIAO (Gauge Including Atomic Orbital) and CSGT (Continuous Set of Gauge Transformation) method which computes the current density induced by the magnetic fields by performing a gauge transformation at every point in space (LODEWYK *et al.,* 2012).

The molecular geometry optimization is often the most time consuming step in determining the chemical shifts for the DFT and *ab initio* level calculations. Therefore much effort has been paid to identify computational methods that afford good geometries for further high quality NMR predictions at minimal computational cost (SAROTTI *et al.,* 2009). The use of DFT functionals (such as B3LYP) coupled with the 6-31G(d) basis set (or superior) provides

satisfactory results for common organic compounds (LODEWYK *et al.,* 2012). CPU time is particularly important in conformationally flexible compounds in which an extensive conformational search is necessary to determine the relative contribution of each conformer by means of a Boltzmann analysis (LODEWYK *et al.,* 2012).

Much effort has been directed toward the goal of calculating accurate magnetic shielding tensors (LODEWYK *et al.,* 2012; SAROTTI *et al.,* 2012). However, it is impractical to carry out such elaborate calculations for large molecules more likely to be of interest to experimental organic chemists. It is known that large basis sets are required to calculate accurate magnetic shielding values and also that corrections due to electron correlation are desirable (LODEWYK *et al.,* 2012).

Recently, Sarotti (SAROTTI, 2013) has published a study in which the geometry optimization was carried out using computationally inexpensive methods (MM+, AM1 or HF/3-21G) and the NMR shielding constants were computed at an affordable mPW1PW91/6-31G(d) level. Thus, given a set of statistical parameters computed after correlation between experimental and calculated chemical shifts, were classified using the knowledge derived from trained artificial neural networks. The process was validated with a set of 26 natural products that had been incorrectly assigned along with their 26 revised structures (SAROTTI, 2013). Thus, it was adduced that the use of computational methods achieve results comparable to those obtained at a greater computational cost.

5.3. Results and Discussion

Several research groups have published studies that aim to assess the best methods which need to be applied to a number of molecules in the prediction of the chemical shifts of the atoms, without incurring computational penalties (CHEESEMAN *et al.,* 1996; SAMULTSEV *et al.,* 2014; SAROTTI *et al.,* 2012). These studies have allowed investigators to perform various assignments of chemical shifts of atoms of complex molecules (AMINI, 2013; MARELL *et al.,* 2013). Therefore, researchers are working to develop various

methodologies to be applied to these data in an attempt to evaluate the results available and get the best correlation (ANDREWS *et al.,* 2013; SAROTTI, 2013; SAROTTI *et al.,* 2012; SMITH *et al.,* 2010).

In the present study, we aimed to establish the best methods to for the assignment of the chemical shifts of ^{1}H and ^{13}C NMR signals from theoretical calculations using experimental chemical shifts data obtained from phosphoramidates. For this purpose, molecules whose structures are depicted in Figure 1 were used. Although the number of compounds tested is small, only 3, the chemical shifts values are related to 48 carbon atoms and 63 hydrogen atoms, addressing a wide range of chemical shift.

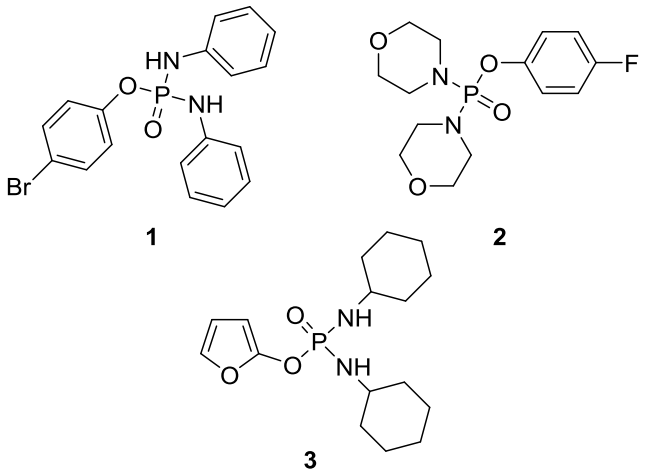

Figure 1 - Phosphoramidate compounds **1**, **2** and **3**.

Magnetic shieldings can depend strongly on the conformation of a molecule (LODEWYK *et al.,* 2012). This is particularly important when dealing with conformationally flexible compounds, from which an extensive conformational search must be done to determine the relative contribution of each conformer for population levels by Boltzmann analysis (SAROTTI, 2013). The structures of the compounds were submitted to a search for the lowest energy conformations employing the PM6 method in the Spartan software (SPARTAN ’10). These conformations were used as input for the geometry optimization using Gaussian software (FRISCH *et al.,* 2009). The geometries of all molecules in the test set were optimized at the B3LYP/6-31G(d,p) level and the contribution of each conformer was determined. One should keep in mind

that Boltzmann statistics dictate that (at room temperature) a 1 kcal/mol difference in free energy corresponds to an ~85:15 ratio and 3 kcal/mol corresponds to a >99:1 ratio of two conformers. Therefore, many conformational minima may not contribute significantly to the experimental spectra (LODEWYK *et al.,* 2012). Therefore, conformers that had a percentage contribution of less than 1% were not considered.

Table 1. Results of Calculations of ^{1}H and ^{13}C NMR Chemical Shifts (Recommended Methods in Italic)

Number	method[a]	functional[b]	basis set[c]	SCRF[d]	^{1}H NMR		^{13}C NMR		CPU time[g]
					MAE[e]	RMSD[f]	MAE[e]	RMSD[f]	
1	GIAO	B3LYP	6-31g(d.p)	no	0.165	0.216	1.469	2.177	6.8
2	GIAO	B3LYP	6-311++g(2d.p)	no	0.140	0.184	1.595	2.258	100.1
3	GIAO	B3LYP	cc-pVTZ	no	0.129	0.173	1.606	2.313	166.1
4	GIAO	WP04	cc-pVTZ	no	0.122	0.159	1.811	2.399	165.9
5	GIAO	TPSSh	cc-pVTZ	no	0.117	0.156	1.753	2.411	127.7
6	GIAO	M062X	cc-pVTZ	no	0.137	0.182	1.783	2.555	114.9
7	GIAO	wB97xD	cc-pVTZ	no	0.129	0.174	1.301	2.121	220.8
8	GIAO	B3LYP	6-31g(d.p)	yes	0.099	0.122	1.393	2.121	9.1
9	GIAO	B3LYP	6-311++g(2d.p)	yes	0.084	0.110	1.507	2.199	98.4
10	GIAO	B3LYP	cc-pVTZ	yes	0.080	0.106	1.502	2.234	175.8
11	GIAO	WP04	cc-pVTZ	yes	0.076	0.099	1.718	2.336	156.7
12	GIAO	TPSSh	cc-pVTZ	yes	0.065	0.088	1.678	2.352	161.2
13	GIAO	M062X	cc-pVTZ	yes	0.097	0.128	1.768	2.537	157.9
14	*GIAO*	*wB97xD*	*cc-pVTZ*	*yes*	*0.089*	*0.116*	*1.243*	*2.073*	*243.1*
15	CSGT	B3LYP	6-311++g(2d.p)	no	0.122	0.164	1.605	2.284	93.8
16	CSGT	B3LYP	cc-pVTZ	no	0.134	0.171	1.629	2.398	143.2
17	CSGT	WP04	cc-pVTZ	no	0.117	0.147	1.836	2.493	130.4
18	CSGT	TPSSh	cc-pVTZ	no	0.125	0.156	1.813	2.520	140.7
19	CSGT	M062X	cc-pVTZ	no	0.126	0.171	1.730	2.476	162.5
20	CSGT	wB97xD	cc-pVTZ	no	0.117	0.154	1.392	2.226	209.6
21	*CSGT*	*B3LYP*	*6-311++g(2d.p)*	*yes*	*0.070*	*0.088*	*1.522*	*2.237*	*96.9*
22	CSGT	B3LYP	cc-pVTZ	yes	0.071	0.082	1.619	2.369	158.4
23	CSGT	WP04	cc-pVTZ	yes	0.056	0.073	1.757	2.444	160.1
24	CSGT	TPSSh	cc-pVTZ	yes	0.053	0.070	1.801	2.485	151.3
25	CSGT	M062X	cc-pVTZ	yes	0.084	0.098	1.704	2.445	135.9
26	*CSGT*	*wB97xD*	*cc-pVTZ*	*yes*	*0.066*	*0.077*	*1.322*	*2.157*	*233.6*

[a] Method for calculating chemical shieldings. [b] B3LYP, WP04, wB97xD, M062X and TPSSh are hybrid functionals. *c* The basis sets are denoted by their corresponding keywords in Gaussian; 6-31G denote double-ζ basis sets; cc-pVTZ and 6-311G denote triple-ζ basis sets. [d] Here, "yes" means that chloroform was included as a solvent in a SMD-SCRF calculation; "no" refers to gas-phase calculations. [e] Mean absolute error. [f] Root mean squared deviation. [g] CPU time in hours for calculating the entire test set of all six conformers on a typical Linux workstation.

Table 1 sums up the results obtained with all combinations of the two methods to calculate magnetic shieldings (GIAO/CSGT), different functionals, and different basis sets that were used. In order to assess the computational cost, we have added in the last column a measure of the CPU time (obtained on a typical Linux workstation) for a calculation of the entire data set of all molecules. It is important to note that the method chosen for computation of isotropic shielding constants need not have any direct connection to that utilized for the geometry optimization step. At this stage, common practice is to average the isotropic shielding constants for all nuclei that are symmetrically equivalent (which should be identical to each other given tight enough convergence criteria in the calculations) and for nuclei that are experimentally indistinguishable due to free rotation around single bonds (for example, methyl hydrogens) (LODEWYK *et al.,* 2012). Diastereotopic or constitutionally heterotopic nuclei are generally not averaged unless they are known to be indistinguishable in the experimental spectrum (LODEWYK *et al.,* 2012). This criterion was adopted in the calculations of the chemical shifts of chemically identical atoms.

Linear regression approach has been extensively applied to predict ^{13}C and ^{1}H NMR chemical shifts in order to reduce systematic errors (JAIN *et al.,* 2009; LODEWYK *et al.,* 2012; WIITALA *et al.,* 2007). Care must be taken in case ^{13}C to avoid specific data that may adversely affect the quality of the linear regression, such as shifts for carbons attached to heavy atoms (LODEWYK *et al.,* 2012). For this reason, the chemical shift related to the carbon atom directly attached to the bromine atom in the compound **1** was removed from the linear regression analysis (the value provided by the method without any treatment was used in the final analysis). The data obtained theoretically were subjected to the process of scaling by linear regression. Although this process does not improve the results in all cases, as discussed by Jain *et al.* (2009) we chose to use this approach in all compounds. This decision was taken considering that it is a method easy to apply and has provided good results in several studies (ALIEV *et al.,* 2009; COSTA *et al.,* 2010).

As shown in Table 1, the accuracy of the predictions shows no correlation with the cost of the calculations. In fact one of the least costly

methods (GIAO/B3LYP/6-31G(d,p)/SCRF) and one which is seventeen times more expensive (GIAO/M062X/cc-pVTZ/SCRF) have almost the same rms deviation (0.122 and 0.128 ppm in ^{1}H NMR, respectively). This value is lower than the value found for the GIAO/wB97xD/cc-pVTZ method (RMSD equal a 0.174), that presents a computational method that much higher (twenty-four times longer) cost. The analysis of the statistical parameters calculated from the ^{13}C NMR data show that the method GIAO/B3LYP/6-31G(d,p)/SCRF presented RMSD value (2.121) equal to or less computational cost methods with more than twenty-two times greater (RMSD 2.121 for GIAO/wB97xD/cc-pVTZ; RMSD 2.226 for CSGT/wB97xD/cc-pVTZ and RMSD 2.157 for CSGT/wB97xD/cc-pVTZ/SCRF).

For ^{1}H shift data, CSGT/TPSSh/cc-pVTZ/SCRF showed RMSD 0.070. The method CSGT/B3LYP/6-311++G(2d,p)/SCRF) provided a good results (RMSD 0.088). For ^{13}C shift data, results from the GIAO/wB97xD/cc-pVTZ/SCRF density functional showed the lowest value of RMSD (2.073), but requiring a high CPU cost. The best cost-benefit in this case was for the method GIAO/B3LYP/6-31G(d,p)/SCRF that provided RMSD 2.121 a CPU cost twenty-six times smaller than CSGT/TPSSh/cc-pVTZ/SCRF.

The B3LYP/cc-pVTZ and wB97xD/cc-pVTZ levels of theory predict ^{1}H chemical shifts with comparable accuracy in GIAO method. The RMSDs for B3LYP/cc-pVTZ are 0.173 and 0.106 ppm (gas phase and chloroform, respectively) for this range of molecules while for wB97xD they are 0.174 and 0.116 ppm. The maximum absolute error for B3LYP predicts ^{1}H shifts which was 0.34 ppm in gas phase (0.21 in chloroform), and 0.37 for wB97xD in gas phase (0.23 in chloroform). Considering the CSGT method, the results obtained by employing the functional wB97xD (RMSD 0.154 in gas phase and RMSD 0.077 in chloroform) were slightly better than the B3LYP functional (RMSD 0.171 in gas phase and RMSD 0.082 in chloroform).

The WP04/cc-pVTZ and TPSSh/cc-pVTZ levels of theory predict ^{13}C chemical shifts with comparable accuracy in GIAO and CSGT methods. However, the results are slightly better when obtained from GIAO method in both functional: WP04 (RMSD 2.399 and 2.336 (gas phase and chloroform) in GIAO; RMSD 2.493 and 2.444 (gas phase and chloroform) in CSGT) and

TPSSh (RMSD 2.411 and 2.352 (gas phase and chloroform) in GIAO; RMSD 2.520 and 2.485 (gas phase and chloroform) in CSGT). Opposite trend was observed for the data obtained for the functional M062X (RMSD 2.555 and 2.537 (gas phase and chloroform) in GIAO; RMSD 2.476 and 2.445 (gas phase and chloroform) in CSGT).

Inclusion of solvation model improves accuracy of predictions, which vary between different methods. While the method GIAO/B3LYP/cc-pVTZ was improved in the amount of 0.079 units in RMSD with the addition of solvent, such improvement was only 0.018 to GIAO/M062X/cc-pVTZ method. This effect is easily seen in the data analysis the statistical parameters obtained from ^{1}H NMR data and summarized in Figure 2. All methods under conditions which considered the effect of the solvent gave the best results. In the case of carbon chemical shifts (statistical parameters from ^{13}C NMR summarized in Figure 2), while the lowest RMSD value (2.073) has been a method for taking into consideration the effect of solvent (GIAO/wB97xD/cc-pVTZ/SCRF), it can be seen that good results were obtained without inclusion of solvent in the calculations (RMSD 2.121 for GIAO/wB97xD/cc-pVTZ and RMSD 2.177 for GIAO/B3LYP/6-31G(d,p)).

Gauge-including atomic orbital (GIAO) and continuous set of gauge transformations (CSGT) are the most frequently employed methods in DFT-NMR calculations, and it is recognized that accurate predictions require the gauge-invariant procedures that these methods implement (LODEWYK *et al.,* 2012). In 1996, Cheeseman *et al.* (1996) concluded that shielding tensor components determined using the GIAO and CSGT methods are found to converge to the same value at sufficiently large basis sets. This observation was confirmed for ^{1}H chemical shifts by Rablen *et al*. (1999). Although we have employed triple-zeta basis, in general, results obtained using method CSGT were even better than those obtained with GIAO. However, it is noteworthy that some methods only showed improvement in ^{1}H NMR data, as is the case of B3LYP/6-311G(2d,p)/SCRF which showed an RMSD value equal to 2.199 when employed GIAO, and a value of 2.237 employing CSGT. Recently, Andrews and Spivey (2013) also reported that the CSGT predictions were significantly more assured than the previous GIAO ones and indicated the correct result via all measures both with and without empirical scaling.

5.3.1. DP4 Analysis

Methods for analyzing the "goodness of fit" have been further developed by Smith and Goodman through statistical treatments that provide numerical probabilities for analyzing various fits (SMITH *et al.,* 2010). The DP4 analysis is based on calculated error probabilities for computed chemical shifts. In this analysis, a statistical student's *t* distribution for these errors is employed. Next, the Bayes's theorem is applied to get an overall probability that the selected structure is correct from the product of the individual error probabilities for each atom (AMINI, 2014). This tool has been used by several research groups and has the advantage of being more robust when compared to traditional statistical methods such as analysis of absolute deviation or standard error (AMINI, 2014; BROWN *et al.,* 2012). Another advantage is the possibility to simultaneously consider the data obtained in ^{1}H and ^{13}C NMR.

One noteworthy example of the utility of the DP4 analysis is the case described by Smith and Goodman (SMITH *et al.,* 2010). With 32 possible diastereomers, standard means of comparison of experimental and computed chemical shifts (e.g., mean absolute error/deviation) do not point to the correct isomer. However, the DP4 analysis indicates a strong match (approximately 85% probability) to the correct structure, with the remaining probability assigned to one other candidate isomer, even with the limited availability of experimental data in this case.

Data evaluation by DP4 analysis allows checking the correlation of the methods tested with the experimental values of ^{1}H and ^{13}C NMR, separately or simultaneously. These analyses are readily employed in due to the availability of a Web-based applet online. In ^{1}H NMR, the methods provided the best results were CSGT/TPSSh/cc-pVTZ/SCRF, which provides a confidence rate of 26.5%, followed the CSGT/WP04/cc-pVTZ with 25.9% and CSGT/wB97xD/cc-pVTZ/SCRF with 11.8%. In that order, these methods were those with the lowest values of RMSD (0.070, 0.073 and 0.077, respectively). Is worth mentioning that if the evaluation is only the chemical shifts of hydrogen, the first two methods provide better results when compared to the third, at a less CPU time (approximately 160 vs. 233 hours). In the case of the ^{13}C NMR chemical

shifts, the best methods obtained from the DP4 analysis were: GIAO/wB97xD/cc-pVTZ/SCRF (DP4 24.1%; RMSD 2.073), CSGT/wB97xD/cc-pVTZ/SCRF (DP4 12.5%; RMSD 2.157), GIAO/wB97xD/cc-pVTZ (DP4 12.4%; RMSD 2.121) and GIAO/B3LYP/6-31G(d,p)/SCRF (DP4 11.6%; RMSD 2.121). These data show that for obtaining of chemical shifts in the ^{13}C NMR spectrum, the GIAO/B3LYP/6-31G(d,p)/SCRF method provides comparable results to those provided by the CSGT/wB97xD/cc-pVTZ/SCRF and GIAO/wB97xD/cc-pVTZ methods, with a computational cost up to twenty-five times smaller.

Considering all the chemical shifts of both hydrogen as carbon, we could perform the DP4 analysis (data not shown). The method gives better results compared to the experimental data was CSGT/wB97xD/cc-pVTZ/SCRF, which provides a confidence rate of 51.9%, followed the CSGT/B3LYP/6-311++G(2d,p) with 13.9% and GIAO/wB97xD/cc-pVTZ/SCRF with 9.9%. This tool works like a strict criterion for choosing a method that provides best results. As an example, we can highlight the CSGT/TPSSh/cc-pVTZ/SCRF and CSGT/WP04/cc-pVTZ/SCRF methods: RMSD 0.070 and 0.073, respectively, for ^{1}H NMR (lower than in CSGT/wB97xD/cc-pVTZ/SCRF method, RMSD 0.077), and RMSD 2.485 and 2.444, respectively, for ^{13}C NMR (higher than that obtained in method CSGT/wB97xD/cc-pVTZ/SCRF, RMSD 2.157). The DP4 analysis allowed to distinguish which of the three methods mentioned that correlates best with the experimental data, which could not be achieved by evaluating only the MAE, Square Deviation and RMDS parameters.

Therefore, the combination of CSGT method with xB97XD functional and cc-pVTZ basis set in chloroform is the best. In order to investigate the quality of the linear relationship between the experimental and the calculated chemical shifts, we used least squares regression. The linear relationships as well as the fit equations are shown in Figure 2. In this condition, as illustrated in Figure 3, the coefficient of determination values (R^2) for ^{1}H and ^{13}C NMR are greater than 0.997. The comparison of the mean absolute error (MAE) between computed/modeled *versus* experimental data sets revealed the MAE is 0.07 for ^{1}H NMR and 1.32 for ^{13}C NMR, this represents an error of less than 2%.

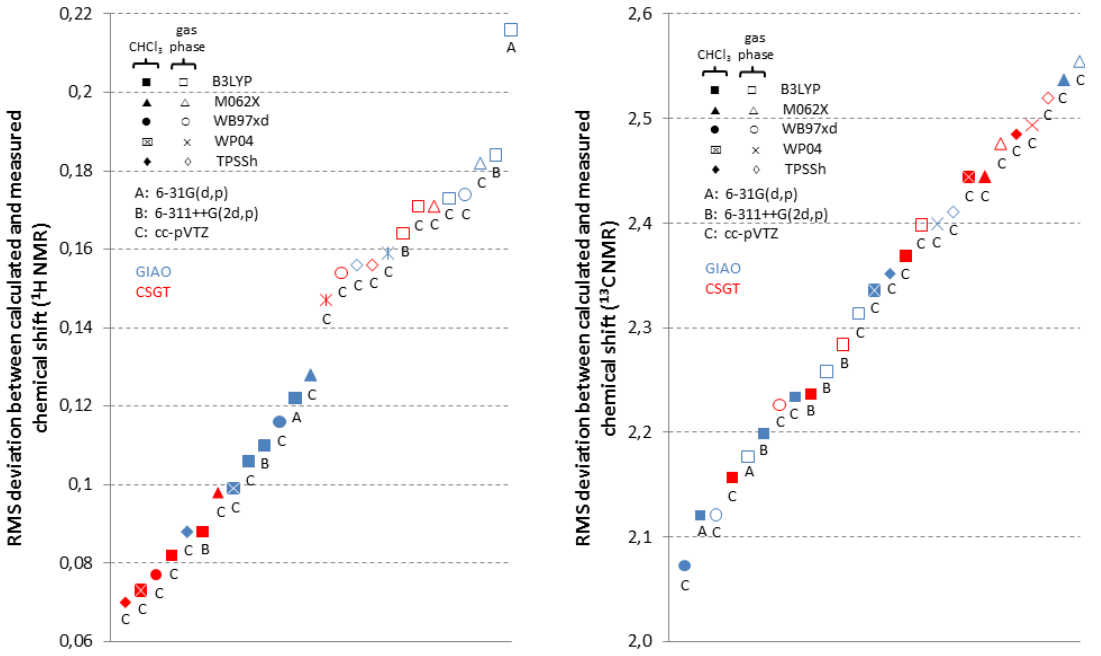

Figure 2 - Graphical representation of results from Table 1 that were obtained by calculations with several methods (explanation of symbols, see inset).

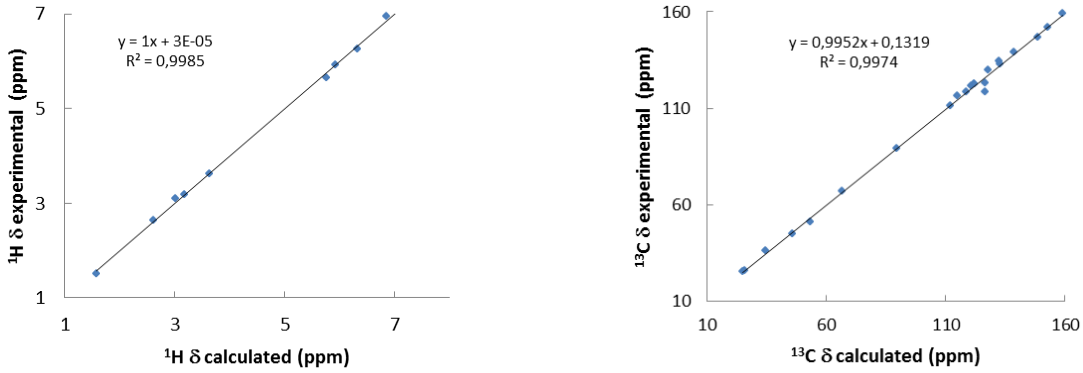

Figure 3 - Correlation plot of ^{1}H and ^{13}C NMR chemical shifts calculated for compounds **1-3** at the CSGT/wB97xD/cc-pVTZ/SCRF level *versus* experiment (best results). Solvent effects ($CDCl_3$) are taken into account within the SMD model.

In order to test which methods offered the best cost/accuracy ratio are bound to the test set that was used to derive the scaling parameters, we carried out calculations on a “probe” set of 6 additional molecules shown in Figure 4. The predetermined conditions have been applied to large complex molecules

with conformational mobility. The lowest energy conformers were considered for calculation of population levels. The experimental structural characterization data are described in a previously published work (OLIVEIRA *et al.,* 2013; OLIVEIRA *et al.,* 2014).

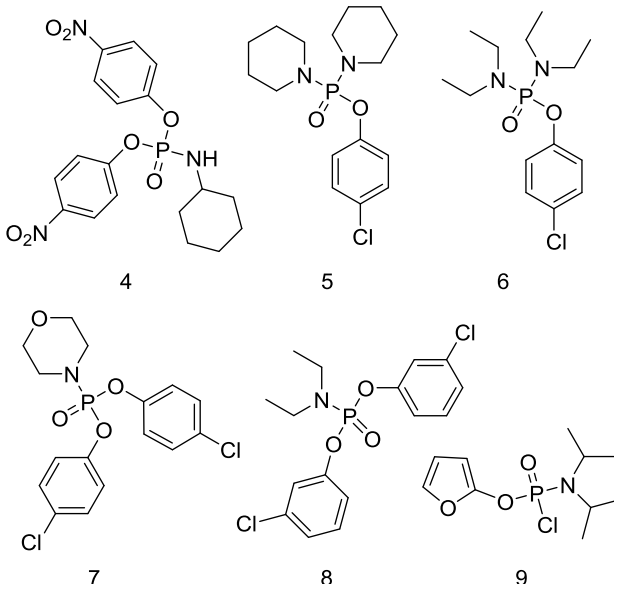

Figure 4 - Molecules in the “probe” set.

The results of this exercise are very encouraging in that the rms errors for the probe set were close to the values obtained for the test set (Table 2). The most notable exceptions to this observation were ^{13}C NMR calculations for compound **8**, for reasons that we do not understand, the rms error for the probe set was much larger than for the test set. The presence of the chlorine atom in this case may have affected the result (LODEWYK *et al.,* 2012). Surprisingly, the best results for the “probe” set turned out to be for this same compound **8** in ^{1}H NMR.

Table 2. Results of calculations of ^{1}H and ^{13}C NMR chemical shifts in the "probe" set

Molecule	^{1}H NMR		^{13}C NMR	
	MAE	RMSD	MAE	RMSD
4	0.169	0.190	1.745	1.727
5	0.101	0.110	1.514	1.768
6	0.126	0.135	0.688	0.862
7	0.077	0.105	1.380	1.683
8	0.012	0.015	4.670	5.404
9	0.026	0.032	1.295	1.480
test set	0.066	0.077	1.322	2.157

5.4. Conclusions

We have tested combinations of various methods, functionals, and basis sets to calculate chemical shifts of a three complex organophosphorus compounds. The most important conclusion of this study is that, contrary to what has been claimed in the literature, it is possible to achieve good results even with less CPU time, according to the needs.

DP4 analysis allowed determining a method that would apply to the ^{1}H and ^{13}C NMR chemical shifts. In this case, the best result has been achieved with the wB97xD functional used in combination with cc-pVTZ basis set (CSGT/wB97xD/cc-pVTZ/SCRF) resulting in the value of MAE as small as 0.066 and 2.157 ppm, respectively. If the only objective is the comparison of the ^{13}C NMR data, the GIAO/wB97xD/cc-pVTZ/SCRF method is recommended. For rapid analysis, the method GIAO/B3LYP/6-31G(d,p)/SCRF with low CPU cost gives results comparable to more robust methods. From the correlation between theoretical and experimental data, it can be concluded that the model adopted was sufficient for calculating the shielding tensors for the studied compounds with accuracy and reduction of the computational time, which validates it as an important tool to confirm the unequivocal assignments of ^{1}H and ^{13}C NMR signals.

5.5. Experimental Section

5.5.1. NMR Studies

One dimensional ^{1}H and ^{13}C NMR spectra were acquired either with an MERCURY-300/Varian spectrometer at 300.069 MHz for ^{1}H (32 k data points, 30^{o} excitation pulse duration of 2.2 μs, spectral width of 6 KHz, acquisition time of 3.3 s and relaxation delay of 10 ms) and at 75.452 MHz for ^{13}C (32 K data points 45^{o} excitation pulse duration of 6.5 μs, spectral width of 19 KHz, acquisition time of 0.8 s and relaxation delay of 2.0 s) in 5 mm probes with direct detection, using deuterated chloroform as a solvent and TMS as internal standard (δ = 0.00).

5.5.2. DFT Studies

The geometries of the phosphoramidates **1-3** were first designed in the SPARTAN´10 software (SPARTAN '10). Using the conformer distribution routine of SPARTAN and the semi-empirical PM6 method (STEWART, 2007) a conformational analysis of species was carried out to identify the most stable conformers in each case. Those conformers were then fully optimized in a gas phase using the Becke three parameter hybrid functional combined with the Lee, Yang, and Parr correlation functional (B3LYP) (BECKER, 1993) and 6-31G(d,p) (RASSOLOV *et al.,* 2001) basis set. NMR chemical shifts were computed at the B3LYP (BECKER, 1993), WP04 (WIITALA *et al.,* 2006), TPSSh (STAROVEROV *et al.,* 2003), M062X (HOHENSTEIN *et al.,* 2008) and wB97xD (MINENKOV *et al.,* 2012) functional and 6-31g(d,p), 6-311++g(2d,p) and cc-pVTZ basis set. WP04 functional was selected since it presented good results similar to B3LYP (JAIN *et al.,* 2009). For comparison, the chemical shifts were calculated in the gas phase and employing Semiempirical Molecular Dynamics (SMD, chloroform as solvent) (LODEWYK *et al.,* 2012). The Continuous Set of Gauge Transformations (CSGT) and Gauge-Including Atomic Orbitals (GIAO) methods were evaluated (LODEWYK *et al.,* 2012). The signal of TMS calculated at the same level of theory was used as reference. Vibrational frequency calculations were performed for all of the previous optimized geometries in order to ascertain the nature of their stationary points on the potential energy surfaces. All the DFT calculations were performed using the Gaussian 09 program package (FRISCH *et al.,* 2009).

The chemical shift values for each isomer were obtained by using Boltzmann weighted average shifts over the set of conformers, calculated by first averaging the chemical shifts for degenerate symmetry related carbon environments within each conformer. Each conformer then contributed a percentage of its chemical shift value to the final total value per environment depending on its Boltzmann weighted energy contribution at 298 K:

$$\sigma^x = \frac{\sum_i \sigma_i^x exp\left(-\frac{E_i}{RT}\right)}{\sum_i exp\left(-\frac{E_i}{RT}\right)}$$

Here, σ^x is the weighted average shielding tensor of the atom(s), σ_i^x is the shielding constant for nucleus x in conformer i, R is the molar gas constant (8.3145 J K^{-1} mol^{-1}), T is the temperature (298 K), and E_i is the energy of the associated conformer. Finally, TMS was optimized in a symmetry restricted (tetrahedral) geometry optimization calculation and the NMR shielding tensor for all atoms (carbon and hydrogen) was obtained at the same levels evaluated. All final shifts were then calculated as $\sigma_{TMS} - \sigma_{calc}$.

Data was scaled according to equation below:

$$\delta_{scaled} = \frac{\delta_{calc} - intercept}{slope}$$

Here, δ_{scaled} is the scaled substrate shift (ppm), δ_{calc} is the calculated compound shift (ppm) and the intercept and slope are the parameters of a linear regression when plotting the experimental shifts against the calculated shifts for a compound.

5.6. Acknowledgments

We thank Conselho Nacional de Desenvolvimento Científico e Tecnológico (CNPq), Coordenação de Aperfeiçoamento de Pessoal de Nível Superior (CAPES) and Fundação de Amparo à Pesquisa do Estado de Minas Gerais (FAPEMIG) for financial support and research fellowships (JWMC, LCAB, SAF and FMO).

5.7. References

ALIEV, A.E.; COURTIER-MURIAS, D.; ZHOU, S. Scaling factors for carbon NMR chemical shifts obtained from DFT B3LYP calculations. *Journal of Molecular Structure: THEOCHEM,* v. 893, p. 1-5, 2009.

ALVARENGA, E.S.; BARBOSA, L.C.A.; SALIBA, W.A.; ARANTES, F.F.P.; DEMUNER, A.J.; SILVA, A.A. Síntese e avaliação da atividade fitotóxica de derivados da alfa-Santonina. *Quimica Nova,* v. 32, p. 401-406, 2009.

AMINI, S. Assignment of absolute configuration of holadyson by computed NMR chemical shifts. *Journal of the Iranian Chemical Society,* v. 11, p. 179-186, 2014.

AMINI, S.K. Assignment of absolute configuration of 8α-hydroxy-13-hydroperoxylabd-14,17-dien-19,16;23,6α-diolide by computed NMR chemical shifts. *Magnetic Resonance in Chemistry,* v. 51, p. 328-333, 2013.

ANDREWS, K.G.; SPIVEY, A.C. Improving the Accuracy of Computed 13C NMR Shift Predictions by Specific Environment Error Correction: Fragment Referencing. *The Journal of Organic Chemistry,* v. 78, p. 11302-11317, 2013.

BARBOSA, L.C.A.; MALTHA, C.R.A.; LAGE, M.R.; BARCELOS, R.C.; DONÀ, A.; CARNEIRO, J.W.M.; FORLANI, G. Synthesis of Rubrolide Analogues as New Inhibitors of the Photosynthetic Electron Transport Chain. *Journal of Agricultural and Food Chemistry,* v. 60, p. 10555-10563, 2012.

BARBOSA, L.C.A.; NOGUEIRA, L.B.; ÁLVARES MALTHA, C.R.; TEIXEIRA, R.R.; SILVA, A.A. Synthesis and Phytogrowth Properties of Oxabicyclic Analogues Related to Helminthosporin. *Molecules,* v. 14, p. 160-173, 2009.

BARBOSA, L.C.A.; PEREIRA, U.A.; MALTHA, C.R.A.; TEIXEIRA, R.R.; VALENTE, V.M.M.; FERREIRA, J.R.O.; COSTA-LOTUFO, L.V.; MORAES, M.O.; PESSOA, C. Synthesis and Biological Evaluation of 2,5-Bis(alkylamino)-1,4-benzoquinones. *Molecules,* v. 15, p. 5629-5643, 2010.

BECKER, A.D. Density-functional thermochemistry. III. The role of exact exchange. *The Journal of Chemical Physics,* v. 98, p. 5648-5652, 1993.

BROWN, S.G.; JANSMA, M.J.; HOYE, T.R. Case Study of Empirical and Computational Chemical Shift Analyses: Reassignment of the Relative Configuration of Phomopsichalasin to That of Diaporthichalasin. *Journal of Natural Products,* v. 75, p. 1326-1331, 2012.

CHEESEMAN, J.R.; TRUCKS, G.W.; KEITH, T.A.; FRISCH, M.J. A comparison of models for calculating nuclear magnetic resonance shielding tensors. *The Journal of Chemical Physics,* v. 104, p. 5497-5509, 1996.

CONGIATU, C.; MCGUIGAN, C.; JIANG, W.G.; DAVIES, G.; MASON, M.D. Naphthyl phosphoramidate derivatives of BVdU as potential anticancer agents: design, synthesis and biological evaluation. *Nucleosides Nucleotides Nucleic Acids,* v. 24, p. 485-489, 2006.

CORRÊA, R.S.; SOUZA E SILVA, S.R.; DUARTE, L.P.; SILVA, G.D.F.; BARBOSA, L.C.A.; ELLENA, J.; DORIGUETTO, A.C. Influence of hydrogen bonds on the molecular structure and conformations of two ($C_{30}H_{48}O_2$) pentacyclic triterpene isomers. *Journal of Structural Chemistry,* v. 53, p. 156-163, 2012.

COSTA, F.L.P.; DE ALBUQUERQUE, A.C.F.; DOS SANTOS, F.M.; DE AMORIM, M.B. GIAO-HDFT scaling factor for ^{13}C NMR chemical shifts calculation. *Journal of Physical Organic Chemistry,* v. 23, p. 972-977, 2010.

DOMÍNGUEZ, M.A.J.; SANMARTÍN, C.; FONT, M.A.; PALOP, J.A.; SAN FRANCISCO, S.; URRUTIA, O.; HOUDUSSE, F.; GARCÍA-MINA, J.M. Design, Synthesis, and Biological Evaluation of Phosphoramide Derivatives as Urease Inhibitors. *Journal of Agricultural and Food Chemistry,* v. 56, p. 3721-3731, 2008.

DUAN, J.X.; JIAO, H.; KAIZERMAN, J.; STANTON, T.; EVANS, J.W.; LAN, L.; LORENTE, G.; BANICA, M.; JUNG, D.; WANG, J.; MA, H.; LI, X.; YANG, Z.;

HOFFMAN, R.M.; AMMONS, W.S.; HART, C.P.; MATTEUCCI, M. Potent and highly selective hypoxia-activated achiral phosphoramidate mustards as anticancer drugs. *Journal of Medicinal Chemistry,* v. 51, p. 2412-2420, 2008.

FRISCH, M.J.; TRUCKS, G.W.; SCHLEGEL, H.B.; SCUSERIA, G.E.; ROBB, M.A.; CHEESEMAN, J.R.; SCALMANI, G.; BARONE, V.; MENNUCCI, B.; PETERSSON, G.A.; NAKATSUJI, H.; CARICATO, M.; LI, X.; HRATCHIAN, H.P.; IZMAYLOV, A.F.; BLOINO, J.; ZHENG, G.; SONNENBERG, J.L.; HADA, M.; EHARA, M.; TOYOTA, K.; FUKUDA, R.; HASEGAWA, J.; ISHIDA, M.; NAKAJIMA, T.; HONDA, Y.; KITAO, O.; NAKAI, H.; VREVEN, T.; MONTGOMERY, J.A., JR.; PERALTA, J.E.; OGLIARO, F.; BEARPARK, M.; HEYD, J.J.; BROTHERS, E.; KUDIN, K.N.; STAROVEROV, V.N.; KOBAYASHI, R.; NORMAND, J.; RAGHAVACHARI, K.; RENDELL, A.; BURANT, J.C.; IYENGAR, S.S.; TOMASI, J.; COSSI, M.; REGA, N.; MILLAM, J.M.; KLENE, M.; KNOX, J.E.; CROSS, J.B.; BAKKEN, V.; ADAMO, C.; JARAMILLO, J.; GOMPERTS, R.; STRATMANN, R.E.; YAZYEV, O.; AUSTIN, A.J.; CAMMI, R.; POMELLI, C.; OCHTERSKI, J.W.; MARTIN, R.L. Gaussian 09. *Revision A1, Gaussian Inc., Wallingford CT,* 2009.

GHOLIVAND, K.; DELLA VÉDOVA, C.O.; ERBEN, M.F.; MAHZOUNI, H.R.; SHARIATINIA, Z.; AMIRI, S. Synthesis, spectroscopic study, X-ray crystallography and ab initio calculations of the two new phosphoramidates: $C_6H_5OP(O)(NHC_6H_{11})_2$ and $[N(CH_3)(C_6H_{11})]P(O)(2\text{-}C_5H_4N\text{-}NH)_2$. *Journal of Molecular Structure,* v. 874, p. 178-186, 2008.

GHOLIVAND, K.; MOSTAANZADEH, H.; KOVAL, T.; DUSEK, M.; ERBEN, M.F.; STOECKLI-EVANS, H.; DELLA VEDOVA, C.O. Syntheses, spectroscopic study and X-ray crystallography of some new phosphoramidates and lanthanide(III) complexes of *N*-(4-nitrobenzoyl)-*N',N''*-bis(morpholino)phosphoric triamide. *Acta Crystallogr B,* v. 66, p. 441-450, 2010.

HOHENSTEIN, E.G.; CHILL, S.T.; SHERRILL, C.D. Assessment of the Performance of the M05−2X and M06−2X Exchange-Correlation Functionals for

Noncovalent Interactions in Biomolecules. *Journal of Chemical Theory and Computation,* v. 4, p. 1996-2000, 2008.

JACINTO DEMUNER, A.; MOREIRA VALENTE, V.M.; ALMEIDA BARBOSA, L.C.; RATHI, A.; DONOHOE, T.; THOMPSON, A. Synthesis and Phytotoxic Activity of New Pyridones Derived from 4-Hydroxy-6-Methylpyridin-2(1*H*)-one. *Molecules,* v. 14, p. 4973-4986, 2009.

JAIN, R.; BALLY, T.; RABLEN, P.R. Calculating accurate proton chemical shifts of organic molecules with density functional methods and modest basis sets. *Journal of Organic Chemistry,* v. 74, p. 4017-4023, 2009.

KATAGI, T. Photochemistry of organophosphorus herbicide butamifos. *Journal of Agricultural and Food Chemistry,* v. 41, p. 496-501, 1993.

KIRAN, Y.B.; DEVENDRANATH REDDY, C.; GUNASEKAR, D.; NAGA RAJU, C.; BARBOSA, L.C.A.; MARNEY, D.C.O.; RUSSELL, L.J. Synthesis and TGA Evaluation of Novel Triphosphate Esters. *Journal of Fire Sciences,* v. 25, p. 193-215, 2007.

KIRAN, Y.B.; DEVENDRANATH REDDY, C.; GUNASEKAR, D.; SURESH REDDY, C.; LEON, A.; BARBOSA, L.C.A. Synthesis and anticancer activity of new class of bisphosphonates/phosphanamidates. *European Journal of Medical Chemistry,* v. 43, p. 885-892, 2008.

LEWANDOWSKA, M.; RUSZKOWSKI, P.; BARANIAK, D.; CZARNECKA, A.; KLECZEWSKA, N.; CELEWICZ, L. Synthesis of 3'-azido-2',3'-dideoxy-5-fluorouridine phosphoramidates and evaluation of their anticancer activity. *European Journal of Medical Chemistry,* v. 67, p. 188-195, 2013.

LODEWYK, M.W.; SIEBERT, M.R.; TANTILLO, D.J. Computational prediction of ^{1}H and ^{13}C chemical shifts: a useful tool for natural product, mechanistic, and synthetic organic chemistry. *Chemical Reviews,* v. 112, p. 1839-1862, 2012.

MARA, C.; DEMPSEY, E.; BELL, A.; BARLOW, J.W. Synthesis and evaluation of phosphoramidate and phosphorothioamidate analogues of amiprophos methyl as potential antimalarial agents. *Bioorganic & Medicinal Chemistry Letters,* v. 21, p. 6180-6183, 2011.

MARELL, D.J.; EMOND, S.J.; KULSHRESTHA, A.; HOYE, T.R. Analysis of Seven-Membered Lactones by Computational NMR Methods: Proton NMR Chemical Shift Data are More Discriminating than Carbon. *The Journal of Organic Chemistry,* v. 79, p. 752-758, 2013.

MCGUIGAN, C.; KELLEHER, M.R.; PERRONE, P.; MULREADY, S.; LUONI, G.; DAVERIO, F.; RAJYAGURU, S.; POGAM, S.L.; NAJERA, I.; MARTIN, J.A.; KLUMPP, K.; SMITH, D.B. The application of phosphoramidate ProTide technology to the potent anti-HCV compound 4′-azidocytidine (R1479). *Bioorganic & Medicinal Chemistry Letters,* v. 19, p. 4250-4254, 2009.

MEHELLOU, Y.; BALZARINI, J.; MCGUIGAN, C. An investigation into the anti-HIV activity of 2',3'-didehydro-2',3'-dideoxyuridine (d4U) and 2',3'-dideoxyuridine (ddU) phosphoramidate 'ProTide' derivatives. *Organic and Biomolecular Chemistry,* v. 7, p. 2548-2553, 2009.

MINENKOV, Y.; SINGSTAD, A.; OCCHIPINTI, G.; JENSEN, V.R. The accuracy of DFT-optimized geometries of functional transition metal compounds: a validation study of catalysts for olefin metathesis and other reactions in the homogeneous phase. *Dalton Transactions,* v. 41, p. 5526-5541, 2012.

NICOLAOU, K.C.; SNYDER, S.A. Chasing Molecules That Were Never There: Misassigned Natural Products and the Role of Chemical Synthesis in Modern Structure Elucidation. *Angewandte Chemie International Edition,* v. 44, p. 1012-1044, 2005.

OLIVEIRA, F.M.; BARBOSA, L.C.A.; DEMUNER, A.J.; MALTHA, C.R.A.; FERNANDES, S.A.; CARNEIRO, J.W.D.M.; CORRÊA, R.S.; DORIGUETTO, A.C. Spectroscopic and dynamic NMR study, X-ray crystallography and DFT calculations of two phosphoramidates: $(C_4H_3O_2)P(O)(Cl)C_6H_{14}N$ and

$(C_4H_3O_2)P(O)(C_6H_{11}NH)_2$. *Journal of Molecular Structure,* v. 1046, p. 64-73, 2013.

OLIVEIRA, F.M.; BARBOSA, L.C.A.; DEMUNER, A.J.; MALTHA, C.R.Á.; PEREIRA, S.R.; HORTA, L.P.; MODOLO, L.V. Synthesis, molecular properties and DFT studies of new phosphoramidates as potential urease inhibitors. *Medicinal Chemistry Research,* v. 23, p. 5174-5187, 2014.

OLIVEIRA, F.M.; BARBOSA, L.C.A.; ISMAIL, F.M.D. The diverse pharmacology and medicinal chemistry of phosphoramidates - a review. *RSC Advances,* v. 4, p. 18998-19012, 2014.

OLIVEIRA, F.M.; BARBOSA, L.C.A.; TEIXEIRA, R.R.; DEMUNER, A.J.; MALTHA, C.R.A.; PICANÇO, M.C.; SILVA, G.A.; PAULA, V.F. Synthesis and insecticidal activity of new phosphoramidates. *Journal of Pesticide Science,* v. 37, p. 85-88, 2012.

PAULA, V.F.; BARBOSA, L.C.A.; TEIXEIRA, R.R.; PICANCO, M.C.; SILVA, G.A. Synthesis and insecticidal activity of new 3-benzylfuran-2-yl *N,N,N',N'*-tetraethyldiamidophosphate derivatives. *Pest Management Science,* v. 64, p. 863-872, 2008.

PERRONE, P.; LUONI, G.M.; KELLEHER, M.R.; DAVERIO, F.; ANGELL, A.; MULREADY, S.; CONGIATU, C.; RAJYAGURU, S.; MARTIN, J.A.; LEVEQUE, V.; LE POGAM, S.; NAJERA, I.; KLUMPP, K.; SMITH, D.B.; MCGUIGAN, C. Application of the phosphoramidate ProTide approach to 4'-azidouridine confers sub-micromolar potency versus hepatitis C virus on an inactive nucleoside. *Journal of Medicinal Chemistry,* v. 50, p. 1840-1849, 2007.

RABLEN, P.R.; PEARLMAN, S.A.; FINKBINER, J. A Comparison of Density Functional Methods for the Estimation of Proton Chemical Shifts with Chemical Accuracy. *The Journal of Physical Chemistry A,* v. 103, p. 7357-7363, 1999.

RASSOLOV, V.A.; RATNER, M.A.; POPLE, J.A.; REDFERN, P.C.; CURTISS, L.A. 6-31G* basis set for third-row atoms. *Journal of Computational Chemistry,* v. 22, p. 976-984, 2001.

SAMULTSEV, D.O.; SEMENOV, V.A.; KRIVDIN, L.B. On the accuracy of the GIAO-DFT calculation of ^{15}N NMR chemical shifts of the nitrogen-containing heterocycles--a gateway to better agreement with experiment at lower computational cost. *Magnetic Resonance in Chemistry,* v. 52, p. 222-230, 2014.

SAROTTI, A.M. Successful combination of computationally inexpensive GIAO ^{13}C NMR calculations and artificial neural network pattern recognition: a new strategy for simple and rapid detection of structural misassignments. *Organic & Biomolecular Chemistry,* v. 11, p. 4847-4859, 2013.

SAROTTI, A.M.; PELLEGRINET, S.C. A Multi-standard Approach for GIAO 13C NMR Calculations. *The Journal of Organic Chemistry,* v. 74, p. 7254-7260, 2009.

SAROTTI, A.M.; PELLEGRINET, S.C. Application of the Multi-standard Methodology for Calculating ^{1}H NMR Chemical Shifts. *The Journal of Organic Chemistry,* v. 77, p. 6059-6065, 2012.

SMITH, S.G.; GOODMAN, J.M. Assigning Stereochemistry to Single Diastereoisomers by GIAO NMR Calculation: The DP4 Probability. *Journal of the American Chemical Society,* v. 132, p. 12946-12959, 2010.

SOFIA, M.J.; CHANG, W.; FURMAN, P.A.; MOSLEY, R.T.; ROSS, B.S. Nucleoside, nucleotide, and non-nucleoside inhibitors of hepatitis C virus NS5B RNA-dependent RNA-polymerase. *Journal of Medicinal Chemistry,* v. 55, p. 2481-2531, 2012.

SPARTAN ’10. Wavefunction Inc., Irvine, CA, USA., 2010.

STAROVEROV, V.N.; SCUSERIA, G.E.; TAO, J.; PERDEW, J.P. Comparative assessment of a new nonempirical density functional: Molecules and hydrogen-

bonded complexes. *The Journal of Chemical Physics,* v. 119, p. 12129-12137, 2003.

STEWART, J.P. Optimization of parameters for semiempirical methods V: Modification of NDDO approximations and application to 70 elements. *Journal of Molecular Modeling,* v. 13, p. 1173-1213, 2007.

TEIXEIRA, R.R.; BARBOSA, L.C.A.; CARNEIRO, J.W.D.M.; CORRÊA, R.S.; ELLENA, J.; DORIGUETTO, A.C. Synthesis, structural characterization and conformational aspects of nostoclide analogues. *Journal of Molecular Structure,* v. 917, p. 1-9, 2009.

WANG, Z.W.; GUO, C.C.; XIE, W.Z.; LIU, C.Z.; XIAO, C.G.; TAN, Z. Novel phosphoramidates with porphine and nitrogenous drug: one-pot synthesis and orientation to cancer cells. *European Journal of Medical Chemistry,* v. 45, p. 890-895, 2010.

WIITALA, K.W.; AL-RASHID, Z.F.; DVORNIKOVS, V.; HOYE, T.R.; CRAMER, C.J. Evaluation of various DFT protocols for computing ^{1}H and ^{13}C chemical shifts to distinguish stereoisomers: diastereomeric 2-, 3-, and 4-methylcyclohexanols as a test set. *Journal of Physical Organic Chemistry,* v. 20, p. 345-354, 2007.

WIITALA, K.W.; HOYE, T.R.; CRAMER, C.J. Hybrid Density Functional Methods Empirically Optimized for the Computation of ^{13}C and ^{1}H Chemical Shifts in Chloroform Solution. *Journal of Chemical Theory and Computation,* v. 2, p. 1085-1092, 2006.

WITTINE, K.; BENCI, K.; RAJIC, Z.; ZORC, B.; KRALJ, M.; MARJANOVIC, M.; PAVELIC, K.; DE CLERCQ, E.; ANDREI, G.; SNOECK, R.; BALZARINI, J.; MINTAS, M. The novel phosphoramidate derivatives of NSAID 3-hydroxypropylamides: synthesis, cytostatic and antiviral activity evaluations. *European Journal of Medical Chemistry,* v. 44, p. 143-151, 2009.

YAN, J.; BU, J.; BAI, X.; LI, J.; REN, T.; ZHAO, Y. The tribological study of novel phosphorous–nitrogen type phosphoramidate additives in rapeseed oil. *Journal of Engineering Tribology,* v. 226, 2012.

ZAKIROVA, N.F.; SHIPITSYN, A.V.; JASKO, M.V.; PROKOFJEVA, M.M.; ANDRONOVA, V.L.; GALEGOV, G.A.; PRASSOLOV, V.S.; KOCHETKOV, S.N. Phosphoramidate derivatives of acyclovir: synthesis and antiviral activity in HIV-1 and HSV-1 models in vitro. *Bioorganic and Medicinal Chemistry,* v. 20, p. 5802-5809, 2012.

CAPÍTULO 6

6. THE DIVERSE PHARMACOLOGY AND MEDICINAL CHEMISTRY OF PHOSPHORAMIDATES – A REVIEW

6.1. Abstract

The phosphoramidates consist of compounds which possess at least one amino group bound directly to the phosphorus atom and are, therefore, phosphoramide acid derivatives. The inherent chemical properties of the element phosphorus include polarizability, low to medium electronegativity and derivatives exhibit low coordination numbers thereby allowing synthesis of a diverse range of compounds. In line with their physicochemical properties, phosphorus compounds have widespread industrial applications and also demonstrate a diverse range of biological activities. In last two decades, notably, phosphoramidates have been evaluated for both their antitumor and antiviral efficacy. This brief review describes the most promising examples of this class which possesses antiviral, antitumor, antibacterial, antimalarial and anti-protozoal activity, as well as urease , acetyl and butyrylcholinesterase enzyme inhibitor activity.

6.2. Introduction

The element phosphorus was discovered in 1669 by Henning Brandt and since then, significant discoveries have been made regarding its biological function (SANTOS *et al.*, 2007).

The advent of suitable synthetic methodology coupled with advances in analytical science has accelerated research into both

isolating and designing both organic and organometallic compounds with evermore diverse applications. Structural incorporation of a phosphorus atom within biomolecules essential for life, notably DNA and RNA, are especially abundant in cells. This element plays a pivotal role within ATP, which is used by most living organisms for storing and translocating energy (Figure 1). Phosphorus compounds also serve as cofactors of multiple enzyme systems whereas others act as essential buffering agents within the cellular mileau (SANTOS *et al.*, 2007; WESTHEIMER, 1987).

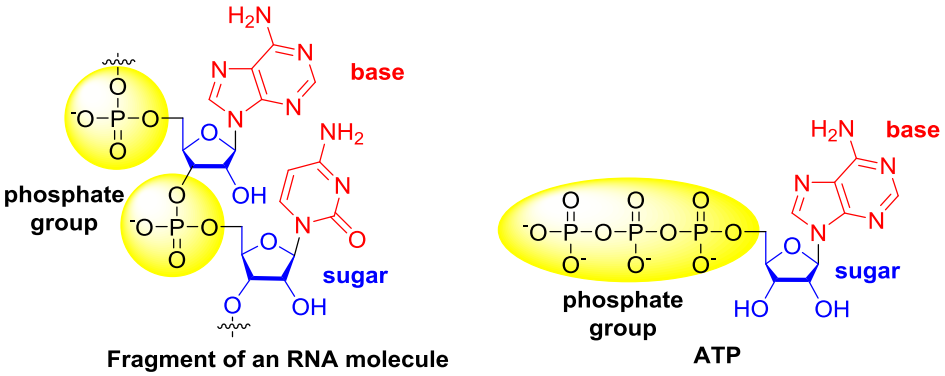

Figure 1 - Fragment of an RNA molecule and the structural formula of adenosine triphosphate (ATP).

The inherent properties of the element phosphorus include: a) polarizability, b) low to medium electronegativity and c) low coordination number, thereby, allowing the synthesis of a diverse range of compounds. Biological and medicinal activities of organophosphorus compounds are modulated, in part, by the nature of the element bound to phosphorus and variations in its own oxidation state. In the last few decades, the phosphoramidates in particular have attracted the attention of many investigators. This class is characterized by having at least one $-NR^1R^2$ group (where R^1 and R^2 = alkyl, aryl, heteroaryl) bound to phosphorus, itself derived from phosphoramidic acid (Figure 2) (WESTHEIMER, 1987).

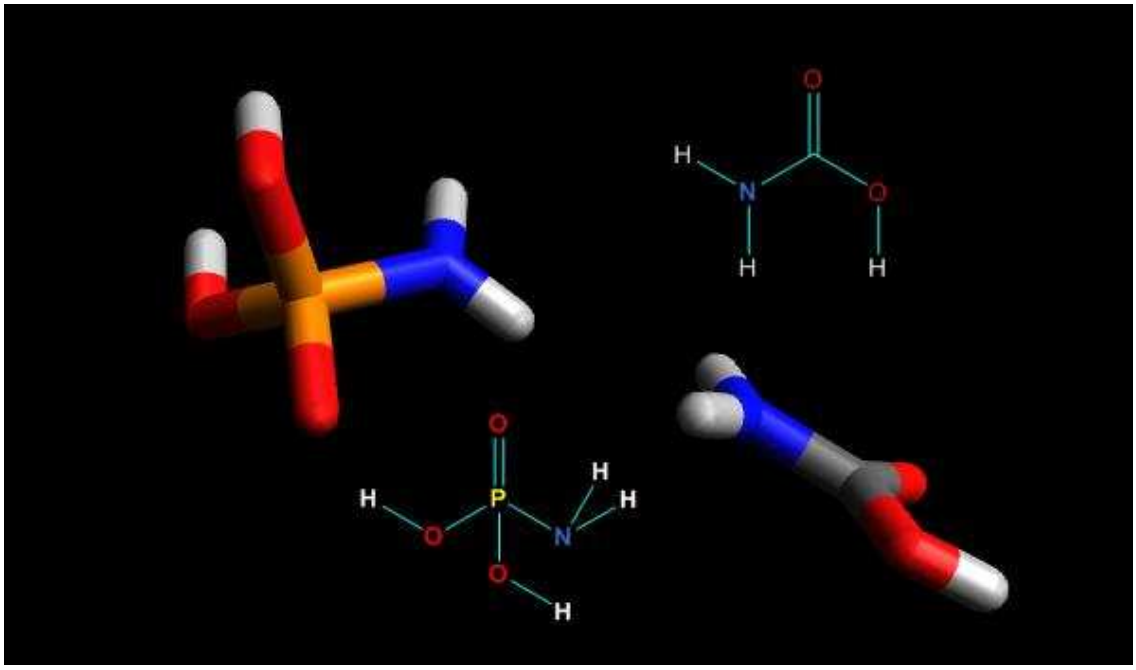

Figure 2 - a) Tetrahedral structure of phosphoramidic acid; b) planar structure of carbamic acid.

Amongst the large array of activities and properties reported for phosphoramidates, the following are particularly noteworthy: biological activities and potential agricultural applications (KATAGI, 1993; OLIVEIRA *et al.*, 2012; PAULA *et al.*, 2008), flame retardant properties (KIRAN *et al.*, 2007; NGUYEN *et al.*, 2013), their use as antirust additives within lubricating oils (YAN *et al.*, 2012) and, notably, pharmaceuticals used for treating and controlling various diseases (CHO *et al.*, 2012; CHO *et al.*, 2013; CONGIATU *et al.*, 2006; DERUDAS *et al.*, 2010; DONGHI *et al.*, 2009; GARDELLI *et al.*, 2009; KIRAN *et al.*, 2008; LIU *et al.*, 2012; LIU *et al.*, 2013; MARA *et al.*, 2011; MCGUIGAN *et al.*, 2009; MCGUIGAN *et al.*, 2011; MCGUIGAN *et al.*, 2010; MCGUIGAN *et al.*, 2011; MCGUIGAN *et al.*, 1992; MCGUIGAN *et al.*, 2005; MENEGHESSO *et al.*, 2013; PERRONE *et al.*, 2007; PRASAD *et al.*, 2006; SANTOS *et al.*, 2007; SOFIA *et al.*, 2012; VALIYEV *et al.*, 2008; WANG *et al.*, 2010; ZAKIROVA *et al.*, 2012). Considering the increasing interest in this class of compound, especially within the pharmaceutical arena, this review discusses the most significant examples of phosphoramidates imbued

with antiviral, antitumor, antibacterial, anti-malarial, anti-protozoal activities, as well as examples of selected compounds that act as inhibitors of urease, butyryl and acetyl cholinesterase. Hopefully, this review will encourage further attention upon this class of compounds, especially that involving the discovery of new drugs for the treatment of various diseases.

The use of vaccines during the last decades has assisted humankind in the fight against diseases caused by viruses such as rubella, measles, mumps and polio. However, for some viral pathogens such as the *Human papilloma virus* (HPV) and human herpes virus (HHV), amongst others, currently, there is neither any small molecule (denoted here as drug) nor vaccine effective for managing such infections. For other diseases, such as herpes simplex virus (HSV) and *Varicella-zoster virus* (VZV), although some effective drugs are available, in many cases off target-side effects in some patients can pose problems, and in such cases, it is imperative to discover new, more efficacious drugs (DE CLERCQ, 2002; SOFIA *et al.*, 2012). For instance, two- drugs Telaprevir and Boceprevir were approved in 2011 for treating hepatitis C virus infection (HCV) in genotype 1 patients. However, these drugs do not exert effect on genotypes 2-6 (SOFIA *et al.*, 2012). In these cases, the treatment also requires regular injections of pegalated α-interferon (PEG-IFN)[1] with daily oral administration of ribavirin (a nucleoside analogue which possesses useful and broad antiviral activity). However, daily administration places additional burden upon the patient arising from management of uncontrolled side effects (Figure 3). Amongst the large array of possible scaffolds for antiviral drugs development, the phosphoramidates promise considerable potential for development into putative drugs (SOFIA *et al.*, 2012).

[1] Interferons (IFNs) are proteins made and released by host cells in response to the presence of pathogens such as viruses, bacteria, parasites or tumor cells. They facilitate communication between cells to trigger the protective defences of the immune system allowing eradicate of either pathogens or tumors. The pegylated form of interferon-alpha, with greater stability and in vivo activity, has substantially improved sustained virological response rates when compared with unmodified interferon-alpha.

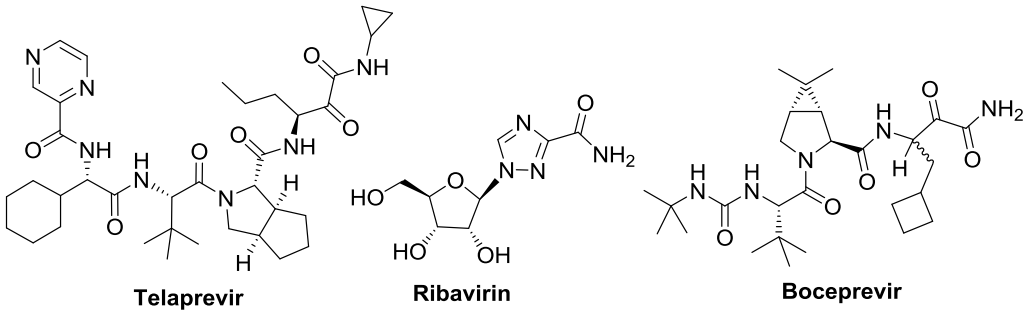

Figure 3 - Structure of Telaprevir, Boceprevir and Ribavirin, drugs approved for treating HCV infection in genotype 1 patients.

Nucleoside analogs are considered an important class of inhibitors of the viral polymerase of several therapeutic targets especially HCMV, HSV, HIV and HBV (ICHIKAWA *et al.*, 2001). Recently some investigators have evaluated phosphoramidate groups covalently linked to nucleosides, a strategy known as 'Phosphoramidate protide' (ARBELO ROMÁN *et al.*, 2011; BORRELLO *et al.*, 2009; CUI *et al.*, 2011; DERUDAS *et al.*, 2010; DERUDAS *et al.*, 2009; DONGHI *et al.*, 2009; GARDELLI *et al.*, 2009; HARRIS *et al.*, 2001; LIU *et al.*, 2012; MCGUIGAN *et al.*, 2009; MCGUIGAN *et al.*, 2011; MCGUIGAN *et al.*, 2005; PERRONE *et al.*, 2007; ZAKIROVA *et al.*, 2012). This approach was introduced by McGuigan *et al*. (1992) as a means of improving the therapeutic potential of a prototype drug. The introduction of this group favors the phosphorylation process *in vivo*, by converting the nucleosides into their active forms as triphosphates derivatives, commonly known as nucleotides. These phosphorylated analogues have significantly advanced both the chemotherapy of neoplasms and antiviral treatments (HILFINGER, 2013; MCGUIGAN *et al.*, 1992). McGuigan *et al.* (2009) have synthesized several phosphorylated nucleoside analogs that proved to be efficient phosphate releasing agents. The phosphoramidate derivatives of 4'-azidocytidine (**R1479**) were effective in inhibiting hepatitis C virus (HCV). From such compounds, pro-nucleoside derivatives were evolved that were up to 3.4 times more potent (**1**; EC_{50} = 0.38 μM) than the standard compounds (**R1479**; EC_{50} = 1.28 μM) (Figure 4). Sofosbuvir (Figure 4) is a drug for the treatment of HCV approved by FDA in December of 2013. This compound suppresses various HCV genotypes in patients exposed to the drug for up to 12 weeks without causing any serious

side effects. Clinical trials revealed a cure rate of 90% when sofosbuvir (Figure 4) is combined with peginterferon and ribavirin. Notably, with conventional treatment that utilizes only peginterferon and ribavirin, the cure rate is less than 50% (HERBST *et al.*, 2013).

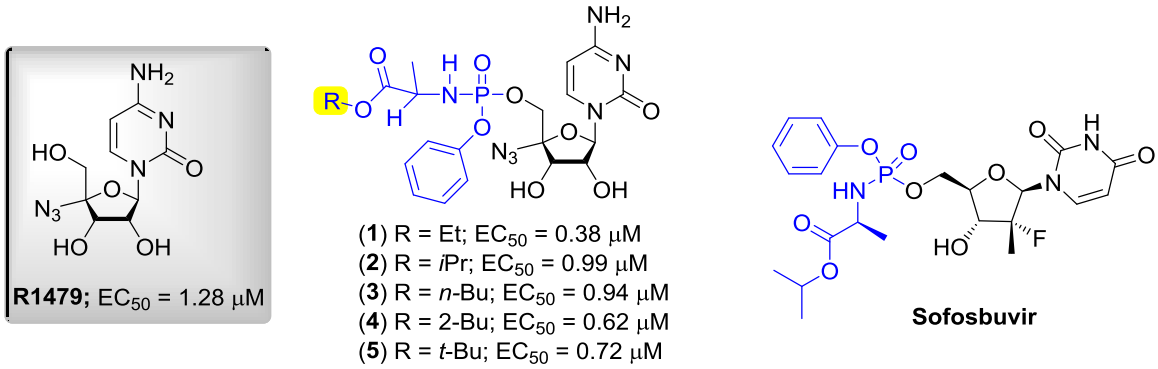

Figure 4 - Structural formulas of compounds with anti-HCV activity.

Acyclovir® (also commercially available as Zovirax®) and a series of derivatives were synthesized by Derudas *et al*. (2009). Acyclovir (ACV), a synthetic purine nucleoside analogue, possesses inhibitory activity *in vitro* and *in vivo* against human herpes viruses including *Herpes simplex virus* (HSV) types 1 and 2, *Varicella-zoster virus* (VZV), *Epstein-Barr virus* (EBV) and *Cytomegalovirus* (CMV) (DE CLERCQ, 2009). ACV is considered inactive against virus HSV thymidine kinase deficient (HSV-1 TK^-) (EC_{50} = 50 µM), whereas in the case of nucleoside, pro-activity was increased 35 fold (EC_{50} = 1.4 µM) (Figure 5). As for activities against HSV-1 and HSV-2, the synthetic compounds proved slightly less active than the standard product ACV employed as a control. Against HSV-1, ACV revealed an EC_{50} = 0.4 µM, whilst for compounds **6-9** the activities were as follows: compound **6**, EC_{50} = 0.9 µM; **7**, 1.4 µM; **8**, 0.8 µM; **9**, 1.1 µM. For HSV-2, ACV had an EC_{50} = 0.2 µM and for the synthetic phosphorous compounds the EC_{50} values were: compound **6**, 0.5 µM; **7**, 1.6 µM; **8**, 0.7 µM; **9**, 1.1 µM. In the same study, the investigators found that pro-nucleoside derivatives **10-16**, incorporating the amino acid alanine, showed high activity (EC_{50} values lay between 0.8 and 42 µM) on three cultures of HIV (HIV-1 CEM, HIV-2 CEM and MT-4) (Figure 5), whilst ACV proved relatively inactive (EC_{50} > 250 for all cultures). The pro-

nucleosides **6-9** were also evaluated against HIV cultures, but failed to demonstrate any useful activity against these infections (DERUDAS *et al*. 2009).

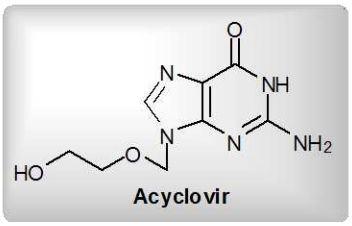

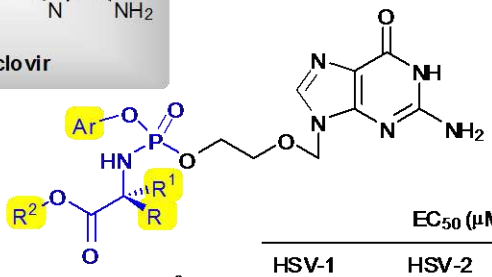

	EC_{50} (μM)		
	HSV-1	HSV-2	HSV-1 TK⁻
(6) Aryl = *p*-F-Ph; AA = L-Ala; R^2 = Bn	0.9	0.5	1.5
(7) Aryl = Naph; AA = DMG; R^2 = Bn	1.4	1.6	3.2
(8) Aryl = Ph; AA = L-Leu; R^2 = Bn	0.8	0.7	1.4
(9) Aryl = Ph; AA = L-Ile; R^2 = Bn	1.1	1.1	1.4

	EC_{50} (μM)		
	HIV-1 CEM	HIV-2 CEM	HIV-1 MT-4
(10) Aryl = Naph; AA = L-Ala; R^2 = Bn	15	8.9	0.8
(11) Aryl = Naph; AA = L-Ala; R^2 = n-Pr	6.6	24	10
(12) Aryl = Naph; AA = L-Ala; R^2 = Me	10	13	4.7
(13) Aryl = Naph; AA = L-Ala; R^2 = Et	12	42	1.7
(14) Aryl = Naph; AA = L-Ala; R^2 = i-Pr	6.2	12	5.4
(15) Aryl = Naph; AA = L-Ala; R^2 = Me	17	26	15
(16) Aryl = Naph; AA = L-Ala; R^2 = Bn	16	11	5.7

Figure 5 - Structure of Acyclovir® and synthetic pro-nucleosides actives against HSV-1 TK- and HIV viruses (Derudas *et al*., 2009).

Phosphoramidate 2'-C-methyl guanosine monophosphate Pro-drugs **18a-i**, were active against HCV (Figure 6). Notably, the addition of a phosphorous group to nucleosides (**17a-i**) enhanced biological activity over 100 fold. Amongst the compounds synthesized, the insertion of the amino acid alanine produced the most favorable modification, with EC_{50} lying within the nanomolar range (Figure 6) (MCGUIGAN *et al.*, 2011). The phosphoramidate derivatives (**20-30**) of 4'-azidouridine (**AZU**, **19**, Figure 7), synthesized by Perrone *et al*., (2007) were up to 450 times more active against HCV when compared with their corresponding, non-phosphorylated, precursors. Data are presented as EC_{50} values (representing the concentration of compounds reducing HCV replication by 50%) and CC_{50} values (representing the concentration of compounds

reducing cell viability by 50%) as determined using the WST assay. All phosphoramidates tested (**20-30**) were non-toxic towards HCV in the replication assay (CC_{50} > 100 μM). In this series, the most active compound was **20** (EC_{50} = 0.22 μM), with the phosphorus atom in either the *R* or *S* configuration. In general, it was observed that compounds bearing naphthyl group (**20-22**) were more active when compared with their corresponding analogues (**23-30**) bearing a phenyl group (Figure 7).

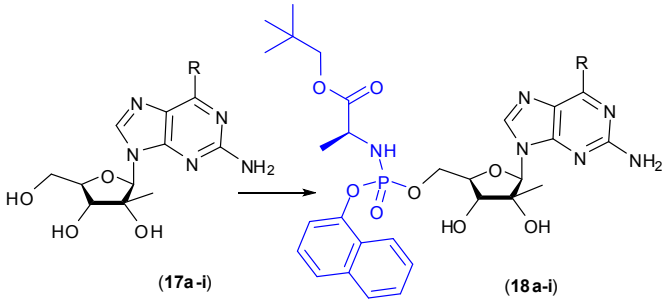

		EC_{50} (μM)	
	R	Series **17**	Series **18**
a	Cl	8.5	0.012
b	OMe	4.6	0.010
c	OEt	8.8	0.08
d	NHMe	13	0.035
e	SMe	11	0.037
f	$O(CH_2)_3OMe$	12	0.043
g	$NHCH_2Bn$	24	0.270
h	NHBn	30	0.79
i	$OCH(CH_3)_2$	9.3	0.023

Figure 6 - HCV Replicon activity of 6-substituted 2´-C-methylguanosine nucleosides (**17a-i**) and ProTides (**18a-i**).

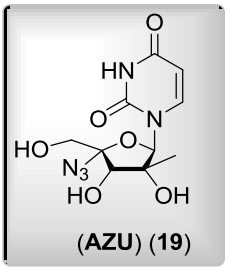

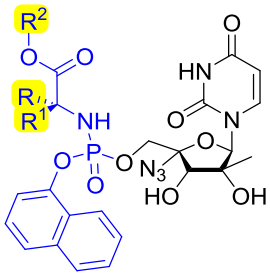

AA = *L*-Ala; ester = Bn

(**19**) 4´azidouridine; EC_{50} > 100 μM
(**20**) Phosphorus configuration: *S/R*; EC_{50} = 0.22 μM
(**21**) Phosphorus configuration: *R*; EC_{50} = 0.39 μM
(**22**) Phosphorus configuration: *S*; EC_{50} = 0.43 μM

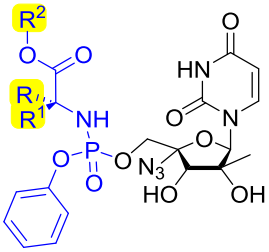

(**23**) AA = *L*-Ala; ester = Et; EC_{50} = 1.3 μM
(**24**) AA = *L*-Ala; ester = Bu; EC_{50} = 1.2 μM
(**25**) AA = *L*-Ala; ester = 2-Bu; EC_{50} = 0.63 μM
(**26**) AA = *L*-Ala; ester = *i*-Pr; EC_{50} = 1.77 μM
(**27**) AA = *L*-Ala; ester = Bn; EC_{50} = 0.61 μM
(**28**) AA = Phe; ester = Et; EC_{50} = 1.37 μM
(**29**) AA = Gly; ester = Bn; EC_{50} = 1.6 μM
(**30**) AA = *D*-Ala; ester = Bn; EC_{50} = 1.2 μM

Figure 7 - HCV Replicon activity of 4´-azidouridine nucleosides derivatives (**20-30**).

In an attempt to increase the concentration of the bioactive ribavirin monophosphate in the cells, some phosphorylated derivatives of ribavirin (Figure 8) were prepared (DERUDAS *et al.*, 2010). Subsequent pharmacological evaluation revealed that compound (**31**) was active against *Vesicular stomatitis virus* (EC_{50} = 20 μM), *Vaccinia virus* (EC_{50} = 100 μM) and Influenza B (EC_{50} = 14 μM); compound (**32**) was active against *Punta Toro virus* (EC_{50} = 100 μM) and (**33**) showed a better effect against *Vesicular stomatitis virus* (EC_{50} = 20 μM), *Vaccinia virus* (EC_{50} = 20 μM) and *Punta Toro virus* (EC_{50} = 58 μM). These values are comparable to the activity of ribavirin (*Vesicular stomatitis virus*, EC_{50} = 22 μM; *Vaccinia virus*, EC_{50} = 22 μM; Influenza B, EC_{50} = 9 μM; *Punta Toro virus*, EC_{50} = 183 μM), clearly indicating that phosphorylation, in this case, did not improve the desired bioactivity. Studies using cell lysate coupled with molecular modeling investigations revealed a weak activation of ProTide in comparison with the free monophosphate, which may provide one explanation for the observed biological activity.

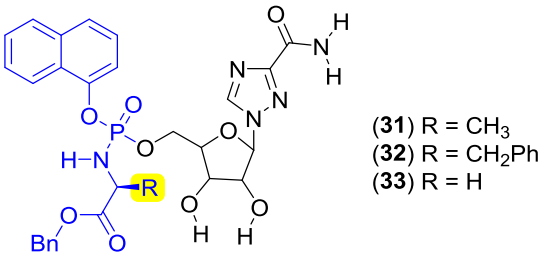

Figure 8 - Phosphorilated derivatives of ribavirine.

Stavudine (d4T), an analogue of thymidine, is the fourth antiretroviral drug to achieve world-wide commercialization (DE CLERCQ, 2009). In 2011, Román *et al*. synthesized several diasteroisomericaly pure derivatives of d4T phosphoramidates (**34-37**). Antiviral activities against HIV-1 and HIV-2 were evaluated and the corresponding EC_{50} against type HIV-1 (IIIB) are shown in Figure 9. Since the phosphorous center is chiral, all compounds can exist in the S_P and R_P forms. All isomers were examined and, in general, compounds with S_P stereochemistry proved superior to the corresponding R_P analogues, compound **36** being a notable exception (ARBELO ROMÁN *et al.*, 2011).

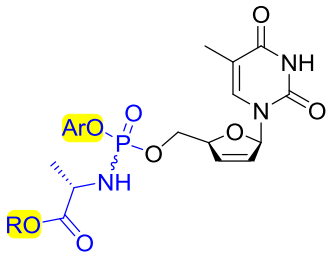

Figure 9 - Structural formulas of diasteroisomericaly pure derivatives of d4T phosphoramidates actives HIV-1 (IIIB)

Some reports have demonstrated that phosphoramidate derivatives of dioxolane sugar nucleosides (DOA) possessing pyrimidines improved the antiviral potency *in vitro* (LIANG *et al.*, 2006; WANG *et al.*, 2012). The phosphoramidates **38** and **39**, synthetized by Bondada *et al*. (2013) had evaluated their activities against HIV-1 and HBV. The compound **38** displayed up to a 1070-fold greater potency versus HIV-1 compared to their corresponding parent nucleoside (**40**), and, notably, were up to 12-

fold more potent versus HBV (Figure 10). The improved and significant dual antiviral activity of these novel phosphoramidate nucleosides was partially explained by the increased intracellular formation of the adenosine dioxolane triphosphate. Cytotoxicity was absent for compound **38** when tested at concentrations of 100 μM in human PBM cells, Vero cells (kidney epithelial cells from the African green monkey) and CEM cells (a human-T-cell-derived cell line), whereas compound **39** showed a value of CC_{50} = 65 μM for Huh7 cells (Human Hepatoma Cell).

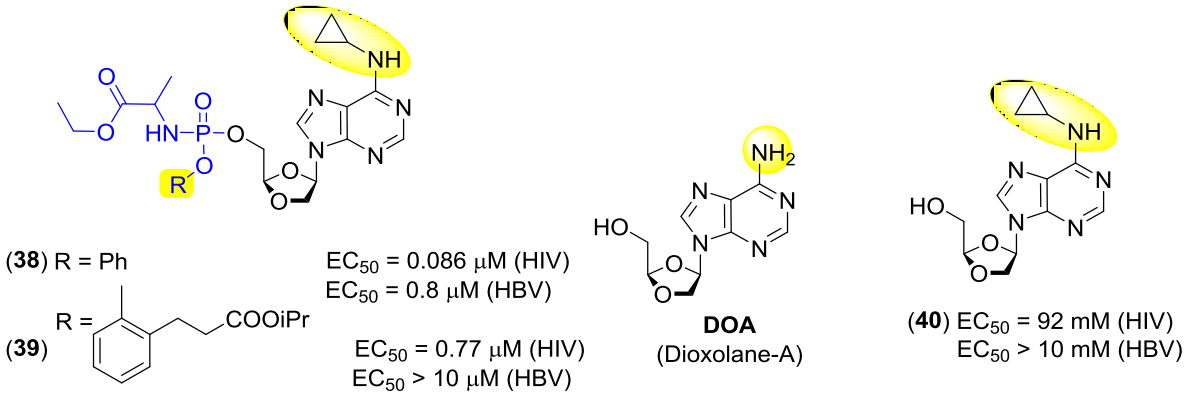

Figure 10 - Adenosine dioxolane nucleoside phosphoramidates as antiviral agents for inhibiting Human Immunodeficiency and Hepatitis B Viruses

Recently, Cho *et al*. (2012) have formulated a structure-activity relationship (SAR) of C-nucleosides containing the 2'-C-Me as putative NS5B inhibitors. In search of compounds with a better selectivity compared to their precursors, structural changes were introduced within both the heteroaromatic portion base and sugar moiety, coupled with a monophosphate prodrug approach. Judicious modification of pharmacokinetic parameters led to the discovery of phosphoramidate **GS-6620** (Figure 11), the first C-nucleoside clinical candidate. During phase I clinical trials **GS-6620** showed potent anti-HCV activity in HCV-infected patients, but with an unexpectedly high variability in PK/PD investigations (CHO *et al.*, 2013).

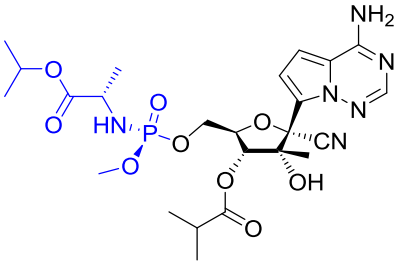

(**GS-6620**)

Figure 11 - Phosphoramidate prodrug possessing HCV replicon activity.

In a study aimed at improving efficacy against HCV, several phosphoramidate derivatives 2'-methycytidine were prepared (Figure 12). Although Valopicitabine 1 (**NM283**) proved highly efficacious, phase II clinical trials revealed some undesirable side effects. In the case of derivative **41**, a thirty fold increase in activity was observed in the replication test, whilst compound **42** proved to be only ten times more active. However, measurements of triphosphate levels in mouse liver after oral administration, showed low levels of nucleoside triphosphate (NTP) for both compounds. In contrast, compound **41**, after six hours of subcutaneous administration (DONGHI *et al.*, 2009), exhibited high levels of NTP.

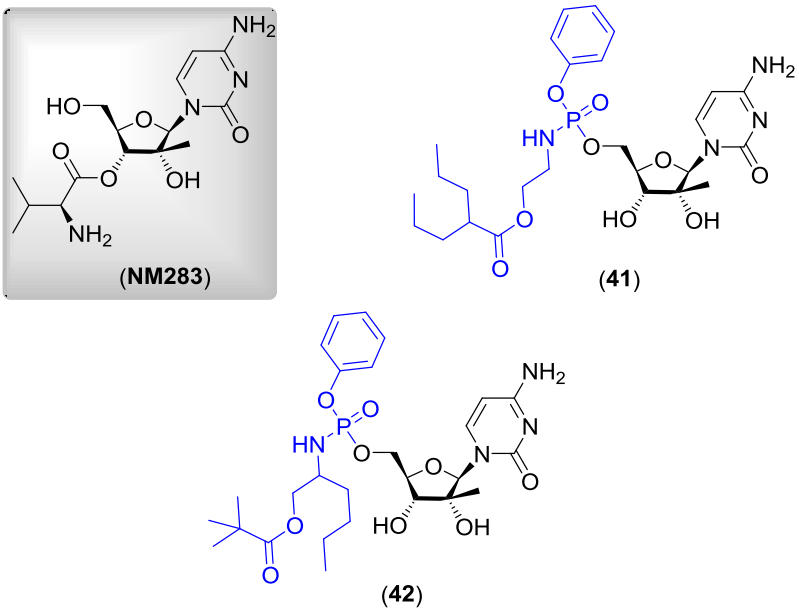

(**NM283**) (**41**) (**42**)

Figure 12 - Structure of **NM283** and 5′-Phosphoramidate prodrugs of 2′-C-methylcytidine inhibitors of NS5B.

The anti-influenza activity of 6-modified 2'-fluoro-2'-phosphoramidate deoxyriboside ProTides was evaluated *in vitro* (Figure 13). Compounds **43-46** showed EC_{99} value ranging from 12 μM to 15 μM. Xenobiotic Metabolism experiments with carboxypeptidase Y and whole-cell lysates demonstrated that the 2'-fluoro-2'-deoxyguanosine ProTides are readily cleaved by cellular enzymes to release the 6-modified 2'-fluoro-2'-deoxyguanosine 5'-monophosphate. Further conversion into 2'-fluoro-2'-deoxyguanosine 5'-triphosphate, the active metabolite that inhibits the viral polymerase then occurs. Antiviral results were supported by drug metabolism studies and calculations suggest that the clogP value (in the range of 2–3) may be favourable. These compounds proved inactive against HSV-1, HSV-2 TK-deficient HSV-1, as well as *Vaccinia* and *Vesicular stomatitis viruses* (MENEGHESSO *et al.*, 2013).

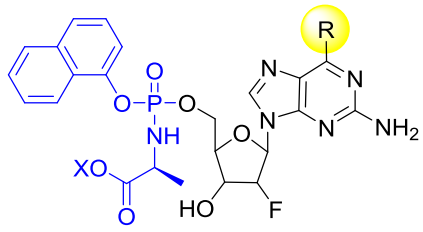

(**43**) R = OCH_3, X = Me; EC_{99} = 15 μM
(**44**) R = OCH_2CH_3, X = Me; EC_{99} = 14 μM
(**45**) R = OCH_2CH_3, X = Et; EC_{99} = 12 μM
(**46**) R = Cl, X = Bn; EC_{99} = 12 μM

Figure 13 - Phosphoramidate ProTides with anti-influenza virus activity.

The synthesis of numerous phosphoramidates with antiviral activities has been described in the literature. Recently, Sofia *et al*. (2012) published a review on inhibitors of hepatitis C virus NS5B RNA-dependent RNA-polymerase highlighting in particular the phosphoramidates. Several other research groups are also engaged in the search for promising bioactive phosphorylated molecules but have only achieved sporadic success (BORRELLO *et al.*, 2009; CUI *et al.*, 2011; DONGHI *et al.*, 2009; GARDELLI *et al.*, 2009; HARRIS *et al.*, 2001; LIANG *et al.*, 2006; LIU *et al.*, 2012; MEHELLOU *et al.*, 2009; MENEGHESSO *et al.*, 2013; UCKUN *et al.*, 2005; VALIYEV *et al.*, 2008; ZAKIROVA *et al.*, 2012; ZLATEV *et al.*, 2009).

6.3. Antitumoral Activity

Cancer is a disease characterized by abnormal cell division and migration, accounting for approximately 13% of all human deaths worldwide. In 2008, 12.4 million cases and 7.6 million deaths have been reported. The forecast is that by 2030 there will be 27 million cancer patients (LI *et al.*, 2012; SHEWACH *et al.*, 2009). Consequently, there is an urgent need to develop new, cost effective and safe drugs (chemotherapy agents) which may be used in combination with surgery and radiation therapy to reduce overall mortality.

Notably, "Phosphoramidate protide" has also been used as a strategy for the development of compounds possessing antitumor activity. This strategy combines, generally, the advantage of high water solubility with low toxicity (to normal cells) of such compounds (WAGNER et al. 2000). For instance, brivudine (**BVdU**) (Figure 14), a potent inhibitor of *Herpes simplex virus* type 1 (HSV-1) and *Varicella-zoster virus* (VZV), has served as a model for the development of newer, active, prototypes drugs (KEAM *et al.*, 2004; RABASSEDA, 2003). The incorporation of a phosphoramidate group within this scaffold led to the discovery of Thymectacin (**NB1011**, **47a**) by the company New Biotics. This compound selectively acts on tumor cells that express high levels of thymidylate synthase (NEUTEBOOM *et al.*, 2002; WILSON, 2006). Subsequently, the replacement of the methyl by a benzyl group within Thymectacin (**47a**) increased the potency against colon cancer HT115 by 175 fold (**47b**, Figure 14) (MCGUIGAN *et al.*, 2005). Cogiatu *et al*. (2006) have synthesized a number BVdU phosphoramidate derivatives (**48-54**) (Figure 14) possessing high cytotoxic activity against the cell lines MDAMB231 (breast cancer) and PC-3 (prostate cancer) cell lines. Compounds **48-50** and **53**, tested as diastereisomer mixtures, were the most active on MDAMB231 cells, with EC_{50} ranging from 0.32 µM to 2.7 µM whilst compounds **49-54** showed EC_{50} values in the range of 1.4-6.9 µM upon PC-3. These compounds were more active than the standard control NB1011 (EC_{50} = 79 and 155 µM on MDAMB231 and PC-3, respectively).

For compound **53**, the mixture was separated by reversed phase chromatography and each diastereoisomer was tested separately against the MDAMB231 (breast cancer) cell line. The rapidly eluting diastereoisomer (*R* stereochemistry on P center) was less active than the mixture with an EC_{50} = 7.4 μM, whilst the slow eluting diastereoisomer (*S* stereochemistry on the P center) was 10 times more potent than the mixture, with an EC_{50} = 0.5 μM highlighting the importance of investigating pharmacology of individual stereoisomers.

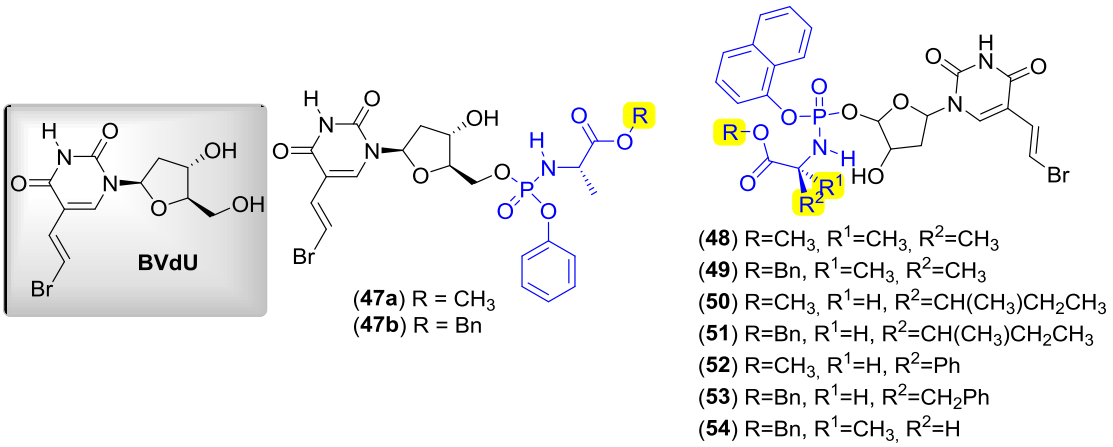

Figure 14 - Structure of Brivudine (BVdU) and various pro-nucleoside derivatives.

Some fluorinated pyrimidine nucleosides (ISMAIL, 2002) have been used as chemotherapeutic agents since 1957 in the treatment of ovarian, breast and gastrointestinal tumors (GREM, 2000; HEIDELBERGER *et al.*, 1957). The fluorinated pyrimidine 5-fluorouracil-2'-deoxynucleoside (**FUDR**) is active against liver metastases, and is beneficially metabolized within the host (HOMSI et al. 2006). In recent studies, McGuigan *et al*. (2011) reported the synthesis of **39** FUDR phosphate pro-drugs derivatives (Figure 15) and measured their relative cytotoxic activity within tumor cell lines L1210/0, L1210/TK-, Cem/0, Cem/TK-, HeLa, HeLa/TK-. The effect on L1210/0 infected with *Mycoplasma hyorhinis* (L1210.Hyor) was also reported. In general, the compounds showed ability to release the nucleoside monophosphate within intact cells whilst maintaining activity in tumor cell cultures infected with mycoplasma. The ProTide's stability in both acidic and neutral pH, as well as host plasma, is of great importance, especially considering that some compounds have proven cytotoxicity within the namomolar range.

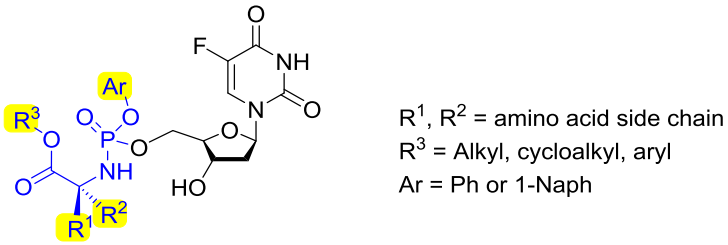

Figure 15 - General structure of FUDR Prodrugs described of McGuigan *et al*. (2011).

In 2013, Lewandowska *et al*. reported the synthesis of 4-chlorophenyl *N*-alkyl phosphoramidate diesters of 3´-azido-2´,3´-dideoxy-5-fluorouridine (**AddFU**) (Figure 16) and evaluation of their cytotoxic activity in three human cancer cell lines: cervical (HeLa), oral (KB) and breast (MCF-7). The most active compound for all cell lines was compound **56**, which displayed IC_{50} = 1.64 μM, IC_{50} = 1.64 μM and IC_{50} = 1.88 μM for HeLa, KB and MCF-7 cells, respectively. This compound was more potent than the parent **AddFU** (IC_{50} = 11.06 μM, IC_{50} = 8.11 μM and IC_{50} = 10.32 μM, respectively). Phosphoramidate **56** also exhibited relatively high activity for these cell lines, displaying IC_{50} = 4.21 μM for HeLa, IC_{50} = 3.81 μM for KB and IC_{50} = 5.41 μM for MCF-7. The authors suggested that the mechanism of inhibition of these compounds differs from that described by McGuigan *et al*. (2011) when devoid of the ester motif, which initiates the hydrolysis process to release the nucleoside analogue 5´-monophosphate.

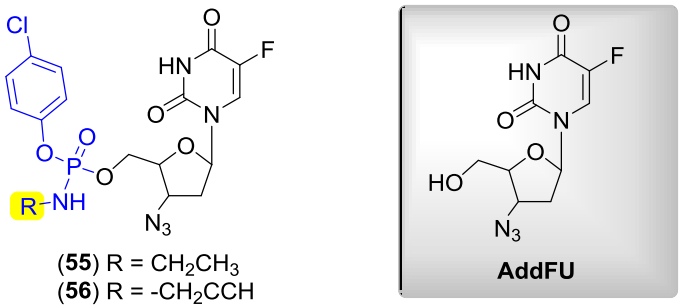

Figure 16 - 3´azido-2´,3´-dideoxy-5-fluorouridine phosphoramidates with anticancer activity.

Other notable examples of compounds demonstrating useful antineoplastic activities include triethylenethiophosphoramides and

cyclophosphamides (Figure 17). For instance, Thio-TEPA®, which has been previously used against a variety of neoplasms, demonstrated consistent efficacy against breast and ovarian adenocarcinomas as well as superficial papillary bladder carcinoma. The pharmacological effect is considered similar to mechlorethamine hydrochloride (**57**), the first systemic chemotherapeutic agent to be approved in the United States for the treatment of Hodgkin's disease, lymphosarcoma, chronic myelocytic or lymphocytic leukemia, polycythemia vera, bronchogenic carcinoma and mycosis fungoides (MF), the most common type of cutaneous T-cell lymphoma (CTCL) (LESSIN *et al.*, 2013; SANTOS *et al.*, 2007). The cyclophosphamide (2*H*-1,3,2-oxazaphosphorin-2-amine, *N,N*-bis(2-chloroethyl)tetrahydro-2-oxide is the active principle of Endoxan®. This genotoxic nitrogen mustard is used in the treatment of many cancers and is also endowed with marked immunosuppressant properties (SANTOS *et al.*, 2007; SUN *et al.*, 2006). In an attempt to alleviate carcinogenic potential and find more selective agents, it has served as a template for the synthesis of **TH-302** (Figure 17). This nitro-1*H*-imidazole has proven effective in the control of pancreatic tumor cells MIA PaCa-2, whilst also surviving microsomal metabolism. In addition, when combined with Gemcitabine®, it has proven particularly effective when tested in mice. Such attractive preclinical properties of **TH-302** have prompted Phase 1 clinical trials for the treatment of solid tumors (DUAN *et al.*, 2008). The presence of the nitro group may engender activity in hypoxic conditions found in these neoplasms. Another series of compounds derived from cyclophosphamide, namely trofosfamide (**58**), mafosfamide (**59**), and ifosfamide (**60**) (Figure 17) represent some of the most widely used anticancer chemotherapeutic agents (SANTOS *et al.*, 2007).

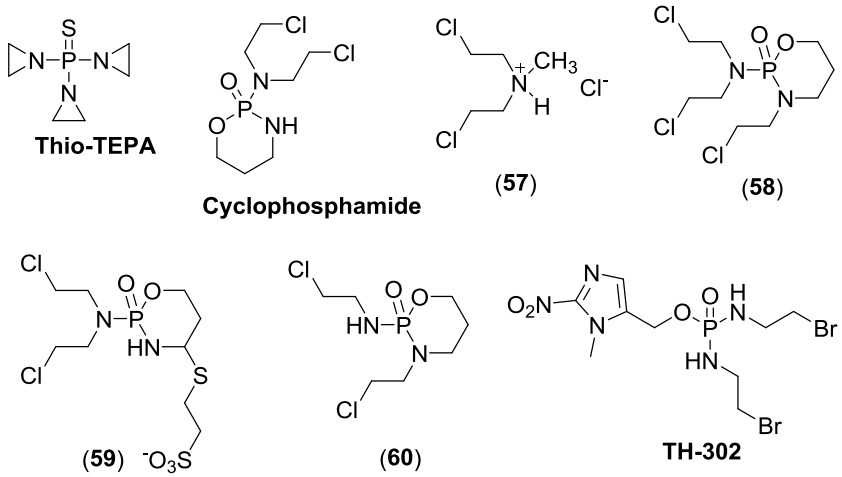

Figure 17 - Chemical structures of some highly effective anticancer agents.

Wang *et al*. (2010) prepared phosphoramidate derivatives of haematoporphine dihydrochloride (**HPD**), a drug with anti-tumor properties marketed under the name Apiabasilon®. For instance, compound (**61**), shows selectivity against the liver tumor cancer cell line (BEL-7402), possessing activity in the micromolar range *in vitro* (IC_{50} = 8.41 μM; Figure 18).

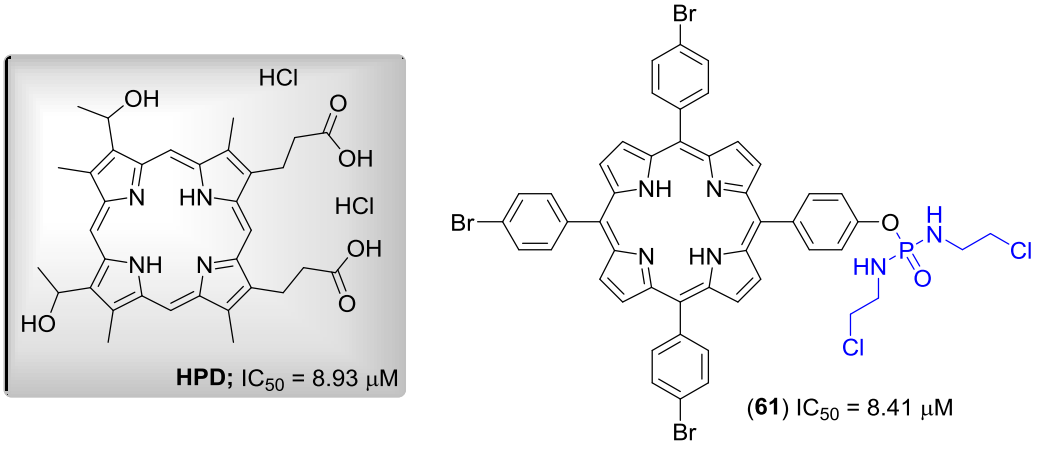

Figure 18 - Structure of the momomeric photosensitiser found within the mixture denoted HpD (LIPSON *et al.*, 1964) and its phosporamide analogue of chlorin (**61**). The IC_{50} reported are against the liver tumor cell line BEL-7402

Some highly potent anticancer heterocyclic phosphoramidates were synthesized by Kiran *et al*. (2008). Tests *in vitro*, involving three human tumor cell lines NCI-H460 (large cell lung), MCF-7 (breast adenocarcinoma) and SF-268 (central nervous system glioblastoma), cyclic compounds like **62** (IC_{50} = 2.8-4.5 μM) showed greater activity when compared to acyclic products such as **63** (IC_{50} = 71.3-90.4 μM) (Figure 19). The investigators did not offer an explanation as to why such cyclic compounds were highly active, and considering the limited number of analogues prepared, further investigations, especially those involving substitutions on the aromatic rings may produce compounds with superior activity.

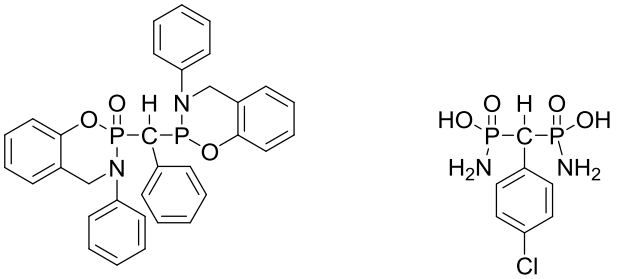

(**62**) (**63**)

Figure 19 - Anticancer phosphoramidates reported by Kiran *et al*. (2008).

Ghosh *et al*. (2009) reported that 7-benzylguanosine monophosphate (GMP-7BN) (**64**) was a potent antagonist of eukaryotic initiation factor 4E (eIF4E) (K_d = 0.8 μM). However, this compound possesses a negative charge at physiological pH preventing penetration across the cell membrane (WAGNER *et al.*, 2000). Consequently, phosphoramidate derivatives of **64** were prepared and the pro-drug **65** was also active against eIF4E (Figure 20). Furthermore, it was found that the zwitterion **65** was very efficient in crossing the membrane of MDA-231 breast cancer and lung cancer (H460, H383 and H2009) cell lines. Hydrolysis of the indolyl side chain once inside the cells provided the active anion form **64** which was then entrapped within the cells (LI *et al.*, 2013).

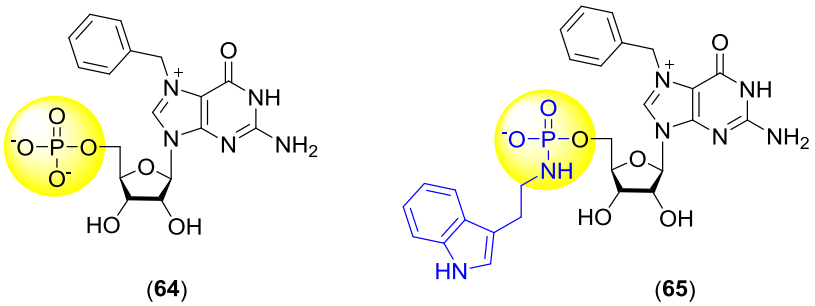

(**64**) (**65**)

Figure 20 - Structures of 7Bn-GMP and 7Bn-GMP pro-drug.

6.4. Antibacterial activity

The incidence of clinically multi-resistant antibiotics bacterial infections caused by bacteria has led to an unacceptable increase in mortality rates. An absence of effective treatments makes it vitally important that both health professionals and the public are sufficiently informed to take necessary precautions so as to maximize the effectiveness and lifetime of currently available antibiotics. Meanwhile, both the pharmaceutical sector and academic investigators continue to search for both novel targets and mechanisms of drug action rational drug design thereby facilitating development of new and effective antibacterial agents (BUSH *et al.*, 2011; CARS *et al.*, 2011; PIDDOCK, 2012). In this context, amongst the several classes of compounds with putative antibacterial activity, phosphoramidates possess considerable potential for further development.

In 2011, Gholivand and Dorosti (2011) reported the synthesis of two new *N*-phosphinyl ureas (Figure 21) and evaluated their antibacterial activities against *Staphylococcus aureus*, *Bacillus subtilis*, *Escherichia coli* and *Salmonella typhi* using the disc diffusion method and also obtained the minimum inhibitory concentration (MIC) for each compound. Compound **66** exhibited high activity against all of the microorganisms under test (MIC = 1.17-18.8 $\mu g.cm^{-3}$ comparable with MIC of Genatamycin used as a positive control) whilst compound **67** was virtually inactive (MIC > 385 $\mu g.cm^{-3}$).

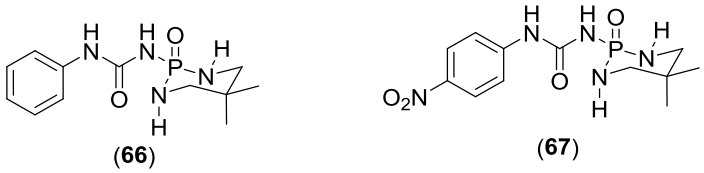

Figure 21 - Two novel *N*-phosphinyl ureas with antibacterial activity.

Prasad *et al*. (2006) have synthesized a series of heterocyclic phosphoramidates (**68-76**), which showed moderate activity against two Gram-positive bacteria (*Staphylococcus aureus*, *Bacillus subtilis*) and four Gram-negative bacteria (*Escherichia coli*, *Pseudomonas aeruginosa*, *Salmonella typhimurium* and *Klebsiella pneumoniae*). Their antibacterial activity was evaluated at concentrations of 20 µg/ml and 40 µg/ml with Ciprofloxacin® a commercial quinolone antibiotic, as a comparator (Figure 22). Compounds **71-74** inhibited bacterial growth at a concentration of 20 µg/mL for both Gram-positive and Gram-negative bacteria. Compounds **73** and **74** exhibited the highest activity. Other diphenylphosphoramidates (**77-78**), have been prepared by Madhala and coworkers (2012). When tested against *Bacillus subtilis*, *Staphylococcus aureus*, *Pseudomonas aeruginosa* and *Escherichia coli*, they were shown to be twice as effective as Cyprofloxacin® (Figure 22).

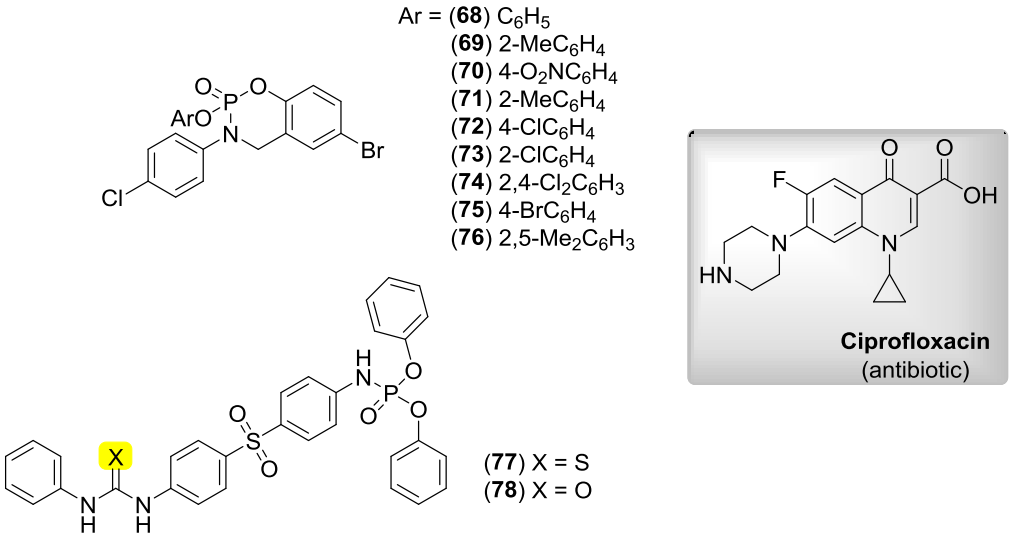

Figure 22 - Structural formulas of Cyprofloxacin® and some synthetic phosphoramidates with antibacterial activity.

6.5. Antiurease activity

Urease is a nickel-dependent enzyme present in various organisms, such as plants, fungi and bacteria, especially *Proteus mirabilis*, *Klebsiella aerogenes* and *Helicobacter pylori* and, consequently, is of considerable biological significance considering its ubiquity in organisms causing diseases of the gastrointestinal and urinary tracts. By neutralizing gastric acid through ammonia production from urea hydrolysis, *H. Pylori*, can maintain 50% to 60% of the metabolic activity at pH = 2.5 (AMTUL *et al.*, 2002; DUCKWORTH *et al.*, 2009; FOLLMER, 2010; KRAJEWSKA, 2009) and is considered the leading cause of stomach ulcers. It has been estimated that around half of the world population is infected with this microorganism, and in some developing countries this can affect up to 85% of the adult population (DUCKWORTH *et al.*, 2009). During the search for novel enzyme inhibitors of urease phosphoramidates showed excellent activity. Amongst putative urease inhibitors, *N*-(but-1-yl)thiophosphoric triamide (**NBPT**, Figure 23) excels in inhibiting the enzyme (AMTUL *et al.*, 2002; KRAJEWSKA, 2009). NBPT is a pro-drug since it has to be oxidized to unmask the active form: *N*-(but-1-yl)phosphoric triamide (**NBPTO**, Figure 23) (AMTUL *et al.*, 2002). In an *in silico* investigation of the active site of urease from *H. pylori*, a molecular modelling study of phenylphosphorodiamidate (**PPD**, Figure 23) demonstrated that this compound interacts with His221 through a hydrogen bond involving its oxygen atoms. A hydrophobic interaction between the benzene group with residues of Ala168, Ala169 and Ala365 (MAO *et al.*, 2009) is also involved. A deeper understanding of such non-covalent interactions may well lead to the design of superior inhibitors.

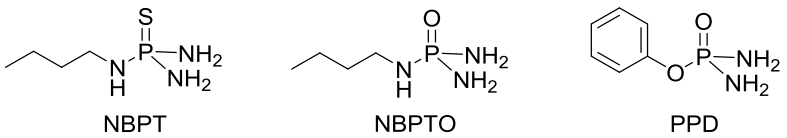

Figure 23 - Chemical structures of phosphoramidates efficient as urease inhibitors.

During 2008, Dominguez *et al*. (2008) described the synthesis of various phosphoramidates all highly active in the nanomolar range against *Jack bean* urease *in vitro* (Figure 24). The reference compounds NBPT and PPD used, showed IC_{50} equal to 100 and 3 nM, respectively. Although no clear structure-activity relationship was found, this series of compounds represents a useful template for further investigation as these are currently the most potent urease inhibitors reported so far.

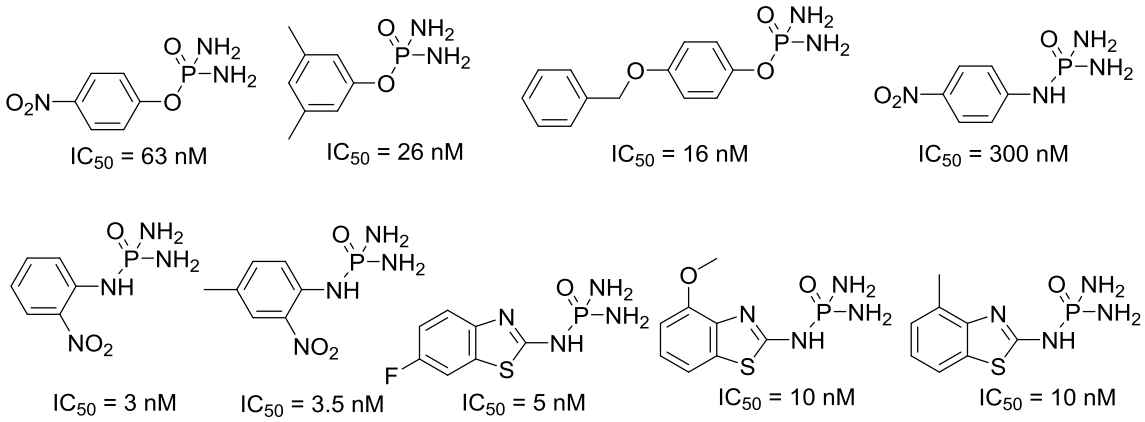

Figure 24 - Aromatic phosphoramidates with high urease inhibitory activity (DOMINGUEZ *et al.*, 2008).

6.6. Miscellaneous

As this survey has shown, the phosphoramidates encompass a diverse range of biological activities. These have, therefore, led several investigators to explore the potential application of this class of compounds against tropical diseases especially malaria and leishmaniasis. Recent investigations include synthesis of nitrobenzyl phosphoramide mustards (compounds **79-90**, Figure 25) that proved active against *Trypanosoma brucei*, *Trypanosoma cruzi* and *Leishmania major*. These protozoan parasites cause major health problems in many countries of the developing world spread across three continents (BAHIA *et al.*, 2009; PARSONS *et al.*, 2005; TURNOCK *et al.*, 2007). The highest biological activity was associated with compounds **84** and **85**, which showed IC_{50} values in the namomolar range against *T. brucei* (HU *et al.*,

2011). Compound **86** revealed selectivity towards *T. brucei* (DARDONVILLE *et al.*, 2004) and served as a prototype for the development of novel phosphonates with EC_{50} lying between 1.7-4.2 μM (structures not shown) (HECKER *et al.*, 2008). Disappointingly, these compounds showed low bioavailability due to their inability to cross cell membranes, therefore, only reaching the site of drug action in sub-therapeutic concentrations *in vivo*. Thus, Ruda *et al*. (2010) prepared a series of phosphoramidate derivatives **86** with better pharmacokinetic properties. Among these compounds **87-90** showed EC_{50} values equal to 90, 40, 50 and 8 nM, respectively, against *T. brucei*.

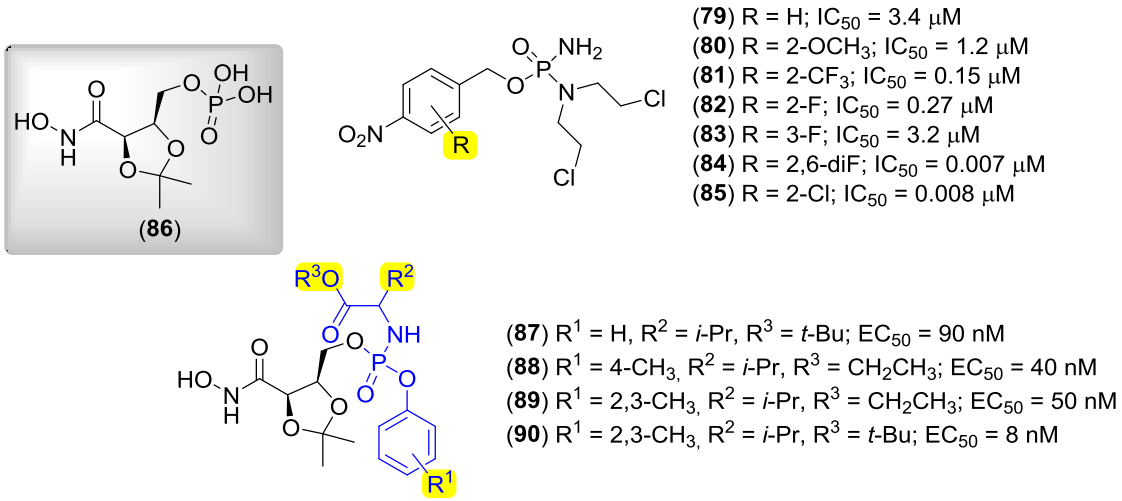

Figure 25 - Compounds with activity against *T. brucei.*

Malaria is a parasitic disease caused by the protozoan of the *Plasmodium genus*, with the most virulent species been *Plasmodium falciparum*. This disease is responsible for about 800,000 deaths per year, many of them including children and pregnant women, and most of them in sub Saharan Africa (WHO, 2010). Amongst a number of compounds described by Mara *et al*. (2011) **91-94** showed good efficacy against *P. falciparum* (IC_{50} = 39-50 μM) (Figure 26). The bio-isosteric replacement of isopropylamino group by other alkylamino substituents resulted in new more pharmacologically potent phosphoramidates **95-104** (Figure 26). Amongst such compounds, **95**, **97**, **99** and **104** (IC_{50} = 17-32 μM) proved most active.[18] Other examples of phosphoramidates (**106-109**) with antimalarial activity were published recently which employed

diphosphonic acid **105** as the lead structure (KEOUGH *et al.*, 2013). Compound **108** (IC_{50} = 3.4 μM) was more potent than **106** (IC_{50} = 6.6 μM), **107** (IC_{50} = 9.7 μM) and **109** (IC_{50} = 42 μM) cells on D6 (wild-type *P. falciparum* strain proved most sensitive to these drugs). In cell lines W2 (chloroquine-and pyrimethamine-resistant *P. falciparum* strain), compound **108** showed IC_{50} value of 4.0 μM as **106**, **107** and **109** had values equal to 7.7, 7.1 and 48 μM, respectively. Compound **109** has little or no effect since it was cytostatic (CC_{50} > 300 μM) on the cell lines A549 (human lung carcinoma cells), C32 (human melonoma cells) and C32TG (and thioguanine-resistant mutant of HGPRT-deficient cell line C32). The pro-drug **107** shows low levels of cytotoxicity against C32 line cell (CC_{50} = 130 μM) and C32TG (CC_{50} = 109 μM). According to the authors, these values are not considered cytotoxic, since these pro-drugs fail to enter mammalian cells. Compound **105** (Figure 26) represents a promising prototype for the development of new phosphoramidates as pro-drugs which may well possess useful antimalarial activity (KEOUGH *et al.*, 2013).

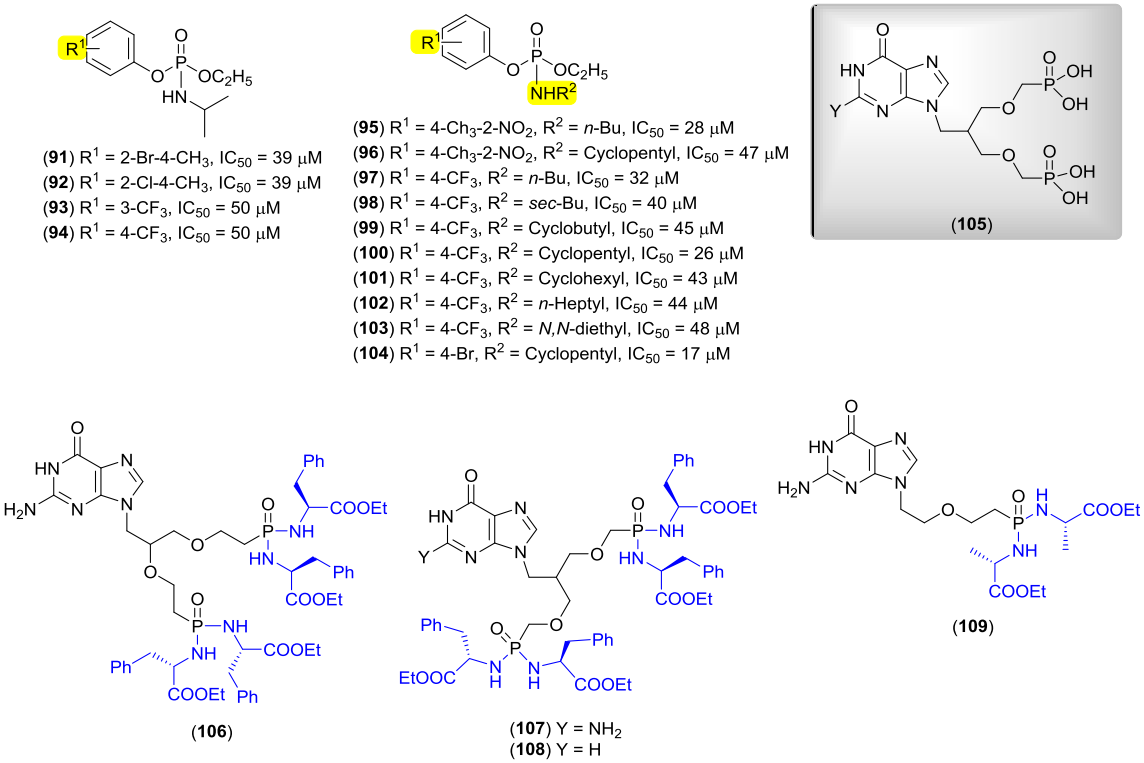

Figure 26 - Chemical structure of compounds with activity against *P. falciparum.*

The major health problems caused by parasites are currently confined to the developing world but climate change may well shift these zones of infection to the more developed areas. Sadly this area of world health has attracted less attention from the pharma sector than desired. In contrast, within several regions of the world, Alzheimer's disease has attracted considerable attention from both pharmaceuticals companies and academic institutions since increasing longevity has led to the emergence of such conditions. Currently, cholinesterase inhibitors (ChEI) are the main drugs commercially available for the treatment of Alzheimer's disease, which is a leading cause of dementia worldwide, with approximately 24 million cases reported annually (BALLARD *et al.*, 2011; REITZ *et al.*, 2011). The rationale behind the use of these inhibitors is based on the assumption that a cholinergic deficit is associated with the disease, and aims at increasing the availability of synaptic acetylcholine by inhibiting its main catalytic enzymes, acetyl (AChE) and butyrylcholinesterase (BChE) (BALLARD *et al.*, 2011; BRADY *et al.*, 2013). In 2010, Gholivand *et al*. (2010) synthesized and evaluated the effect of compounds **110-114** (Figure 27) on the aforementioned enzymes. As a result, these compounds revealed a mixed type mechanism of action with moderate activity against BChE (IC_{50} ranging from 0.43 to 2.45 mM) and AChE (IC_{50} ranging from 1.95 to 18.62 mM).

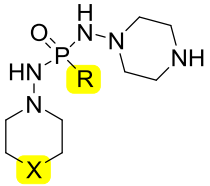

(**110**) R = C_6H_5-; X=O
(**111**) R = C_6H_5O-; X=O
(**112**) R = $C_6H_5C(O)NH$-; X=O
(**113**) R = $C_6H_5C(O)NH$-; X=CH_2

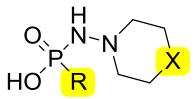

(**114**) R = C_6H_5O-; X=CH_2

Figure 27 - Chemical structure of compounds with activity against AChE and BChE.

6.7. Rational drug design using Phosporamidates

The previous sections demonstrate that the incorporation of a phosphoramidate at a critical point within the agonist or antagonist is essential for success. During a drug design campaign, bioisosteric

substitution should be carried out at a known xenobiotic transformation point inferred from *studies in vitro* using the relevant receptor, usually, but not exclusively an enzyme, which can now be achieved using recombinant methods. For instance, since folate hydrolase I and glutamate carboxypeptidase II, PSMA possess proteolytic activities toward γ-glutamyl folic acid derivatives and the neuropeptide N-acetylaspartylglutamate (PINTO *et al*., 1996). Studies involving PSMA substrate specificity revealed that acidic residues at the P1 and P19 positions are suitable targets for modification, and several folate-like and *N*-acetylaspartylglutamate-like dipeptides with modest hydrolytic efficiency were reported (BARINKA *et al.*, 2002). Later, by adapting the dipeptide motif for PSMA targeting, Lapi *et al.* developed a library of tetrahedral phosphoramidates for PSMA inhibition (Figure 28) (MALLARI *et al.*, 2004).

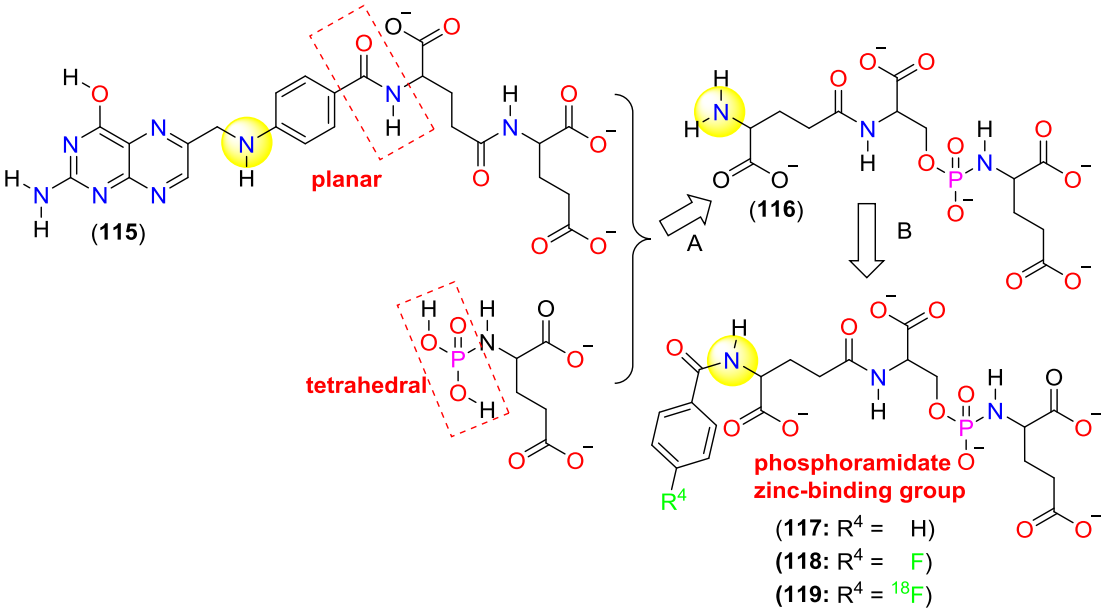

Figure 28 - Rational approaches towards the design of inhibitors active *in vivo*

Through adopting a *seco*-analogue approach (molecular pruning), Wu *et al*. systematically identified several potent inhibitors (WU *et al.*, 2007) (Figure 29 & 30) and proposed a pharmacophore model involving the zinc binding site which pseudo-irreversibly bind to PSMA (LIU *et al.*, 2008).

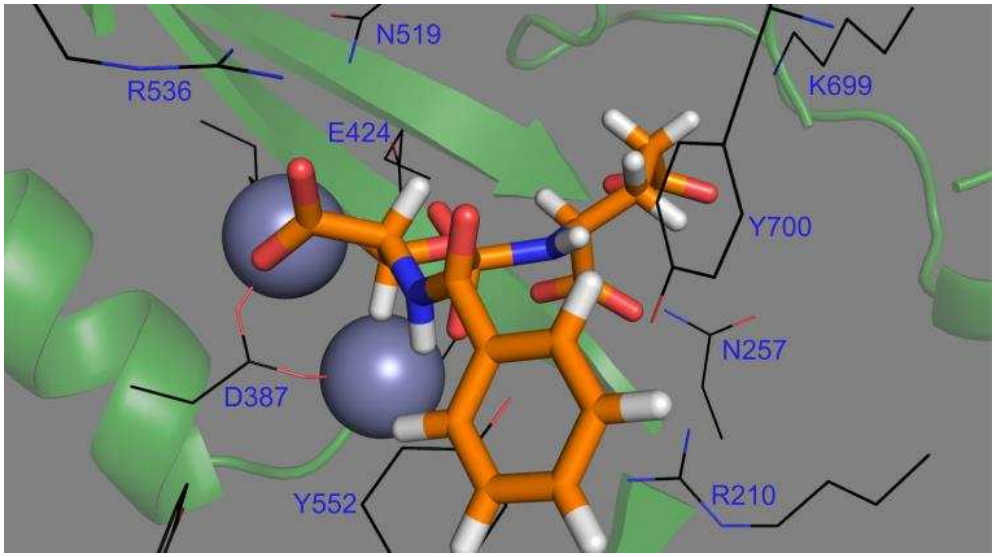

Figure 29 - Computational docking of phosphoramidate inhibitors into the active site of PSMA binding with Zinc represented by two spheres: (See panel a, inhibitor 1a: (((S)-2-benzamido-2-carboxylatoethoxy)oxidophosphoryl)-L-glutamatej; yellow; re-rendered using PyMol from (WU *et al.*, 2007); see original paper for details of interactions with relevant amino acids).

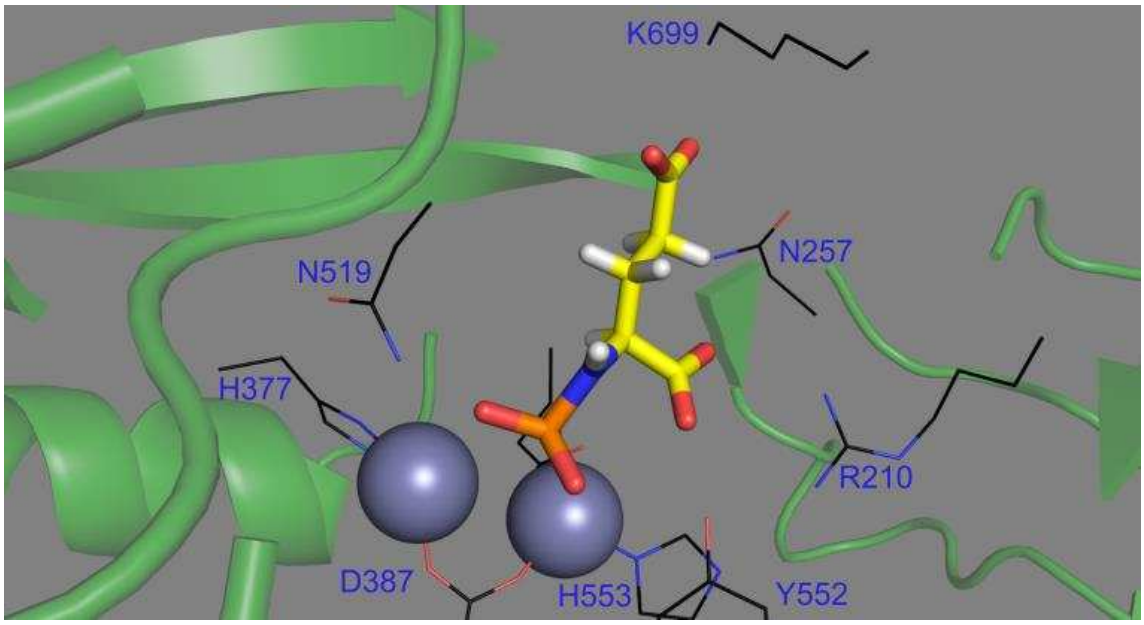

Figure 30 - Computational docking of phosphoramidate inhibitors into the active site of PSMA binding with Zinc represented by two spheres: (See panel c, inhibitor 1j, phosphonato-D-glutamate, yellow; re-rendered using PyMol from (WU *et al.*, 2007); see original paper for details of interactions with relevant amino acids).

An ^{18}F labelled analogue of phosphoramidate (**117**, R^4 = H) showed their suitability in PSMA-targeted delivery for prostate cancer using positron emission tomography (ISMAIL *et al.*, 2009) allowing them to track its biodistribution data in murine xenografts *in vivo*. The uptake of ^{18}F-fluorobenzamido-phosphoramidate *in vivo* **119** in both PSMA+ and PSMA− tumor models by PET and *ex vivo* biodistribution study revealed that phosphoramidate probe **119** rapidly localized at the LNCaP PSMA+ tumor, whereas there was significantly less activity within the PC-3 PSMA− tumor model (Fig 31).

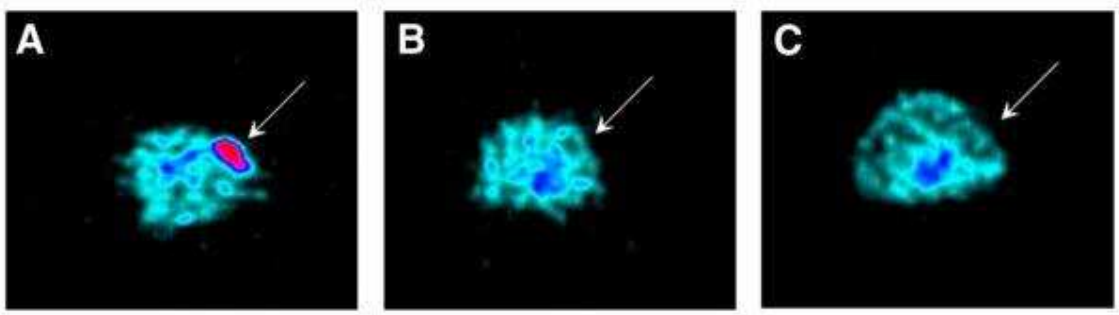

Figure 31 - PET transaxial images of male nude mice bearing subcutaneous LNCaP (A and C) and PC-3 (B) tumor xenografts at 2 h after injection of ^{18}F-fluorobenzamido-phosphoramidate **(3)**. Arrows indicate tumor placement. Blocked LNCaP is shown in C. Reproduced with permission from LAPI *et al.*, 2009.

As an imaging agent, the ^{18}F-labeled phosphoramidate, had high uptake in the PSMA-expressing tumor and low background and some of the accumulation seen in the kidney may be specific to the mouse. Such findings clearly demonstrate that the leading phosphoramidate is a PSMA-specific targeting ligand *in vivo* and uptake was specific to PSMA. Consequently, these findings will allow further development of this class of compounds and also provide a sensitive and specific imaging agent for prostate cancer. Knowledge of drug action through crystallography is the ideal guide for rational synthesis. For instance, the mode of binding to thermolysin of the unsubstituted phosphoramidate inhibitor *N*-phosphoryl-L-leucinamide was studied by single crystal x-ray diffraction methods (Figure 32) and these were considered transition state analogues (TRONRUD *et al.*, 1986).

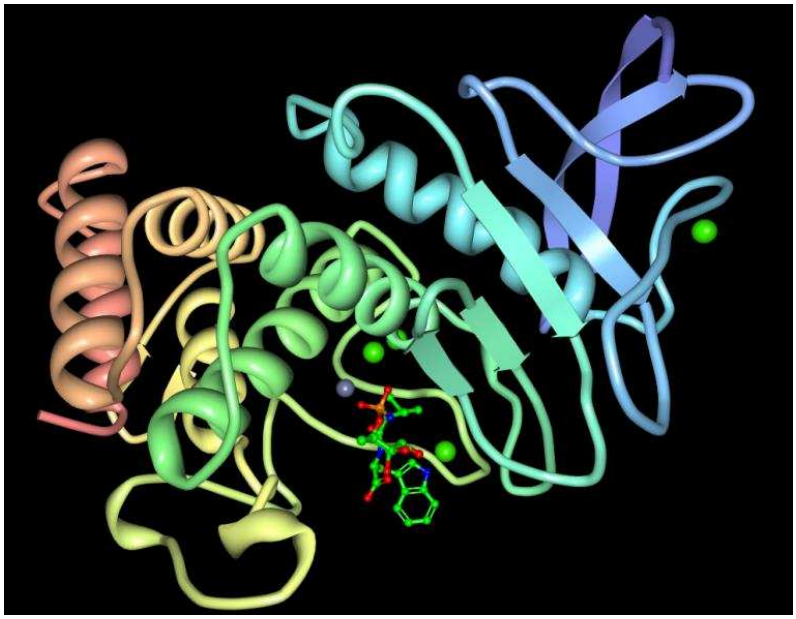

Figure 32 - Binding to thermolysin of the unsubstituted phosphoramidate inhibitor *N*-phosphoryl-L-leucinamide.

In general, the bond that is known to be cleaved is usually modified and, in our experience, often tends to be the weakest bond possessing dimensions that are normally longer than those averages culled from crystal structure databases[98] (F. M. D. Ismail & M. G. B. Drew Unpublished study).

6.8. Conclusion

In this review, we briefly reported promising pharmacological activities displayed by the phosphoramidate class of compounds. Although various applications have been discussed in the literature, the biological activity of this class deserves further investigation since they reveal considerable potential for improving drug action especially with respect to antitumor and antiviral activities. Rational drug design will be improved as the structure of the target receptors and underlying biochemistry and genetics becomes available. By a careful consideration of ADMET approaches, more robust series of compounds can be developed especially using 3D-QSARs.

6.9. Acknowledgements

We thank Conselho Nacional de Desenvolvimento Científico e Tecnológico (CNPq) and Fundação de Amparo à Pesquisa do Estado de Minas Gerais (FAPEMIG) for financial support and research fellowships (LCAB and FMO). FMDI thanks LJMU for a research allocation. We sincerely thank both Professors C. E. Berkman (Washington State University) and M. O. Anderson (San Francisco State University) for useful correspondence and generously providing re-rendered figures originally published in 2007[93].

6.10. Abbreviations Used

7Bn-GMP, 7-benzyl guanosine monophosphate; A549 cell, human lung carcinoma cells; AChE, Acetylcholinesterase; ACV, Acyclovir; AddFU, 3´-azido-2´,3´-dideoxy-5-fluorouridine; ADMET, absorption, distribution, metabolism, and excretion - toxicity in pharmacokinetics; Ala, alanine; APM, amiprophos methyl; ATP, adenosine triphosphate; AZU, 4'-azidouridine; BChE, Butyrylcholinesterase; BEL-7402 cell, liver tumor cancer cell line; BVdU, brivudine; C32 cell, human melonoma cells; C32TG, thioguanine-resistant mutant of HGPRT-deficient cell line C32; CEM cell, Human T cell lymphoblast-like cell line; ChEI, cholinesterase inhibitors; d4T, stavudine; DNA, deoxyribonucleic acid; DOA, dioxolane sugar nucleosides; EBV, *Epstein-Barr virus*; eIF4E, eukaryotic initiation factor 4E; MIC, minimum inhibitory concentration; FUDR, 5-fluorouracil 2´-deoxynucleoside; Gly, glycine; H460, H383 and H2009 cells, human lung cancer cell lines; HBV, hepatitis B virus; HCMV, human cytomegalovirus; HCV, hepatitis C virus; HeLA cell, human cervical cancer cell lines; HHV, human herpes virus; HIV, human immunodeficiency virus; HPD, haematoporphine dihydrochloride; HPV, *Human papilloma virus*; HSV, herpes simplex virus; HSV-1 TK-, HSV-deficient thymidine kinase; KB cell, human oral cancer cell lines; MCF-7 cell, human breast cancer cell lines; MDA-231 cell, human membrane of breast cancer cell lines; MDAMB231 cell, human breast cancer cell lines; MIC, minimum inhibitory concentration; MT-4 cell, human T cell line MT4; NBPT, *N*-(n-butyl)

thiophosphoric triamide; NBPTO, *N*-(n-butyl)phosphoric triamide; NCI-H460 cell, human large cell lung cancer cell lines; NS5B, non-structural protein 5B; NTP, nucleoside triphosphate; PC-3 cell, human prostate cancer cell lines; PEG-IFN, pegalated α-interferon; Phe, phenylalanine; PK/PD, pharmacokinetic/ pharmacodynamics; PSMA, prostate-specific membrane antigen, PPD, phenylphosphorodiamidate; RNA, ribonucleic acid; SF-268 cell, human central nervous system glioblastoma cell lines; VZV, *Varicella-zoster virus*.

6.11. References

AMTUL, Z.; RAHMAN, A.U.; SIDDIQUI, R.A.; CHOUDHARY, M.I. Chemistry and mechanism of urease inhibition. *Current Medicinal Chemistry,* v. 9, p. 1323-1348, 2002.

ARBELO ROMÁN, C.; WASSERTHAL, P.; BALZARINI, J.; MEIER, C. Diastereoselective Synthesis of (Aryloxy)phosphoramidate Prodrugs. *European Journal of Organic Chemistry,* v. 2011, p. 4899-4909, 2011.

BAHIA, D.; OLIVEIRA, L.M.; LIMA, F.M.; OLIVEIRA, P.; SILVEIRA, J.F.; MORTARA, R.A.; RUIZ, J.C. The TryPIKinome of five human pathogenic trypanosomatids: *Trypanosoma brucei*, *Trypanosoma cruzi, Leishmania major, Leishmania braziliensis* and *Leishmania infantum*--new tools for designing specific inhibitors. *Biochemical and Biophysical Research Communications,* v. 390, p. 963-970, 2009.

BALLARD, C.; GAUTHIER, S.; CORBETT, A.; BRAYNE, C.; AARSLAND, D.; JONES, E. Alzheimer's disease. *Lancet,* v. 377, p. 1019-1031, 2011.

BARINKA, C.; RINNOVA, M.; SACHA, P.; ROJAS, C.; MAJER, P.; SLUSHER, B.S.; KONVALINKA, J. Substrate specificity, inhibition and enzymological analysis of recombinant human glutamate carboxypeptidase II. *Journal of Neurochemistry*, v. 80, p. 477-487, 2002.

BONDADA, L.; DETORIO, M.; BASSIT, L.; TAO, S.; MONTERO, C.M.; SINGLETARY, T.M.; ZHANG, H.; ZHOU, L.; CHO, J.-H.; COATS, S.J.;

SCHINAZI, R.F. Adenosine Dioxolane Nucleoside Phosphoramidates As Antiviral Agents for Human Immunodeficiency and Hepatitis B Viruses. *ACS Medicinal Chemistry Letters,* v. 4, p. 747-751, 2013.

BORRELLO, L.; CHIACCHIO, U.; CORSARO, A.; PISTARÀ, V.; IANNAZZO, D. Phosphoroamidate derivatives of N,O-nucleosides as inhibitors of reverse transcriptase. *Archive for Organic Chemistry,* v. 2009, p. 112-124, 2009.

BRADY, R.; WEINMAN, J. Adherence to Cholinesterase Inhibitors in Alzheimer's Disease: A Review. *Dementia and Geriatric Cognitive Disorders,* v. 35, p. 351-363, 2013.

BUSH, K.; COURVALIN, P.; DANTAS, G.; DAVIES, J.; EISENSTEIN, B.; HUOVINEN, P.; JACOBY, G.A.; KISHONY, R.; KREISWIRTH, B.N.; KUTTER, E.; LERNER, S.A.; LEVY, S.; LEWIS, K.; LOMOVSKAYA, O.; MILLER, J.H.; MOBASHERY, S.; PIDDOCK, L.J.V.; PROJAN, S.; THOMAS, C.M.; TOMASZ, A.; TULKENS, P.M.; WALSH, T.R.; WATSON, J.D.; WITKOWSKI, J.; WITTE, W.; WRIGHT, G.; YEH, P.; ZGURSKAYA, H.I. Tackling antibiotic resistance. *Nature Reviews Microbiology,* v. 9, p. 894-896, 2011.

CARS, O.; HEDIN, A.; HEDDINI, A. The global need for effective antibiotics—Moving towards concerted action. *Drug Resistance Updates,* v. 14, p. 68-69, 2011.

CHO, A.; ZHANG, L.; XU, J.; BABUSIS, D.; BUTLER, T.; LEE, R.; SAUNDERS, O.L.; WANG, T.; PARRISH, J.; PERRY, J.; FENG, J.Y.; RAY, A.S.; KIM, C.U. Synthesis and characterization of 2′-C-Me branched C-nucleosides as HCV polymerase inhibitors. *Bioorganic & Medicinal Chemistry Letters,* v. 22, p. 4127-4132, 2012.

CHO, A.; ZHANG, L.; XU, J.; LEE, R.; BUTLER, T.; METOBO, S.; AKTOUDIANAKIS, V.; LEW, W.; YE, H.; CLARKE, M.; DOERFFLER, E.; BYUN, D.; WANG, T.; BABUSIS, D.; CAREY, A.C.; GERMAN, P.; SAUER, D.; ZHONG, W.; ROSSI, S.; FENAUX, M.; MCHUTCHISON, J.G.; PERRY, J.; FENG, J.; RAY, A.S.; KIM, C.U. Discovery of the First C-Nucleoside HCV

Polymerase Inhibitor (GS-6620) with Demonstrated Antiviral Response in HCV Infected Patients. *Journal of Medicinal Chemistry,* v. 13, p. 1812-1825, 2013.

CONGIATU, C.; MCGUIGAN, C.; JIANG, W.G.; DAVIES, G.; MASON, M.D. Naphthyl phosphoramidate derivatives of BVdU as potential anticancer agents: design, synthesis and biological evaluation. *Nucleosides Nucleotides Nucleic Acids,* v. 24, p. 485-489, 2006.

CUI, Q.B.; ZHANG, G.X.; YU, P.; WANG, Y.Q. Synthesis and preliminary evaluation of anti-HIV agent AZT prodrug. *Yao Xue Xue Bao. Acta Pharmaceutica Sinica,* v. 46, p. 1015-1018, 2011.

DARDONVILLE, C.; RINALDI, E.; BARRETT, M.P.; BRUN, R.; GILBERT, I.H.; HANAU, S. Selective inhibition of *Trypanosoma brucei* 6-phosphogluconate dehydrogenase by high-energy intermediate and transition-state analogues. *Journal of Medicinal Chemistry,* v. 47, p. 3427-3437, 2004.

DE CLERCQ, E. Anti-HIV drugs: 25 compounds approved within 25 years after the discovery of HIV. *International Journal of Antimicrobial Agents,* v. 33, p. 307-320, 2009.

DE CLERCQ, E. Strategies in the design of antiviral drugs. *Nature Reviews Drug Discovery,* v. 1, p. 13-25, 2002.

DERUDAS, M.; BRANCALE, A.; NAESENS, L.; NEYTS, J.; BALZARINI, J.; MCGUIGAN, C. Application of the phosphoramidate ProTide approach to the antiviral drug ribavirin. *Bioorganic and Medicinal Chemistry,* v. 18, p. 2748-2755, 2010.

DERUDAS, M.; CARTA, D.; BRANCALE, A.; VANPOUILLE, C.; LISCO, A.; MARGOLIS, L.; BALZARINI, J.; MCGUIGAN, C. The application of phosphoramidate protide technology to acyclovir confers anti-HIV inhibition. *Journal of Medicinal Chemistry,* v. 52, p. 5520-5530, 2009.

DOMÍNGUEZ, M.A.J.; SANMARTÍN, C.; FONT, M.A.; PALOP, J.A.; SAN FRANCISCO, S.; URRUTIA, O.; HOUDUSSE, F.; GARCÍA-MINA, J.M. Design, Synthesis, and Biological Evaluation of Phosphoramide Derivatives as Urease Inhibitors. *Journal of Agricultural and Food Chemistry,* v. 56, p. 3721-3731, 2008.

DONGHI, M.; ATTENNI, B.; GARDELLI, C.; MARCO, A.D.; FIORE, F.; GIULIANO, C.; LAUFER, R.; LEONE, J.F.; PUCCI, V.; ROWLEY, M.; NARJES, F. Synthesis and evaluation of novel phosphoramidate prodrugs of 2'-methyl cytidine as inhibitors of hepatitis C virus NS5B polymerase. *Bioorganic & Medicinal Chemistry Letters,* v. 19, p. 1392-1395, 2009.

DUAN, J.X.; JIAO, H.; KAIZERMAN, J.; STANTON, T.; EVANS, J.W.; LAN, L.; LORENTE, G.; BANICA, M.; JUNG, D.; WANG, J.; MA, H.; LI, X.; YANG, Z.; HOFFMAN, R.M.; AMMONS, W.S.; HART, C.P.; MATTEUCCI, M. Potent and highly selective hypoxia-activated achiral phosphoramidate mustards as anticancer drugs. *Journal of Medicinal Chemistry,* v. 51, p. 2412-2420, 2008.

DUCKWORTH, M.J.; OKOLI, A.S.; MENDZ, G.L. Novel Helicobacter pylori therapeutic targets: the unusual suspects. *Expert Review of Anti-Infective Therapy,* v. 7, p. 835-867, 2009.

FOLLMER, C. Ureases as a target for the treatment of gastric and urinary infections. *Journal of Clinical Pathology,* v. 63, p. 424-430, 2010.

GARDELLI, C.; ATTENNI, B.; DONGHI, M.; MEPPEN, M.; PACINI, B.; HARPER, S.; DI MARCO, A.; FIORE, F.; GIULIANO, C.; PUCCI, V.; LAUFER, R.; GENNARI, N.; MARCUCCI, I.; LEONE, J.F.; OLSEN, D.B.; MACCOSS, M.; ROWLEY, M.; NARJES, F. Phosphoramidate prodrugs of 2'-C-methylcytidine for therapy of hepatitis C virus infection. *Journal of Medicinal Chemistry,* v. 52, p. 5394-5407, 2009.

GHOLIVAND, K.; DOROSTI, N. Synthesis, spectroscopic characterization, crystal structures, theoretical studies, and antibacterial evaluation of two novel N-phosphinyl ureas. *Monatshefte fur Chemie,* v. 142, p. 183-192, 2011.

GHOLIVAND, K.; HOSSEINI, Z.; FARSHADIAN, S.; NADERI-MANESH, H. Synthesis, characterization, oxidative degradation, antibacterial activity and acetylcholinesterase/butyrylcholinesterase inhibitory effects of some new phosphorus(V) hydrazides. *European Journal of Medical Chemistry,* v. 45, p. 5130-5139, 2010.

GHOSH, B.; BENYUMOV, A.O.; GHOSH, P.; JIA, Y.; AVDULOV, S.; DAHLBERG, P.S.; PETERSON, M.; SMITH, K.; POLUNOVSKY, V.A.; BITTERMAN, P.B.; WAGNER, C.R. Nontoxic chemical interdiction of the epithelial-to-mesenchymal transition by targeting cap-dependent translation. *ACS Chemical Biology,* v. 4, p. 367-377, 2009.

GREM, J.L. 5-Fluorouracil: forty-plus and still ticking. A review of its preclinical and clinical development. *Investigational New Drugs,* v. 18, p. 299-313, 2000.

HARRIS, S.A.; MCGUIGAN, C.; ANDREI, G.; SNOECK, R.; DE CLERCQ, E.; BALZARINI, J. Synthesis and antiviral evaluation of phosphoramidate derivatives of (E)-5-(2-bromovinyl)-2'-deoxyuridine. *Antiviral Chemistry and Chemotherapy,* v. 12, p. 293-300, 2001.

HECKER, S.J.; ERION, M.D. Prodrugs of phosphates and phosphonates. *Journal of Medicinal Chemistry,* v. 51, p. 2328-2345, 2008.

HEIDELBERGER, C.; CHAUDHURI, N.K.; DANNEBERG, P.; MOOREN, D.; GRIESBACH, L.; DUSCHINSKY, R.; SCHNITZER, R.J.; PLEVEN, E.; SCHEINER, J. Fluorinated pyrimidines, a new class of tumour-inhibitory compounds. *Nature,* v. 179, p. 663-666, 1957.

HERBST, D.A., JR.; REDDY, K.R. Sofosbuvir, a nucleotide polymerase inhibitor, for the treatment of chronic hepatitis C virus infection. *Expert Opinion on Investigational Drugs,* v. 22, p. 527-536, 2013.

HILFINGER, J. Solving the Prodrug Design and Activation Puzzle. *Molecular Pharmaceutics,* v. 10, p. 429-429, 2013.

HOMSI, J.; GARRETT, C.R. Hepatic arterial infusion of chemotherapy for hepatic metastases from colorectal cancer. *Cancer Control,* v. 13, p. 42-47, 2006.

HU, L.; WU, X.; HAN, J.; CHEN, L.; VASS, S.O.; BROWNE, P.; HALL, B.S.; BOT, C.; GOBALAKRISHNAPILLAI, V.; SEARLE, P.F.; KNOX, R.J.; WILKINSON, S.R. Synthesis and structure–activity relationships of nitrobenzyl phosphoramide mustards as nitroreductase-activated prodrugs. *Bioorganic & Medicinal Chemistry Letters,* v. 21, p. 3986-3991, 2011.

ICHIKAWA, E.; KATO, K. Sugar-modified nucleosides in past 10 years, a review. *Current Medicinal Chemistry,* v. 8, p. 385-423, 2001.

ISMAIL, F.M.D. Important fluorinated drugs in experimental and clinical use. *Journal of Fluorine Chemistry,* v. 118, p. 27-33, 2002.

ISMAIL, F.M.D; DREW, M.G.B.; DASCOMBE, M.J. *Chimica Oggi: Chemistry Today*, v. 27, p. 18-22, 2009.

KATAGI, T. Photochemistry of organophosphorus herbicide butamifos. *Journal of Agricultural and Food Chemistry,* v. 41, p. 496-501, 1993.

KEAM, S.J.; CHAPMAN, T.M.; FIGGITT, D.P. Brivudin (bromovinyl deoxyuridine). *Drugs,* v. 64, p. 2091-2097, 2004.

KEOUGH, D.T.; SPACEK, P.; HOCKOVA, D.; TICHY, T.; VRBKOVA, S.; SLAVETINSKA, L.; JANEBA, Z.; NAESENS, L.; EDSTEIN, M.D.; CHAVCHICH, M.; WANG, T.H.; DE JERSEY, J.; GUDDAT, L.W. Acyclic nucleoside phosphonates containing a second phosphonate group are potent inhibitors of 6-oxopurine phosphoribosyltransferases and have antimalarial activity. *Journal of Medicinal Chemistry,* v. 56, p. 2513-2526, 2013.

KIRAN, Y.B.; DEVENDRANATH REDDY, C.; GUNASEKAR, D.; SURESH REDDY, C.; LEON, A.; BARBOSA, L.C.A. Synthesis and anticancer activity of

new class of bisphosphonates/phosphanamidates. *European Journal of Medical Chemistry,* v. 43, p. 885-892, 2008.

KIRAN, Y.B.; REDDY, C.D.; GUNASEKAR, D.; RAJU, C.N.; BARBOSA, L.C.A.; MARNEY, D.C.O.; RUSSEL, L.J. Synthesis and TGA Evaluation of Novel Triphosphate Esters. *Journal of Fire Sciences,* v. 25, p. 193-215, 2007.

KRAJEWSKA, B. Ureases I. Functional, catalytic and kinetic properties: A review. *Journal of Molecular Catalysis B: Enzymatic,* v. 59, p. 9-21, 2009.

LAPI, S.E.; WAHNISHE, H.; PHAM, D.; WU, L.Y.; NEDROW-BYERS, J.R.; LIU, T.; VEJDANI, K.; VANBROCKLIN, H.F.; BERKMAN, C.E.; JONES, E.F. Assessment of an 18F-labeled phosphoramidate peptidomimetic as a new prostate-specific membrane antigen-targeted imaging agent for prostate cancer. *Journal of Nuclear Medicine*, v. 50, p. 2042-2048, 2009.

LESSIN, S.R.; DUVIC, M.; GUITART, J.; ET AL. Topical chemotherapy in cutaneous t-cell lymphoma: Positive results of a randomized, controlled, multicenter trial testing the efficacy and safety of a novel mechlorethamine, 0.02%, gel in mycosis fungoides. *JAMA Dermatology,* v. 149, p. 25-32, 2013.

LEWANDOWSKA, M.; RUSZKOWSKI, P.; BARANIAK, D.; CZARNECKA, A.; KLECZEWSKA, N.; CELEWICZ, L. Synthesis of 3'-azido-2',3'-dideoxy-5-fluorouridine phosphoramidates and evaluation of their anticancer activity. *European Journal of Medical Chemistry,* v. 67, p. 188-195, 2013.

LI, J.; CHEN, F.; CONA, M.M.; FENG, Y.; HIMMELREICH, U.; OYEN, R.; VERBRUGGEN, A.; NI, Y. A review on various targeted anticancer therapies. *Targeted Oncology,* v. 7, p. 69-85, 2012.

LI, S.; JIA, Y.; JACOBSON, B.; MCCAULEY, J.; KRATZKE, R.; BITTERMAN, P.B.; WAGNER, C.R. Treatment of Breast and Lung Cancer Cells with a N-7 Benzyl Guanosine Monophosphate Tryptamine Phosphoramidate Pronucleotide (4Ei-1) Results in Chemosensitization to Gemcitabine and Induced eIF4E Proteasomal Degradation. *Molecular Pharmaceutics,* v. 10, p. 523-531, 2013.

LIANG, Y.; NARAYANASAMY, J.; SCHINAZI, R.F.; CHU, C.K. Phosphoramidate and phosphate prodrugs of (-)-beta-D-(2*R*,4*R*)-dioxolane-thymine: synthesis, anti-HIV activity and stability studies. *Bioorganic and Medicinal Chemistry,* v. 14, p. 2178-2189, 2006.

LIPSON, R.L.; BALDES, E.J.; OLSEN, A.M. Further evaluation of the use of hematoporphyrin derivative as a new AID for the endoscopic detection of malignant disease. *Diseases of the Chest,* v. 46, p. 676-679, 1964.

LIU, J.; DU, J.; WANG, P.; NAGARATHNAM, D.; ESPIRITU, C.L.; BAO, H.; MURAKAMI, E.; FURMAN, P.A.; SOFIA, M.J. A 2'-deoxy-2'-fluoro-2'-C-methyl uridine cyclopentyl carbocyclic analog and its phosphoramidate prodrug as inhibitors of HCV NS5B polymerase. *Nucleosides Nucleotides Nucleic Acids,* v. 31, p. 277-285, 2012.

LIU, T.; TORIYABE, Y.; KAZAK, M.; BERKMAN, C.E. Pseudoirreversible inhibition of prostate-specific membrane antigen by phosphoramidate peptidomimetics. *Biochemistry*, v. 47, p. 12658-12660, 2008.

LIU, W.; ZHANG, L.; ZHOU, H.; YANG, C.; MIAO, Z.; ZHAO, Y. Synthesis of Novel Nucleoside Analogue Phosphorothioamidate Prodrugs and in vitro Anticancer Evaluation Against RKO Human Colon Carcinoma Cells. *Nucleosides, Nucleotides and Nucleic Acids,* v. 32, p. 161-173, 2013.

MADHAVAA, G.; SUBBAIAHB, K.V.; SREENIVASULU, R.; RAJUA, C.N. Synthesis of novel urea and thiourea derivatives of diphenylphosphoramidate and their antimicrobial activity. *Der Pharmacia Lettre,* v. 4, p. 1194-1201, 2012.

MALLARI, J.P.; CHOY, C.J.; HU, Y.; MARTINEZ, A.R.; HOSAKA, M.; TORIYABE, Y.; MAUNG, J.; BLECHA, J.E.; PAVKOVIC, S.F.; BERKMAN, C.E. Stereoselective inhibition of glutamate carboxypeptidase by organophosphorus derivatives of glutamic acid. *Bioorganic and Medicinal Chemistry*, v. 12, p. 6011-6020, 2004.

MAO, W.-J.; LV, P.-C.; SHI, L.; LI, H.-Q.; ZHU, H.-L. Synthesis, molecular docking and biological evaluation of metronidazole derivatives as potent Helicobacter pylori urease inhibitors. *Bioorganic & Medicinal Chemistry,* v. 17, p. 7531-7536, 2009.

MARA, C.; DEMPSEY, E.; BELL, A.; BARLOW, J.W. Synthesis and evaluation of phosphoramidate and phosphorothioamidate analogues of amiprophos methyl as potential antimalarial agents. *Bioorganic & Medicinal Chemistry Letters,* v. 21, p. 6180-6183, 2011.

MCGUIGAN, C.; KELLEHER, M.R.; PERRONE, P.; MULREADY, S.; LUONI, G.; DAVERIO, F.; RAJYAGURU, S.; POGAM, S.L.; NAJERA, I.; MARTIN, J.A.; KLUMPP, K.; SMITH, D.B. The application of phosphoramidate ProTide technology to the potent anti-HCV compound 4′-azidocytidine (R1479). *Bioorganic & Medicinal Chemistry Letters,* v. 19, p. 4250-4254, 2009.

MCGUIGAN, C.; MADELA, K.; ALJARAH, M.; GILLES, A.; BATTINA, S.K.; RAMAMURTY, C.V.; SRINIVAS RAO, C.; VERNACHIO, J.; HUTCHINS, J.; HALL, A.; KOLYKHALOV, A.; HENSON, G.; CHAMBERLAIN, S. Dual pro-drugs of 2'-C-methyl guanosine monophosphate as potent and selective inhibitors of hepatitis C virus. *Bioorganic & Medicinal Chemistry Letters,* v. 21, p. 6007-6012, 2011.

MCGUIGAN, C.; MADELA, K.; ALJARAH, M.; GILLES, A.; BRANCALE, A.; ZONTA, N.; CHAMBERLAIN, S.; VERNACHIO, J.; HUTCHINS, J.; HALL, A.; AMES, B.; GOROVITS, E.; GANGULY, B.; KOLYKHALOV, A.; WANG, J.; MUHAMMAD, J.; PATTI, J.M.; HENSON, G. Design, synthesis and evaluation of a novel double pro-drug: INX-08189. A new clinical candidate for hepatitis C virus. *Bioorganic & Medicinal Chemistry Letters,* v. 20, p. 4850-4854, 2010.

MCGUIGAN, C.; MURZIANI, P.; SLUSARCZYK, M.; GONCZY, B.; VANDE VOORDE, J.; LIEKENS, S.; BALZARINI, J. Phosphoramidate ProTides of the anticancer agent FUDR successfully deliver the preformed bioactive monophosphate in cells and confer advantage over the parent nucleoside. *Journal of Medicinal Chemistry,* v. 54, p. 7247-7258, 2011.

MCGUIGAN, C.; PATHIRANA, R.N.; MAHMOOD, N.; HAY, A.J. Aryl phosphate derivates of AZT inhibit HIV replication in cells where the nucleoside is poorly active. *Bioorganic & Medicinal Chemistry Letters,* v. 2, p. 701-704, 1992.

MCGUIGAN, C.; THIERY, J.C.; DAVERIO, F.; JIANG, W.G.; DAVIES, G.; MASON, M. Anti-cancer ProTides: tuning the activity of BVDU phosphoramidates related to thymectacin. *Bioorganic and Medicinal Chemistry,* v. 13, p. 3219-3227, 2005.

MEHELLOU, Y.; BALZARINI, J.; MCGUIGAN, C. An investigation into the anti-HIV activity of 2',3'-didehydro-2',3'-dideoxyuridine (d4U) and 2',3'-dideoxyuridine (ddU) phosphoramidate 'ProTide' derivatives. *Organic and Biomolecular Chemistry,* v. 7, p. 2548-2553, 2009.

MENEGHESSO, S.; VANDERLINDEN, E.; BRANCALE, A.; BALZARINI, J.; NAESENS, L.; MCGUIGAN, C. Synthesis and biological evaluation of purine 2'-fluoro-2'-deoxyriboside ProTides as anti-influenza virus agents. *ChemMedChem,* v. 8, p. 415-425, 2013.

NEUTEBOOM, S.T.; KARJIAN, P.L.; BOYER, C.R.; BERYT, M.; PEGRAM, M.; WAHL, G.M.; SHEPARD, H.M. Inhibition of cell growth by NB1011 requires high thymidylate synthase levels and correlates with p53, p21, bax, and GADD45 induction. *Molecular Cancer Therapeutics,* v. 1, p. 377-384, 2002.

NGUYEN, T.-M.; CHANG, S.; CONDON, B.; SLOPEK, R.; GRAVES, E.; YOSHIOKA-TARVER, M. Structural Effect of Phosphoramidate Derivatives on the Thermal and Flame Retardant Behaviors of Treated Cotton Cellulose. *Industrial & Engineering Chemistry Research,* v. 52, p. 4715-4724, 2013.

OLIVEIRA, F.M.; BARBOSA, L.C.A.; TEIXEIRA, R.R.; DEMUNER, A.J.; MALTHA, C.R.A.; PICANÇO, M.C.; SILVA, G.A.; PAULA, V.F. Synthesis and insecticidal activity of new phosphoramidates. *Journal of Pesticide Science,* v. 37, p. 85-88, 2012.

PARSONS, M.; WORTHEY, E.A.; WARD, P.N.; MOTTRAM, J.C. Comparative analysis of the kinomes of three pathogenic trypanosomatids: Leishmania major, Trypanosoma brucei and Trypanosoma cruzi. *BMC Genomics,* v. 6, p. 127, 2005.

PAULA, V.F.; BARBOSA, L.C.A.; TEIXEIRA, R.R.; PICANCO, M.C.; SILVA, G.A. Synthesis and insecticidal activity of new 3-benzylfuran-2-yl *N,N,N',N'*-tetraethyldiamidophosphate derivatives. *Pest Management Science,* v. 64, p. 863-872, 2008.

PERRONE, P.; LUONI, G.M.; KELLEHER, M.R.; DAVERIO, F.; ANGELL, A.; MULREADY, S.; CONGIATU, C.; RAJYAGURU, S.; MARTIN, J.A.; LEVEQUE, V.; LE POGAM, S.; NAJERA, I.; KLUMPP, K.; SMITH, D.B.; MCGUIGAN, C. Application of the phosphoramidate ProTide approach to 4'-azidouridine confers sub-micromolar potency versus hepatitis C virus on an inactive nucleoside. *Journal of Medicinal Chemistry,* v. 50, p. 1840-1849, 2007.

PIDDOCK, L.J.V. The crisis of no new antibiotics—what is the way forward? *The Lancet Infectious Diseases,* v. 12, p. 249-253, 2012.

PINTO, J.T.; SUFFOLETTO, B.P.; BERZIN, T.M.; QIAO, C.H.; LIN, S.; TONG, W.P.; MAY, F.; MUKHERJEE, B.; HESTON, W.D. Prostate-specific membrane antigen: a novel folate hydrolase in human prostatic carcinoma cells. *Clinical Cancer Research*, v. 2, p. 1445-1451, 1996.

PRASAD, G.S.; BABU, B.H.; REDDY, K.R.K.K.; HARANATH, P.R.; REDDY, C.S. Synthesis and antibacterial activity of new 2-aryloxy-6-bromo-3-(4-chlorophenyl)-3,4-dihydrobenzo[e][1,3,2]oxazaphosphinine-2-oxides. *Archive for Organic Chemistry,* v. 2006, p. 165-170, 2006.

RABASSEDA, X. Brivudine: a herpes virostatic with rapid antiviral activity and once-daily dosing. *Drugs of Today,* v. 39, p. 359-371, 2003.

REITZ, C.; BRAYNE, C.; MAYEUX, R. Epidemiology of Alzheimer disease. *Nature Reviews Neurology,* v. 7, p. 137-152, 2011.

RUDA, G.F.; WONG, P.E.; ALIBU, V.P.; NORVAL, S.; READ, K.D.; BARRETT, M.P.; GILBERT, I.H. Aryl phosphoramidates of 5-phospho erythronohydroxamic acid, a new class of potent trypanocidal compounds. *Journal of Medicinal Chemistry,* v. 53, p. 6071-6078, 2010.

SANTOS, V.M.R.D.; DONNICI, C.L.; DACOSTA, J.B.N.; CAIXEIRO, J.M.R. Compostos organofosforados pentavalentes: histórico, métodos sintéticos de preparação e aplicações como inseticidas e agentes antitumorais. *Quimica Nova,* v. 30, p. 159-170, 2007.

SHEWACH, D.S.; KUCHTA, R.D. Introduction to Cancer Chemotherapeutics. *Chemical Reviews,* v. 109, p. 2859-2861, 2009.

SOFIA, M.J.; CHANG, W.; FURMAN, P.A.; MOSLEY, R.T.; ROSS, B.S. Nucleoside, nucleotide, and non-nucleoside inhibitors of hepatitis C virus NS5B RNA-dependent RNA-polymerase. *Journal of Medicinal Chemistry,* v. 55, p. 2481-2531, 2012.

SUN, Q.; LI, R.-T.; GUO, W.; CUI, J.-R.; CHENG, T.-M.; GE, Z.-M. Novel class of cyclophosphamide prodrug: Cyclophosphamide spiropiperaziniums (CPSP). *Bioorganic & Medicinal Chemistry Letters,* v. 16, p. 3727-3730, 2006.

TRONRUD, D.E.; MONZINGO, A.F.; MATTHEWS, B.W. Crystallographic structural analysis of phosphoramidates as inhibitors and transition-state analogs of thermolysin. *European Journal of Biochemistry*, v. 157, p. 261-268, 1986.

TURNOCK, D.C.; FERGUSON, M.A.J. Sugar nucleotide pools of *Trypanosoma brucei, Trypanosoma cruzi*, and *Leishmania major*. *Eukaryot Cell,* v. 6, p. 1450-1463, 2007.

UCKUN, F.M.; VENKATACHALAM, T.K.; ERBECK, D.; CHEN, C.L.; PETKEVICH, A.S.; VASSILEV, A. Zidampidine, an aryl phosphate derivative of AZT: *in vivo* pharmacokinetics, metabolism, toxicity, and anti-viral efficacy

against hemorrhagic fever caused by *Lassa virus*. *Bioorganic and Medicinal Chemistry,* v. 13, p. 3279-3288, 2005.

VALIYEV, F.; TSAI, F.Y.; SABOURY, A.A.; LIU, H.J.; MOOSAVI-MOVAHEDI, A.A.; HAKIMELAHI, G.H. Design, synthesis, and antiviral activity of novel phosphoramidates. *Journal of the Iranian Chemical Society,* v. 5, p. 228-237, 2008.

WAGNER, C.R.; IYER, V.V.; MCINTEE, E.J. Pronucleotides: toward the *in vivo* delivery of antiviral and anticancer nucleotides. *Medicinal Research Reviews,* v. 20, p. 417-451, 2000.

WANG, P.; RACHAKONDA, S.; ZENNOU, V.; KEILMAN, M.; NIU, C.; BAO, D.; ROSS, B.S.; FURMAN, P.A.; OTTO, M.J.; SOFIA, M.J. Phosphoramidate prodrugs of (-)-beta-D-(2*R*,4*R*)-dioxolane-thymine (DOT) as potent anti-HIV agents. *Antiviral Chemistry and Chemotherapy,* v. 22, p. 217-238, 2012.

WANG, Z.W.; GUO, C.C.; XIE, W.Z.; LIU, C.Z.; XIAO, C.G.; TAN, Z. Novel phosphoramidates with porphine and nitrogenous drug: one-pot synthesis and orientation to cancer cells. *European Journal of Medical Chemistry,* v. 45, p. 890-895, 2010.

WESTHEIMER, F. Why nature chose phosphates. *Science,* v. 235, p. 1173-1178, 1987.

WHO. World Malaria Report., 2010.

WILSON, R.H. Novel therapeutic developments other than EGFR and VEGF inhibition in colorectal cancer. *Oncologist,* v. 11, p. 1018-1024, 2006.

WU, L.Y.; ANDERSON, M.O.; TORIYABE, Y.; MAUNG, J.; CAMPBELL, T.Y.; TAJON, C.; KAZAK, M.; MOSER, J.; BERKMAN, C.E. The molecular pruning of a phosphoramidate peptidomimetic inhibitor of prostate-specific membrane antigen. *Bioorganic and Medicinal Chemistry*, v. 15, p. 7434-7443, 2007.

YAN, J.; BU, J.; BAI, X.; LI, J.; REN, T.; ZHAO, Y. The tribological study of novel phosphorous–nitrogen type phosphoramidate additives in rapeseed oil. *Journal of Engineering Tribology,* v. 226, p. 377–388, 2012.

ZAKIROVA, N.F.; SHIPITSYN, A.V.; JASKO, M.V.; PROKOFJEVA, M.M.; ANDRONOVA, V.L.; GALEGOV, G.A.; PRASSOLOV, V.S.; KOCHETKOV, S.N. Phosphoramidate derivatives of acyclovir: synthesis and antiviral activity in HIV-1 and HSV-1 models *in vitro*. *Bioorganic and Medicinal Chemistry,* v. 20, p. 5802-5809, 2012.

ZLATEV, I.; GIRAUT, A.; MORVAN, F.; HERDEWIJN, P.; VASSEUR, J.-J. δ-Di-carboxybutyl phosphoramidate of 2′-deoxycytidine-5′-monophosphate as substrate for DNA polymerization by HIV-1 reverse transcriptase. *Bioorganic & Medicinal Chemistry,* v. 17, p. 7008-7014, 2009.

7. SPECTROSCOPIC AND DYNAMIC NMR STUDY, X-RAY CRYSTALLOGRAPHY AND DFT CALCULATIONS OF TWO PHOSPHORAMIDATES: $(C_4H_3O_2)P(O)(CL)C_6H_{14}N$ AND $(C_4H_3O_2)P(O)(C_6H_{11}NH)_2$

7.1. Abstract

In recent years, research in organophosphorus compounds, particularly phosphoramidates, have attracted attention because of their many applications. In this work, we report a combined experimental and theoretical study on the molecular structure and NMR spectra of two phosphoramidates (furan-2-yl *N,N*-diisopropylamidochlorophosphate (**1**) and furan-2-yl *N,N,N′,N′*-dicyclohexylamidophosphate (**2**)). In the NMR time scale a free rotation of the C-N/P-N single bonds was observed at room temperature (298 K) while the rotation freezes below 195 K for compound **1**. From dynamic NMR analysis, the activation free energy ($\Delta G^{\#}$) for rotation of the C-N bond was calculated as 9.9 ± 0.3 kcal mol^{-1}. The experimental data were reinforced by theoretical calculation using the density functional theory method B3LYP and the 6-31G(d) basis set which provided activation energy *($\Delta E^{\ddagger}$)* of 9.2 kcal mol^{-1}. The structures of compounds **1** and **2** were determined by single crystal X-ray diffraction method. Compound **1** is formed by a racemic mixture, whose presence was evidenced only in the structure determination by X-ray

7.2. Introduction

Organophosphorus compounds have attracted great attention due to their biological activities. Among these, one of the most common class are the phosphoramidates, which are characterized by the presence of at least one –NR^1R^2 group (R^1 and R^2 = alkyl, aryl) in their structures. Phosphoramidates are extensively studied due to their potential applications as acetylcholinesterase and urease inhibitors [1], insecticides [2,3], herbicides [4], antifire [5], anticancer drugs [6-8], anti HIV [9-10], inhibitors of hepatitis C virus [11-12], antimalarial agents [13], and antirust additives in lubricating oils [14]. Moreover, novel

synthesized phosphoramidate derivatives of fenoprofen, ketoprofen, ibuprofen, indomethacine and diclofenac possess significantly higher antiproliferative activities than the corresponding nonsteroidal anti-inflammatory drugs (NSAID) 3-hydroxypropylamides [15].

Continuing our effort to develop new compounds with insecticidal [2,3] and phytotoxic activity [16-19], we have synthesized new phosphoramidates and quantified their activity against the Lepidoptera species that attack important commercial crops [3]. Among the synthesized compounds, only furan-2-yl *N,N*-diisopropylamidochlorophosphate (**1**) and furan-2-yl *N,N,N′,N′*-dicyclohexylamidophosphate (**2**) were obtained as single crystals (Figure 1).

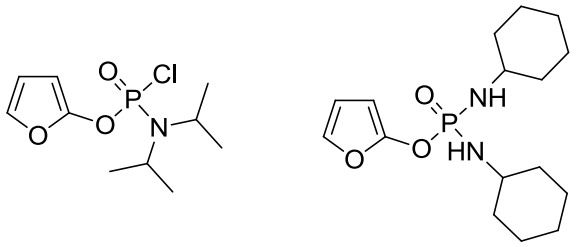

1 **2**

Figure 1 - Structure of compounds **1** and **2**.

The biological functions of the phosphoramidates most probably are correlated to their molecular properties [20-23]. Although the crystal structures of some phosphoramidates have been reported recently [24-27], only a few details about the structural and spectral properties of such substances have been described in the literature. Knowledge of structure and molecular properties are important for the detailed understanding of their effect on the biological functions and help the rational design of new compounds [28].

Our aim is to provide valid support to the structural characterization of the phosphoramidates. Dynamic NMR studies have been extensively used to explore the kinetics and thermodynamics of stereo dynamic processes [29]. Thus, we report the dynamic ^{1}H and ^{13}C NMR spectra and use them to estimate the rotational barrier activation free energy ($\Delta G^{\ddagger}$) for hindered rotation of the C-N bond [30] in phosphoramidate **1**. Additionally, the single crystal X-ray diffraction data and quantum chemical calculations using Density Functional Theory (DFT) are also reported.

7.3. Experimental

7.3.1. NMR Studies

One dimensional ^{1}H- and ^{13}C-NMR spectra were acquired either with an MERCURY-300/Varian spectrometer at 300.069 MHz for ^{1}H (32 k data points, 30° excitation pulse duration of 2.2 μs, spectral width of 6 KHz, acquisition time of 3.3 s and relaxation delay of 10 ms) and at 75.452 MHz for ^{13}C (32 K data points 45° excitation pulse duration of 6.5 μs, spectral width of 19 KHz, acquisition time of 0.8 s and relaxation delay of 2.0 s) in 5 mm probes with direct detection, using deuterated dichloromethane or chloroform as a solvent and TMS as internal standard (δ = 0.00).

7.3.2. Single-crystal X-ray diffraction

Crystals of compounds **1** and **2** were obtained by gently warming each compound in hexane, followed by addition of dichloromethane dropwise until the solid was completely dissolved. The resulting solution was left undisturbed at room temperature. After 24 hours, white crystals, suitable for X-ray analyses, were formed. They were separated, washed with cold hexane, and dried.

Well-shaped single crystals of **1** and **2** were chosen for the X-ray experiment. The measurements were made at 298 K on an Enraf-Nonius Kappa-CCD difractometer with graphite monochromated Mo Kα. Data were collected up to ~50° in 2θ, with a redundancy of 4. The final unit cell parameters were based on all reflections. The temperature was controlled using an Oxford Cryosystem low temperature device. Data collection was made using the *COLLECT* software [31]; integration and scaling of the reflections were performed with the HKL Denzo-Scalepack software system [32]. The structures were solved and the models refined using the SHELXL-97 software [33]. H atoms on C atoms were positioned stereochemically and were refined with fixed individual displacement parameters [$U_{iso}(H) = 1.5U_{eq}(C)$ for methyl groups or $1.2U_{eq}(C)$ for aromatic, methine and methylene groups], using the SHELXL riding model with C—H bond lengths of 0.96, 0.98 and 0.97 Å for methyl, methine and methylene groups, respectively. The hydrogen atoms bonded to

the nitrogen atoms in **2** were found in successive difference Fourier maps and were refined with free coordinates and $U_{iso}(H) = 1.2U_{eq}(O)$. WINGX software was used to analyze and prepare the data for publication. Molecular graphics were prepared using ORTEP-3 for Windows [34] and Mercury [35]. Crystal data, data collection procedures, structure determination methods and refinement results are summarized below.

7.3.3. Computational Details

The geometries of the two phosphoramidates **1** and **2** were first designed in the SPARTAN´10 software [36]. Using the conformer distribution routine of SPARTAN and the semi-empirical PM3 method [37] a conformational analysis of both species was carried out to identify the most stable conformers in each case. Those conformers were then reoptimized with the B3LYP functional [38,39] and the 6-311++G(2d,p) basis set. Approximated activation energies for rotation around either the P-N or the C-N bonds were obtained by a relaxed dihedral scan (by 30º step) around the corresponding bond using the 6-31G(d) basis set. All the DFT calculations were performed using the Gaussian 09 program package [40].

7.4. Results and discussion

In a previous work we have described the preparation of some lactone analogous to the natural compounds called nostoclides [17]. Lactone **3**, used as starting material, was synthesized previously [2]. The treatment of **3** with $POCl_3$ in the presence of triethylamine afforded compound **4** (Scheme 1), which was not isolated. Subsequent reaction of **4** with diisopropylamine (2 eq.) and DMAP (5 mol%) furnished **1** in 14% yield. Formation of **1** resulted from substitution of one of the chlorine atoms in **4** by the diisopropylamino group. Treatment of **4** with cyclohexylamine (2 eq.) and DMAP (5 mol%) furnished **2** in 10% yield, with the complete substitution of chlorine atoms in **4** by the nucleophilic cyclohexylamine [3]. The products were obtained as white crystals and the structures of compounds **1** and **2** were confirmed by single crystal X-ray diffraction (Figures 2 and 6).

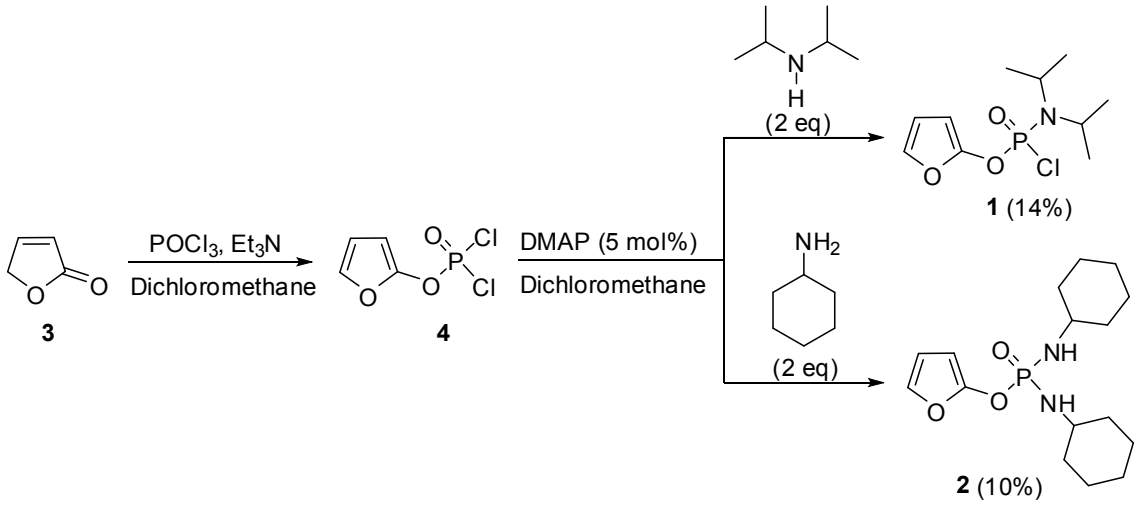

Scheme 1 - Synthesis of phosphoramidates **1** and **2** described by Oliveira and co-workers (2012).

7.4.1. Crystal structure analysis

Crystal data, data collection procedures, structure determination methods and refinement results are summarized in Table 1. Crystallographic data for the structural analysis of the compounds discussed here have been deposited at the Cambridge Crystallographic Data Centre, 12 Union Road, Cambridge CB2 1EZ, UK, and are available on request quoting the deposition numbers CCDC 902881 and 902882, for **1** and **2**, respectively.

Figure 2 shows the *R* enantiomer of **1**. Table 2 gives selected experimental and calculated bond length and angles. Since **1** is a chiral molecule crystallized in a centrosymmetric space group, its crystal structure is formed by an equimolar mixture of a pair of enantiomers (*R/S*: 50/50) (Figure 3). The intermolecular geometry of **1** was analyzed using Mogul [41], a knowledge base of molecular geometry derived from the Cambridge Structural Database (CSD; Version 5.33 of November 2011, with January 2012 and May 2012 updates) [42]. This analysis shows that all bond lengths and bond angles are in agreement with the values expected for a good X-ray diffraction structure refinement. The extended least-squares plane through the furan ring including the exocyclic atom O2 [r.m.s = 0.0024 Å and largest deviation = 0.003(2) Å for O3], shows that this moiety is planar, as expected

Table 1 - Crystal data, data collection details and structure refinement results for **1** and **2**.

	1	**2**
Empirical formula	$C_{10}H_{17}N_1O_3P_1$	$C_{16}H_{27}N_2O_3P_1$
Formula weight	265.67	326.27
Crystal system	Triclinic	Orthorhombic
Space Group	P-1	Pbca
Unit cell (Å, º)	*a*=7.4216(2) *b*=8.4341(3) *c*=11.9649(4) α=87.914(2) β=73.647(2) γ=70.935(2)	*a*=11.8810(5) *b*=8.9415(3) *c*=32.847(1) $\alpha=\beta=\gamma=90^o$
Volume ($Å^3$)	677.94(4)	3489.5(2)
Z	2	8
Density (mg/m^3)	1.301	1.242
μ (mm^{-1})	0.393	0.171
F (000)	280	1408
Crystal size (mm^3)	0.21 x 0.24 x 0.38	0.19 x 0.23 x 0.26
θ_{max} (º)	26	25
Index ranges	-9<=h<=9, -10<=k<=10, -14<=l<=14	-13<=h<=14, -9<=k<=10, -19<=l<=40
Reflections collected	9784	16902
Independent reflections	2681 [R(int) = 0.0741]	3396 [R(int) = 0.0944]
Completeness to θ_{max} (%)	99.1	98.6
Data/restraints/parameters	2681 / 0 / 149	3396 /0/ 205
Goodness-of-fit on F^2	1.048	0.979
Final R índices [I>2σ(I)]	R1 = 0.0462, wR2 = 0.1236	R1 = 0.0477, wR2 = 0.1099
R indices (all data)	R1 = 0.0588, wR2 = 0.1323	R1 = 0.0981, wR2 = 0.1298
$\Delta\rho_{max}$ and $\Delta\rho_{min}$ ($e.Å^{-3}$)	0.390 and -0.315 e.Å-3	0.156 and -0.211

Table 2 - Experimental (X-ray) and calculated selected bond lengths [Å] and angles [°] for **1** and MOGUL [41] bond analysis.

Geometric Parameter	Bond length	Mogul average query	B3LYP/ 6-311++G(2d,p)	Geometric parameter	Bond angle	Mogul average query	B3LYP/ 6-311++G(2d,p)
C10–C8	1.516(4)	1.52(3)	1.536	C2–C3–C4	108.0(3)	107(2)	106.524
C6–C5	1.506(4)	1.52(3)	1.529	O3–C4–C3	109.7(2)	110(2)	110.280
C7–C5	1.528(4)	1.52(3)	1.533	C10–C8–N1	111.9(2)	113(2)	114.579
C9–C8	1.512(4)	1.52(3)	1.531	C6–C5–N1	111.1(2)	113(2)	114.144
C3–C2	1.422(4)	1.42(5)	1.434	C7–C5–N1	112.0(2)	113(2)	112.490
O3–C4	1.406(3)	1.38(3)	1.369	C9–C8–N1	110.8(2)	113(2)	113.037
C3–C4	1.292(4)	1.32(4)	1.354	C8–N1–C5	117.3(2)	118(3)	124.980
C5–N1	1.500(3)	1.49(2)	1.501	O2–P1–O1	114.95(9)	110(4)	115.699
C8–N1	1.490(3)	1.49(2)	1.493	C4–O3–C1	104.2(2)	107(1)	106.292
P1–O2	1.605(1)	1.57(1)	1.640	O3–C1–C2	113.2(2)	109(4)	111.650
P1–Cl1	2.015(1)	2.02(5)	2.071	C3–C2–C1	105.0(2)	108(1)	105.252
O3–C1	1.329(3)	1.35(3)	1.350	P1–N1–C5	121.6(2)	121(3)	116.189
C2–C1	1.311(3)	1.39(4)	1.355	P1–N1–C8	119.9(2)	121(3)	118.680
O2–C1	1.365(3)	1.36(2)	1.358	O2–P1–N1	107.0(1)	104(5)	106.524
P1–N1	1.606(2)	1.62(2)	1.645	O1–P1–N1	116.6(1)	114(2)	115.699
P1–O1	1.452(2)	1.47(3)	1.465	Cl1–P1–N1	109.2(1)	107(2)	107.994
				O2–P1–Cl1	95.12(6)	103(2)	95.664
C10–C8–C9	112.7(3)	112(3)	111.194	O2–C1–C2	131.4(2)	132(3)	132.586
C7–C5–C6	113.2(3)	112(3)	111.977	O1–P1–Cl1	111.8()	109(1)	113.175

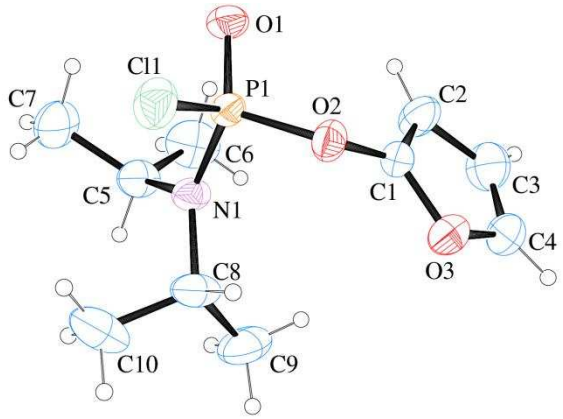

Figure 2 - The molecular structure of **1** (*R* enantiomer), showing the atom numbering scheme. Displacement ellipsoids are drawn at the 30% probability level and H atoms are shown as small spheres of arbitrary radii.

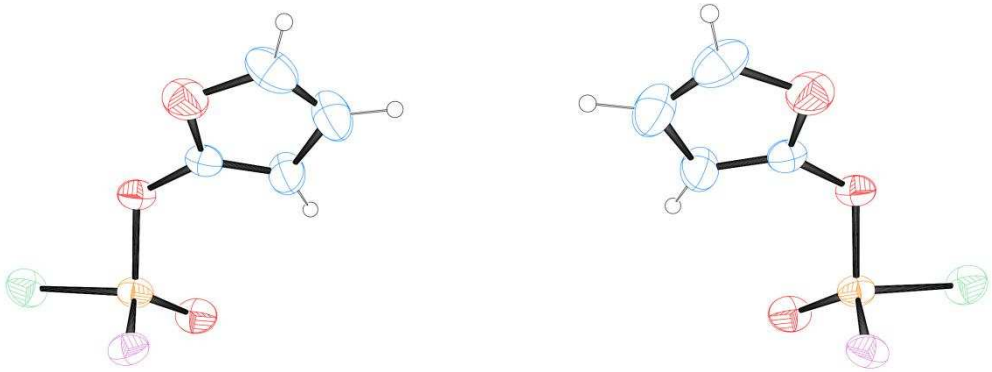

(a) (b)

Figure 3 - Molecular fragments highlighting the two enantiomers, a) *R* (molecule in x, y, z) and b) *S* (molecule in -x, -y, -z).

The intermolecular analysis of **1** shows that a non-classical hydrogen bond [C—H = 0.93 Å, C…O = 3.364(3) Å, H4…O = 2.502(3) Å, C—H…O = 154.26^{o}] involving the furan and P=O group is the main intermolecular force that contributes to the stabilization of the crystal packing (Figures 4 and 5). The individual chains are themselves linked by VDW interactions forming a racemic double chain along [010]. The furan rings in the double chains are laid in plane parallel to (101) forming a ribbon along [010] (Figures 4 and 5). The shortest Cl…Cl separation is 5.581(3) Å, which is slightly longer than the limit (3.52 Å) to be considered as an intermolecular halogen-halogen interaction involving chlorine [43].

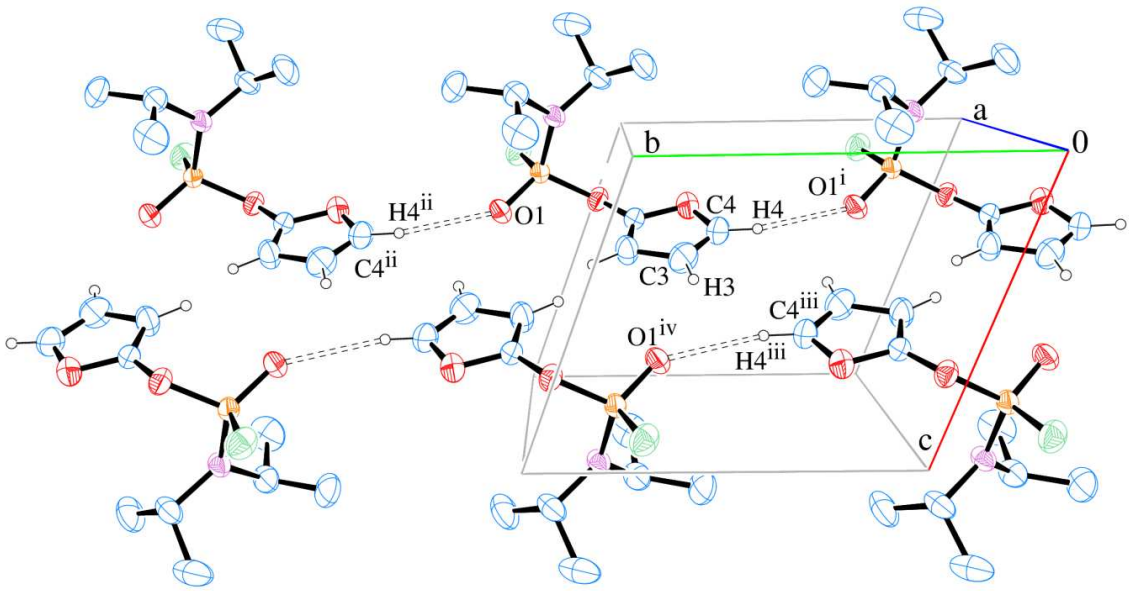

Figure 4 - A partial packing diagram for **1**, showing the racemic double chain formed along [010]. Hydrogen bonds are shown as dashed lines. [Symmetry codes: (i) x, y-1, z; (ii) x, y+1, z; (iii) -x+1, -y+1, -z+1; (iv) -x+1, -y+2, -z+1].

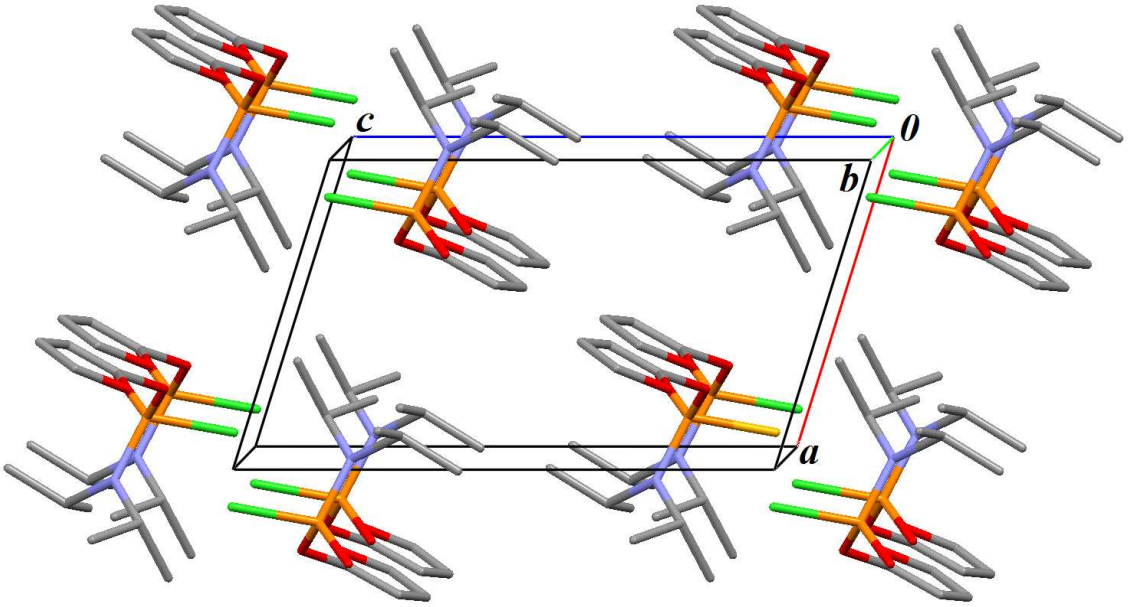

Figure 5 - The crystal packing illustration of **1** onto the plane ac. Hydrogen atoms were omitted for clarity.

Figure 6 shows an ORTEP view of **2** with the ring label scheme. The main geometric parameters are given in Table 1 and some experimental and calculated bond length and bond angles are given in Table 3. Similarly to compound **1**, the molecular conformation of **2** was also analyzed using the

MOGUL software, which revealed a good X-ray diffraction refinement. The extended least-squares plane through the furan ring including the exocyclic O2 atom [r.m.s = 0.0206 Å and largest deviation = -0.029(1) Å for O2] shows that also in this case this moiety is considerably planar. The intermolecular arrangement of the furan rings in **1** and **2** shows that they are similar, as expected. However, their orientations are different in relation to the O1=P1-O2 plane in the phosphorus tetrahedral moiety (Figure 7). The least-squares plane through the furan ring and the O1=P1-O2 triad form angles of 73.97(7)° and 53.6(1)° for **1** and **2**, respectively. Moreover, in **1** the P=O bond is oriented *anti* to the C1—O3 bond, whereas in **2** the corresponding arrangement is *syn* (Figure 7). Both cyclohexyl moieties have chair conformation with weighted average absolute torsion angles of 54.87(10.52)° and 55.42(12.23)° for rings B and C, respectively (1st is the e.s.d. internal and 2nd is the external one) [44]. Considering the two possible chair conformations of the cyclohexylamine ring, the C5—N1 and C11—N2 bonds are both in equatorial orientation.

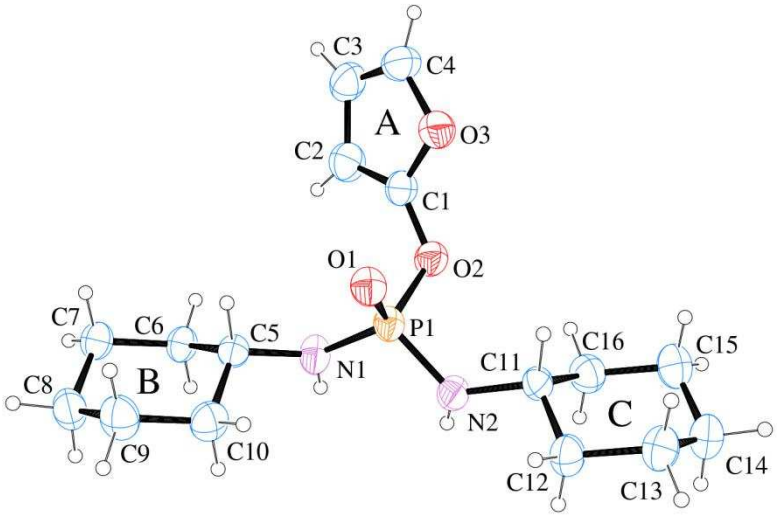

Figure 6 - The molecular structure of **2** with atom and ring labeling. Displacement ellipsoids are drawn at the 30% probability level and H atoms are shown as small spheres of arbitrary radii.

Table 3. Experimental (X-ray) and calculated selected bond lengths [Å] and angles [°] for **2** and MOGUL [41] bond analysis.

Geometric Parameter	Bond length	Mogul average query	B3LYP/ 6-311++G(2d,p)	Geometric parameter	Bond angle	Mogul average query	B3LYP/ 6-311++G(2d,p)
C13–C12	1.528(3)	1.53(3)	1.534	C8–C7–C6	112.0(2)	111(2)	111.787
C14–C13	1.501(4)	1.51(4)	1.533	C8–C9–C10	111.0(2)	111(3)	111.675
C15–C14	1.513(3)	1.51(4)	1.534	C9–C8–C7	110.7(2)	111(4)	111.255
C15–C16	1.520(3)	1.53(3)	1.534	C2–C3–C4	107.1(2)	107(2)	106.842
C7–C6	1.518(3)	1.53(3)	1.534	O3–C4–C3	110.5(2)	110(2)	110.089
C8–C7	1.498(3)	1.51(4)	1.532	C13–C12–C11	111.4(2)	111(2)	111.864
C9–C10	1.510(3)	1.53(3)	1.534	C15–C16–C11	111.6(2)	111(2)	111.747
C9–C8	1.517(3)	1.51(4)	1.533	C7–C6–C5	111.8(2)	111(2)	111.861
C3–C2	1.424(4)	1.42(5)	1.435	C9–C10–C5	112.0(2)	111(2)	111.883
O3–C4	1.371(3)	1.38(3)	1.374	C10–C5–C6	110.6(2)	111(2)	110.945
C3–C4	1.315(4)	1.32(4)	1.353	C12–C11–C16	110.9(2)	111(2)	110.803
C10–C5	1.505(3)	1.51(3)	1.535	C10–C5–N1	112.6(2)	111(2)	111.889
C12–C11	1.515(3)	1.51(3)	1.536	C12–C11–N2	109.6(2)	111(2)	109.983
C16–C11	1.515(3)	1.51(3)	1.535	C16–C11–N2	112.8(2)	111(2)	112.456
C6–C5	1.505(3)	1.51(3)	1.536	C6–C5–N1	111.0(2)	111(2)	110.999
C11–N2	1.471(3)	1.47(2)	1.464	P1–N1–C5	123.2(1)	124(2)	127.827
C5–N1	1.471(3)	1.47(2)	1.472	P1–N2–C11	123.7(1)	124(2)	129.383
P1–O1	1.461(1)	1.48(1)	1.472	O2–P1–O1	108.3(8)	113(2)	116.179
O3–C1	1.346(2)	1.35(3)	1.355	C4–O3–C1	105.7(2)	107(1)	106.196
C2–C1	1.336(3)	1.39(4)	1.355	O3–C1–C2	111.4(2)	109(4)	111.658
O2–C1	1.353(2)	1.36(2)	1.349	C3–C2–C1	105.3(2)	108(1)	105.214
P1–O2	1.640(1)	1.60(1)	1.651	O1–P1–N1	113.63(9)	113(4)	110.529
P1–N1	1.612(2)	1.62(1)	1.656	O1–P1–N2	117.47(9)	113(4)	115.129
P1–N2	1.601(2)	1.62(1)	1.649	O2–P1–N1	107.47(9)	103(5)	104.340
				O2–P1–N2	101.67(9)	103(5)	97.831
C14 C13 C12	111.1(2)	111(2)	111.750	N2–P1–N1	107.3(1)	109(2)	111.768
C14 C15 C16	111.1(2)	111(2)	111.698	O2–C1–C2	133.4(2)	131(3)	133.844
C15 C14 C13	111.3(2)	111(3)	111.193				

Table 4. Intermolecular hydrogen bond length (Å) and angles (°) for **1**. 'D' and 'A' mean hydrogen donor and acceptor, respectively.

D-H...A	D-H	H...A	D...A	D-H...A
N1-H1...O1^{i}	0.77(3)	2.44(2)	3.110(2)	147(2)
N2-H2b…O1^{i}	0.72(3)	2.22(3)	2.908(2)	162(3)

Symmetry codes (as Figure 8: $^{(i)}$ -x-1/2, y+1/2, z

Either the N1—H1 or N2—H2b groups act as intermolecular H bond donor to the O1, giving rise to an infinite one-dimensional chain parallel to the [010] direction (Figure 8 and Table 4). The linkage takes place through the phosphorous tetrahedron by glide b (normal to *a* axis)- and translation-related molecules. The orientation of individual chains along [010] is shown in the packing illustration of **2** onto the plane ac (Figure 9).

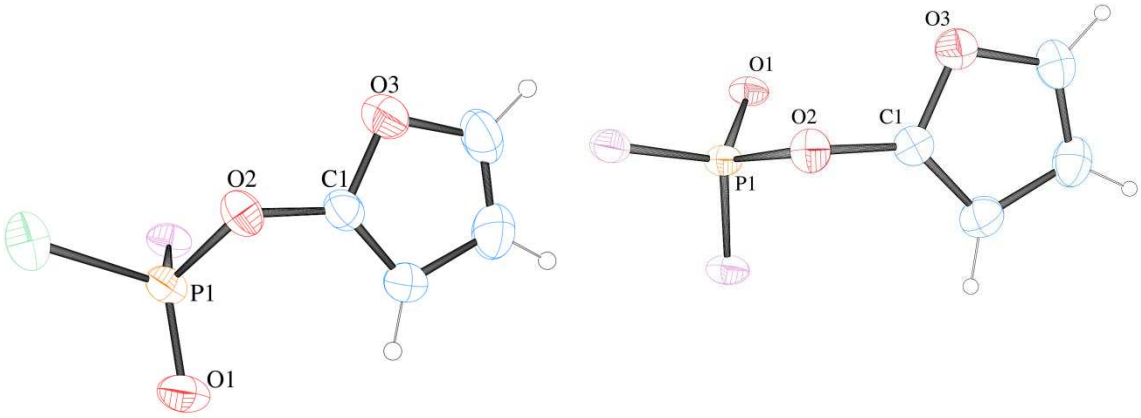

(a) (b)

Figure 7 - Relative orientation of the furan ring and phosphorus tetrahedron in (a) **1** and (b) **2**.

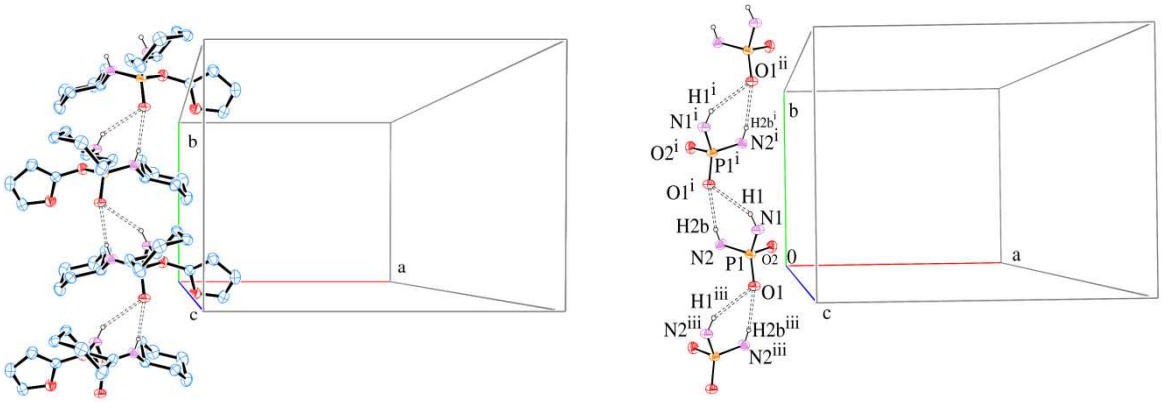

(a) (b)

Figure 8 - (a) View of the network of hydrogen bonds parallel to [001] which stabilizes the packing of **2**. (b) View showing only the phosphorous tetrahedral and atom labeling involved in the hydrogen bonds. Symmetry codes: $^{(i)}$ = *-x-1/2, y+1/2, z;* $^{(ii)}$ = *x, y+1, z;* $^{(iii)}$ *-x-1/2, y-1/2, z.*

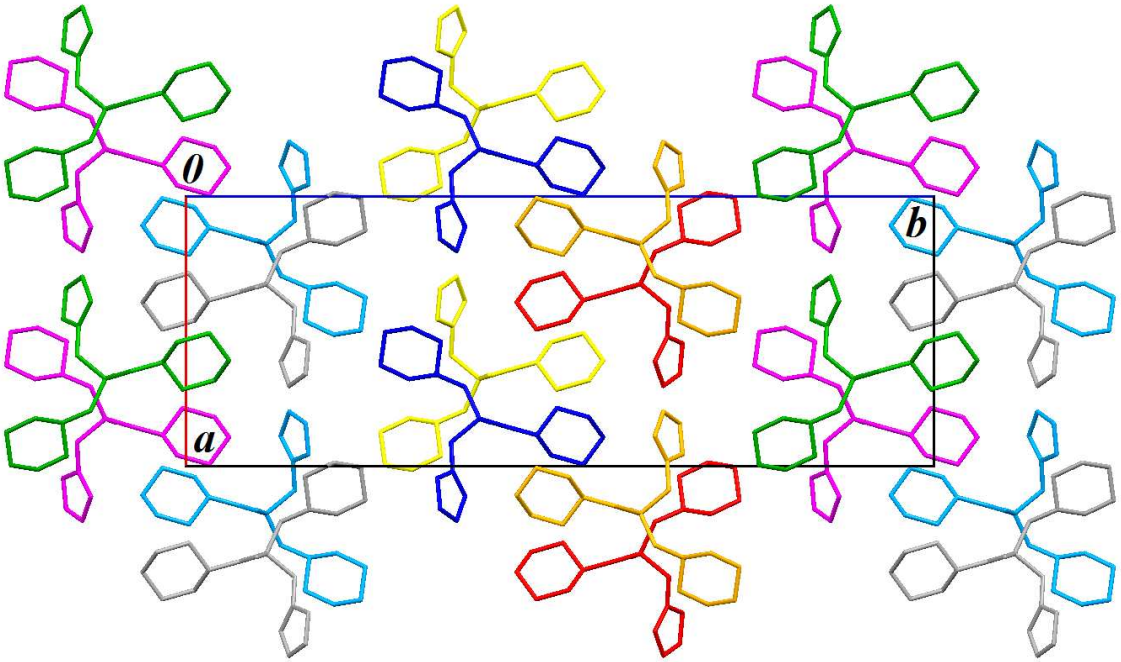

Figure 9 - Packing illustration of **2** onto the plane ac. Hydrogen atoms were omitted for clarity. The colors represent the eight equivalent positions of Pbac space group.

7.4.2. NMR study

The ^{1}H- and ^{13}C-NMR spectra at 298K evidence couplings over long distances in both phosphoramidates, **1** and **2**. The ^{1}H-NMR spectra of compounds **1** and **2** show three double double doublets corresponding to H-3, H-4 and H-5 (Figure 10). The furan hydrogen couples with neighboring hydrogen atoms and shows a ddd splitting pattern due to its coupling with phosphorus atom at 4 to 5 bond distance (Figure 10). The *J* values at 298 K are shown in Table 5. The NMR spectrum of compound **2** also shows a multiplet at δ 3.03-3.18 for the –CH group coupled with the H_{ax} and H_{eq}. A multiplet integrated for 20 hydrogen atoms at δ 1.05-1.96 for the hydrogens of cyclohexyl coupled with neighboring hydrogen atoms was also observed. For the NH signal of compound **2** a two bond distance coupling with the P atom and a two bond distance coupling with –CH of cyclohexyl were observed. A triplet signal at δ 2.64 is obtained for NH with $^{2}J_{P,NH} \approx {}^{2}J_{NH,CH} \approx 10$ Hz, a value similar to that described in the literature [25]. The ^{1}H NMR spectrum of **1** displays two doublets at δ 1.29 and 1.34 integrated for 6 hydrogen atoms each ($^{2}J_{CH3,CH}$ =

6.9 Hz) for the two types of CH_3 groups of the isopropyl moieties due to the fact that the carbon atom of the CH group in the isopropyl substituent is prochiral. The methine hydrogen of the isopropyl groups appears as a double septet at δ 3.63 and 3.69 integrated for 2 hydrogens ($^3J_{P,\ CH}$ = 24.3 Hz) due to its coupling with the methyl groups and the phosphorus atom. This analysis indicates that the rotational energy barrier around the C-N and P-N bonds must be low, consistent with the equivalent chemical shifts shown by the isopropyl moieties on the NMR timescale.

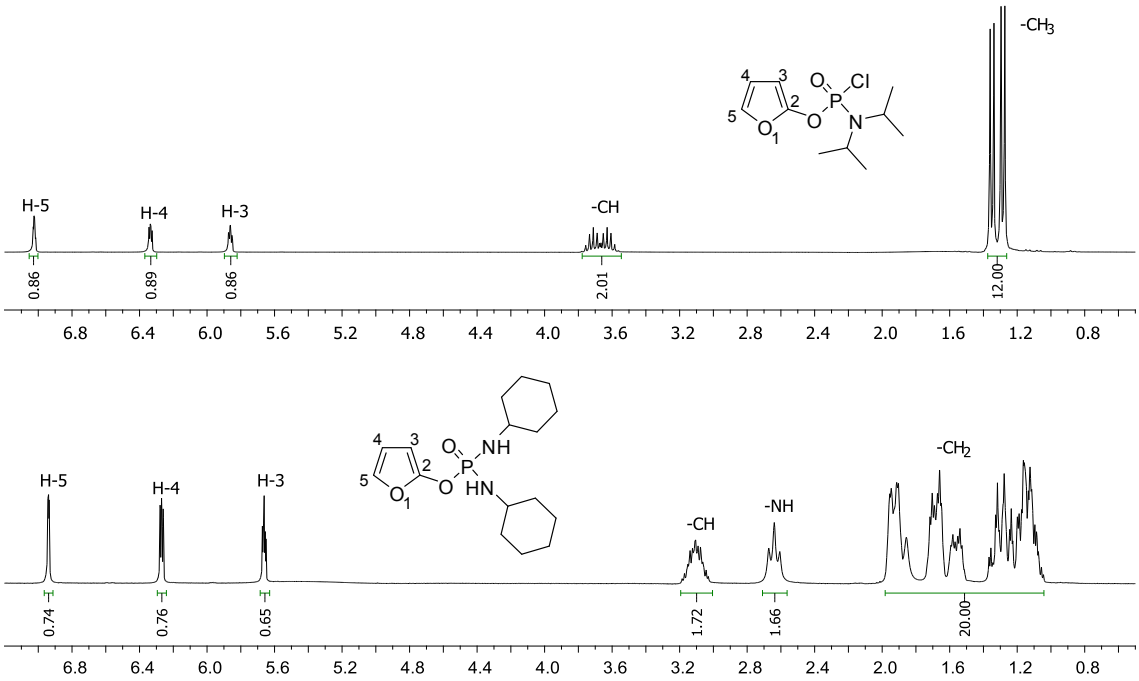

Figure 10 - The ^{1}H NMR spectra of compounds **1** and **2** at 298 K in $CDCl_3$.

The ^{13}C NMR spectra of compounds **1** and **2** show three doublets (δ89, 111 and 135, respectively) due to carbon atoms C-3, C-4 and C-5 (Figure 11). The signal multiplicities are due to carbon coupling with phosphorus atom at a distance of 3-4 bonds. Curiously, lower $J_{P,C}$ were obtained for compound **2** (Table 5) than for compound **1**. The quaternary carbon atoms of compounds **1** and **2**, C-2 (Figure 11), are coupled to phosphorus at δ 149-152 ($^2J_{P,C}$ = 6.5 and 5.1 Hz, respectively). For both compounds couplings at long distances were observed, but $^2J_{P,CH}$ coupling was not observed for compound **2**. A similar behavior was observed for the phosphoramidates described by Souza et al. (2006) [45]. The ^{13}C spectrum of compound **1** shows distinct signals for the diastereotopic methyl carbon atoms which appeared as doublets ($^3J_{CH3,P}$ = 2.5

and 1.6 Hz) due to $^{3}J_{PNC}$ coupling, whereas the methine carbon atom doublet shows larger $^{2}J_{PNC}$ coupling ($^{2}J_{CH,P}$ = 4.9 Hz). The ^{13}C NMR spectrum of compound **2** exhibits three signals for the ten carbon atoms of the $–CH_2$ cyclohexyl moieties. These results indicate that the spatial orientations of the aliphatic six-membered rings are the same. A ($^{3}J_{P,CH2}$) coupling constant of 5.4 Hz was observed for the splitting of the -CH_2 carbon atom with the phosphorus atom. The spectrum observed in this experiment for compound **1** was found to correspond to that of a racemic mixture, whose evidence appeared only in structure determination by X-ray (Figure 3).

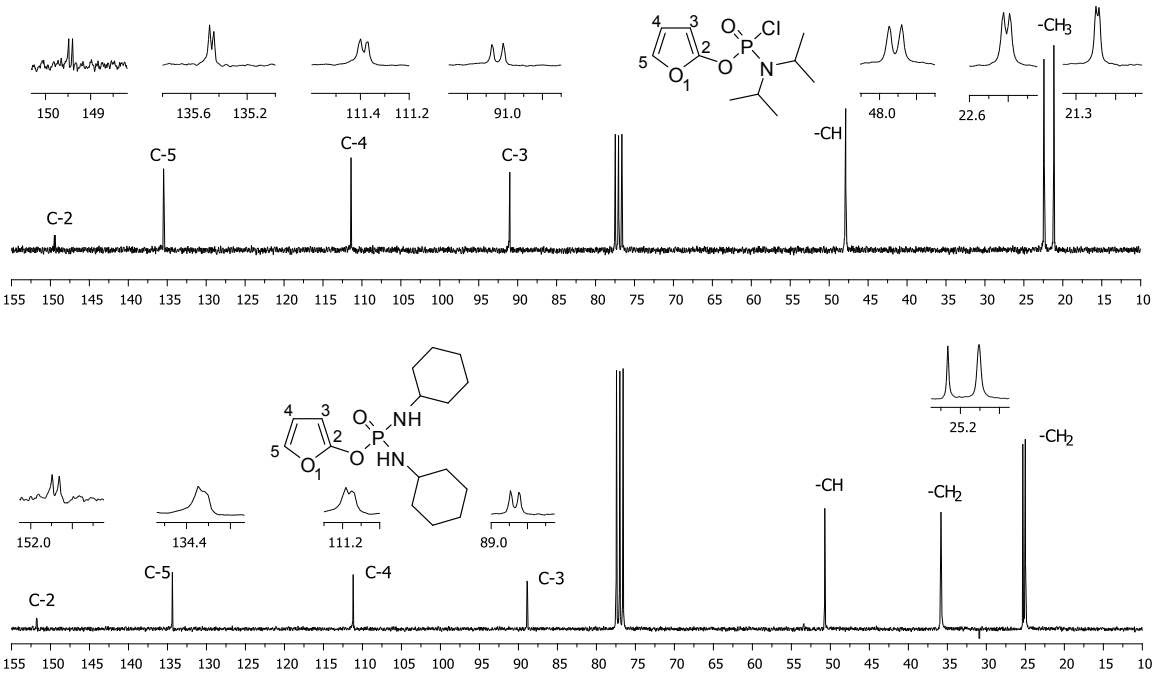

Figure 11 - The ^{13}C NMR spectra of the compounds **1** and **2** at 298 K in $CDCl_3$.

Table 5. Selected coupling constant at 298 K of compounds **1** and **2**.

Compound	$^{4}J_{H3,P}$	$^{5}J_{H4,P}$	$^{5}J_{H5,P}$	$^{3}J_{C3,P}$	$^{4}J_{C4,P}$	$^{4}J_{C5,P}$
1	1.2	0.9	0.9	4.4	2.1	2.2
2	1.2	0.3	0.6	3.5	1.2	1.2

An important point in the discussion of the equilibrium geometries of the phosphoramidates is the activation barrier for rotation around the C-N and P-N bonds. From the analysis of a molecular model, a 180º rotation around the P-N bond, followed by a 180º rotation around each C-N bonds, results in the

equivalence of the two isopropyl groups. With this in mind, we carried out a NMR variable temperature study for compound **1**. The results allowed calculation of the higher free energy barrier for rotation, but would not allow us to know which bond (C-N or P-N) correspond to the experimental data. From the temperature of coalescence of the hydrogen lines the first-order rate constant ($k_{coalescence}$) was calculated from the expression $k_{coalescence} = \pi(\Delta\nu^2 + 6J^2)^{1/2}/(2^{1/2})$ where $\Delta\nu$ is the difference in chemical shift between the centers of the two doublets arising from the methyl hydrogens, and *J* is the coupling constant. From the ^{13}C NMR and the coalescence temperature, the rate constant is related to the chemical shift difference from the expression $k_{coalescence} = \pi(\Delta\nu)/(2^{1/2})$ where $\Delta\nu$ is the difference in chemical shift. Substituting this value into the Eyring rate equation gives the expression $\Delta G^{\ddagger} = RTln(6.62x10^{12}/k_{coalescence})$ [46]. For comparison, the value of the free energy barrier was calculated from the coalescence of the resonances and by theoretical methods.

The behavior of **1** was monitored by ^1H-NMR techniques at variable temperatures. From the data, the relevant thermodynamic parameters were calculated. To examine their behavior, the NMR tube containing compound **1** was placed in the NMR probe and cold slowly from 298 K to 178 K.

The determination of the exact temperature inside the sample is crucial for the determination of the thermodynamic parameters. An error of ± 2 °C in the temperature causes an error in $\Delta G^{\#}$ of 0.15 to 0.2 kcal mol^{-1} and this is usually the main source of errors in the dynamic NMR technique [47]. Therefore, the coalescence temperature was determined by performing several ^1H NMR experiments (Figures 12 and 13).

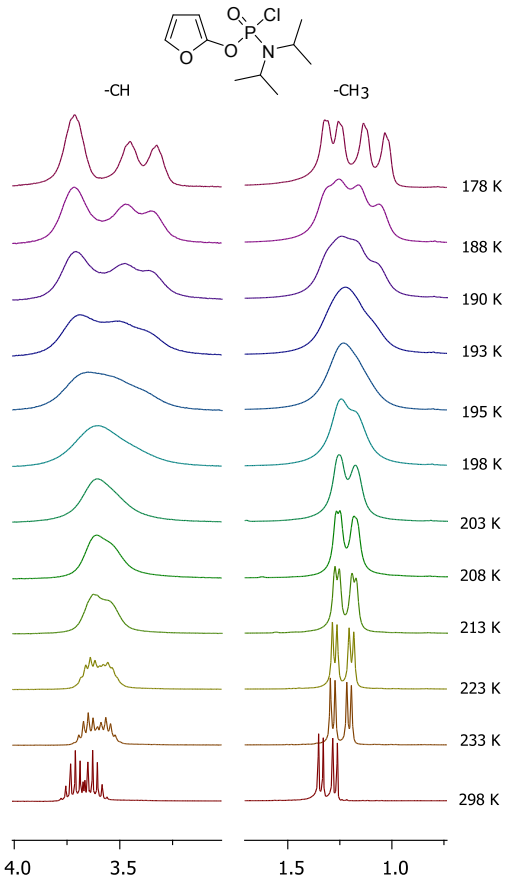

Figure 12 - The variable temperature ^{1}H NMR spectra of **1** from 298 to 178 K in CD_2Cl_2.

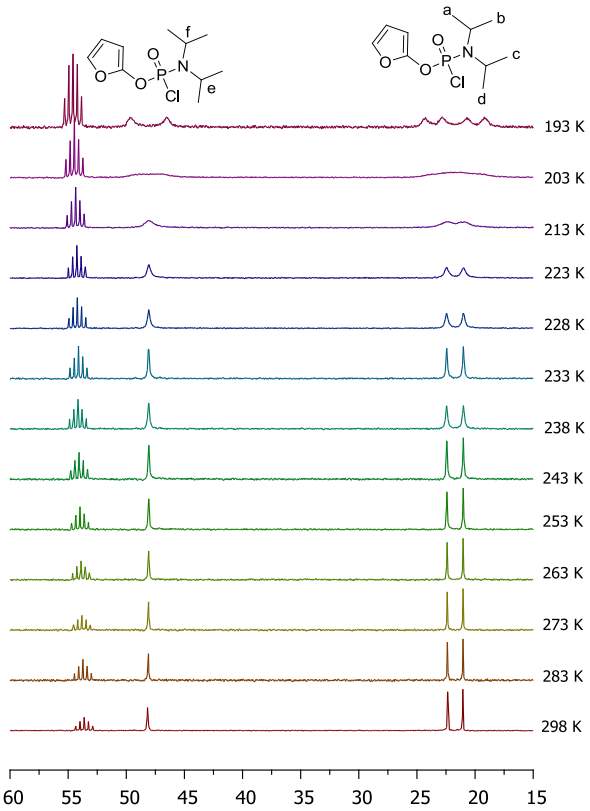

Figure 13 - The variable temperature ^{13}C NMR spectra of **1** from 298 to 193 K in CD_2Cl_2.

For compound **1**, two separate doublets appeared in the ^{1}H-NMR spectrum at 298 K for the methyl carbons of the isopropyl groups since they are diastereotopic. In this condition there is a free rotation of the C-N and P-N single bonds so that the isopropyl groups become equivalent. Also, in the ^{13}C NMR spectrum of **1** at this temperature, two signals (Figure 13: a = c ≠ b = d and Scheme 2) are observed for the methyl carbons of the isopropyl groups. At low-temperature (< 195K), ^{1}H and ^{13}C NMR spectra of compound **1** show signals for two diastereotopic isopropyl groups. Therefore, four signals are observed for the methyl carbons (Figure 13: a ≠ c ≠ b ≠ d and Scheme 2) and two signals for –CH (Figure 13: e ≠ f and Scheme 2).

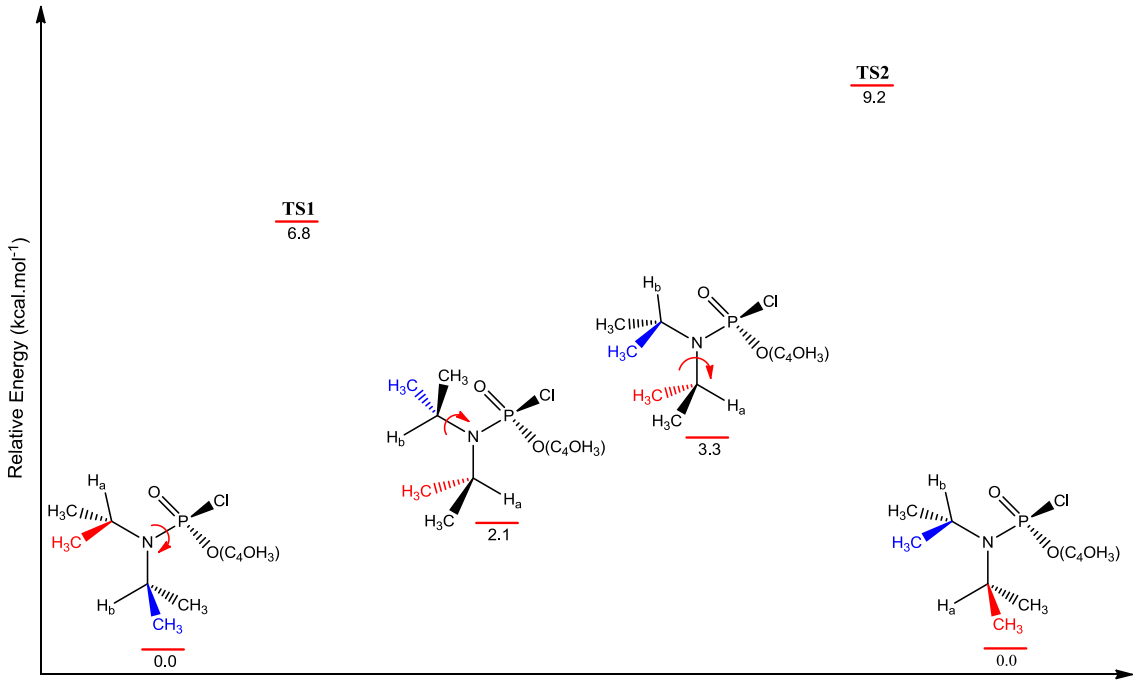

Scheme 2 - Interchangeable processes of compound **1** at 298K.

The collected ^{1}H NMR spectra relevant to the dynamic effect are shown in the following variable-temperature NMR (Figures 12 and 13).

The coalescence temperature was eventually observed at T_C = 195 K in ^{1}H NMR, and the higher activation energy ($\Delta G^{\#}$) for rotation around the C-N and P-N single bonds was calculated as 9.9 ± 0.3 kcal mol^{-1}. From this experiment we cannot attribute calculated value to $\Delta G^{\#}$ for rotation of C-N or P-N. So, in order to better understand this process, a molecular computational analysis was carried out.

7.4.3. Computational analysis

To help rationalize the experimental findings, we carried out a set of calculations for phosphoramidates **1** and **2**. The most stable conformers of **1** and **2** were obtained using the semi-empirical PM3 method [37] in the Spartan software. The geometry of that conformations were then reoptimized using the B3LYP/6-311++G(2d,p) approach. Each optimized geometry was confirmed as a local minimum on the potential energy surface. Selected parameters of the most stable optimized geometries are compared with the X-ray diffraction data in Tables 2 and 3, which show that in general the experimental and computed parameters are in close agreement. The only cases that deserve some attention are the bond angles O1-P1-O2, C8-N1-C5 in **1** and O2-P1-N2 in **2**. The computed values for the O1–P1–O2 bond angles for compounds **1** and **2** are 115.70 and 116.18(^{o}), respectively. The corresponding experimental bond angles are 110(4)(^{o}) and 113(2)(^{o}). For the C8–N1–C5 bond angle in **1** the difference between the experimental and theoretical values is a bit larger, amounting to 6.9^o. For the O2-P1-N2 bond angle in **2** the corresponding difference is 5.7^o.

In addition to the determination of the most stable geometry for each phosphoramidate we also calculated the approximated activation energy for rotation around the P-N and C-N single bonds for **1**. The goal was to identify whether the activation parameters determined in the dynamic NMR studies are consistent with activation energies for rotation around these bonds.

The dynamic process represented in Scheme 2 is enough to interconvert the pairs of diastereotopic isopropyl groups, however, to completely equilibrate the four methyl groups (a, b, c and d in Scheme 2) we have also to consider rotation around the C-N bonds. To determine the activation parameter in each case we performed a set of calculations with the dihedral angle involving both the P-N and the C-N bonds fixed at a given value and optimization of the additional degree of freedom. Starting from 0^o the dihedral angle was increased by a 30^o step in each case up to the value of 330^o. With this, we could not only confirm the structure of minimal energy but also determine the transition structure for rotation around the corresponding bond. The B3LYP/6-31G(d) approach was employed for these calculations.

Rotation around the P-N bond revealed two minima, the global minimum energy structure, with one of the C-N bonds eclipsing the phosphoryl P=O bond and a local minimum energy structure with the lone pair on the nitrogen atom eclipsing the P-Cl bond, 2.1 kcal.mol^{-1} less stable than the global minimum. The activation energy for interconversion between these two minima is 6.8 kcal mol^{-1} (TS1). On the other hand, rotation around each of the C-N bond also revealed two minima, the global minimum energy structure and a second one, 3.3 kcal mol^{-1} above the global minimum. The activation barrier for rotation around the C-N bond is 9.2 kcal mol^{-1} (TS2). The last value closely fits the experimental 9.9±0.3 kcal mol^{-1} obtained by dynamic NMR studies. Based on these results we are suggesting that the dynamic behaviour in these phosphoramidates is characterized by rotation around both the P-N and the C-N bonds, with activation energy for rotation around the C-N bonds being the higher value. According to Scheme 2 rotation around the P-N bond interchanges the isopropyl groups but not the methyl groups within each isopropyl groups. Complete equilibration of the methyl groups occurs only after rotation around the C-N bond, which is the process with the higher activation energy.

7.5. Conclusion

In an effort to prepare new compounds with potential biological activity and rationalize their molecular properties, two phosphoramidates have been studied by dynamic NMR, theoretical calculation, spectroscopic data and X-ray crystallography. Compound **1** is a chiral molecule crystallized in a centrosymmetric space group as an equimolar mixture of a pair of enantiomers (*R/S*: 50/50). Geometrical parameters calculated with DFT methods are consistent with the experimental X-ray data. The dynamic behavior of **1** was investigated by NMR spectroscopy, which revealed the activation energy of 9.9 ± 0.3 kcal mol^{-1}. Based on computational calculation of the activation energies for rotation around the P-N and C-N bonds, this experimental value was attributed to the C-N bond.

7.6. Acknowledgments

We thank Conselho Nacional de Desenvolvimento Científico e Tecnológico (CNPq), Fundação de Amparo à Pesquisa do Estado de Minas Gerais (FAPEMIG) and Fundação Arthur Bernardes (FUNARBE) for financial support and research fellowships (ACF, AJD, JWMC, ACD, LCAB,SAF and FMO). We thank Prof. Javier Ellena for support during the single-crystal diffraction measurements.

7.7. References

[1] M.J. Dominguez, C. Sanmartin, M. Font, J.A. Palop, S.S. Francisco, O. Urrutia, F.Houdusse, J.M. Garcia-Mina, J. Agric. Food Chem., 56 (2008) 3721-3731.

[2] V.F. Paula, L.C.A. Barbosa, R.R. Teixeira, M.C. Picanço, G.A. Silva, Pest Manag. Sci., 64 (2008) 863-872.

[3] F.M. Oliveira, L.C.A. Barbosa, R.R. Teixeira, A.J. Demuner, C.R.A. Maltha, M.C. Picanço, G.A. Silva, V.F. Paula, J. Pestic Sci., 37 (2012) 85-88.

[4] T. Katagi, J. Agric. Food Chem., 41 (1999) 496-501.

[5] Y.B. Kiran, C.D. Reddy, D. Gunasekar, C.N. Raju, L.C.A. Barbosa, D.C.O. Marney, L.J. Russell, J. Fire Sci., 25 (2007) 193-215.

[6] Y.B. Kiran, C.D. Reddy, D. Gunasekar, C.S. Reddy, A. Leon, L.C.A. Barbosa, Eur. J. Med. Chem., 43 (2008) 885-892.

[7] D.I. Niculescu, I. Scanlon, D. Niculescu, F. Friedlos, J. Martin, R. Marais, C.J. Springer, J. Med. Chem., 47 (2004) 2651-2658.

[8] Z. Wang, C. Guo, W. Xie, C. Liu, C. Xiao, Z. Tan, Eur. J. Med. Chem., 45 (2010) 890-895.

[9] Y. Mehellou, J. Balzarini, C. McGuigan, Org. Biomol. Chem., 7 (2009) 2548-2553.

[10] I. Zlatev, A. Giraut, F. Morvan, P. Herdewijn, J. Vasseur, Bioorg. Med. Chem., 17 (2009) 7008-7014.

[11] C. McGuigan, M.R. Kelleher, P. Perrone, S. Mulready, G. Luoni, F. Daverio, S. Rajyaguru, S.L. Pogam, I. Najera, J.A. Martin, K. Klumpp, D.B. Smith, Bioorg. Med. Chem. Lett., 19 (2009) 4250-4254.

[12] M. Donghi, B. Attenni, C. Gardelli, A.D. Marco, F. Fiore, C. Giuliano, R. Laufer, J.F. Leone, V. Pucci, M. Rowley, F. Narjes, Bioorg. Med. Chem. Lett., 19 (2009) 1392-1395.

[13] C. Mara, E. Dempsey, A. Bell, J.W. Barlow, Bioorg. Med. Chem. Lett., 21 (2011) 6180-6183.

[14] J. Yan, J. Bu, X. Bai, J. Li, T. Ren, Y. Zhao, J. Engineering Tribology, 226 (2012) 377-388.

[15] K. Wittine, K. Benci, Z. Rajic, B. Zorc, M. Kralj, M. Marjanovic, K. Pavelic, E. De Clercq, G. Andrei, R. Snoeck, J. Balzarini, M. Mintas, Eur. J. Med. Chem., 44 (2009) 143-151.

[16] L.C.A. Barbosa, C.R.A. Maltha, A.J. Demuner, F.R. Ganen, A.A. Silva, Quim. Nova, 28 (2005) 444-450.

[17] L.C.A. Barbosa, A.J. Demuner, E.S. Alvarenga, A. Oliveira, B. King-Diaz, B. Lotina-Hennsen, Pest Manag. Sci., 62 (2006) 214-222.

[18] L.C.A. Barbosa, U.A. Pereira, R.R. Teixeira, C.R.A. Maltha, S.A. Fernandes, G. Forlani, J. Agric. Food Chem., 56 (2008) 9434-9440.

[19] L.C.A. Barbosa, C.R.A. Maltha, R.C. Cusati, R.R. Teixeira, F.F. Rodrigues, A. A. Silva, M.G.B. Drew, F.M.D. Ismail, J. Agric. Food Chem., 57 (2009) 10107-10115.

[20] R.S. Corrêa, S.R. Souza e Silva, L.P. Duarte, G.D.F. Silva, L.C.A. Barbosa, J. Ellena, A.C. Doriguetto, J. Struct. Chem., 53 (2012) 156-163.

[21] R.R. Teixeira, L.C.A. Barbosa, J.W.M. Carneiro, R.S. Corrêa, J. Ellena, A.C. Doriguetto, J. Mol. Struct., 917 (2009) 1–9.

[22] F.T. Martins, I. Campsa, A.C. Doriguetto, M.H. dos Santos, J. Ellena, L.C.A. Barbosa, Helv. Chim. Acta, 91 (2008) 1313-1324.

[23] R.R. Teixeira, L.C.A. Barbosa, J.O. Santana, D.P. Veloso, J. Ellena, A.C. Doriguetto, M.G.B. Drew, F.M.D. Ismail, J. Mol. Struct., 837 (2007) 197-205.

[24] K. Gholivand, C.O.D. Védova, M.F. Erben, H.R Mahzouni, Z. Shariatinia, S. Amiri, J. Mol. Struct., 874 (2008) 178-186.

[25] K. Gholivand, M. Pourayoubi, Z. Shariatinia, H. Mostaanzadeh, Polyhedron, 24 (2005) 655-662.

[26] K. Gholivand, H. Mostaanzadeh, T. Koval, M. Dusek, M.F. Erben, H. Stoeckli-Evans, C.O.D. Védova, Acta Cryst., B66 (2010) 441-450.

[27] K. Gholivand, F. Afshar, Z. Shariatinia, K. Zare, Struct. Chem., 21 (2010) 629-636.

[28] S. Dehghanpour, R. Welter, A.H. Barry, F. Tabasi, Spectrochim. Acta Part A, 75 (2010) 1236-1243.

[29] T.G. Peck, Y.H. Lai, Tetrahedron, 65 (2009) 3664-3667.

[30] K. Marjani, M. Mousavi, H.T. Nahzomic, O. Arazi, R. Jafari, Spectrochim. Acta Part A, 79 (2011) 1798-1802.

[31] Nonius, COLLECT. Nonius BV, Delft, The Netherlands, 1999.

[32] Z. Otwinowski, and W. Minor, Methods in Enzymology, (1997) Vol. 276, Macromolecular Crystallography, Part A, edited by C. W. Carter Jr & R. M. Sweet, pp. 307–326. New York: Academic Press.

[33] G.M. Sheldrick, Acta Cryst., A64 (2008) 112–122.

[34] L.J. Farrugia, J. Appl. Cryst., 30 (1997) 565.

[35] C.F. Macrae, P.R. Edgington, P. McCabe, E. Pidcock, G.P. Shields, R. Taylor, M. Towler, and J. van de Streek, J. Appl. Cryst., 39 (2006) 453–457.

[36] Spartan ’10, Wavefunction Inc., Irvine, CA, USA.

[37] J.J.P.J. Stewart, Comput. Chem., 10 (1989) 221-264

[38] A.D. Becke, Phys. Rev. A, 38 (1988) 3098-3100.

[39] C. Lee, W. Yang, R.G. Parr, Phys. Rev. B, 37 (1988) 785-789.

[40] M.J. Frisch, G.W. Trucks, H.B. Schlegel, G.E. Scuseria, M.A. Robb, J.R. heeseman, G. Scalmani, V. Barone, B. Mennucci, G.A. Petersson, H. Nakatsuji, M. Caricato, X. Li, H.P. Hratchian, A.F. Izmaylov, J. Bloino, G. Zheng, J.L. Sonnenberg, M. Hada, M. Ehara, K. Toyota, R. Fukuda, J. Hasegawa, M. Ishida, T. Nakajima, Y. Honda, O. Kitao, H. Nakai, T. Vreven, J.A. Montgomery, Jr., J.E. Peralta, F. Ogliaro, M. Bearpark, J.J. Heyd, E. Brothers, K.N. Kudin, V.N. Staroverov, R. Kobayashi, J. Normand, K. Raghavachari, A. Rendell, J.C. Burant, S.S. Iyengar, J. Tomasi, M. Cossi, N. Rega, J.M. Millam, M. Klene, J.E. Knox, J.B. Cross, V. Bakken, C. Adamo, J. Jaramillo, R. Gomperts, R.E. Stratmann, O. Yazyev, A.J. Austin, R. Cammi, C. Pomelli, J.W. Ochterski, R.L. Martin, K. Morokuma, V.G. Zakrzewski, G.A. Voth, P. Salvador, J.J. Dannenberg, S. Dapprich, A.D. Daniels, Ö. Farkas, J.B. Foresman, J.V. Ortiz, J. Cioslowski, D.J. Fox, Gaussian 09, Revision A1, Gaussian Inc., Wallingford CT, 2009.

[41] I.J. Bruno, J.C. Cole, M. Kessler, J. Luo, W.D.S. Motherwell, L.H. Purkis, B.R. Smith, R. Taylor, R.I. Cooper, S.E. Harris, and A.G. Orpen, J. Chem. Inf. Comput. Sci., 44 (2004) 2133–2144.

[42] F.H. Allen, Acta Cryst., B58 (2002) 380–388.

[43] G.R. Desiraju, and R. Parthasarathy, J. Am. Chem., 111 (1989) 8725-8726.

[44] A. Domenicano, A. Vaciago, and C.A. Coulson, Acta Cryst., B31 (1975) 221-234.

[45] M.C. de Souza, W.P. de Macedo, T.S. Torres, L.F. Pedrosa, H.G. Alt, Phosphorus, Sulfur, and Silicon and the Related Elements, 181 (2006) 1885-1893.

[46] E. Breitmaier, W. Voelter, ^{13}C NMR Spectroscopy, 3nd ed., Verlag Chemie, Weinheim, New York, 1987.

[47] B.F. Bonini, L. Grossi, L. Lunazzi, D. Macciantelli, J. Org. Chem., 51 (1986) 517-522.

8. ANEXO

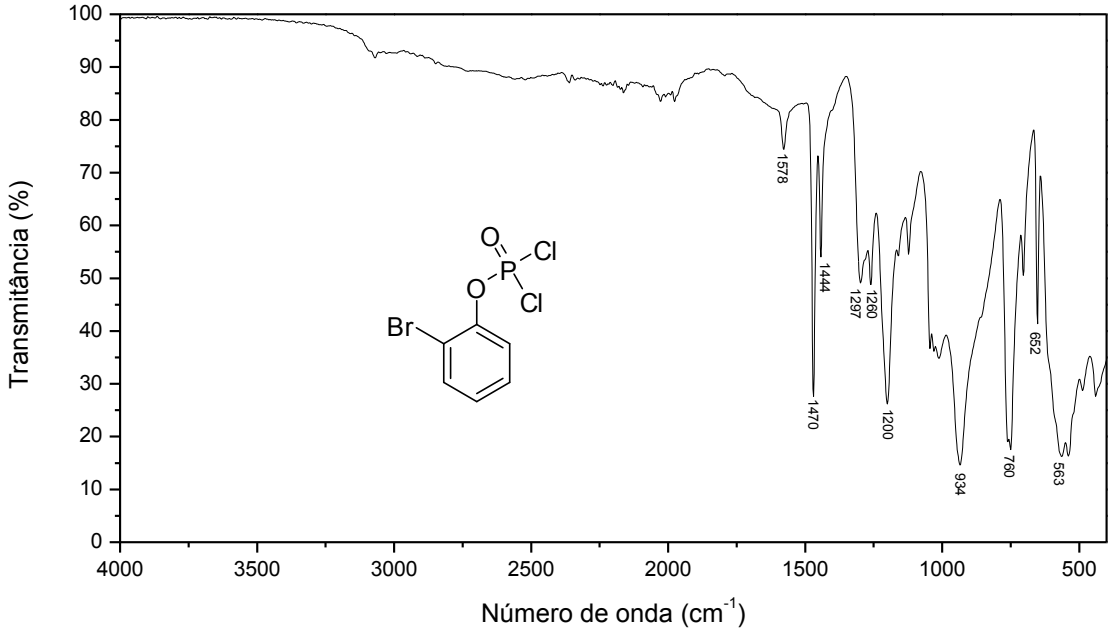

Figura 1 - Espectro no IV do diclorado **63**.

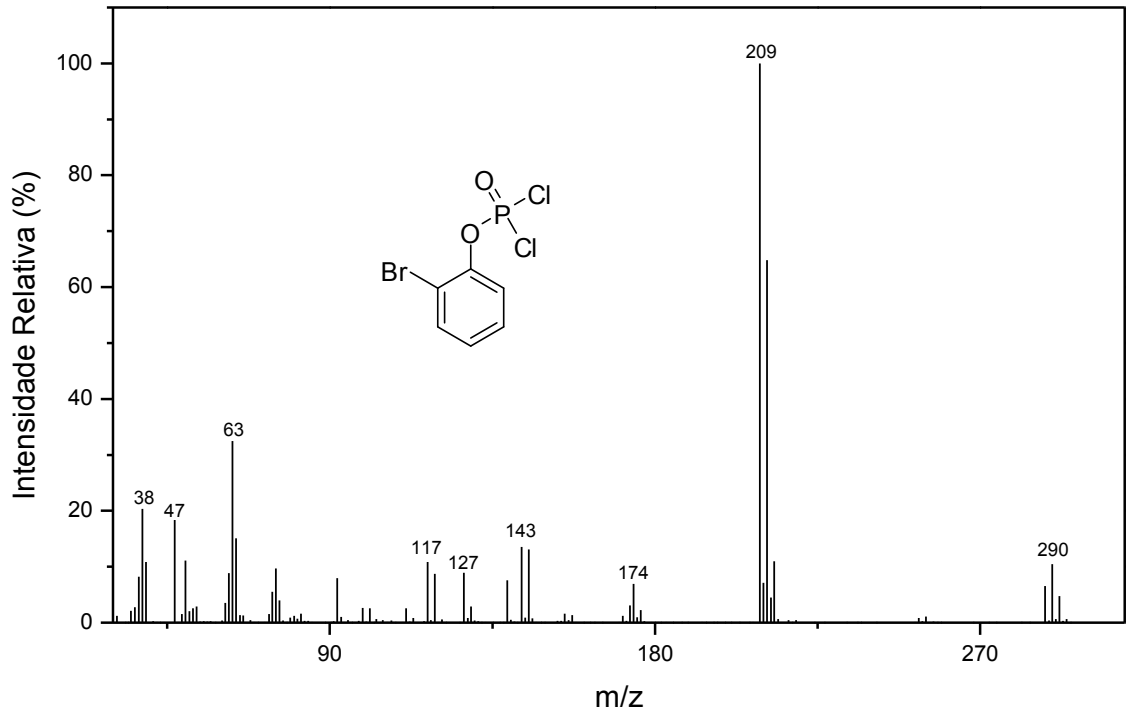

Figura 2 - Espectro de massas do diclorado **63**.

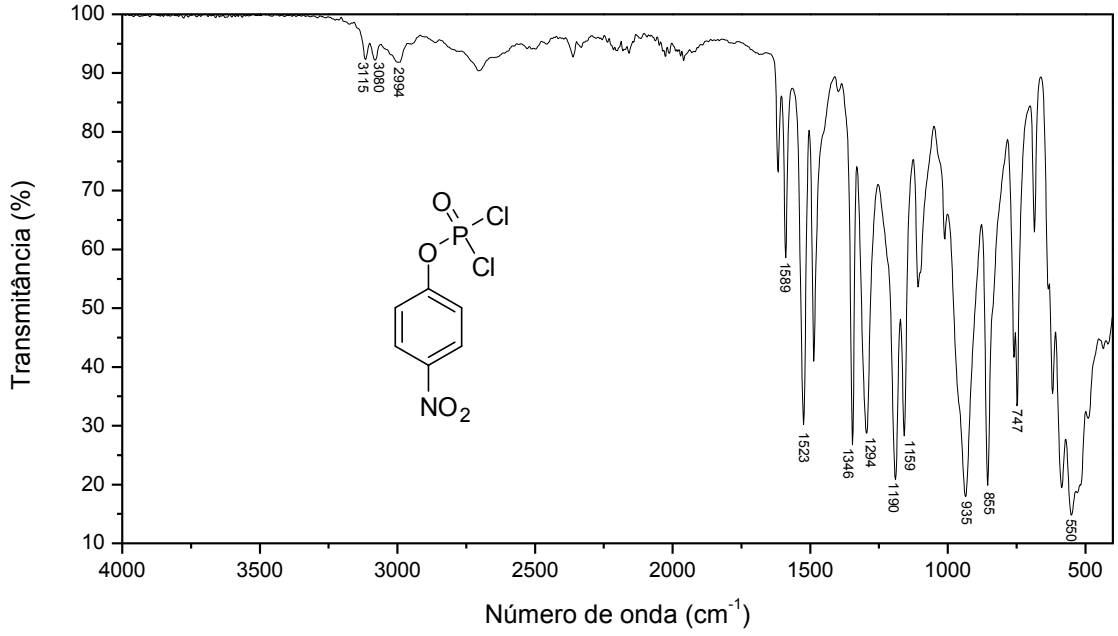

Figura 3 - Espectro no IV do diclorado **64**.

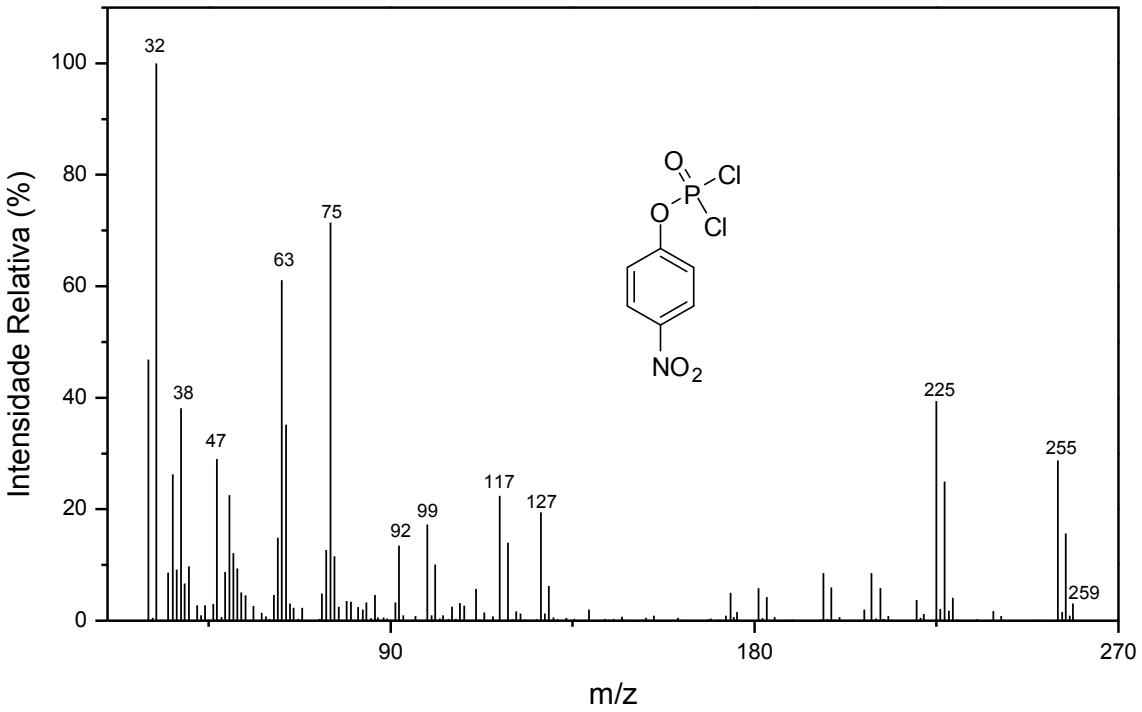

Figura 4 - Espectro de massas do diclorado **64**.

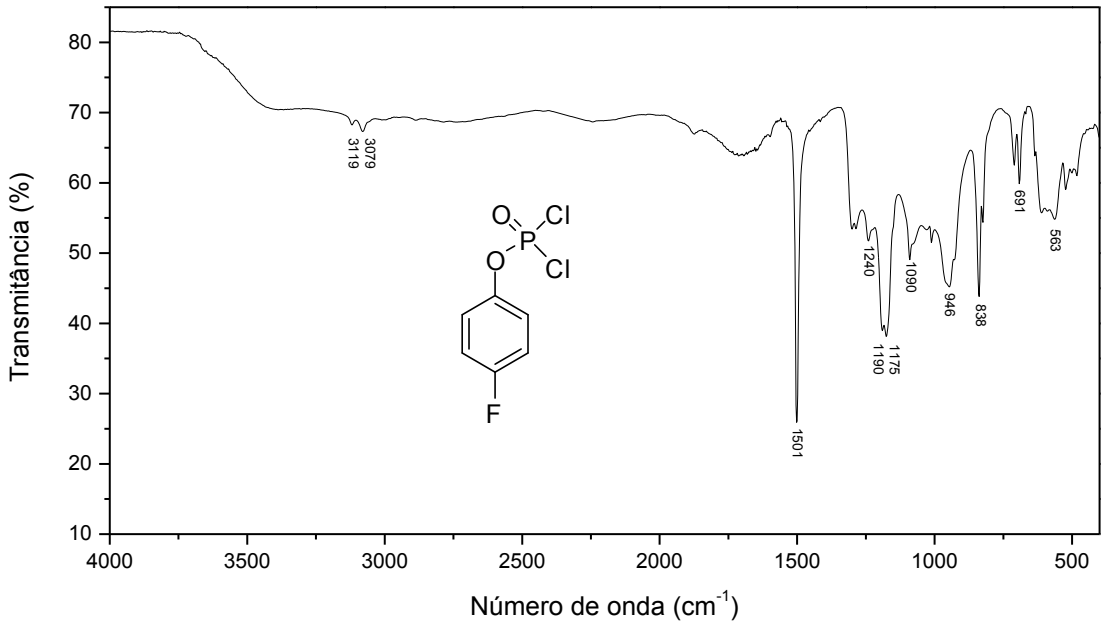

Figura 5 - Espectro no IV do diclorado **65**.

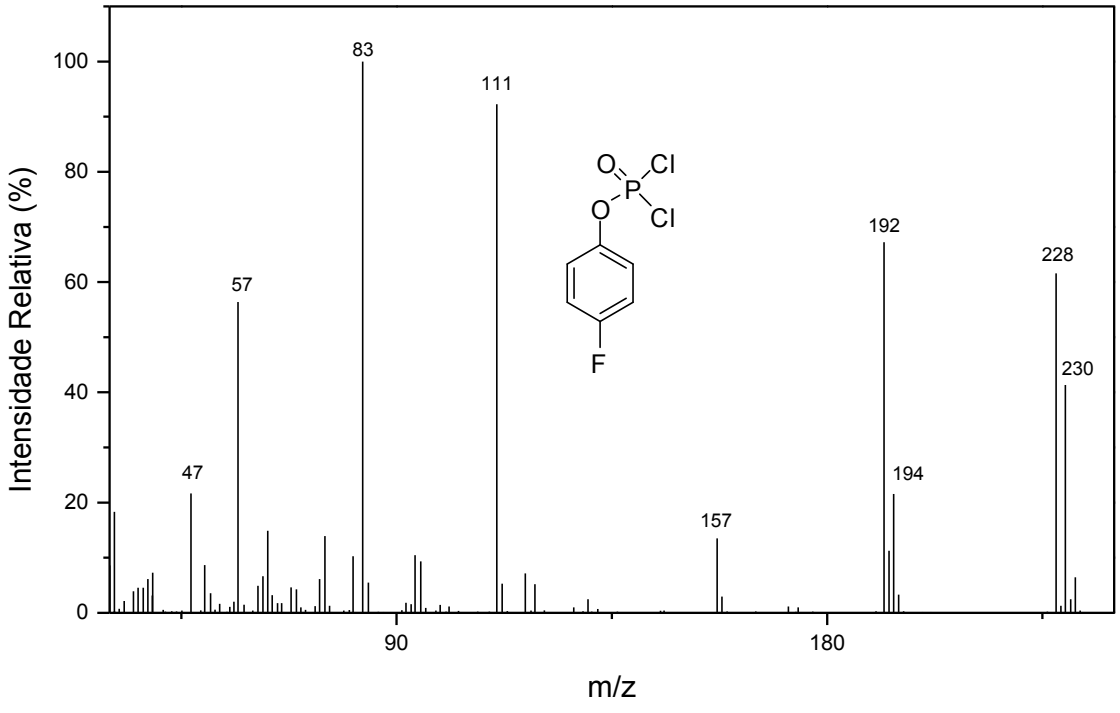

Figura 6 - Espectro de massas do diclorado **65**.

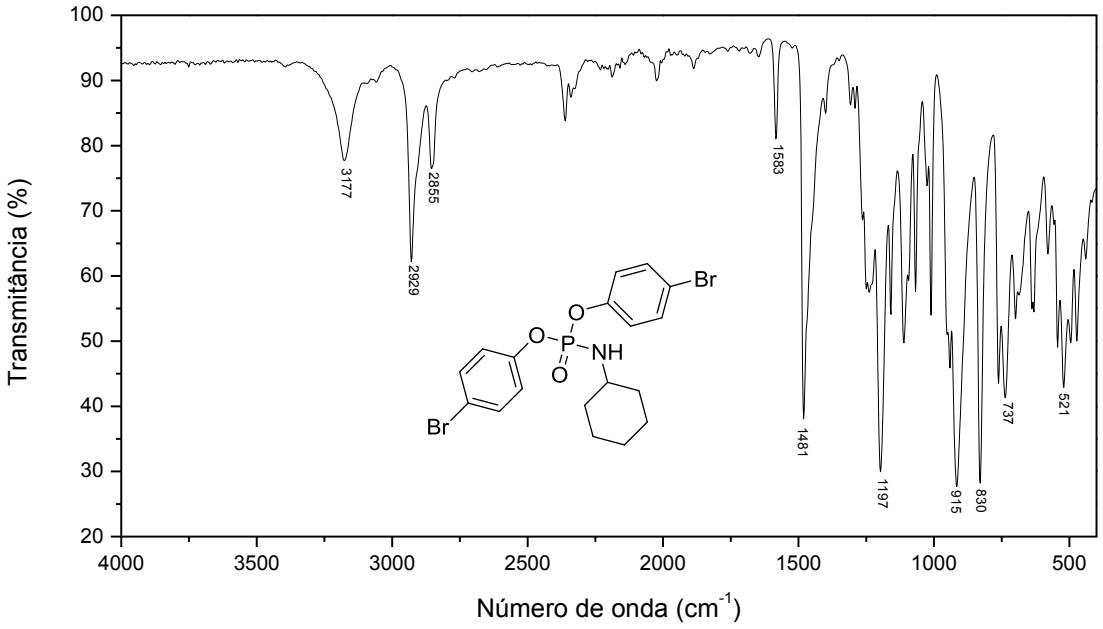

Figura 7 - Espectro no IV do composto **67**.

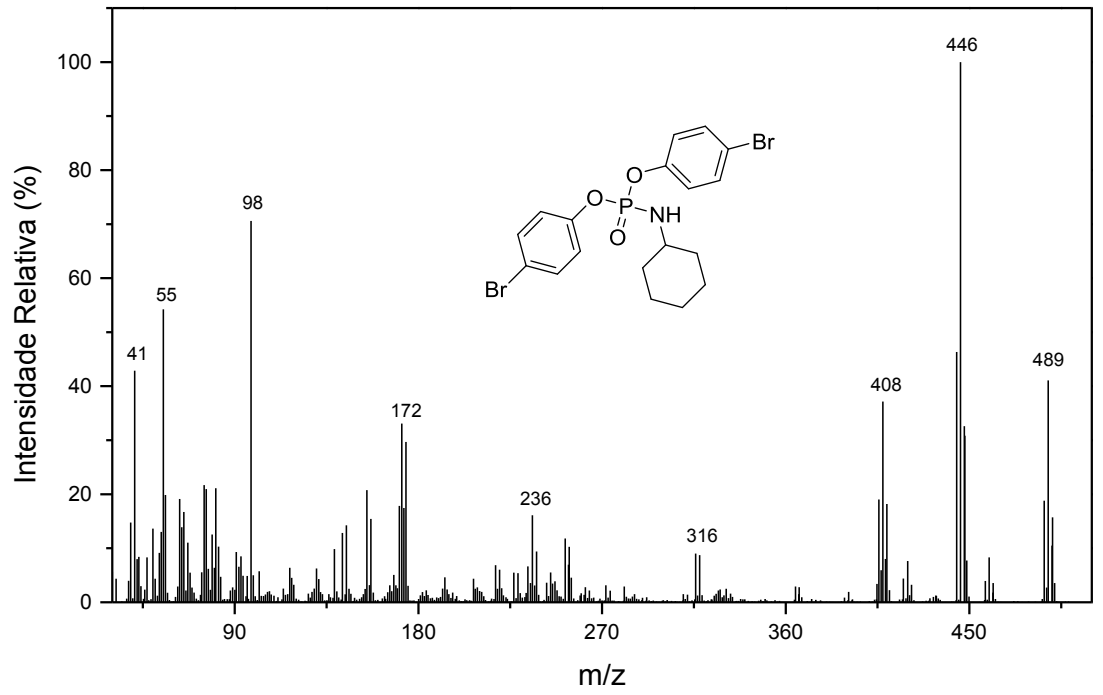

Figura 8 - Espectro de massas do composto **67**.

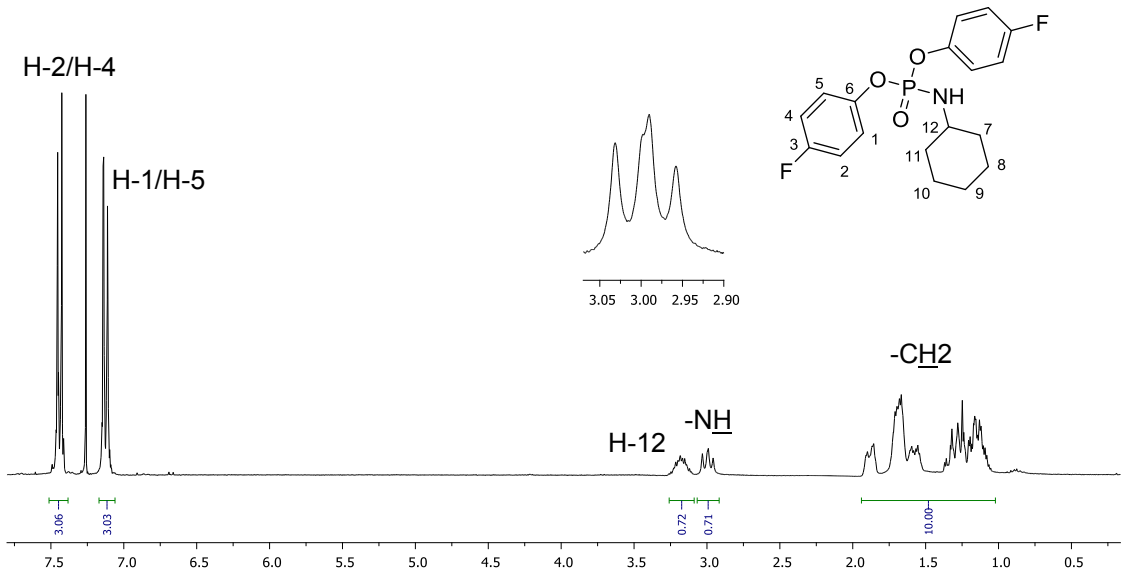

Figura 9 – Espectro de RMN de ^{1}H (300 MHz, $CDCl_3$) do composto **67**.

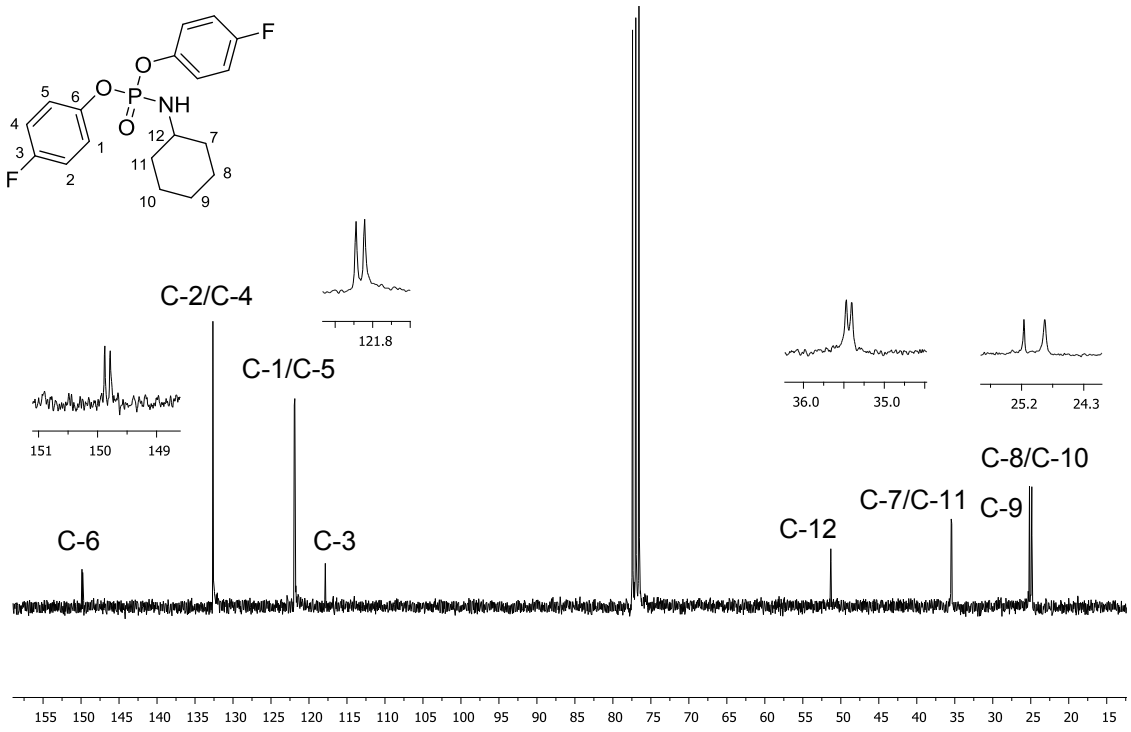

Figura 10 - Espectro de RMN de ^{13}C (75 MHz, $CDCl_3$) do composto **67**.

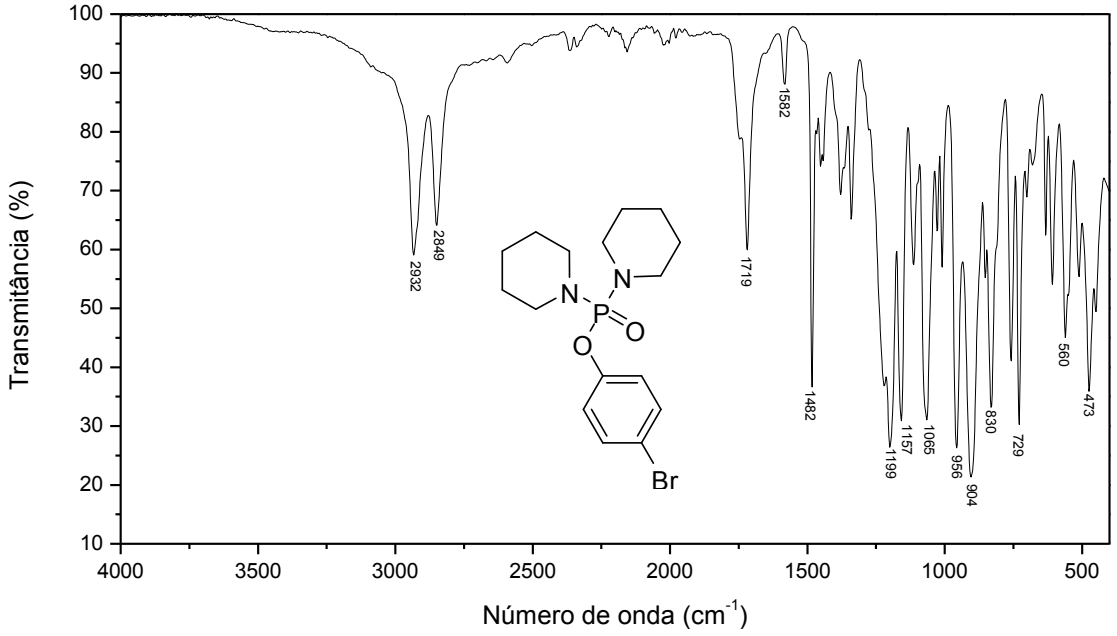

Figura 11 - Espectro no IV do composto **68**.

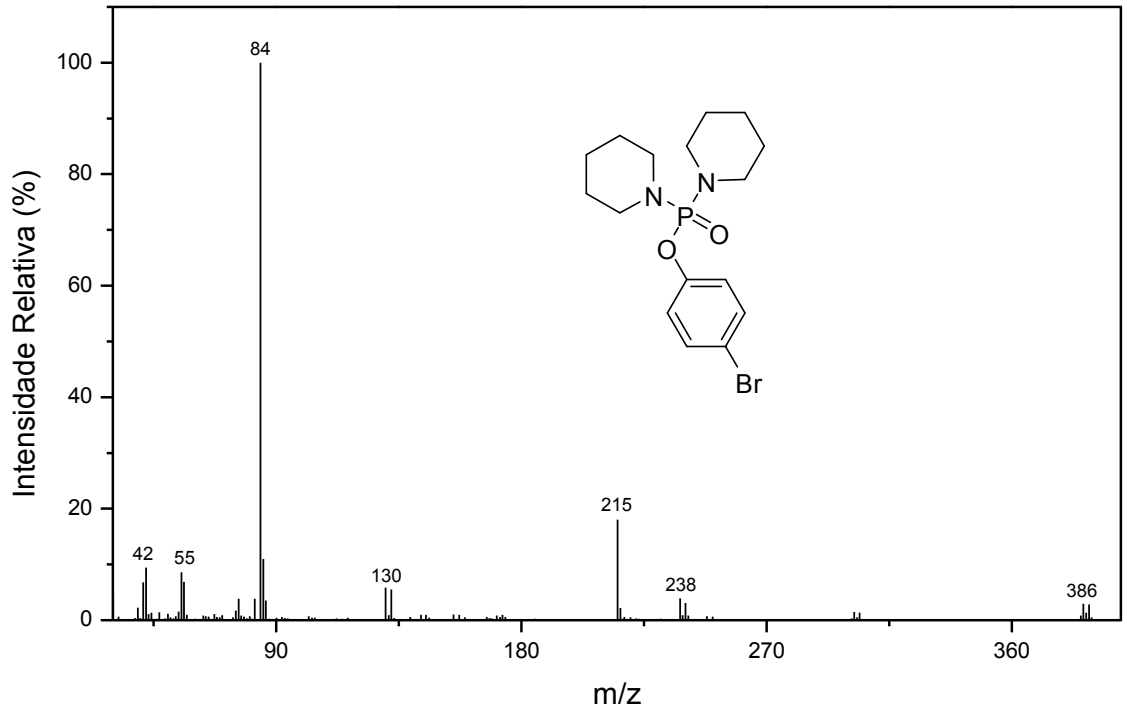

Figura 12 - Espectro de massas do composto **68**.

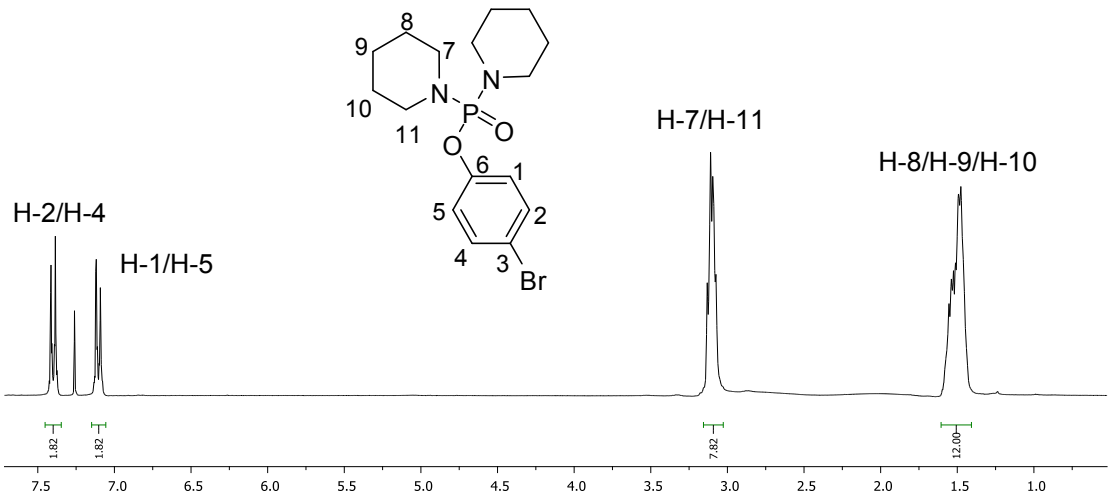

Figura 13 – Espectro de RMN de ^{1}H (300 MHz, $CDCl_3$) do composto **68**.

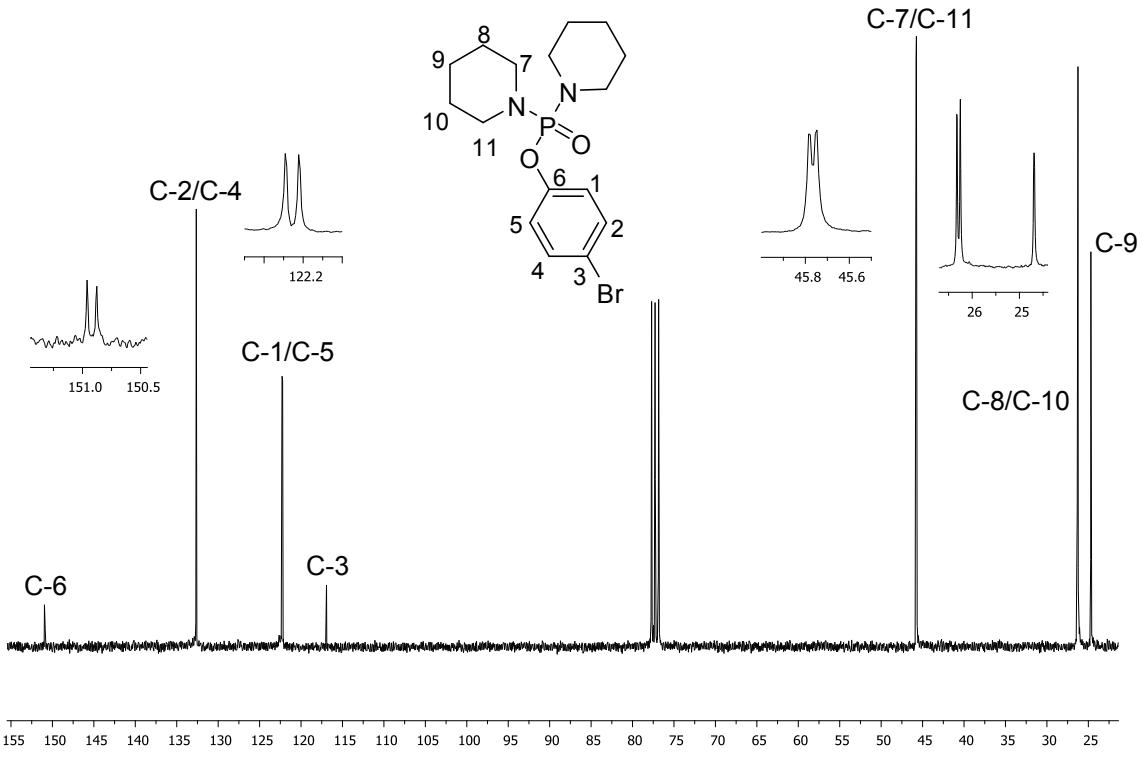

Figura 14 - Espectro de RMN de ^{13}C (75 MHz, $CDCl_3$) do composto **68**.

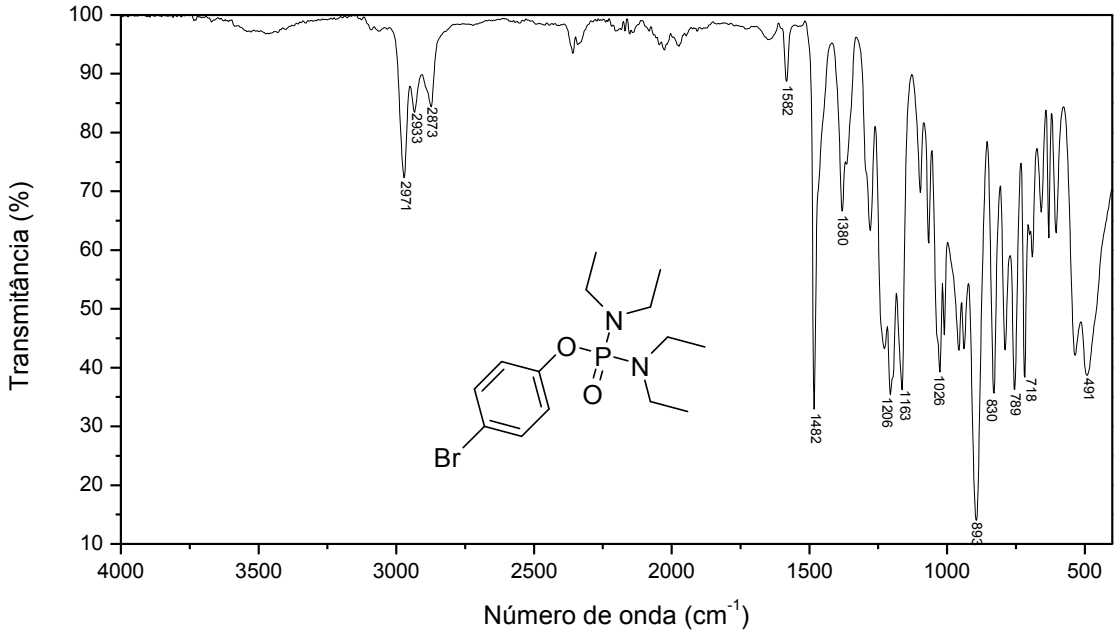

Figura 15 - Espectro no IV do composto **69**.

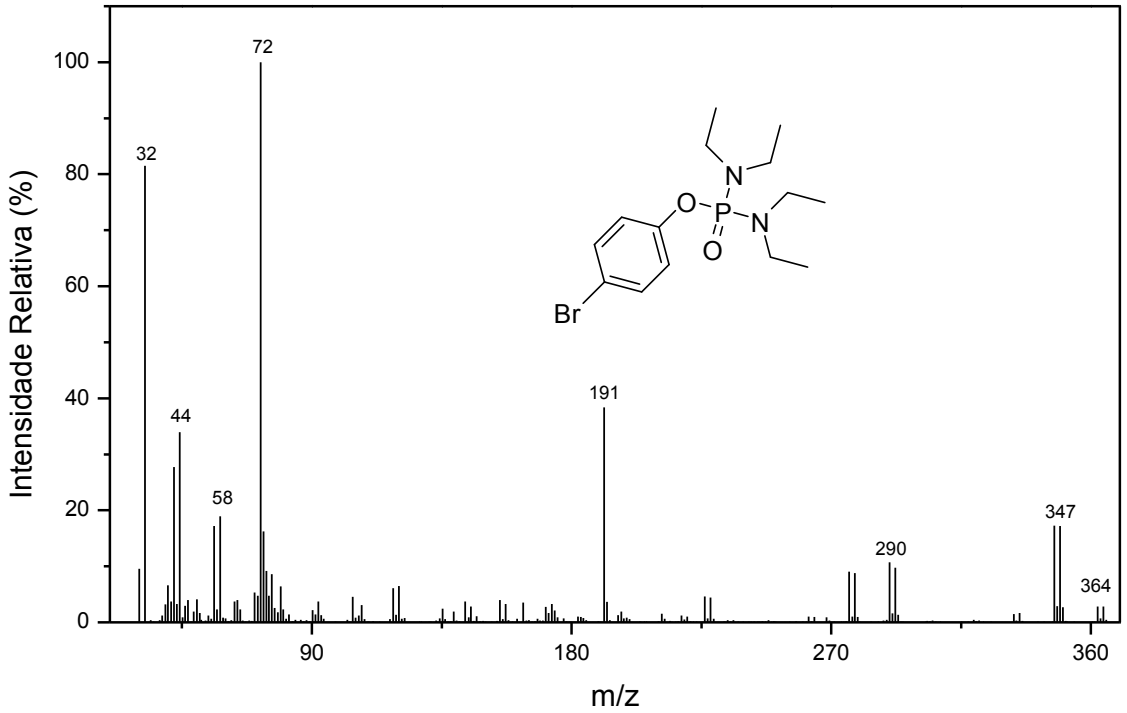

Figura 16 - Espectro de massas do composto **69**.

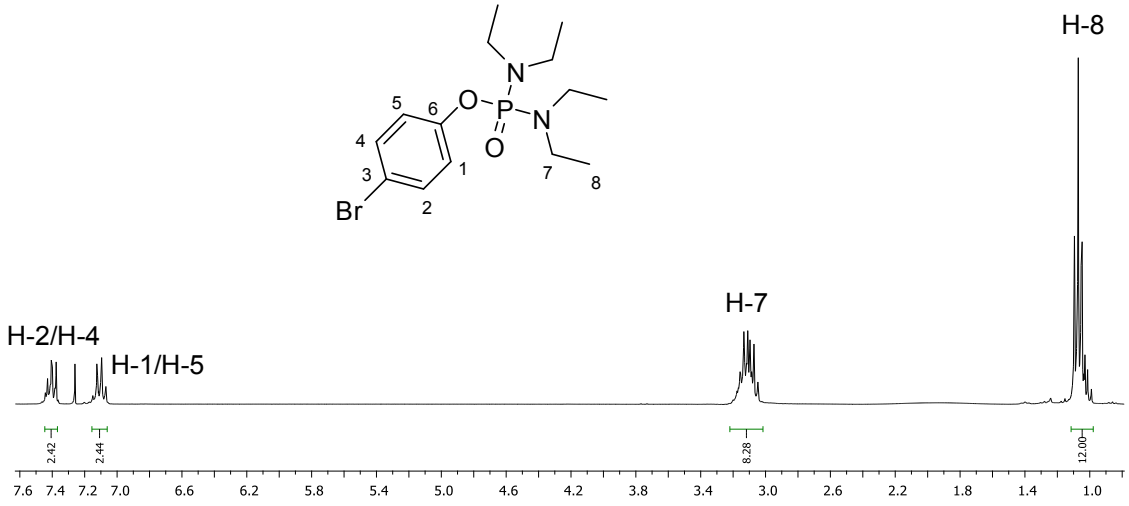

Figura 17 – Espectro de RMN de ^{1}H (300 MHz, $CDCl_3$) do composto **69**.

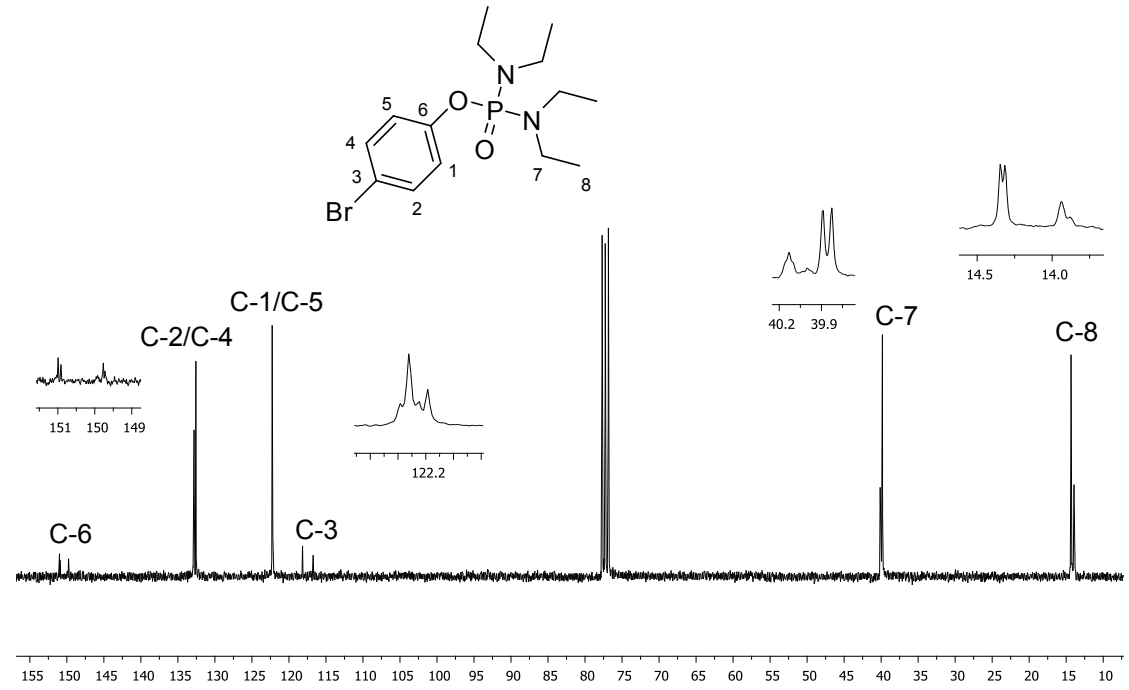

Figura 18 - Espectro de RMN de ^{13}C (75 MHz, $CDCl_3$) do composto **69**.

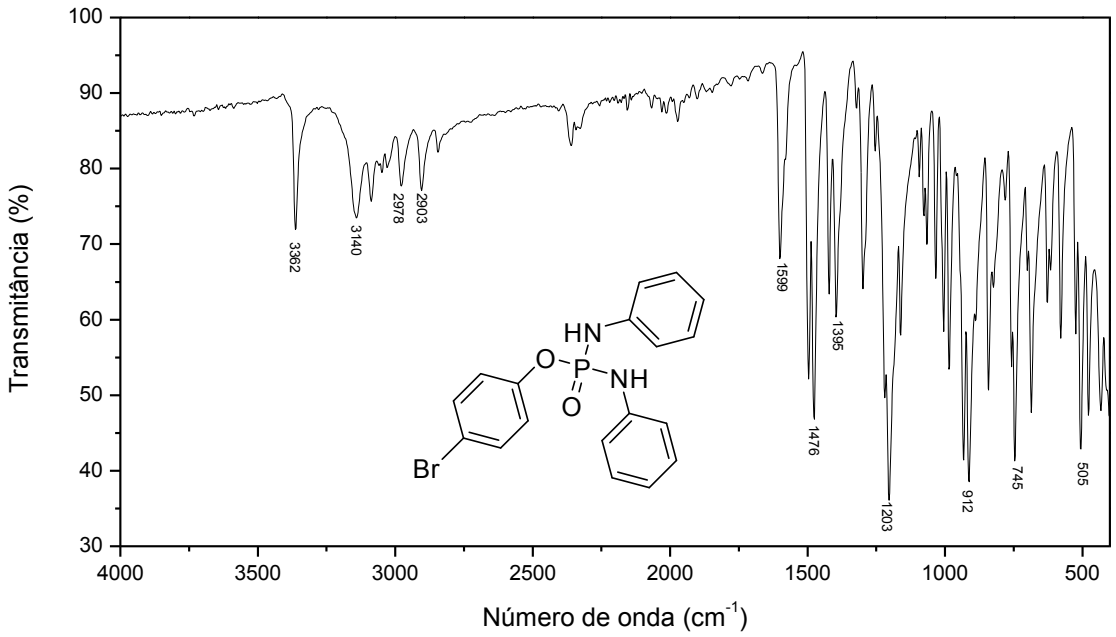

Figura 19 - Espectro no IV do composto **70**.

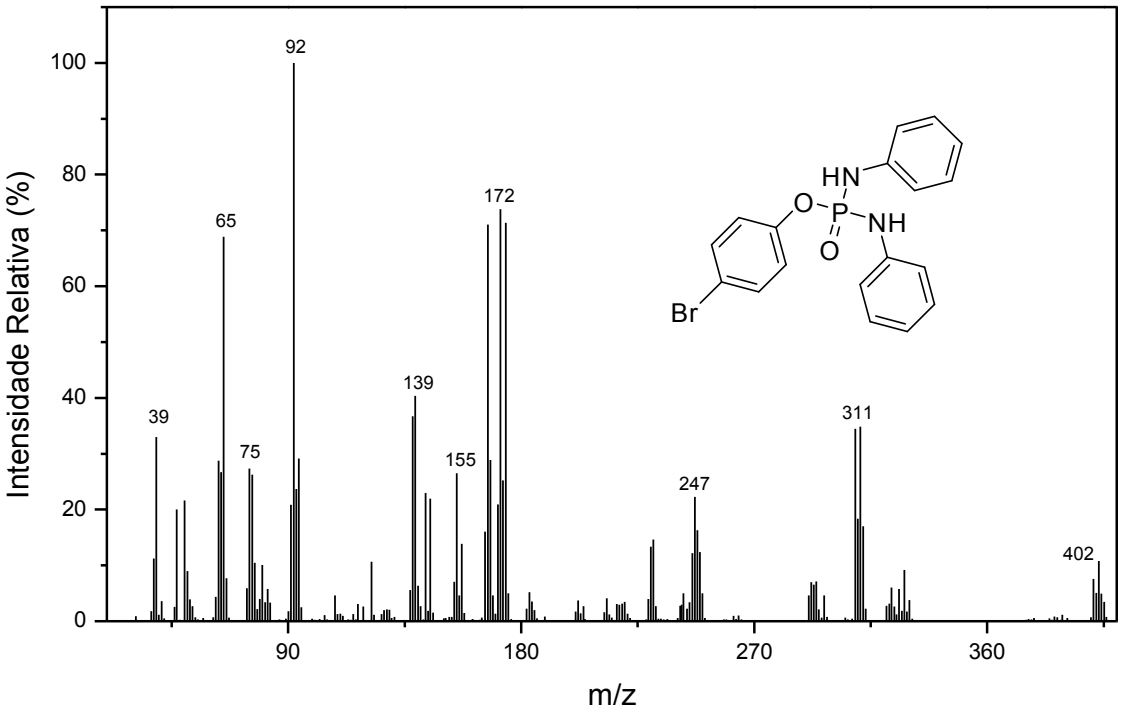

Figura 20 - Espectro de massas do composto **70**.

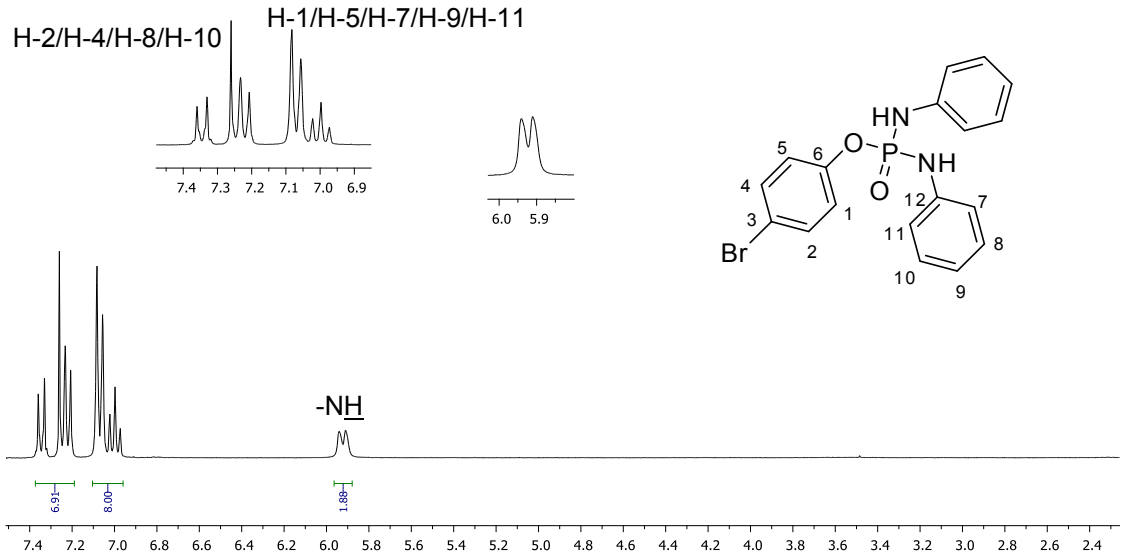

Figura 21 – Espectro de RMN de ^{1}H (300 MHz, $CDCl_3$) do composto **70**.

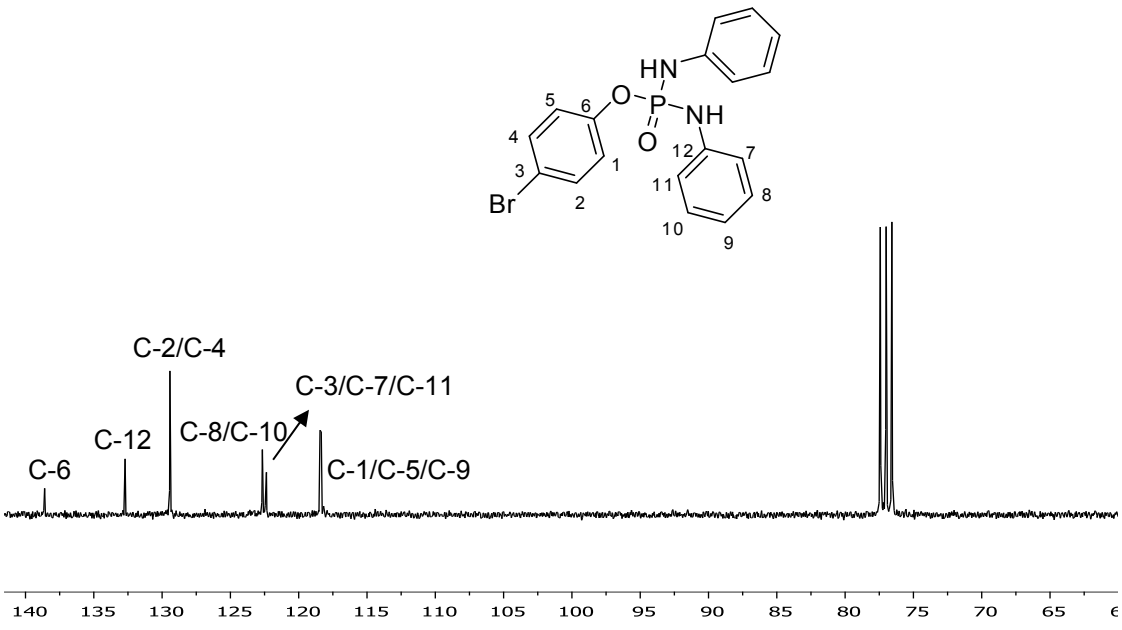

Figura 22 - Espectro de RMN de ^{13}C (75 MHz, $CDCl_3$) do composto **70**.

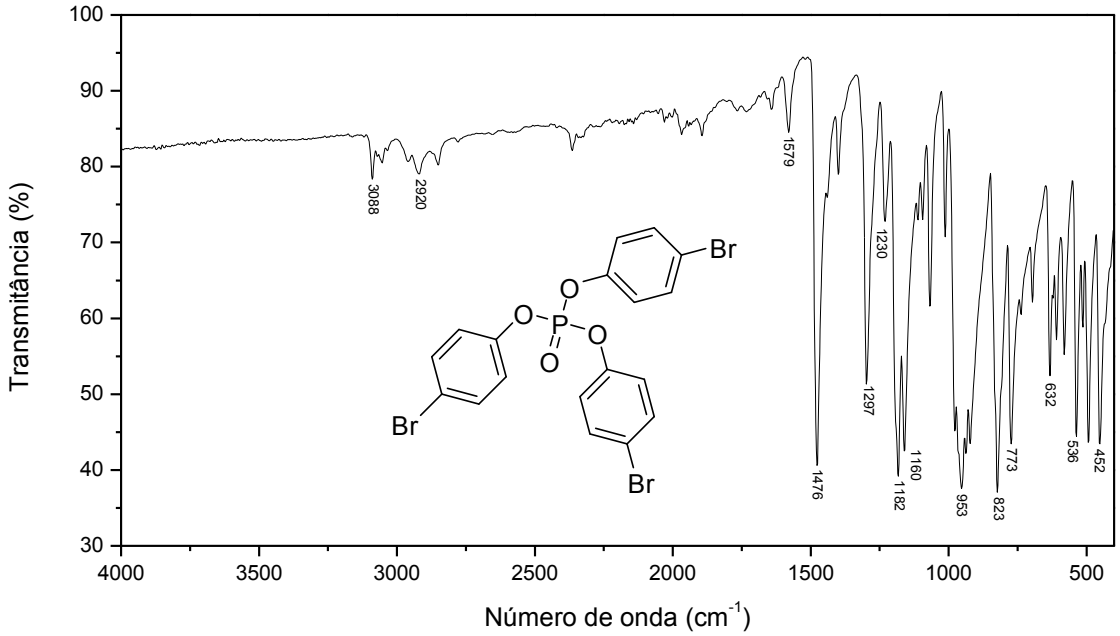

Figura 23 - Espectro no IV do composto **71**.

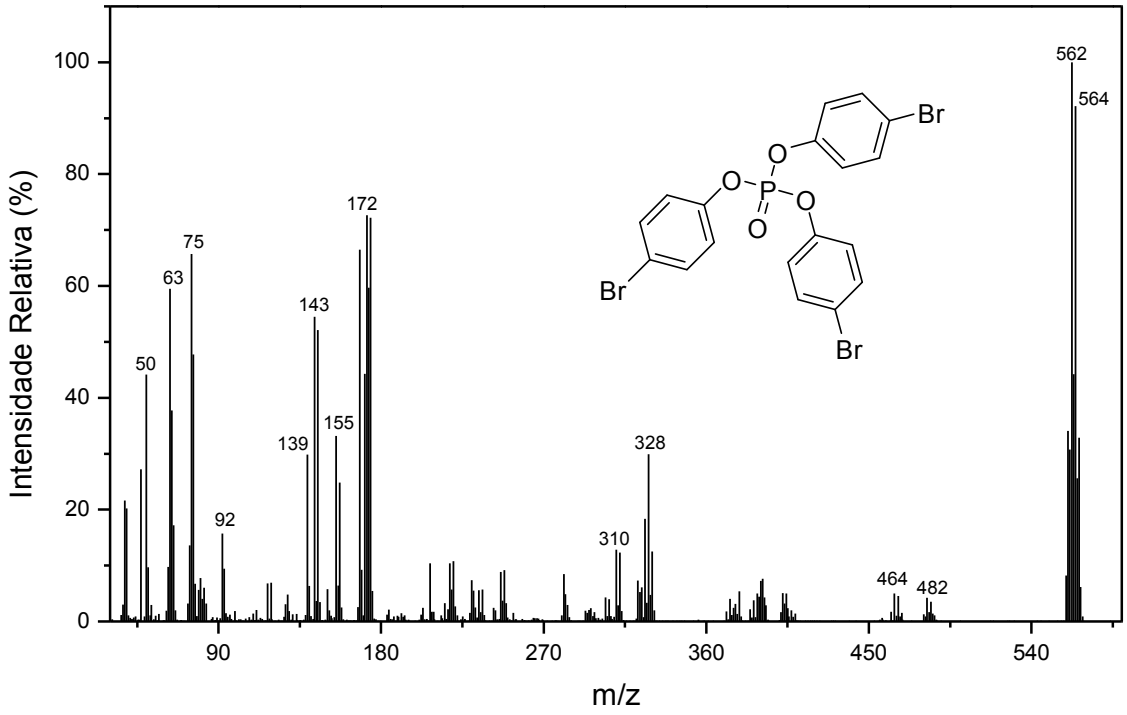

Figura 24 - Espectro de massas do composto **71**.

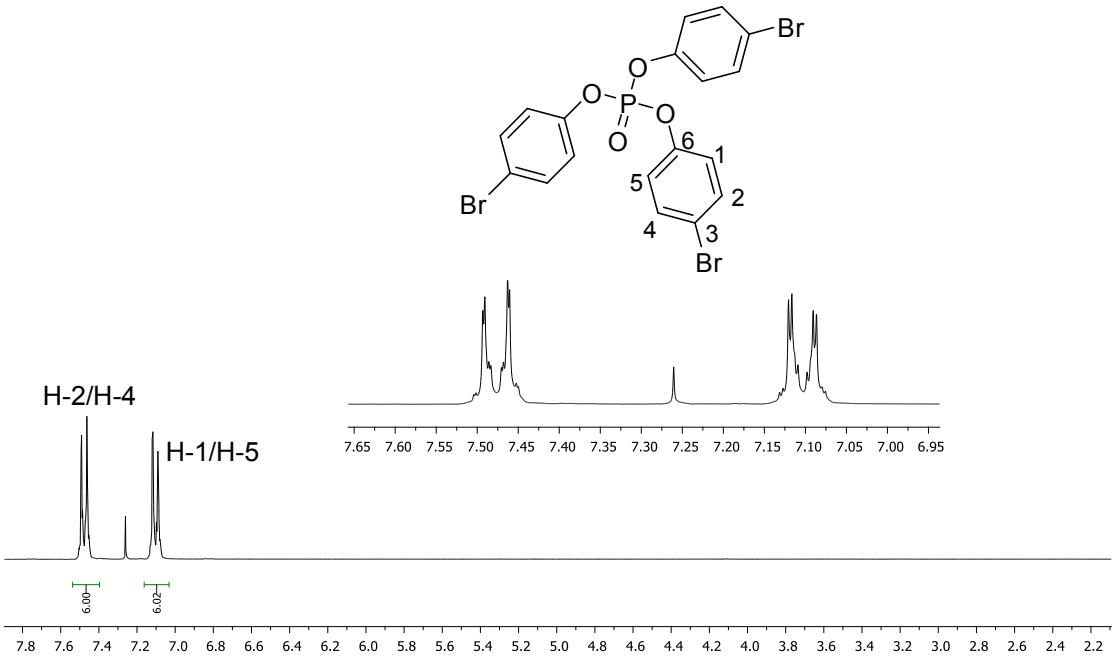

Figura 25 – Espectro de RMN de ^{1}H (300 MHz, $CDCl_3$) do composto **71**.

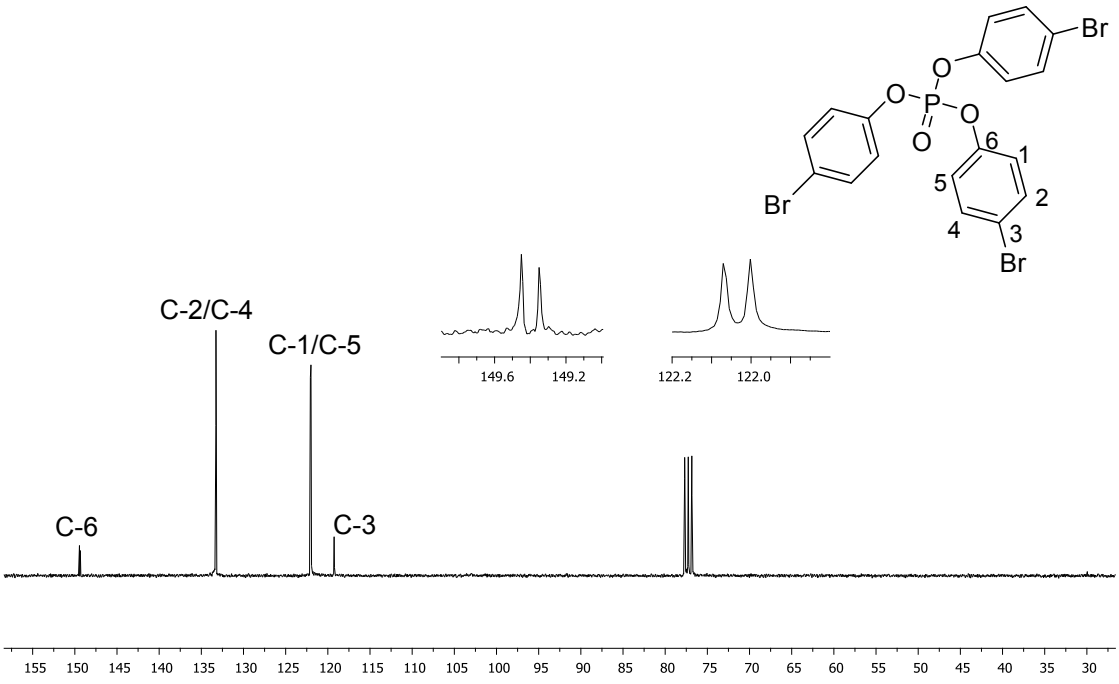

Figura 26 - Espectro de RMN de ^{13}C (75 MHz, $CDCl_3$) do composto **71**.

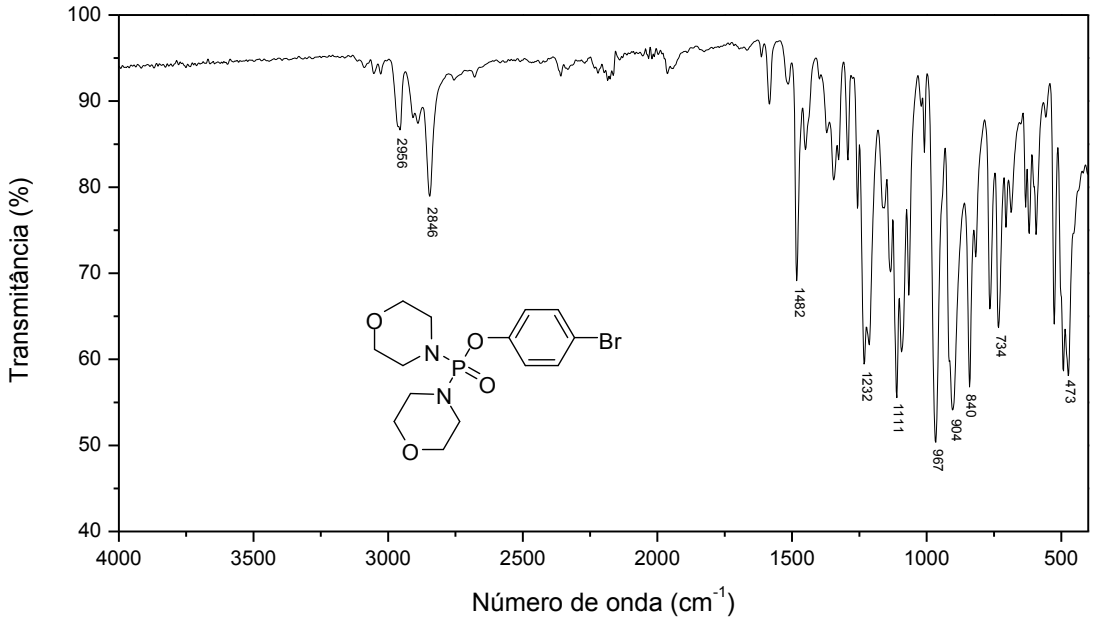

Figura 27 - Espectro no IV do composto **72**.

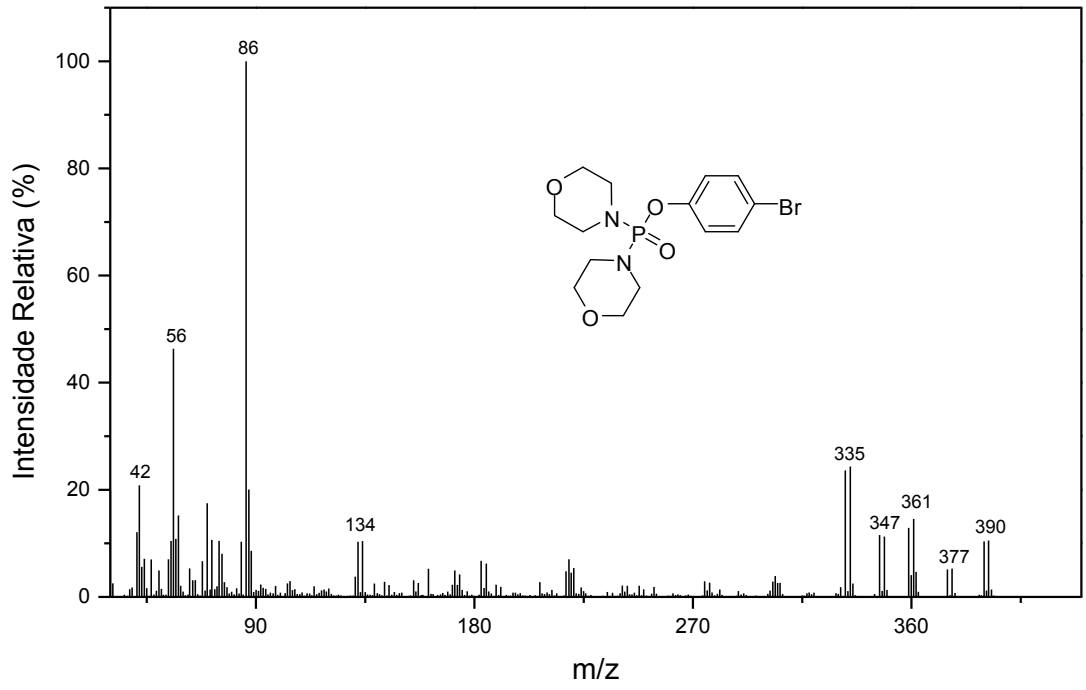

Figura 28 - Espectro de massas do composto **72**.

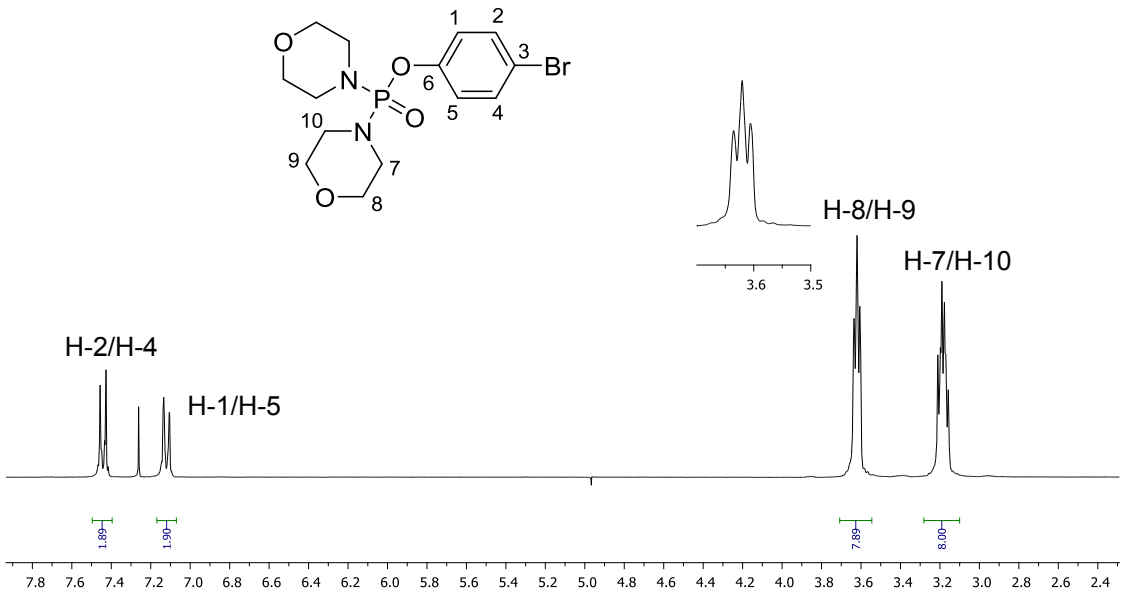

Figura 29 – Espectro de RMN de ^{1}H (300 MHz, $CDCl_3$) do composto **72**.

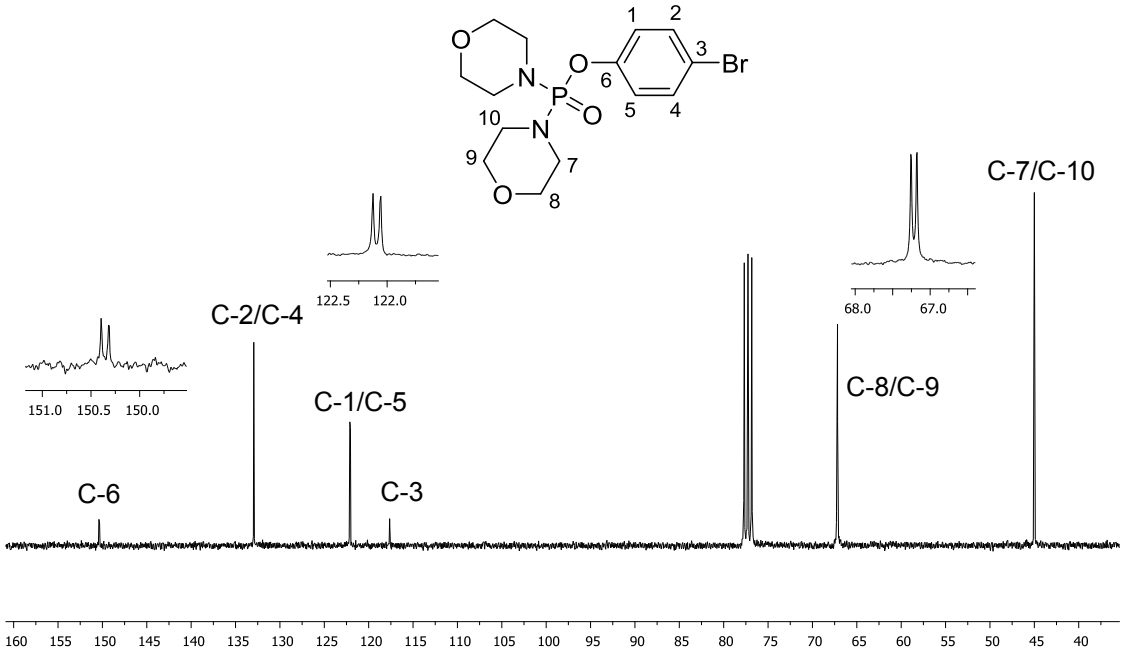

Figura 30 - Espectro de RMN de ^{13}C (75 MHz, $CDCl_3$) do composto **72**.

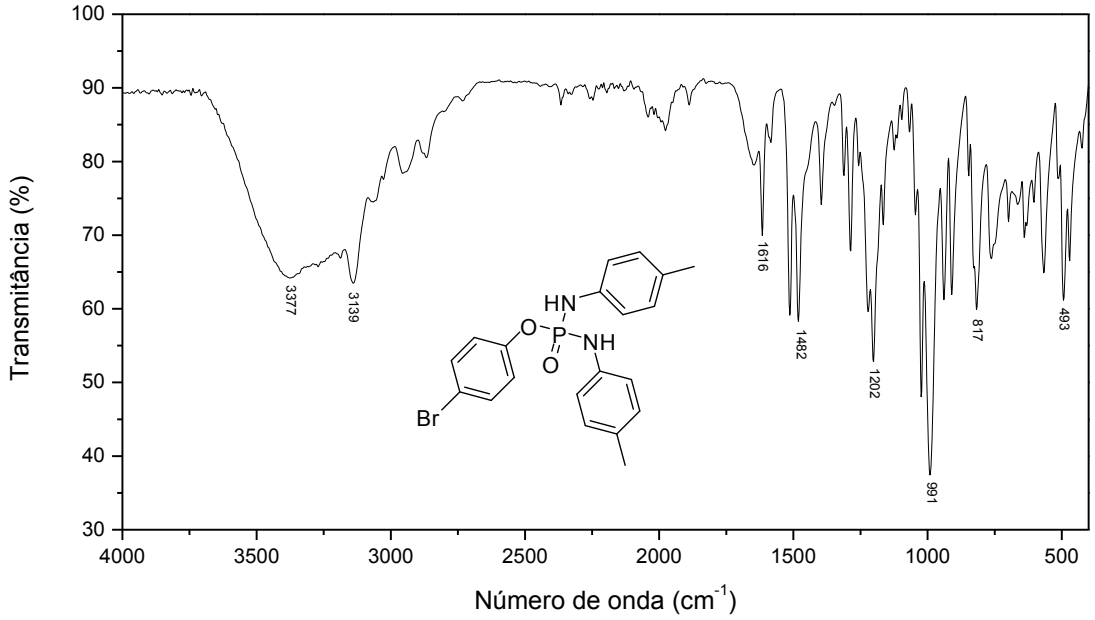

Figura 31 - Espectro no IV do composto **73**.

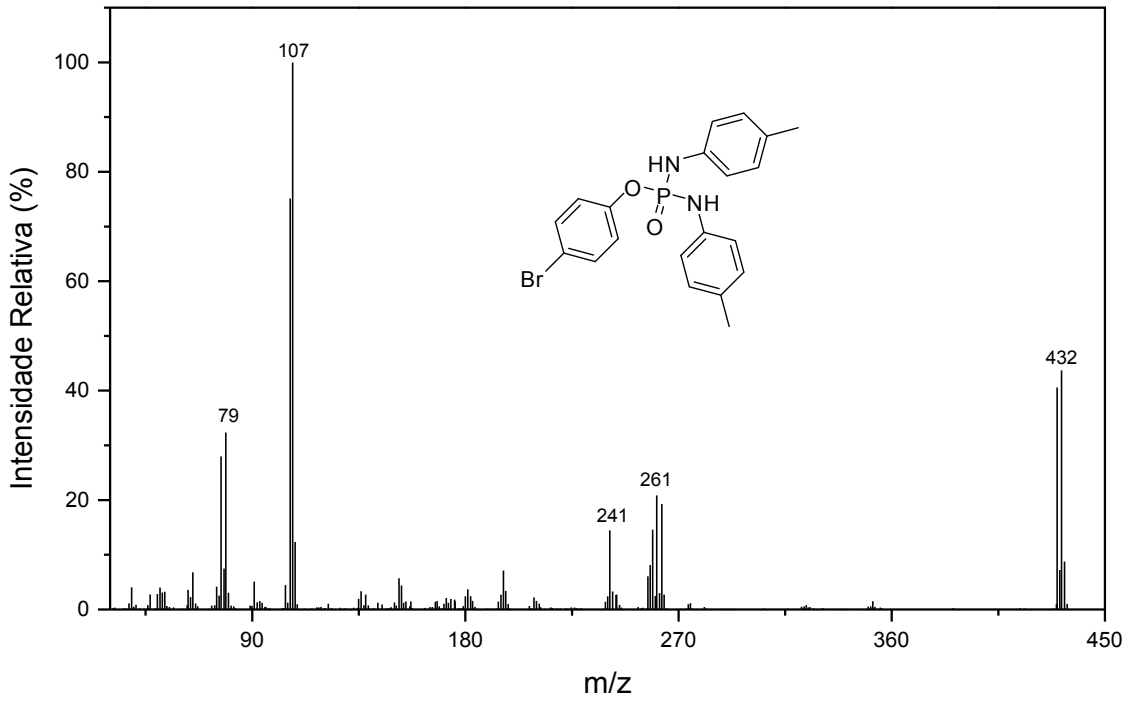

Figura 32 - Espectro de massas do composto **73**.

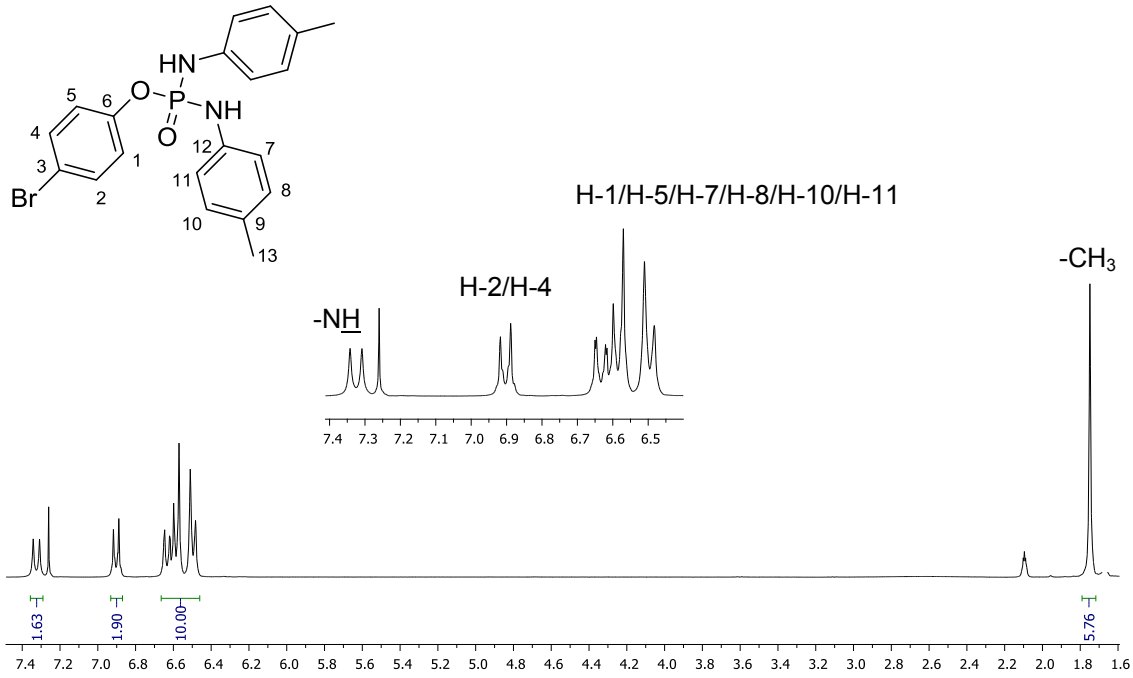

Figura 33 – Espectro de RMN de ^{1}H (300 MHz, $CDCl_3$) do composto **73**.

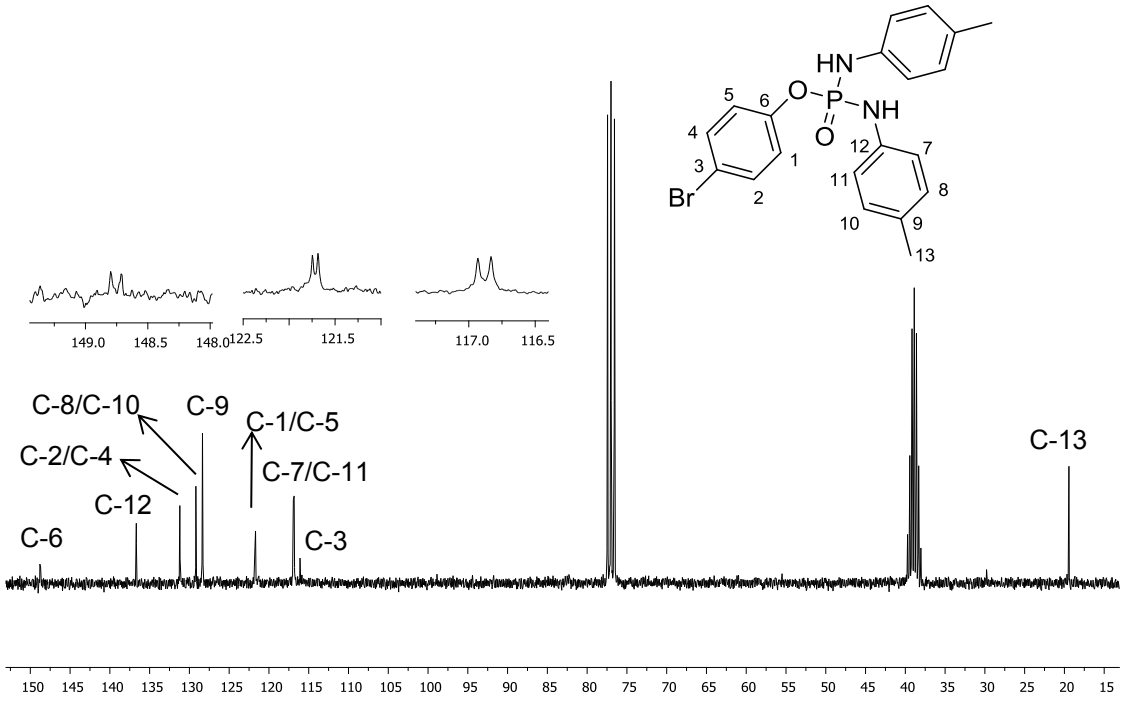

Figura 34 - Espectro de RMN de ^{13}C (75 MHz, $CDCl_3$) do composto **73**.

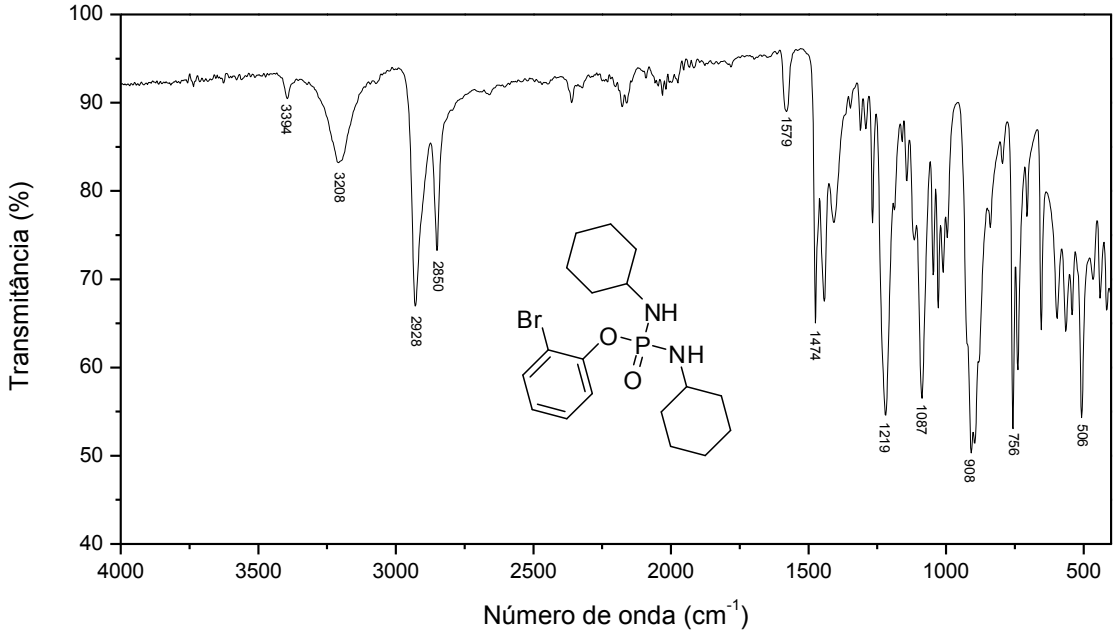

Figura 35 - Espectro no IV do composto **75**.

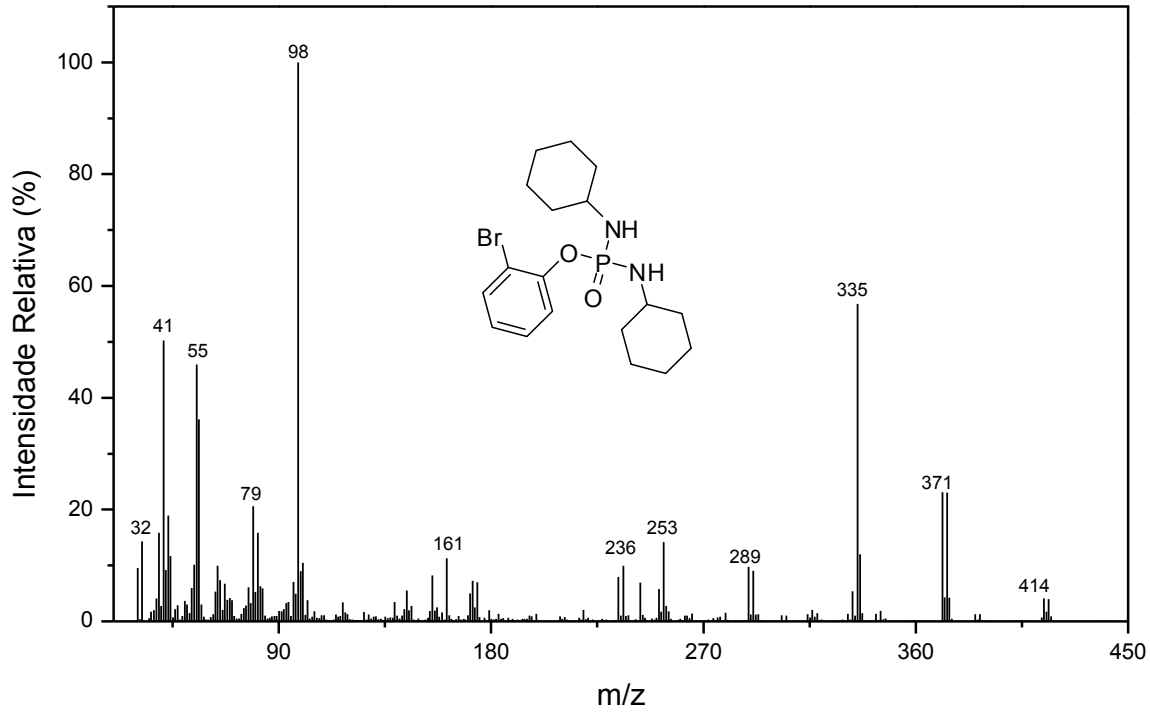

Figura 36 - Espectro de massas do composto **75**.

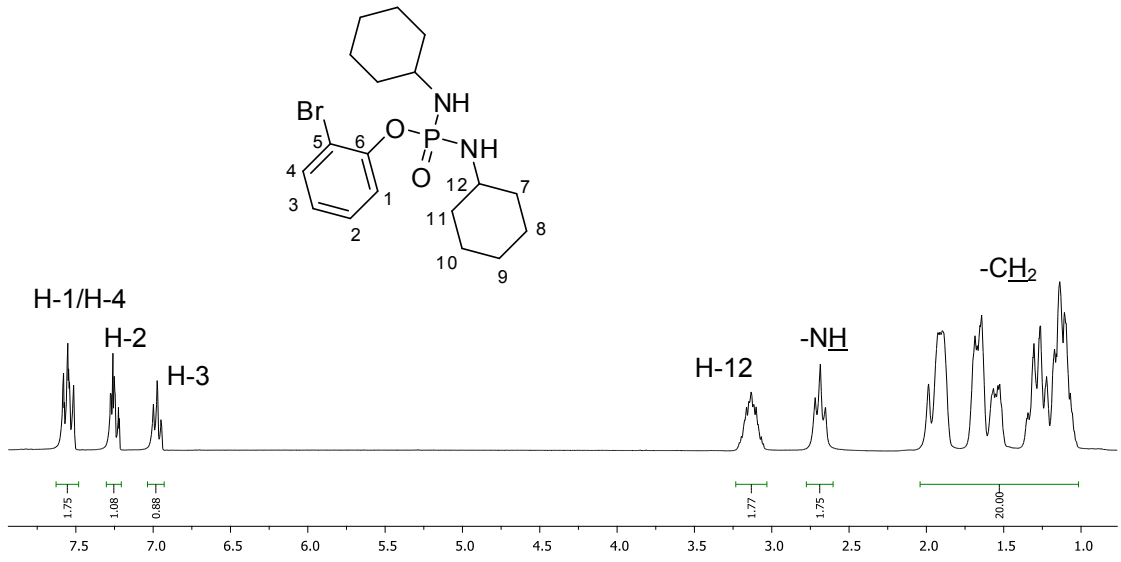

Figura 37 – Espectro de RMN de ^{1}H (300 MHz, $CDCl_3$) do composto **75**.

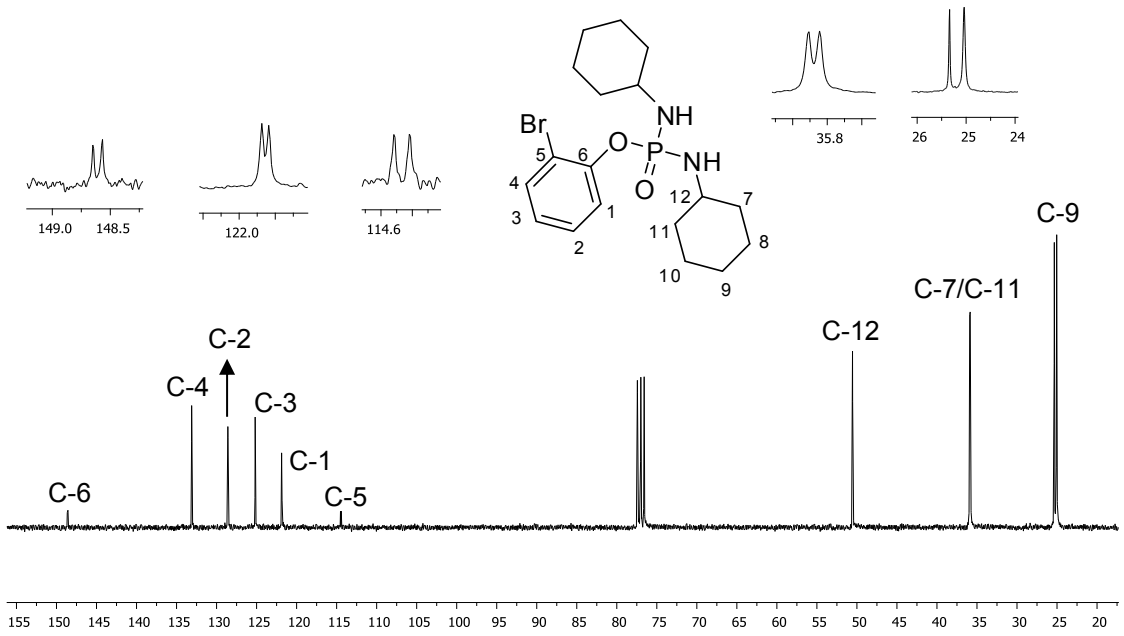

Figura 38 - Espectro de RMN de ^{13}C (75 MHz, $CDCl_3$) do composto **75**.

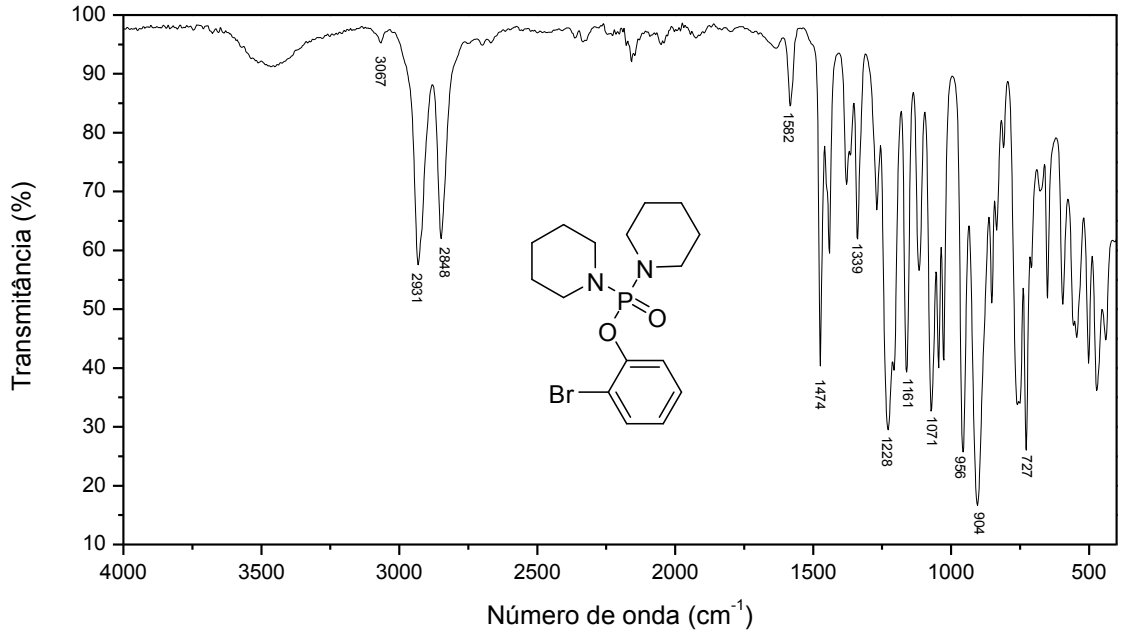

Figura 39 - Espectro no IV do composto **76**.

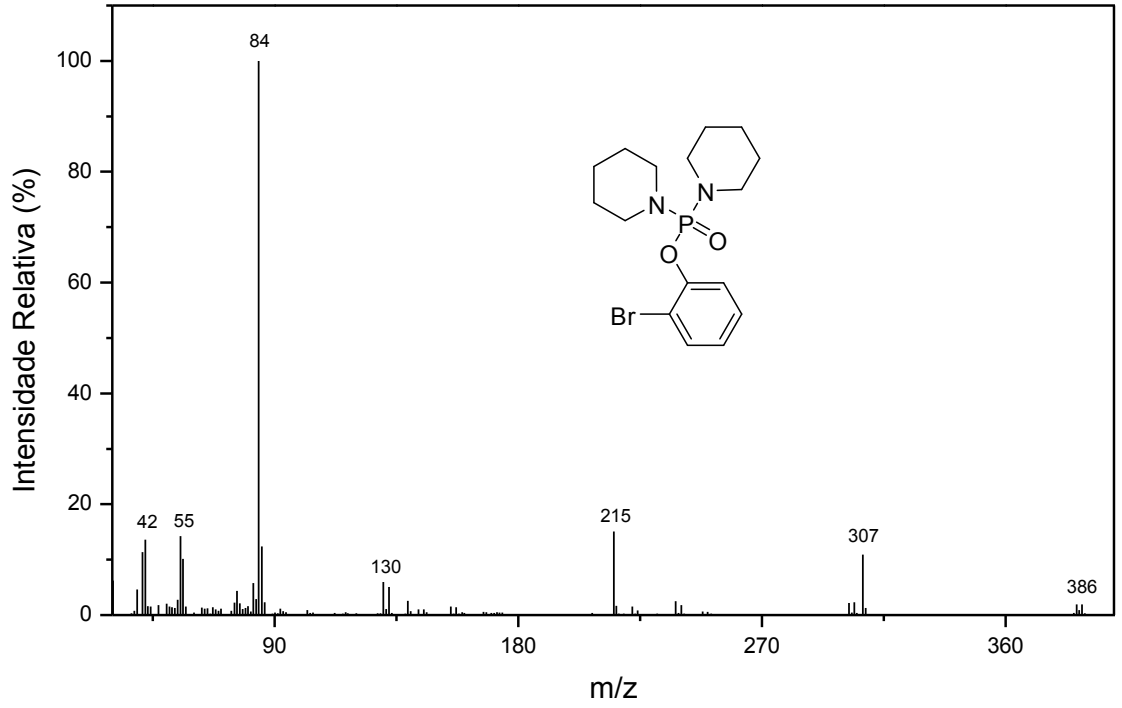

Figura 40 - Espectro de massas do composto **76**.

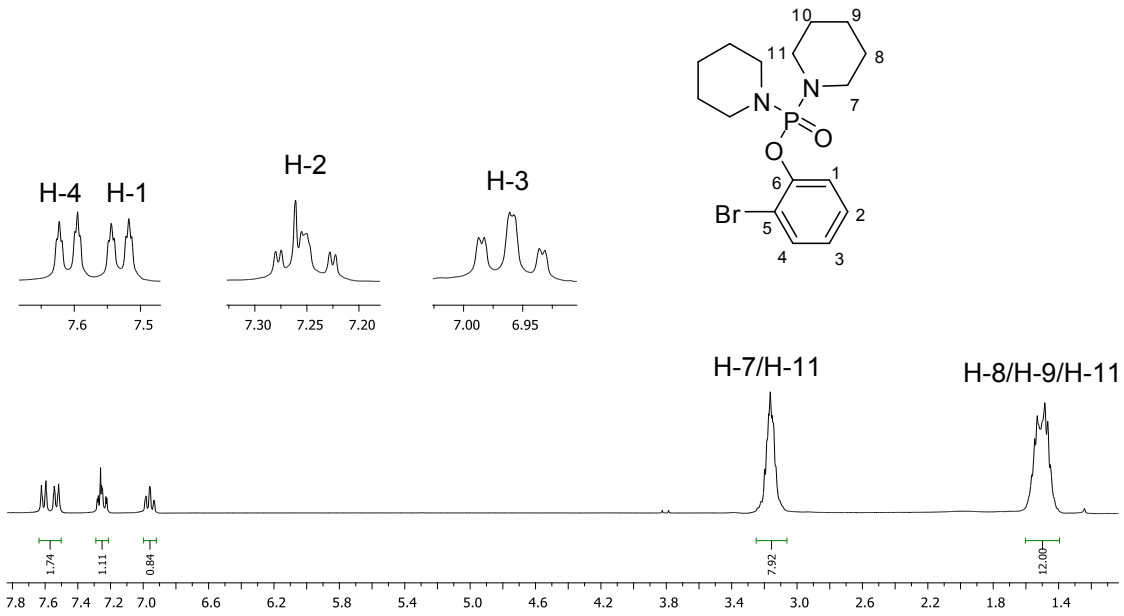

Figura 41 – Espectro de RMN de ^{1}H (300 MHz, $CDCl_3$) do composto **76**.

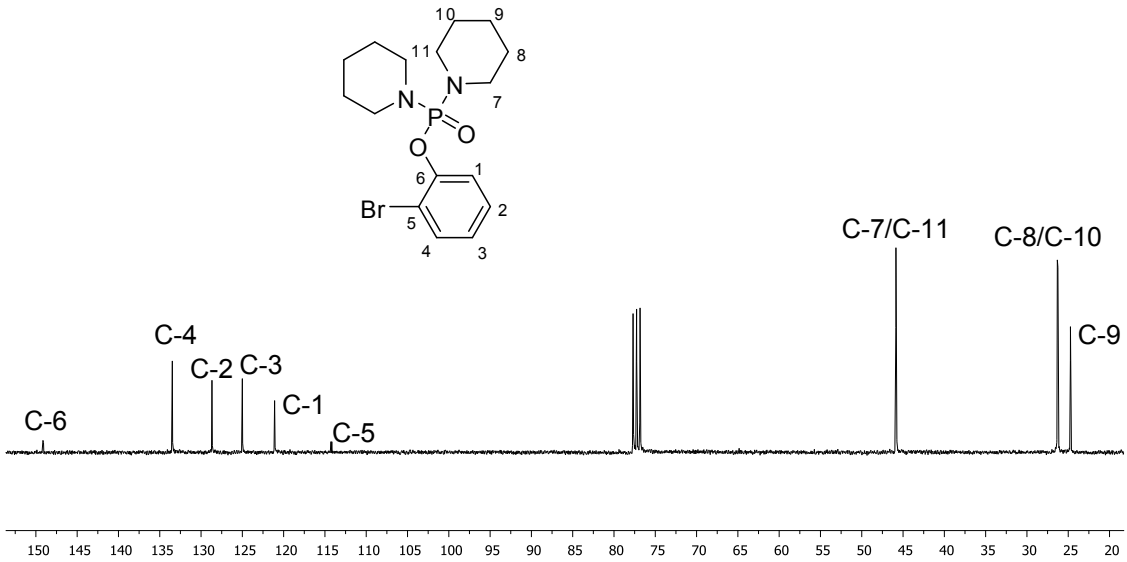

Figura 42 - Espectro de RMN de ^{13}C (75 MHz, $CDCl_3$) do composto **76**.

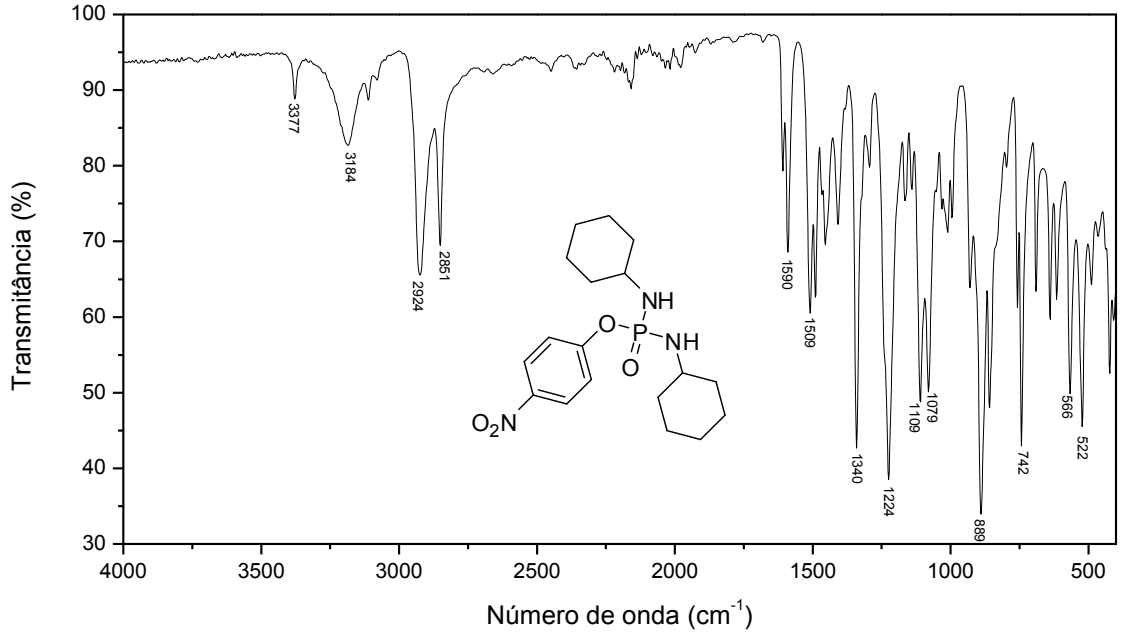

Figura 43 - Espectro no IV do composto **78**.

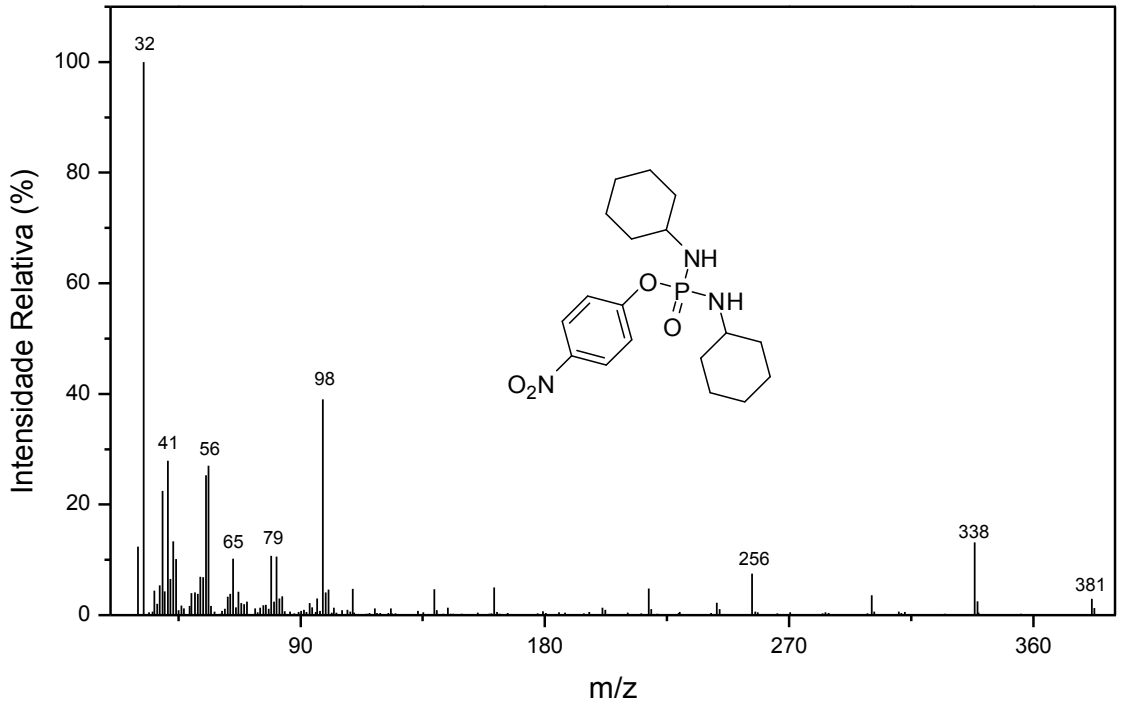

Figura 44 - Espectro de massas do composto **78**.

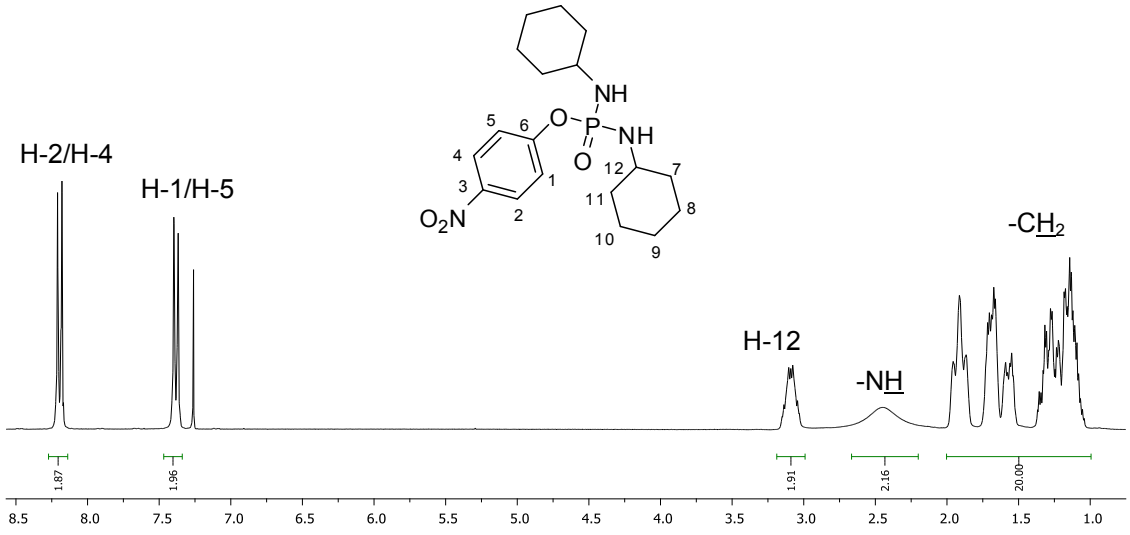

Figura 45 – Espectro de RMN de ^{1}H (300 MHz, $CDCl_3$) do composto **78**.

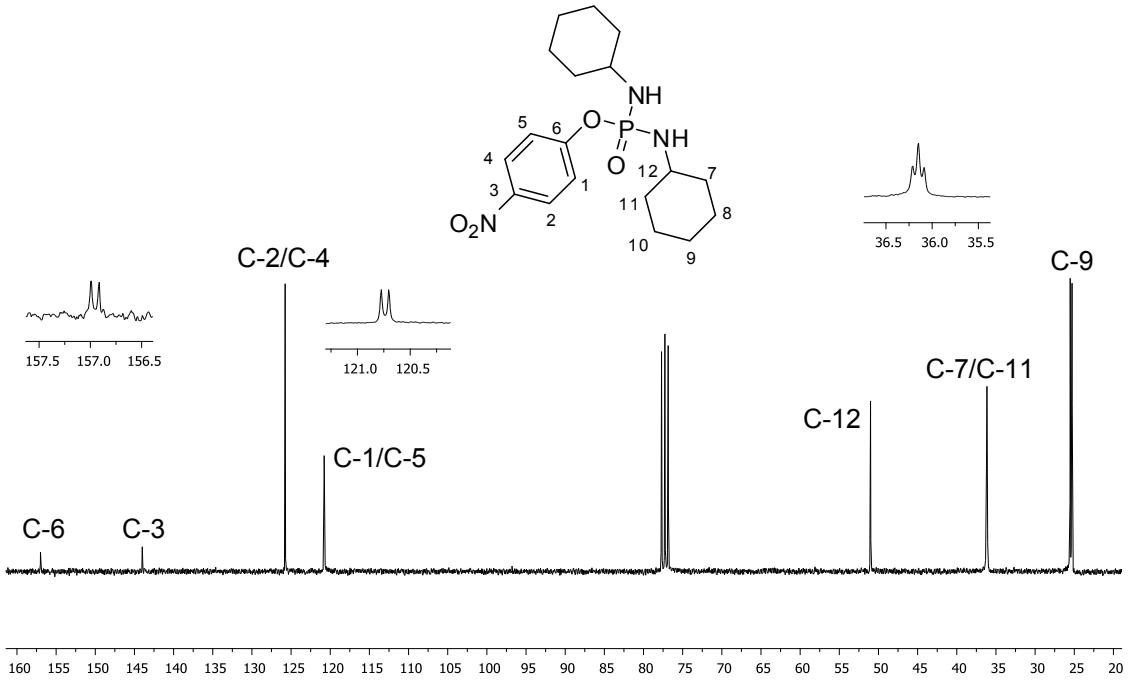

Figura 46 - Espectro de RMN de ^{13}C (75 MHz, $CDCl_3$) do composto **78**.

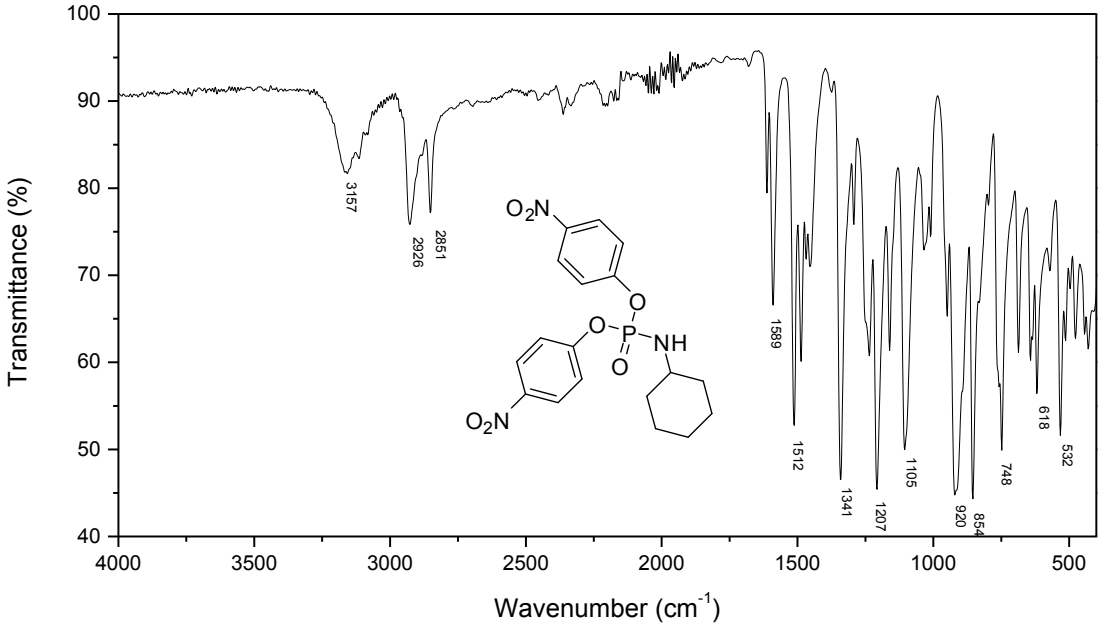

Figura 47 - Espectro no IV do composto **79**.

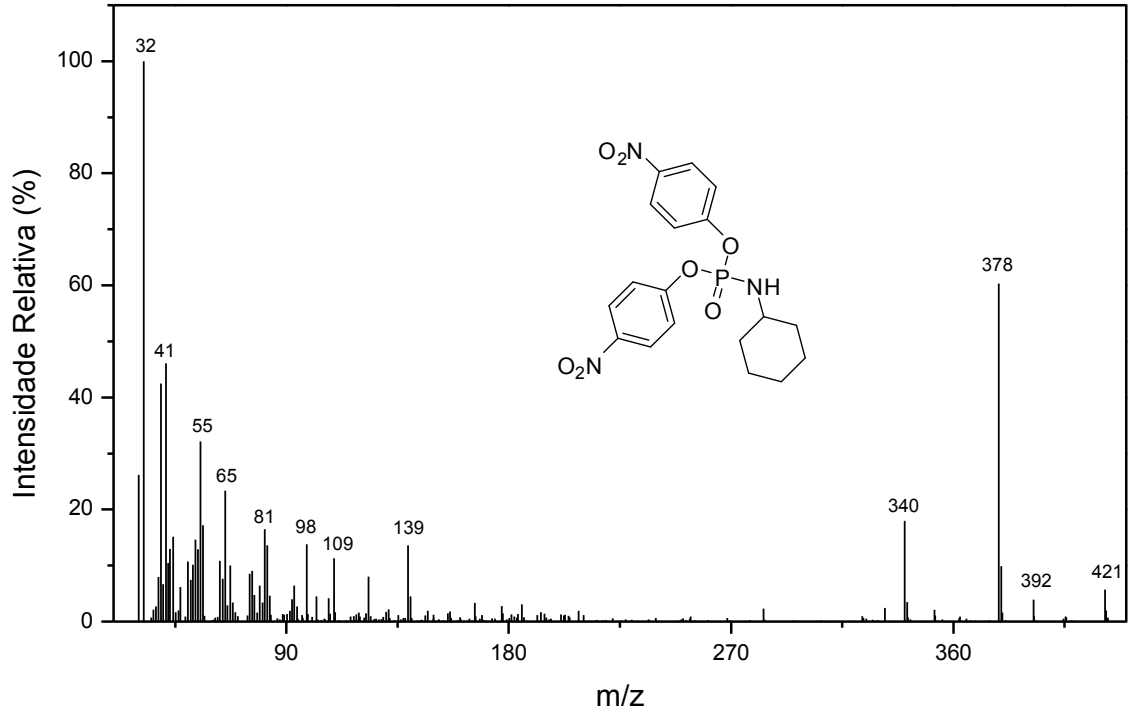

Figura 48 - Espectro de massas do composto **79**.

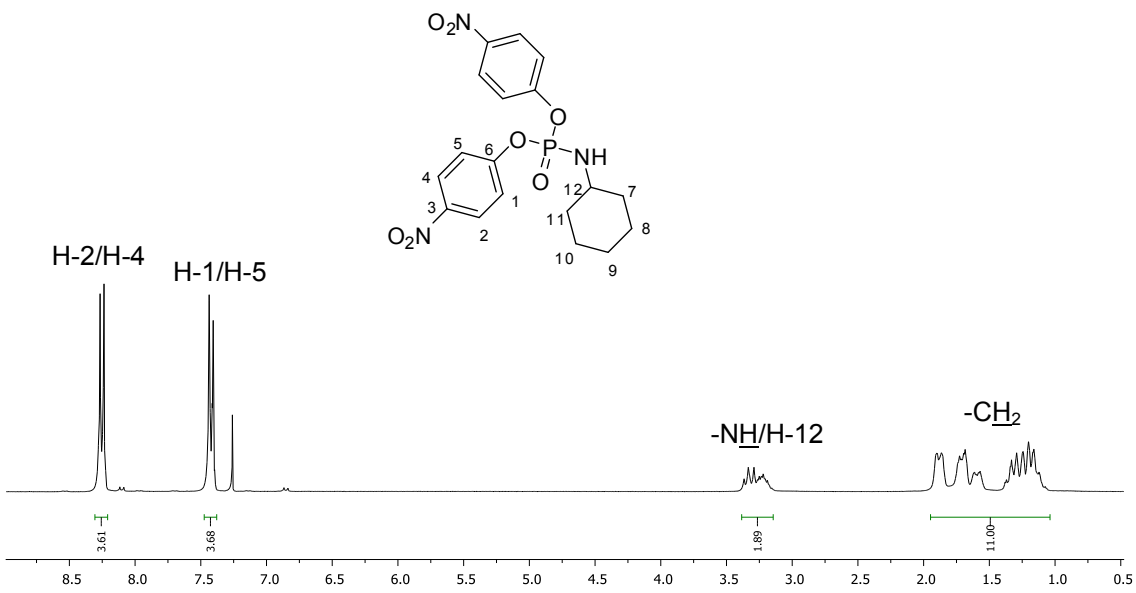

Figura 49 – Espectro de RMN de ^{1}H (300 MHz, $CDCl_3$) do composto **79**.

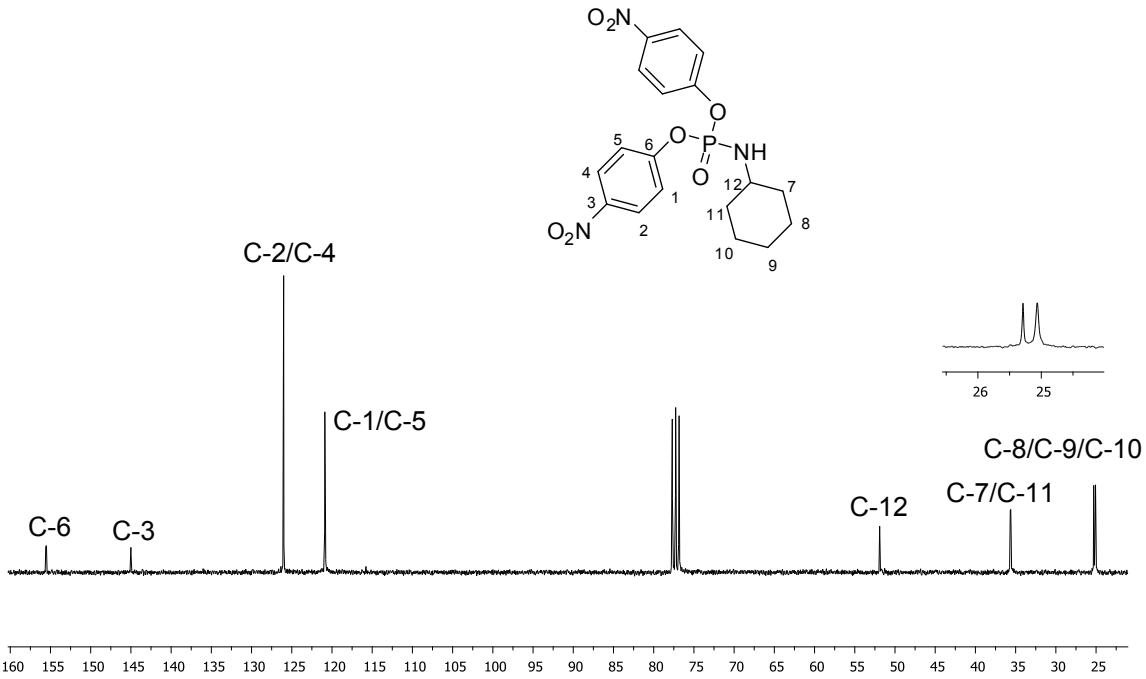

Figura 50 - Espectro de RMN de ^{13}C (75 MHz, $CDCl_3$) do composto **79**.

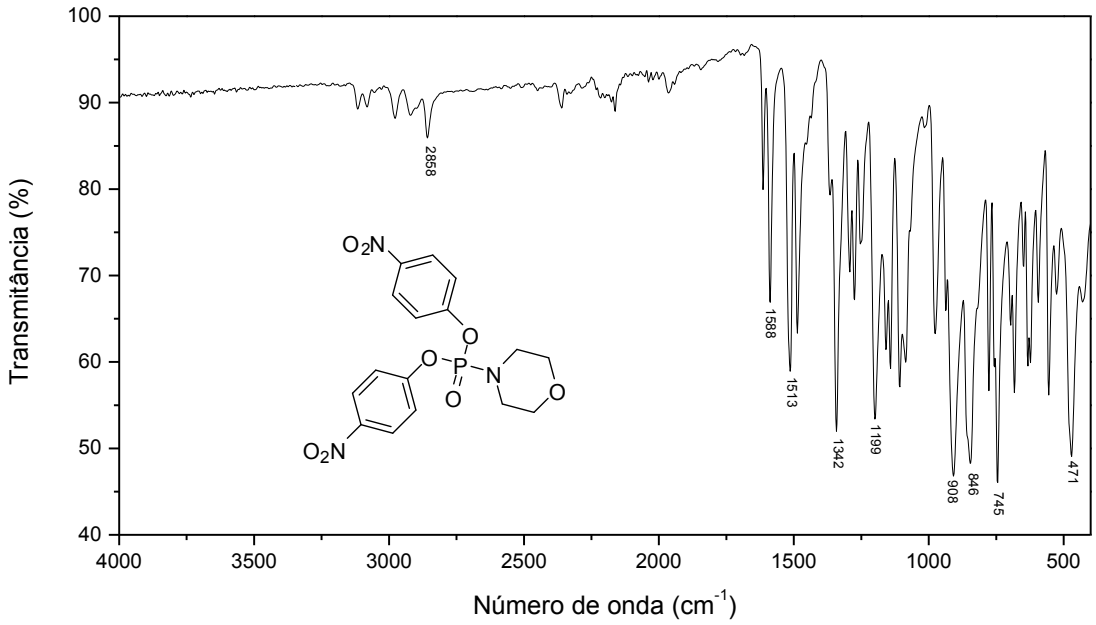

Figura 51 - Espectro no IV do composto **80**.

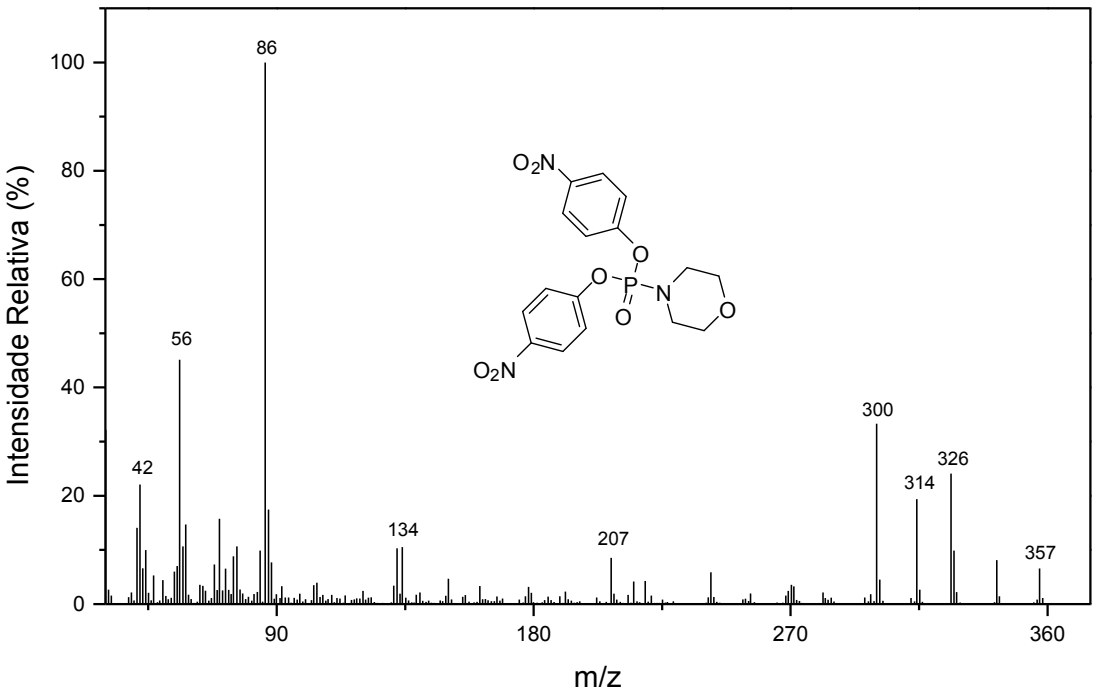

Figura 52 - Espectro de massas do composto **80**.

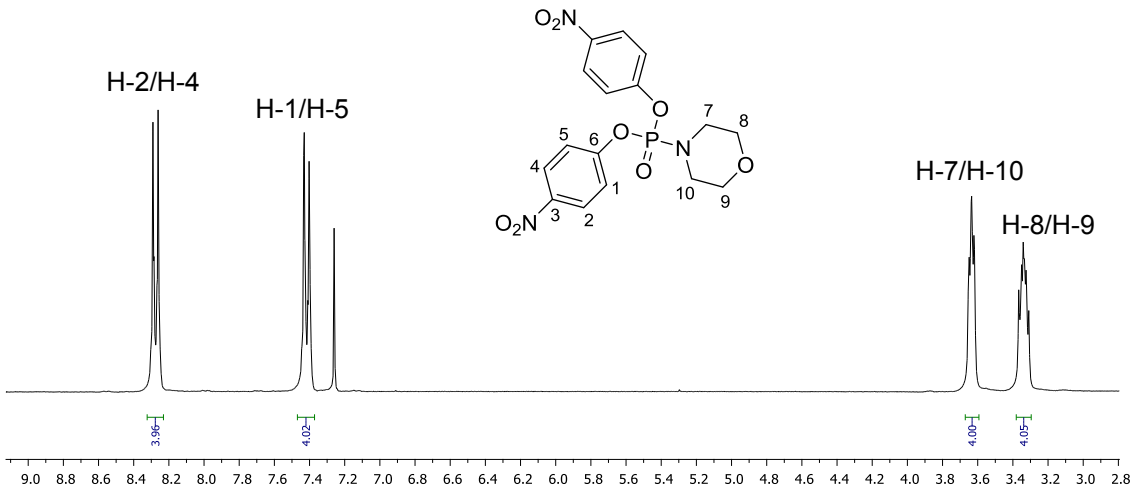

Figura 53 – Espectro de RMN de ^{1}H (300 MHz, $CDCl_3$) do composto **80**.

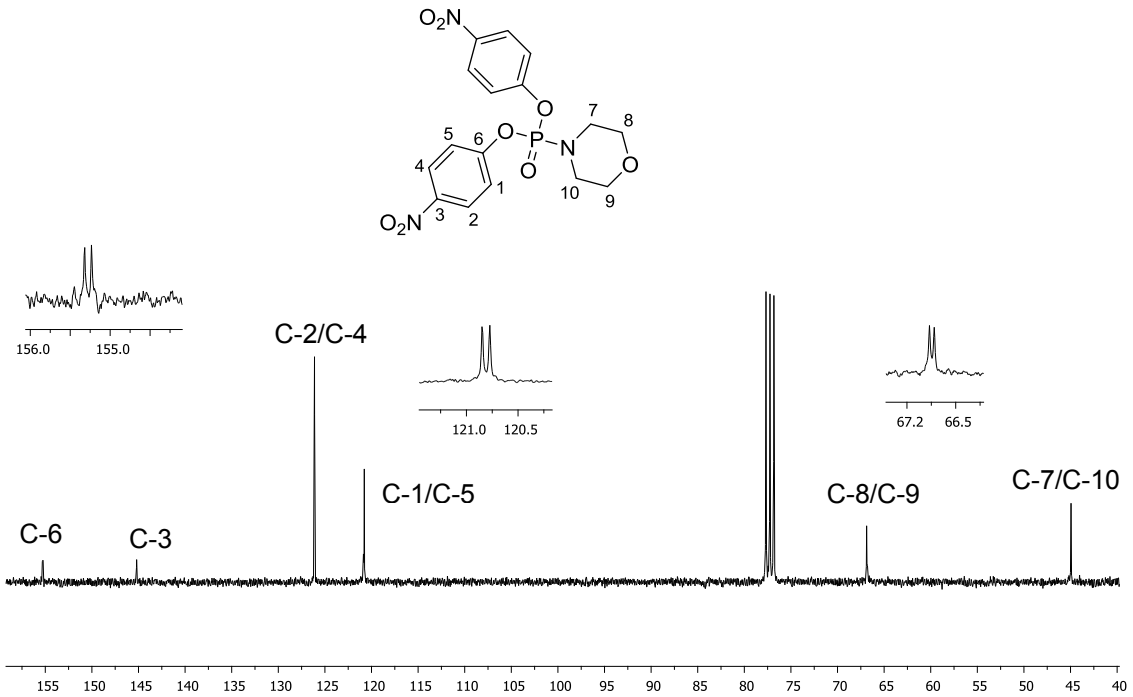

Figura 54 - Espectro de RMN de ^{13}C (75 MHz, $CDCl_3$) do composto **80**.

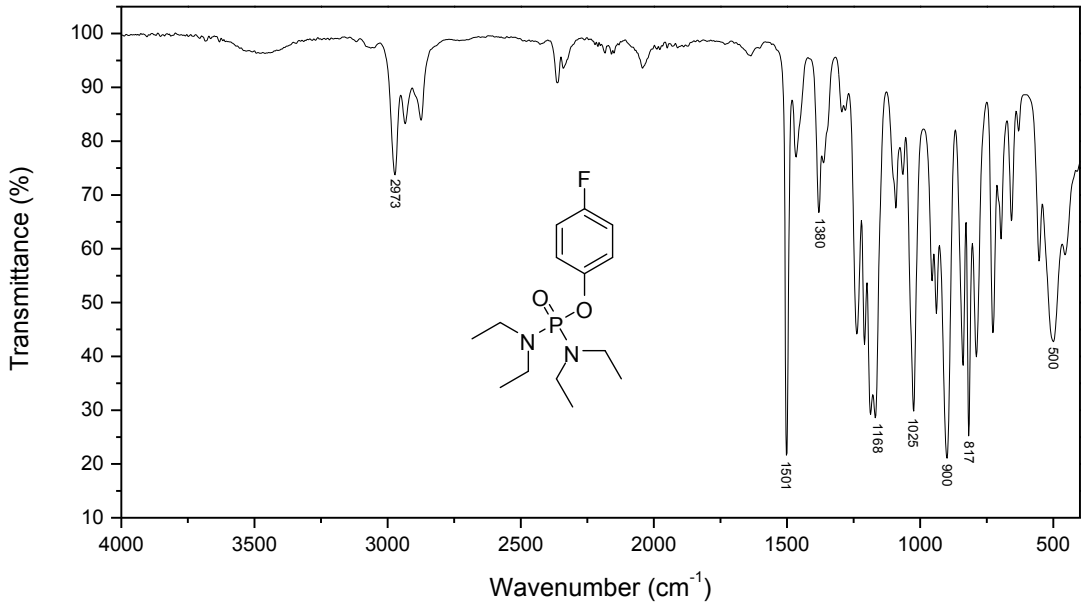

Figura 55 - Espectro no IV do composto **81**.

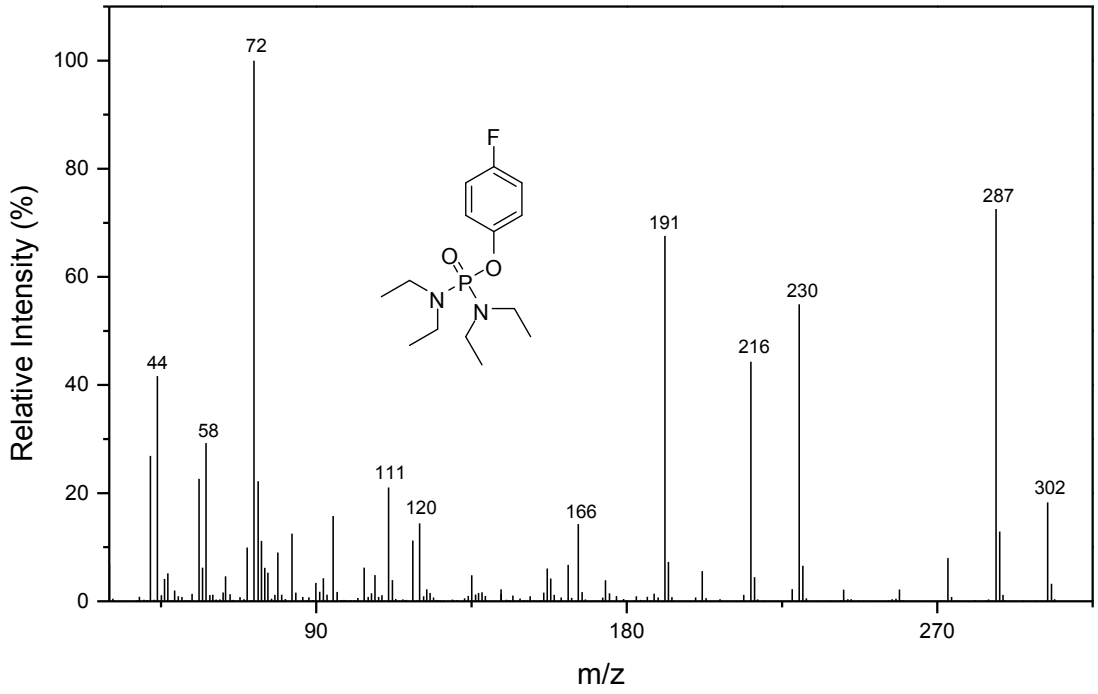

Figura 56 - Espectro de massas do composto **81**.

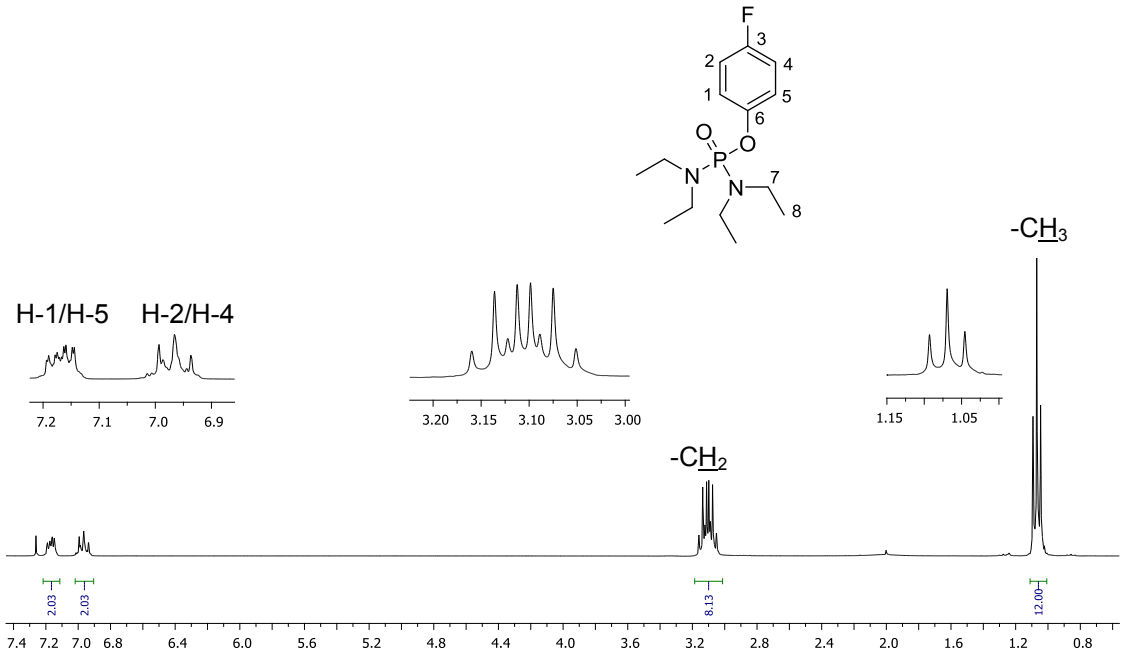

Figura 57 – Espectro de RMN de ^{1}H (300 MHz, $CDCl_3$) do composto **81**.

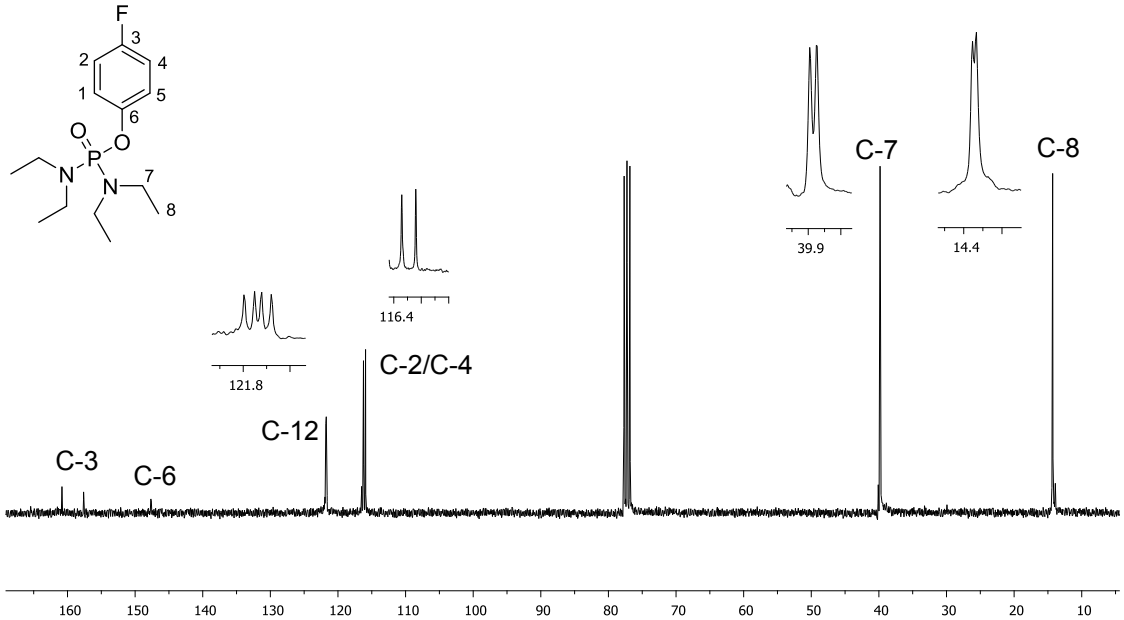

Figura 58 - Espectro de RMN de ^{13}C (75 MHz, $CDCl_3$) do composto **81**.

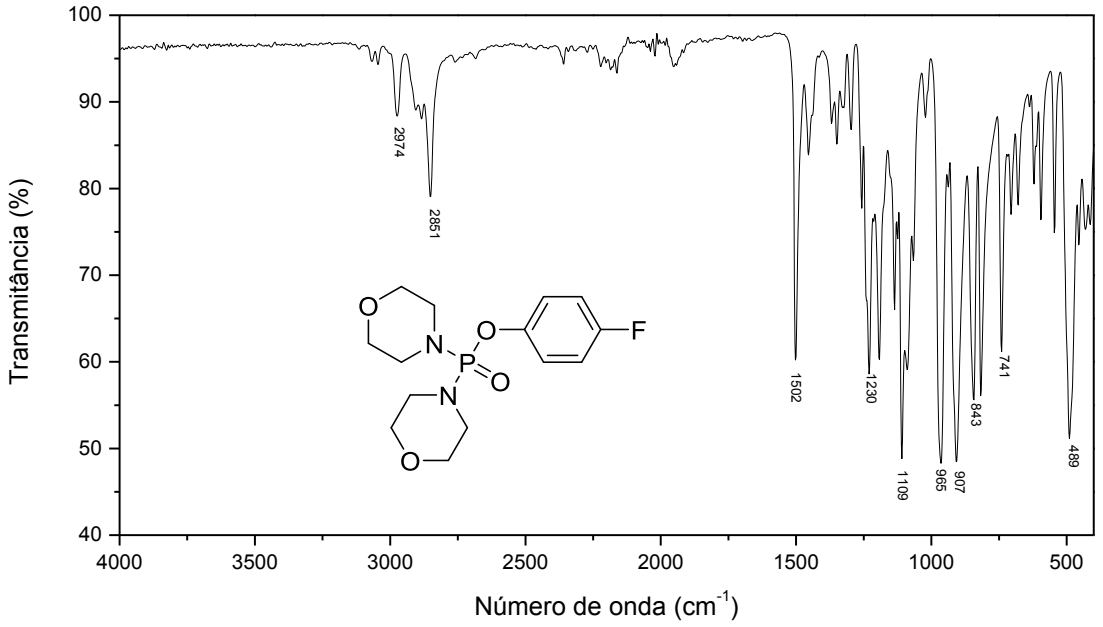

Figura 59 - Espectro no IV do composto **82**.

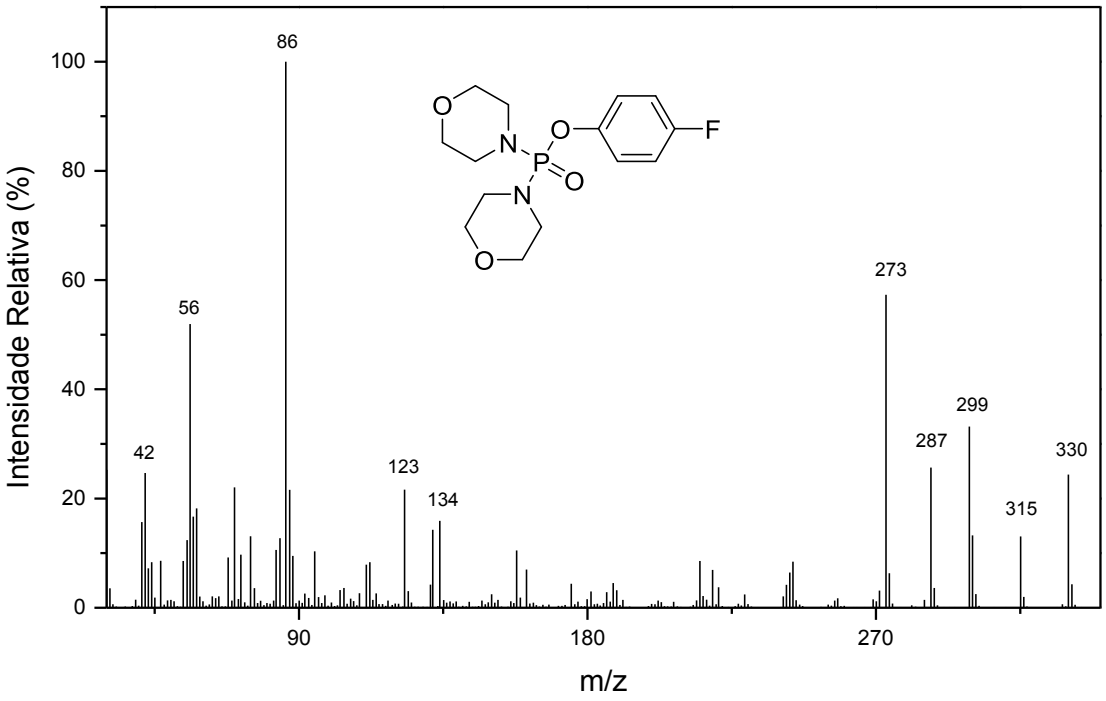

Figura 60 - Espectro de massas do composto **82**.

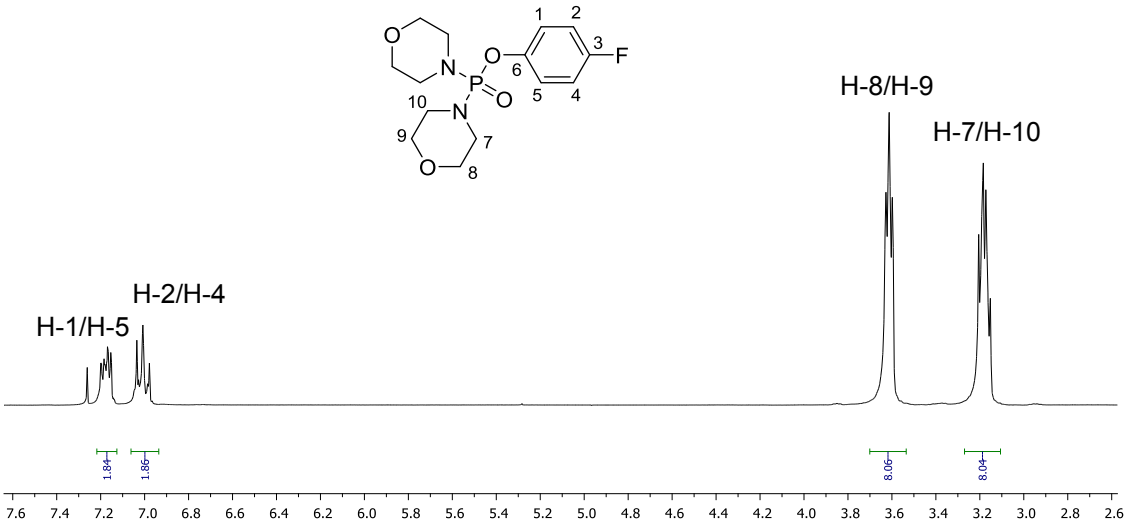

Figura 61 – Espectro de RMN de ^{1}H (300 MHz, $CDCl_3$) do composto **82**.

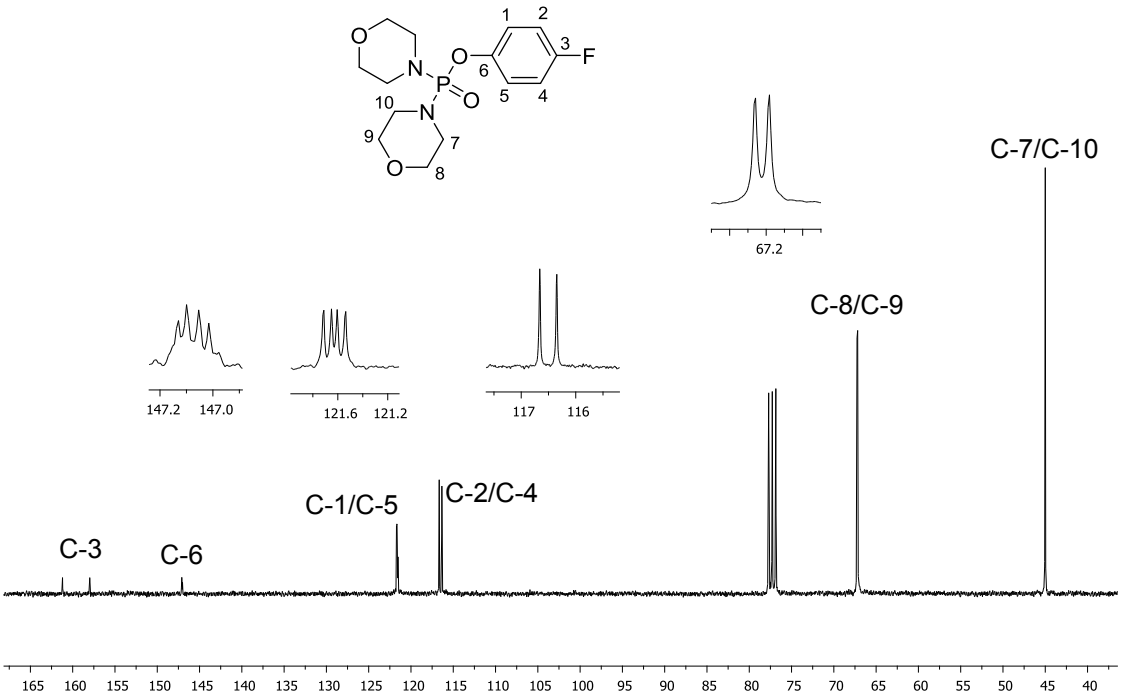

Figura 62 - Espectro de RMN de ^{13}C (75 MHz, $CDCl_3$) do composto **82**.

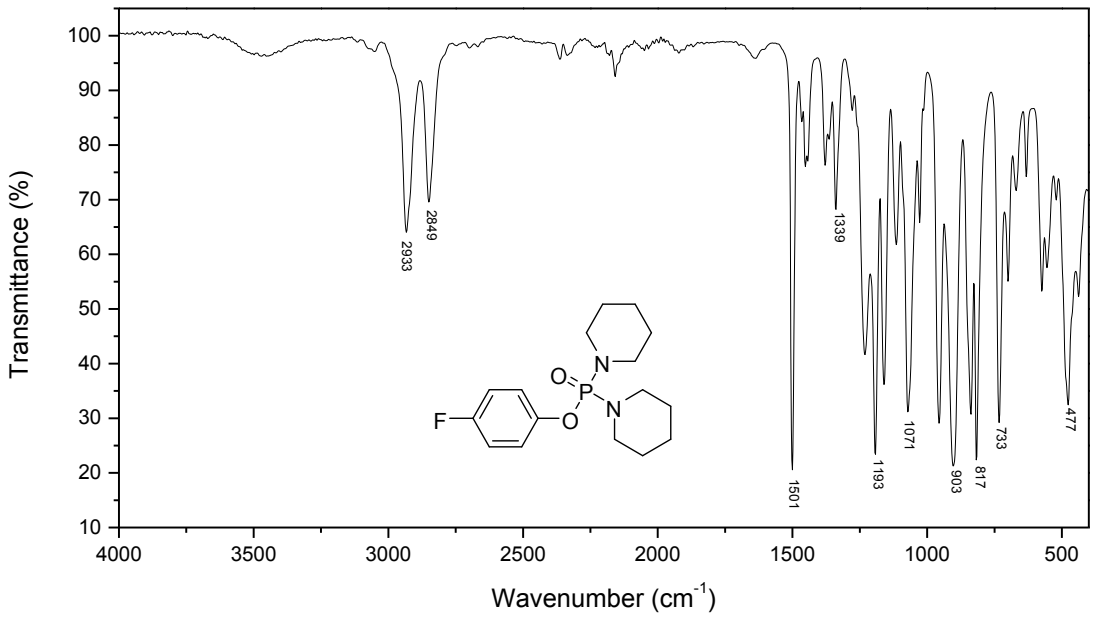

Figura 63 - Espectro no IV do composto **83**.

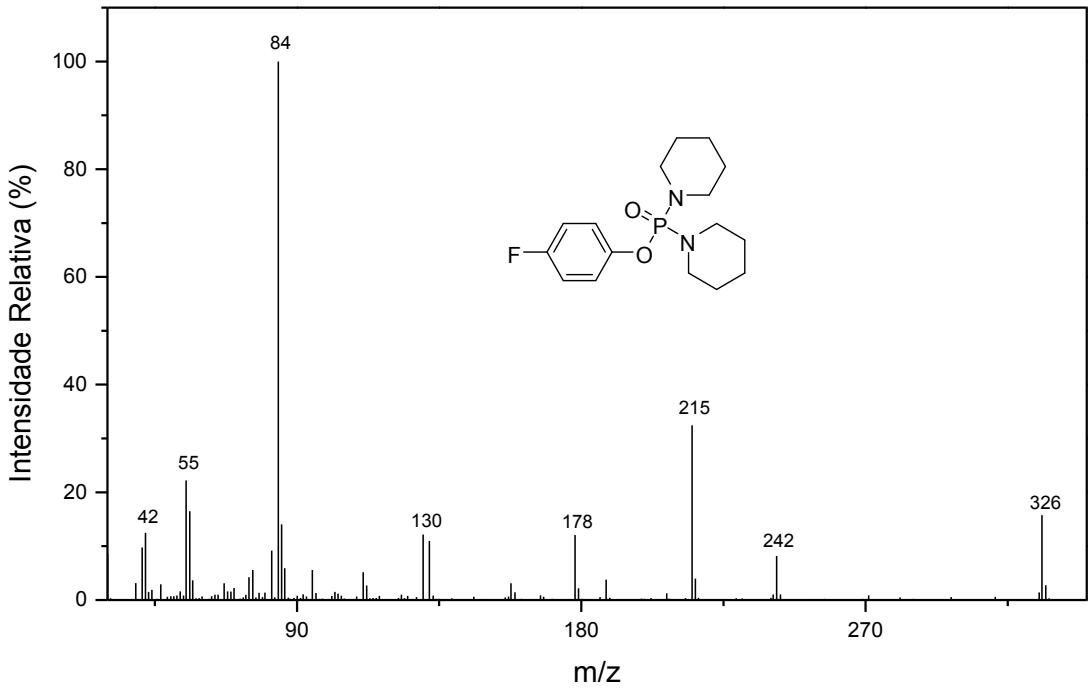

Figura 64 - Espectro de massas do composto **83**.

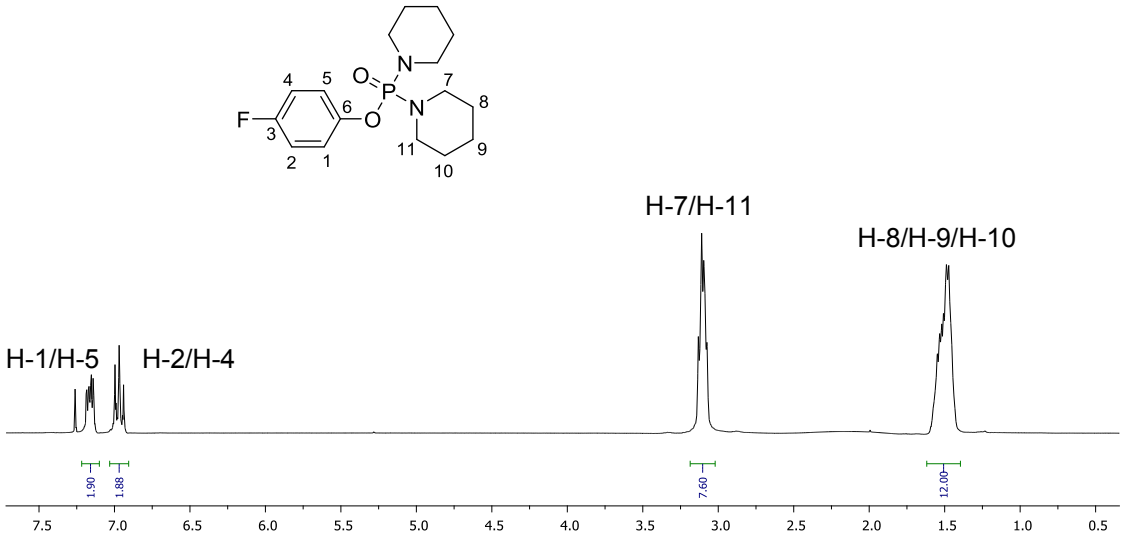

Figura 65 – Espectro de RMN de ^{1}H (300 MHz, $CDCl_3$) do composto **83**.

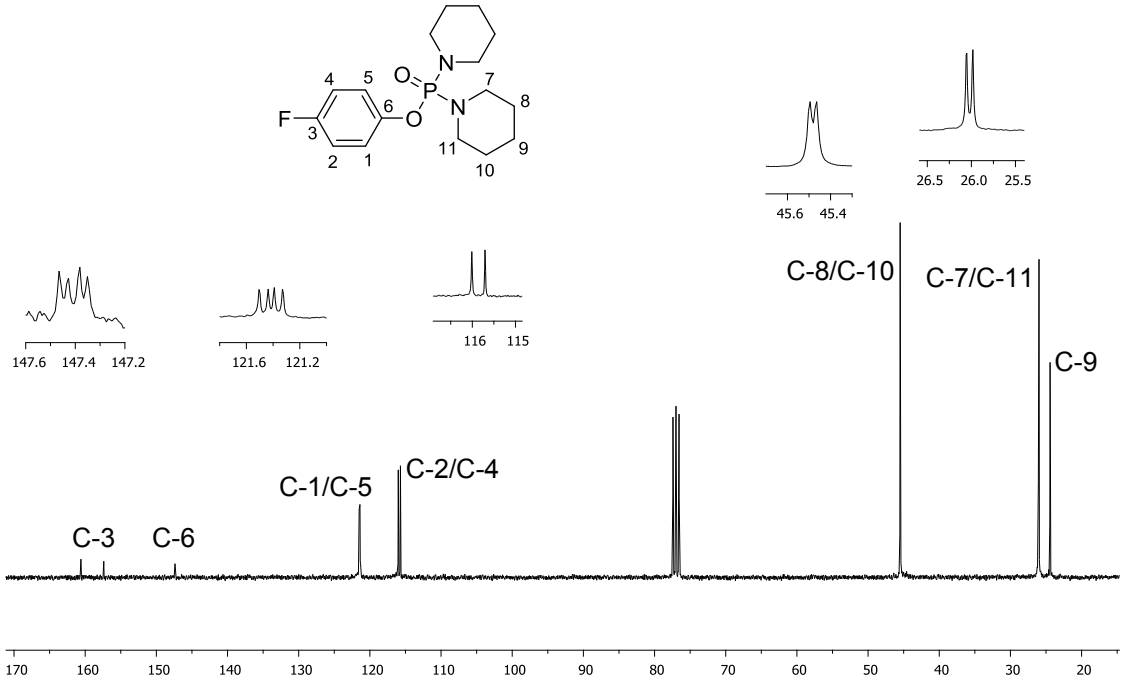

Figura 66 - Espectro de RMN de ^{13}C (75 MHz, $CDCl_3$) do composto **83**.

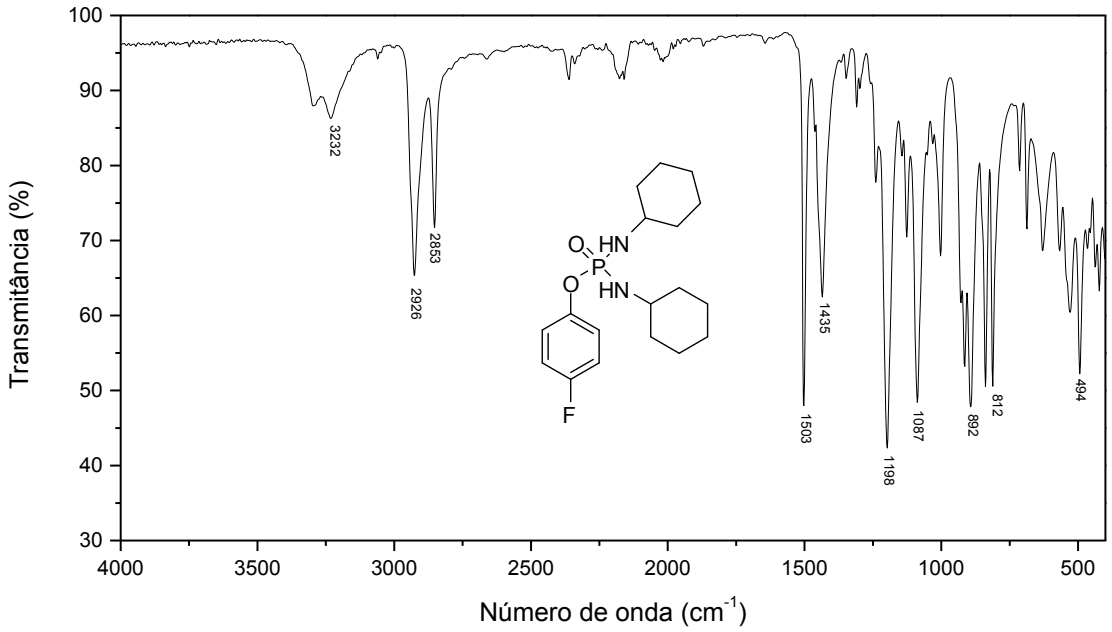

Figura 67 - Espectro no IV do composto **84**.

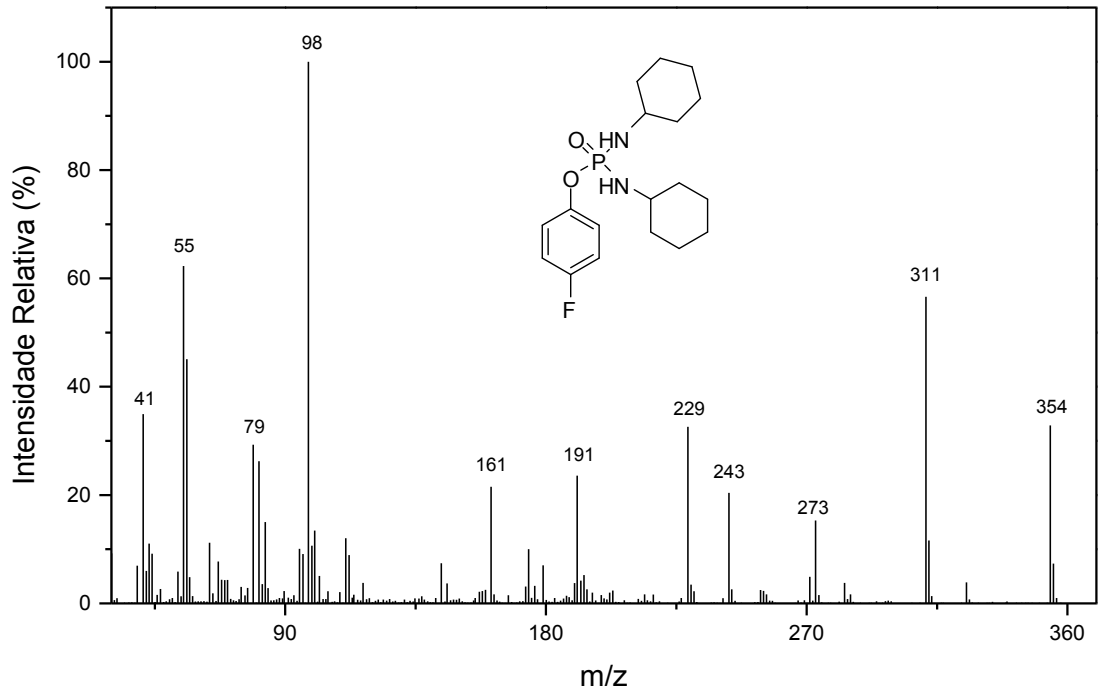

Figura 68 - Espectro de massas do composto **84**.

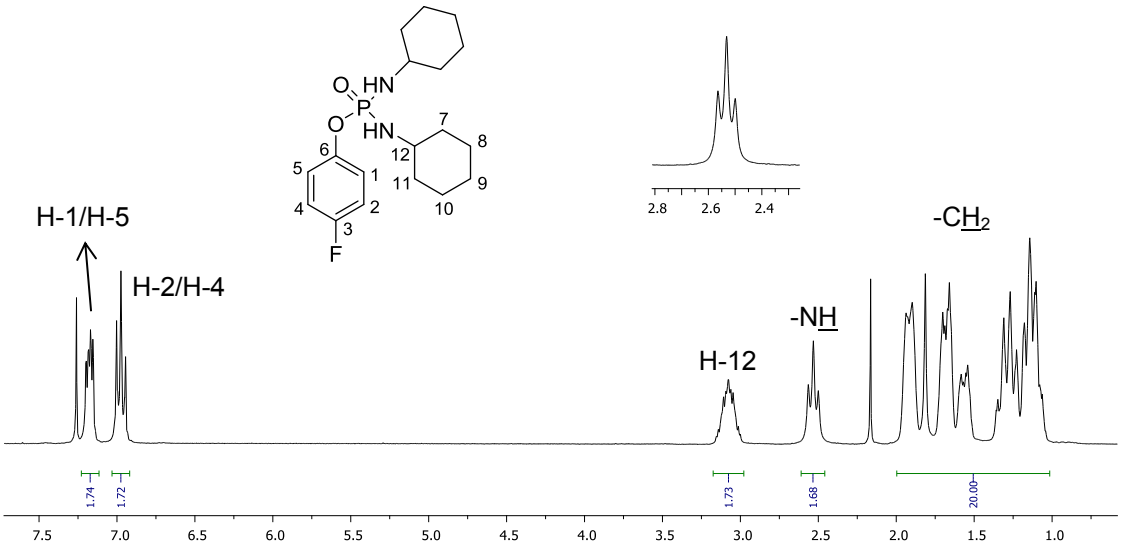

Figura 69 – Espectro de RMN de ^{1}H (300 MHz, $CDCl_3$) do composto **84**.

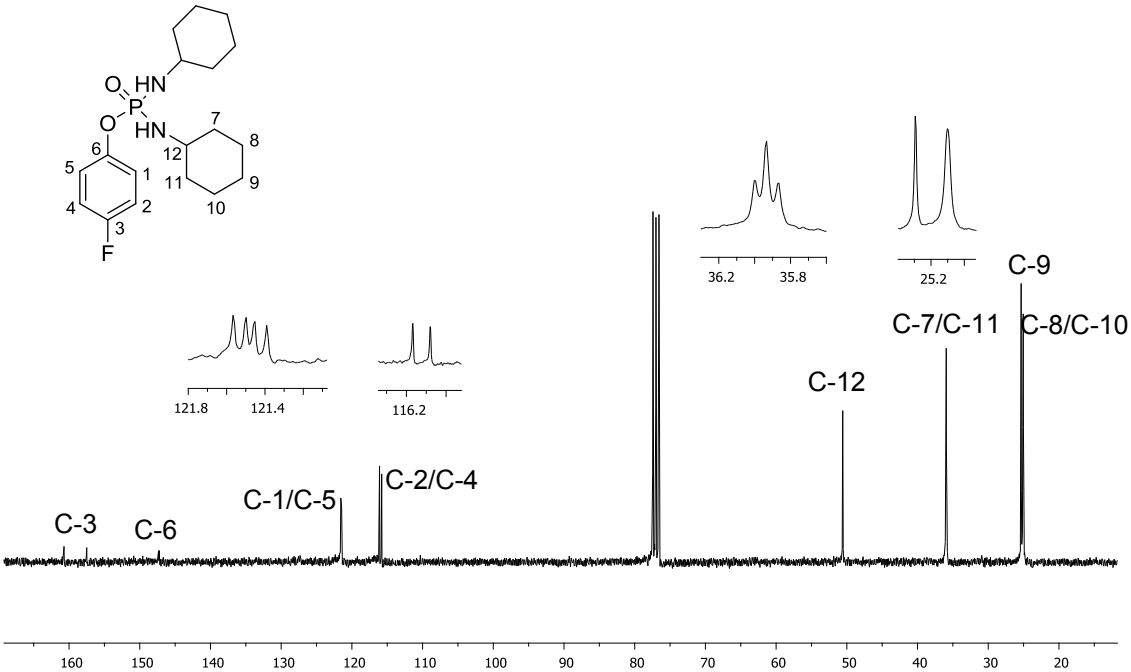

Figura 70 - Espectro de RMN de ^{13}C (75 MHz, $CDCl_3$) do composto **84**.

9. ARTIGOS PUBLICADOS

OLIVEIRA, F.M.; BARBOSA, L.C.A.; DEMUNER, A.J.; MALTHA, C.R.A.; PEREIRA, S.R.; HORTA, L.P.; MODOLO, L.V. Synthesis, molecular properties and DFT studies of new phosphoramidates as potential urease inhibitors, *Medicinal Chemistry Research*, v. 23, p.5174-5187, 2014.

OLIVEIRA, F.M.; BARBOSA, L.C.A.; ISMAIL, F.M.D. The diverse pharmacology and medicinal chemistry of phosphoramidates – a review, *RSC Advances*, v. 4, p. 18998-19012, 2014.

OLIVEIRA, F.M.; BARBOSA, L.C.A.; DEMUNER, A.J.; MALTHA, C.R.A.; FERNANDES, S.A.; CARNEIRO, J.W.M.; CORRÊA, R.S.; DORIGUETTO, A.C. Spectroscopic and dynamic NMR study, X-ray crystallography and DFT calculations of two phosphoramidates: $(C_4H_3O_2)P(O)(Cl)C_6H_{14}N$ and $(C_4H_3O_2)P(O)(C_6H_{11}NH)_2$, *Journal of Molecular Structure*, v. 1046, p.64–73, 2013.

TEIXEIRA, R.R.; BRESSAN, G.C.; PEREIRA, W.L.; FERREIRA, J.G.; OLIVEIRA, F.M.; THOMAZ, D.C. Synthesis and Antiproliferative Activity of C-3 Functionalized Isobenzofuran-1(3*H*)-ones, *Molecules*, v. 18, p. 1881-1896, 2013.

TEIXEIRA, R.R.; PEREIRA, W.L.; FERREIRA, J.G.; TOMAZ, D.C.; OLIVEIRA, F.M.; GIBERTI, S.; FORLANI, G. Synthetic Analogues of the Natural Compound Cryphonectric Acid Interfere with Photosynthetic Machinery through Two Different Mechanisms, *Journal of Agricultural and Food Chemistry*, v. 61, p. 5540−5549, 2013.

OLIVEIRA, F.M.; BARBOSA, L.C.A.; VALENTE, V.M.M.; DEMUNER, A.J.; MALTHA, C.R.A.; OLIVEROS-BASTIDAS, A.J. Structure–activity relationship of pyridin-2(1*H*)-ones derivatives as urease inhibitors, *Journal of Pharmacy Research*, v. 5, p. 5326-5333, 2012.